

NASA-CR-65178

THE DESIGN
OF AN
OMNIDIRECTIONAL
ANTENNA SYSTEM
FOR THE
APOLLO SPACECRAFT

FACILITY FORM 602

N 66-12503	
(ACCESSION NUMBER)	(THRU)
236	1
(PAGES)	(CODE)
	07
(NASA CR OR TMX OR AD NUMBER)	(CATEGORY)

GPO PRICE \$ _____

CFSTI PRICE(S) \$ _____

Hard copy (HC) 6.00

Microfiche (MF) 1.25

653 July 65

DORNE AND MARGOLIN, INC., 29 NEW YORK AVE., WESTBURY, N. Y.



THE DESIGN OF AN OMNIDIRECTIONAL
ANTENNA SYSTEM FOR THE APOLLO
SPACECRAFT



Report 1791.1

PREPARED FOR: NASA Manned Spacecraft Center
Houston, Texas

DATE: September 22, 1964

CONTRACT NO: NAS 9-2286

PREPARED BY: Arthur Dorne
Eugene Shube
Ray Anderson
Louis Leopold

DORNE AND MARGOLIN, INC., 29 NEW YORK AVE., WESTBURY, N. Y.



ACKNOWLEDGMENT

The work described herein would not have been possible without the co-operation of NASA Manned Spacecraft Center, Houston, Texas, and of North American Aviation, Inc., Downey, California. These organizations furnished a substantial amount of background information and technical detail upon which much of the study and subsequent design recommendations are based.

TABLE OF CONTENTS

	<u>Page</u>
LIST OF ILLUSTRATIONS	ii-xiv
ABSTRACT	xv
1.0 INTRODUCTION	1
1.1 Statement of Problem	1
1.2 Objectives of Work Performed	3
1.3 Specific Details of the Problem	5
2.0 THE DESIGN APPROACH	9
2.1 Discussion of the Problem	9
2.2 The Design Approach	17
3.0 THE ANTENNA DESIGN STUDY	29
3.1 The Electrical Portion of the Design Study	30
3.2 Mechanical Design	73
3.2.1 Materials	73
4.0 FINAL DESIGN AND LABORATORY PROTOTYPES	120
4.1 Recommended Designs	120
4.2 Description of Laboratory Models	123
4.3 Performance of Laboratory Models	135
5.0 MODEL RADIATION PATTERN STUDY	155
5.1 Discussion of Test Facility and Pattern Testing Procedure	156
5.2 Model Pattern Measurements	159
6.0 CONCLUSIONS	214

LIST OF ILLUSTRATIONS

<u>FIGURE NO.</u>	<u>TITLE</u>	<u>PAGE NO.</u>
1	Undershoot Entry, Total Heating Rate for Antennas Located Near $+Y_c$, $-Z_c$, $-Y_c$ Meridians at Maximum Capsule Diameter	12
2	Overshoot Entry, Total Heating Rate for Antennas Located Near $+Y_c$, $-Z_c$, $-Y_c$ Meridians at Maximum Capsule Diameter	13
3	General Construction of Antennas (Except C Band)	25
4	Detail of Antenna Retaining and Insulating Flange	26
5	General Construction of C Band Antenna	28
6	Diagrammatic Representations of Flat, Round Cavity Antennas with Flush Strap Feed, Excited in Various Ways to Determine Effect Upon Input Impedance	33
7	Measured Impedance of Flat Round Cavity Antennas with Various Flush Feeds Shown in Figure 6	34
8	Measured Impedances of Flat Round Cavity Antenna with Flush Feed with Various Terminating Capacitors as Shown in Figure 6d	36
9	Diagrammatic Representation of Flat, Round Cavity Antennas with Elevated Feed Straps Showing Basic Configuration	38
10	Measured Input Impedance of Flat Round Cavity Antennas with Elevated Feed Straps Shown in Figure 9	39
11	Diagrammatic Representations of Flat Cavity Antennas Showing Progression to Capacitively Excited Radiator Embedded in Fused Quartz	41

LIST OF ILLUSTRATIONS

(Continued)

<u>FIGURE NO.</u>	<u>TITLE</u>	<u>PAGE NO.</u>
12	Measured Input Impedances of Flat Cavity Antennas Shown in Figure 11	42
13	Measured Input Impedance of Flat Round Cavity Antennas with Elevated Feed Strap after Matching, Both with and without Quartz Cover as Shown in Figure 9 (With Strap 3.2" Wide) and Figure 11c (With Shunt Matching Capacitor Added)	43
14	Measured Input Impedances of Flat Round Cavity with Elevated Strap Radiator Covered with 3 Different Thicknesses of Quartz	44
15	Principal Plane Patterns of Quartz Covered Cavity Antenna Shown in Figure 11c, Mounted in Center of Flat Five Foot Square Ground Plane, Measured at 258 mc	46
16	Cavity Shapes Tested to Determine Effect of Enlarging Diameter of Backing Cavity While Holding Radiating Aperture and Feed Configuration Constant	47
17	Relative Bandwidth Versus Volume of Backing Cavity for Antennas like that Shown in Figure 9, but with Backing Cavity as Shown in Figure 15	49
18	Diagramatic Representation of Flat Round Duplexed Cavity Antenna with Radiators for Two Different Frequencies	50
19	Measured Input Impedance at Input Number 1 of Duplexed Antenna like that Shown in Figure 18 but with Radiator Number 1 Matched at 259 mc and Radiator Number 2 Matched at 283 mc	52
20	Measured Input Impedance of Input Number 1 of Duplexed Antenna Shown in Figure 18 for Various Terminations of Input Number 2	53

LIST OF ILLUSTRATIONS

(Continued)

<u>FIGURE NO.</u>	<u>TITLE</u>	<u>PAGE NO.</u>
21	Measured Input Impedance of Input Number 2 of Duplexed Antenna Shown in Figure 18 for Various Terminations of Input Number 1	54
22	Sketch of Duplexed "VHF" and "S" Band Cavity Antenna	55
23	Radiation Pattern (E Plane) of "S" Band Portion of Duplexed Antenna Shown in Figure 22 in a 30 Inch Circular Ground Plane	57
24	Study Layout of Cavity Antenna	59
25	Diagramatic Representations of Strap Radiators	61
26	Measured Impedances of Strap Radiators Shown in Figure 25	63
27	Principal Plane Patterns of Strap Antenna Shown in Figure 25b Mounted in Center of Flat Five Foot Diameter Ground Plane Measured at 258 mc	64
28	Sketch of First Quartz Laboratory Model of VHF Strap Antenna	66
29	Measured Impedance of Final Laboratory Model of VHF Strap Antenna Shown in Figure 26	67
30	Outline Drawings of Ablative Shield Antennas	69
31	E Plane Patterns of Small S Lot in 3 Foot Square Ground Plane	71
32	Thermal Conductivity of Clear Fused Silica	75
33	Specific Heat of Clear Fused Silica	76
34	Thermal Diffusivity of Clear Fused Silica	77
35	Dielectric Constant of Clear Fused Silica	78

LIST OF ILLUSTRATIONS

(Continued)

<u>FIGURE NO.</u>	<u>TITLE</u>	<u>PAGE NO.</u>
36	Loss Tangent of Clear Fused Silica	79
37	Emissivity of Clear Fused Silica	80
38	Conductivity of Clear Fused Silica Showing Operation of Radiant Heat Transfer Mechanism	81
39	Thermal Conductivity of Multiform Fused Silica	83
40	Specific Heat of Multiform Fused Silica	84
41	Thermal Diffusivity of Multiform Fused Silica	85
42	Dielectric Constant of Multiform Fused Silica	86
43	Loss Tangent of Multiform Fused Silica	87
44	Estimated Emissivity for Multiform Fused Silica	88
45	Mechanical Properties of Imidite 1850	94
46	Antenna, Convective Heating Rate Aft of Maximum Heating Zone. $X_c = 59.0$ at $+Z_c$ Axis	99
47	Antenna Convective Heating Rate Aft of Maximum Heating Zone. $X_c = 59.0$ at $+Z_c$ Axis. Overshoot Entry.	100
48	Temperature Distribution in Prism Shaped Window. Simplified Problem Statement. Surrounding Ablator Does Not Change in Thickness. Antenna 1.4 Inches Thick Exposed to Overshoot Entry per Figure 2	105

LIST OF ILLUSTRATIONS

(Continued)

<u>FIGURE NO.</u>	<u>TITLE</u>	<u>PAGE NO.</u>
49	Temperature Distribution in Prism Shaped Window. Ablator Recedes 0.7 Inch During Heat Pulse. Antenna Exposed to Overshoot Entry per Figure 2	106
50	Temperature Distribution in Prism Shaped Window as Influenced by Local Thermal Short Circuits. Antenna Exposed to Overshoot Entry per Figure 2	107
51	Temperature in Prism Shaped Window as Influenced by Local Thermal Short Circuits. Antenna Exposed to Overshoot Entry per Figure 2.	109
52	Temperature Distribution in Conical Frustrum Window. 3 Inch Top Diameter. 60° Included Angle. 1.4 Inches Thick. Antenna Exposed to Overshoot Entry per Figure 2	110
53	Temperature Distribution in Semi-Infinite Slab Window 1.4 Inches Thick. Antenna Exposed to Overshoot Entry per Figure 2	112
54	Temperature Distribution in Semi-Infinite Slab Window 1.4 Inches Thick. Antenna Exposed to Undershoot Entry per Figure 1	113
55	Temperature Distribution in Semi-Infinite Slab Window 1.3 Inches Thick. Antenna Exposed to Overshoot Entry per Figure 47	115
56	Temperature Distribution in Semi-Infinite Slab Window 1.3 Inches Thick. Antenna Exposed to Undershoot Entry per Figure 46	116
57	Schematic Diagram of Analog Computer	118

LIST OF ILLUSTRATIONS

(Continued)

<u>FIGURE NO.</u>	<u>TITLE</u>	<u>PAGE NO.</u>
58	Temperature - Time Plot of Spacecraft Heat Shield Wall Under Antenna. Analog Computer Output	119
59	Comparison between Laboratory Model Design and Operational Model Design of Antennas	124
60	Assembly Drawing for Laboratory Prototypes for VHF Through S Band	125
61	Laboratory Prototype of VHF Antenna	127
62	Laboratory Prototype of S Band Antenna	129
63	Layout of C Band Antenna	131
64	Laboratory Prototype of C Band Antenna	132
65	Temperature Profile in C Band Antenna at Completion of Overshoot Entry Heat Pulse	134
66	Measured Input Impedance of 237.8 mc Prototype	136
67	Measured Input Impedance of 243 mc Prototype	137
68	Measured Input Impedance of 247.3 mc Prototype	138
69	Measured Input Impedance of 259.7 mc Prototype	139
70	Measured Input Impedance of 296.7 mc Prototype	140
71	Measured Input Impedance of 450 mc Prototype	141

LIST OF ILLUSTRATIONS

(Continued)

<u>FIGURE NO.</u>	<u>TITLE</u>	<u>PAGE NO.</u>
72	Measured Input Impedance of S Band Prototype	142
73	Measured Input Impedance of C Band Prototype	143
74	Prototype Antennas Under Pattern Test	145
75	Measured E Plane Radiation Patterns of 237.8 mc Prototype and Half Loop Reference Antenna	147
76	Measured E Plane Patterns of 296.7 mc Prototype and Half Loop Reference Antenna	148
77	Radiation Patterns of S Band Prototype Measured at 2100 mc	150
78	Radiation Patterns of C Band Prototype Measured at 5500 mc	151
79	Radiation Patterns of C Band Prototype Measured at 5600 mc	152
80	Radiation Patterns of C Band Prototype Measured at 5700 mc	153
81	Radiation Patterns of C Band Prototype Measured at 5800 mc	154
82	One-Fourth Scale Model Used for Pattern Study	157
83	Sketch of Model Pattern Test Setup	158
84	Radiation Pattern Coordinate System	160

LIST OF ILLUSTRATIONS

(Continued)

<u>FIGURE NO.</u>	<u>TITLE</u>	<u>PAGE NO.</u>
85	Sketch of Unbalanced Half-Loop Antenna	161
86	Computed Roll Plane Pattern for Two Sets of Two Antennas on a Cylinder (Linear Slot and Annular Slot)	163
87	Relative Field Radiation Patterns in Roll Plane of 230 mc Antennas at Station 30	164
88	Relative Field Radiation Patterns in Roll Plane of 230 mc Antennas at Station 68	165
89	Relative Field Radiation Patterns in Roll Plane of 230 mc Antennas at Station 107	166
90	Relative Field Radiation Patterns in Pitch-Yaw Planes of Arrays of 8 230 mc Antennas	168
91	Relative Field Radiation Patterns in Pitch-Yaw Planes of Arrays of 4 230 mc Antennas	169
92	Relative Field Radiation Patterns in Pitch-Yaw Planes of Arrays of 3 230 mc Antennas	170
93	Relative Field Radiation Patterns in Pitch Plane Showing Effect of Service Module on 230 mc Antennas at Station 30	172
94	Relative Field Radiation Patterns in Pitch Plane Showing Effect of Service Module on 230 mc Antennas at Station 68	173
95	Measured Pattern of Small Half-Loop Antenna on Two Foot Diameter Ground Plane at 920 mc	175

LIST OF ILLUSTRATIONS

(Continued)

<u>FIGURE NO.</u>	<u>TITLE</u>	<u>PAGE NO.</u>
96	Relative Field Radiation Patterns in Roll Plane of Two Canted 230 mc antennas at Station 68	177
97	Relative Field Radiation Patterns in Pitch-Yaw Planes of Two Canted 230 mc Antennas at Station 68	178
98	Relative Field Radiation Patterns in Pitch-Yaw Planes of Two Canted 230 mc Antennas at Station 68 - Continued	179
99	Relative Field Radiation Patterns in Pitch-Yaw Planes of Two Canted 230 mc Antennas at Station 68 - Continued	180
100	Relative Field Radiation Patterns of Three Element Array of 450 mc Antennas at Station 25	181
101	Relative Field Radiation Patterns of Three Element Array of 450 mc Antennas at Station 25 - Continued	182
102	Relative Field Radiation Patterns in Roll plane of Two Element Array of 450 mc Antennas (Not Canted) at Station 25	183
103	Relative Field Radiation Patterns in Pitch-Yaw Planes of Two Element Array of 450 mc Antennas (Not Canted) at Station 25	184
104	Relative Field Radiation Patterns in Pitch-Yaw Planes of Two Element Array of 450 mc Antennas (Not Canted) at Station 25 - Continued	185
105	Relative Field Radiation Pattern in Roll Plane of Two Element Array of Canted 450 mc Antennas at Station 25	186

LIST OF ILLUSTRATIONS

(Continued)

<u>FIGURE NO.</u>	<u>TITLE</u>	<u>PAGE NO.</u>
106	Relative Field Radiation Patterns in Pitch-Yaw Planes of Two Elements Array of Canted 450 mc Antennas at Station 25	187
107	Relative Field Radiation Patterns in Pitch-Yaw Planes of Two Element Array of Canted 450 mc Antennas at Station 25 - Continued	188
108	Relative Field Radiation Patterns in Pitch-Yaw Planes of Two Element Array of Canted 450 mc Antennas at Station 25 - Continued	189
109	Relative Field Radiation Patterns of Single, One-Quarter Scale S Band Antenna on Flat Sectional Mockup	191
110	Relative Field Roll Plane Radiation Pattern of Single S Band Antenna at Station 21. Principal Polarization Component; Gap Unbridged	193
111	Relative Field Roll Plane Radiation Pattern of Single S Band Antenna at Station 21. Cross Polarization Component; Gap Unbridged	194

LIST OF ILLUSTRATIONS

(Continued)

<u>FIGURE NO.</u>	<u>TITLE</u>	<u>PAGE NO.</u>
112	Relative Field Pitch Plane Radiation Pattern of Single S Band Antenna at Station 21. Principal Polarization Component; Gap Unbridged	195
113	Relative Field Pitch Plane Radiation Pattern of Single S Band Antenna at Station 21. Principal Polarization Component; Gap Unbridged	198
114	Relative Field Roll Plane Radiation Pattern of three S Band Antennas at Station 21. Principal Polarization Component; Gap Unbridged. Antennas at 0°, 120° and 240°	199
115	Relative Field Roll Plane Radiation Pattern of Three S Band Antennas at Station 21. Cross Polarization Component; Gap Unbridged. Antennas at 0°, 120° and 240°	200
116	Relative Field Pitch-Yaw Plane Radiation Pattern of Three S Band Antennas at Station 21. Principal Polarization Component; Gap Unbridged. One Antenna in Plane of Pattern	201
117	Relative Field Pitch-Yaw Plane Radiation Pattern of Three S Band Antennas at Station 21. Cross Polarization Component; Gap Unbridged. One Antenna in Plane of Pattern.	202
118	Relative Field Pitch-Yaw Plane Radiation Pattern of Three S Band Antennas at Station 21. Principal Polarization Component; Gap Unbridged. Plane of Pattern 30° from Plane Containing Antenna	203

LIST OF ILLUSTRATIONS

(Continued)

<u>FIGURE NO.</u>	<u>TITLE</u>	<u>PAGE NO.</u>
119	Relative Field Pitch-Yaw Plane Radiation Pattern of Three S Band Antennas at Station 21. Cross Polarization Component of Radiation; Gap Unbridged. Plane of Pattern 30° from Plane Containing Antenna.	204
120	Relative Field Pitch-Yaw Plane Radiation Pattern of Three S Band Antennas at Station 21. Principal Polarization Component; Gap Unbridged. Plane of Pattern 60° from Plane Containing Antenna.	205
121	Relative Field Pitch-Yaw Plane Radiation Pattern of Three S Band Antennas at Station 21. Principal Polarization Component; Gap Unbridged. Plane of Pattern 60° from Plane Containing Antenna.	206
122	Relative Field Pitch-Yaw Plane Radiation Pattern of Three S Band Antennas at Station 21. Principal Polarization Component; Gap Bridged. One Antenna in Plane of Pattern	207
123	Relative Field Pitch-Yaw Plane Radiation Pattern of Three S Band Antennas at Station 21. Cross Polarization Component; Gap Bridged. One Antenna in Plane of Pattern	208
124	Relative Field Pitch-Yaw Plane Radiation Pattern of Three S Band Antennas at Station 21. Principal Polarization Component; Gap Bridged. Plane of Pattern 30° from Plane Containing Antenna	209
125	Relative Field Pitch-Yaw Plane Radiation Pattern of Three S Band Antennas at Station 21. Cross Polarization Component of Radiation; Gap Bridged. Plane of Pattern 30° from Plane Containing Antenna.	210
126	Relative Field Pitch-Yaw Plane Radiation Pattern of Three S Band Antennas at Station 21. Principal Polarization Component; Gap Bridged. Plane of Pattern 60° from Plane Containing Antenna	211

LIST OF ILLUSTRATIONS

(Continued)

<u>FIGURE NO.</u>	<u>TITLE</u>	<u>PAGE NO.</u>
127	Relative Field Pitch-Yaw Plane Radiation Pattern of Three S Band Antennas at Station 21. Principal Polarization Component; Gap Bridged. Plane of Pattern 60° from Plane Containing Antenna	212
128	Relative Field Roll Plane Radiation Pattern of Three S Band Antennas at Station 40. Principal Polarization Component; Gap Unbridged. Antennas at 0° , 120° and 240°	213

ABSTRACT

12503

A study was carried out to select an approach to the design of an omnidirectional antenna system for the Apollo Command module. It was concluded that radiating elements embedded in fused silica blocks installed in the ablative shield, would best meet the requirements. A laboratory prototype was made of each of the nine different versions of this kind of antenna that a complete system would require. These prototypes are described and their performance characteristics presented. Scale model radiation pattern measurements, using a one-fourth scale model of the vehicle, were also performed. Based upon these measurements recommendations for the location of the antennas upon the capsule are made.

1.0 INTRODUCTION

1.1 Statement of Problem

The Apollo mission requires a multifrequency non-directional antenna system for use in radio transmissions to and from the Apollo command module. It is possible to install such a system either on the command module itself or (at least in part) on the accompanying service module. Command module installation poses many more problems, but offers the major advantage that antenna availability is not terminated when the service module is jettisoned*.

The study described in this report was performed to provide basic information pertaining to the design and installation of a flush-mounted system of antennas suitable for use on the command module.

The precise functions which will require this non-directional antenna system will be subject to change during the course of the program. Not only have the exact frequencies to be used not yet been finally determined, but it is expected that they will not be the same for all flights. For the purposes of this study it was assumed that the following services would be utilized:

* During a normal mission this will occur during the transearth period shortly before entry.

<u>FUNCTION</u>	<u>FREQUENCY</u> mc/sec	<u>MISSION PHASE</u>
Telemetry	237.8	Entry, Launch, Near Earth
Beacon	243.0	Descent
Telemetry	247.3	Lunar Operations
Voice-Receiving Only	259.7	Entry
Voice-Two Way	296.8	Entry, Launch, Near Earth, Lunar Operations Post Landing
Up Data (Receiving Only)	450	Launch, Near Earth
Voice, Up Data Ranging Receiving Only	2106	Near Earth to Deployment of High Gain Antenna, Backup to High Gain Antenna. Voice code only at Lunar Distance.
Voice, TM, TV Ranging Transmit Only	2287	All - If Available
Beacon	Two Frequencies in Band 5600 to 5815 mc	All - If Available

The problem in meeting these requirements all arise from the particular characteristics of the Apollo vehicle and its mission. The restrictions imposed by weight considerations and by the heat flux that will be encountered during entry into the atmosphere are the most severe. Almost as important are those that arise from the

shape and structure of the vehicle as well as the competing requirements of other equipment on, or in, the outer surface of the vehicle.

1.2 Objectives of Work Performed

The objectives of this program comprised the following three separate parts:

a. Design Study: A study of the basic problem of designing antennas suitable for use as elements in the required non-directional antenna system. The recommendation of a particular design approach, and the design of breadboard models to demonstrate the feasibility of the approach. This study was to include the determination of the requirements, restrictions and conditions applicable to the antennas.

b. Radiation Pattern Study: An experimental program of scale model measurements to determine the relationship between the form and quality of the patterns (i.e., the extent of approach to omnidirectionality) and the number and location of the antennas on the vehicle. The particular objective of this study was to obtain information which would indicate the broad general trends of the patterns as the antenna locations and their numbers were varied, and which would be of value in considering tradeoffs between antenna pattern performance, weight and other requirements.

There is an unlimited number of possible cases to consider in making a pattern study of this kind. Consequently, there is no limit to the amount of data that might be gathered. It is necessary therefore to select for study those possibilities which appear most significant. It was initially planned to make measurements at frequencies corresponding to 230, 450 and 2,100 mc on a 1/5th scale model with sets at each frequency of 4, 6 and 8 antennas installed successively at three representative stations on the command module. It was also planned that measurements would be made both with and without the service module attached to the command module in order to determine its effect. Finally, it was planned in some of the cases to vary the phase relationships between the antennas tested to find out if, for example, progressive phasing between antennas yields significantly better patterns than does incoherent excitation.

During the course of the work several changes were made to this program. In order to improve the precision of the modeling, the model was made 1/4th scale rather than 1/5th scale. Because it was learned as the program progressed that weight considerations ruled out the practical possibility of using large sets of antennas, the emphasis was shifted to study of those of the minimum possible number. To have adhered to the initial plan would have yielded results that were of academic interest at best.

c. Prototype Fabrication: A laboratory prototype of each of the antenna types recommended as a result of the design study were to be fabricated. These prototypes were required neither to utilize the exact fabrication techniques nor the exact materials that would be used in operational units, but they were required to establish the feasibility of the recommended designs and to demonstrate that the size and form factors, the impedance characteristics and the radiation patterns of the recommended designs would meet the requirements for an antenna system for the Apollo Spacecraft.

1.3 Specific Details of the Problem

The formal specifications which operational antennas, based upon the results of this study, would have to meet do not, of course, exist as yet. However, in the course of its Apollo work North American Aviation has prepared specifications* for Apollo Spacecraft Command module antennas that substantially describe the conditions and requirements that would apply to any antennas that would be utilized on the capsule. Accordingly, this study was carried out with the understanding that any design approaches produced should be capable of leading to units which would meet and, if need be, exceed the pertinent portions of these specifications. The following are key points from these specifications

* See, for example, NAA Specification MC481-0001 dated 9 March 1962 and MC481-0005 dated 20 June 1963.

that relate particularly to the antenna problem.

a. The General Specification for Military Aircraft Electrical Equipment MIL-E-5400 must be complied with, as well as the other specifications and standards commonly called out for aerospace electrical equipment.

b. Environmental requirements include the following:

- i. Temperature - normal operating temperatures of -200 to +225 degrees F and extreme temperatures of -290 degrees F to a maximum temperature of many thousands of degrees F encountered during entry. (This point is discussed in detail in Section 2.1.)
- ii. Sunshine - solar radiation of 360 B.T.U. per square foot per hour for a six-hour period each day for 42 days.
- iii. Pressure - 7.5×10^{-10} millimeters of mercury for 336 hours.
- iv. Acceleration - 7 g for 147 seconds during lift-off

Other important pertinent facts are the following:

a. The command module is constructed of an inner pressure vessel, surrounded by an outer structural shell separated from it and made up of 1/2 inch stainless steel honeycomb. The entire command module is covered by a heat shield of ablative material. The outer wall of the inner pressure vessel is thermally insulated from the outer shell and is at temperatures close to those of the astronauts' compartment. The ablative cover is of varying thickness around the capsule; but in those regions where antennas would be installed is in the neighborhood of 1.4 inches thick. A key design condition is that the outer skin temperature remain below 600 degrees F during entry and that the outside surface of the inner pressure vessel remain below 200 degrees F. The antennas must not introduce any thermally conducting paths which would upset these conditions.

b. The depth available below the outer metal skin of the vehicle for any antenna structures penetrating it is 1.5 inches. The total distance from the structural mold line of the capsule to the inner pressure vessel is about 1.85 inches. The antenna must clear it by about 0.25 inch.

c. Although it is of course vital that the antennas not deteriorate during entry in such a way as to jeopardize the

integrity of the thermal design of the vehicle, they themselves are not expected to function during this period. Further, although it is desired that the basic designs be such that they will function after entry, the achievement of this is not essential.

d. Radio blackout problems as a result of plasma are outside the scope of this project.

e. The polarization of the earth antennas are such that all of the vehicle antennas should be linearly polarized except for the C-band beacon antenna which is to be circularly polarized. All of the antennas are required to have VSWR's of less than 2:1 except for the C-band antenna which is required to be less than 1.5:1.

f. The heat shield will be of phenolic or electrically similar material which chars when extremely hot. It has a dielectric constant of around 1.95 and a loss tangent of .015.

g. Weight control of the command module is one of the most important design considerations.

2.0 THE DESIGN APPROACH

2.1 Discussion of the Problem

A single requirement dominates the entire problem and is a prime consideration in determining the means by which each of the other requirements can be acceptably met. It is the need to achieve minimum weight. If this objective were not of such over-riding importance a great variety of designs could be achieved without difficulty. There is no absolute lower limit to the size of antennas of this kind. Rather as they are made smaller, they become more critical and less efficient. In essence, therefore, the design problem is to minimize such effects to the greatest possible extent.

The weight of the antenna system will depend upon four factors: (1) the weights of the individual antennas, (2) the weight increases resulting from the structural provisions that must be made to permit the antennas to be installed, (3) the number of antennas, and (4) the amount of ancillary equipment such as cables, filters, and multiplexers which the antennas require. Minimization of the first two of these factors depends upon the design of the antennas themselves. Minimization of the second two is more a matter of tradeoff between weight and antenna performance than it is of design. The more antennas for use at each frequency that are distributed around the capsule, the more nearly omni-directional can the radiation patterns be made and obviously the heavier will be the installation.

The electrical and mechanical aspects of the design problem are so inter-related that they cannot be truly separated. However, the problem may be viewed as consisting in essence of performing the following design steps:

1. Determining the minimum size that would be possible for the antennas if there were no mechanical or thermal restrictions to be met.

2. Determination of a basic electrical design that is compatible with a structure that is judged potentially capable of meeting the mechanical and thermal requirements without exceeding the size determined under step 1.

3. Evolving a mechanical design that embodies the electrical designs while meeting the environmental requirements.

If the problem is viewed from the mechanical-thermal design point of view the antennas are seen as aberrations in, but nevertheless part of, the continuous ablative heat shield which covers the command module. Therefore, the antennas must not only exist in the same thermal environment as the ablative heat shield but must also afford the same thermal protection to the capsule as the portions of ablator which they displace as noted earlier. The spacecraft construction in the areas of interest consists of an outer heat

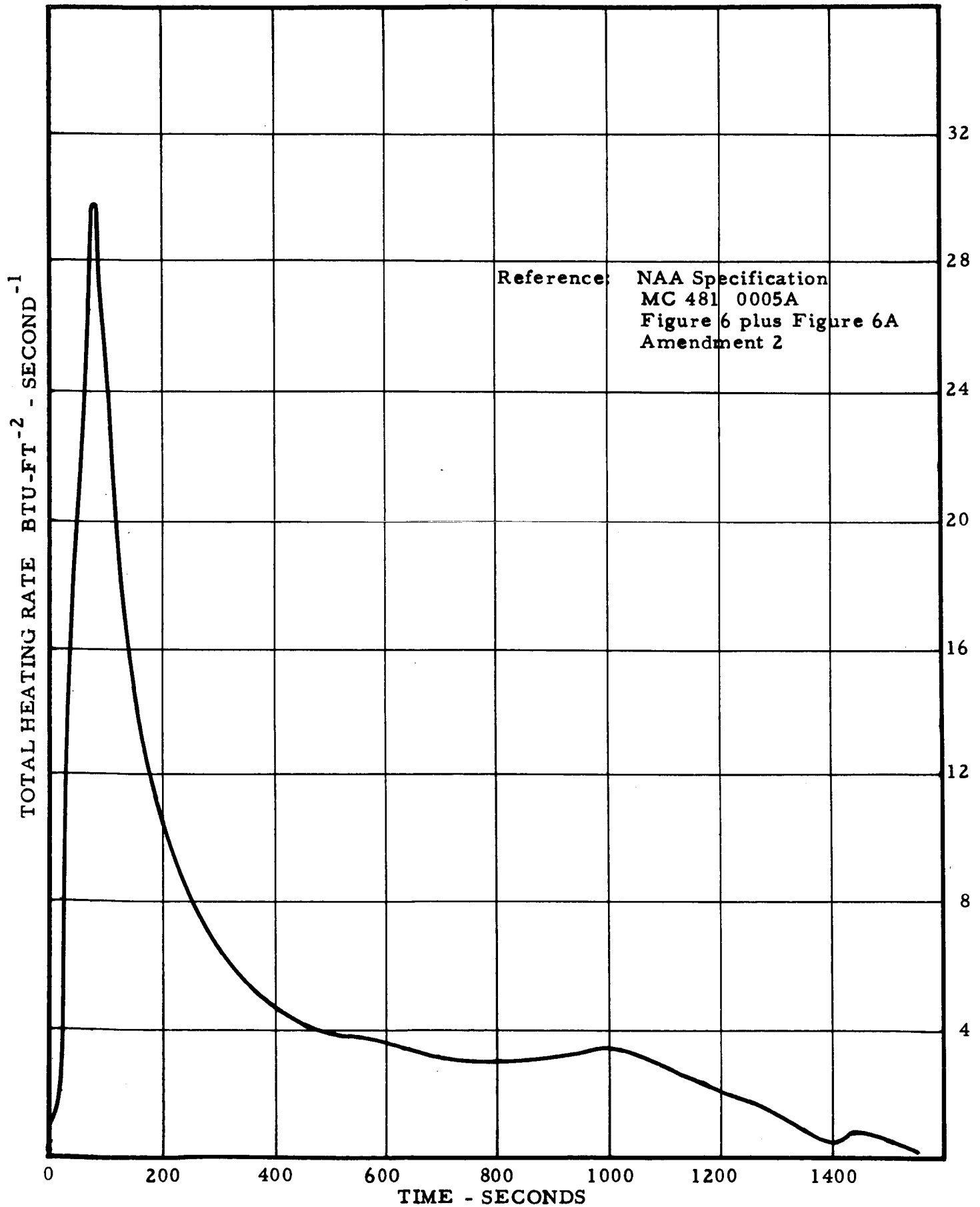


Figure 2 Overshoot Entry, Total Heating Rate For Antennas Located Near +Y_C, -Z_C, -Y_C Meridians At Maximum Capsule Diameter

for the protection of the remainder. The overshoot, which turns out to be the more severe design problem, requires a great deal of isolation of the heat receiving surface from the remainder of the antenna, and a means for storing or rejecting a great deal of heat over a long period of time without bringing the mounting surface above an acceptable limit temperature. The actual temperatures reached will depend on the antenna mechanical design. Proposed designs must be analyzed against the heat pulse in order to find the temperatures. In short, the problem is not actually defined in terms of ambient temperature. However, the temperatures illustrate the nature of the problem which thus oversimplified can be stated: Design a device which will withstand an outer surface temperature which goes from 2800 degree Rankine (about 2340°F) to about 1700 degrees Rankine while its mounting surface, 1.4 inches away, is not heated above 600 degrees F after 40 minutes from the start of the exposure. The device so designed must also function as an antenna of very high efficiency. This device must also withstand vibration, mechanical and thermal shock, humidity, salt spray, acoustic noise and other mechanical environments, and must exhibit a very high order of reliability, on order of 0.999999 probability of success for a two-week mission.

shield of 1/2 inch thick metal honeycomb construction covered by approximately 1.4 inches of a lightweight ablative material layer. Beneath the metal outer heat shield is a space of approximately 1.3 inches filled with felt-like insulative material. Below this space is an inner metal honeycomb wall which constitutes the main life support vessel.

Any antenna that penetrates into the space between the outer and inner walls must not act as a thermal short circuit. The life support system of the spacecraft will be overloaded if portions of the inner wall are heated about 200 degree F.

Any antenna that penetrates into the ablative covering above the outer heat shield must protect the metal heat shield structure from temperatures exceeding 600 degrees F, since this is the temperature above which the bond line between the spacecraft ablator and the heat shield structure will fail.

Local peak heating rates reach 190 B.T.U. per second for each square foot of exposed surface in a short (undershoot) entry of 120 seconds (see Figure 1), or 31 B.T.U. per second per square foot over a long (overshoot) entry of 1500 seconds (see Figure 2). The undershoot emphasizes the requirement for very high temperature resistance and the possibility of sacrifice of some surface material

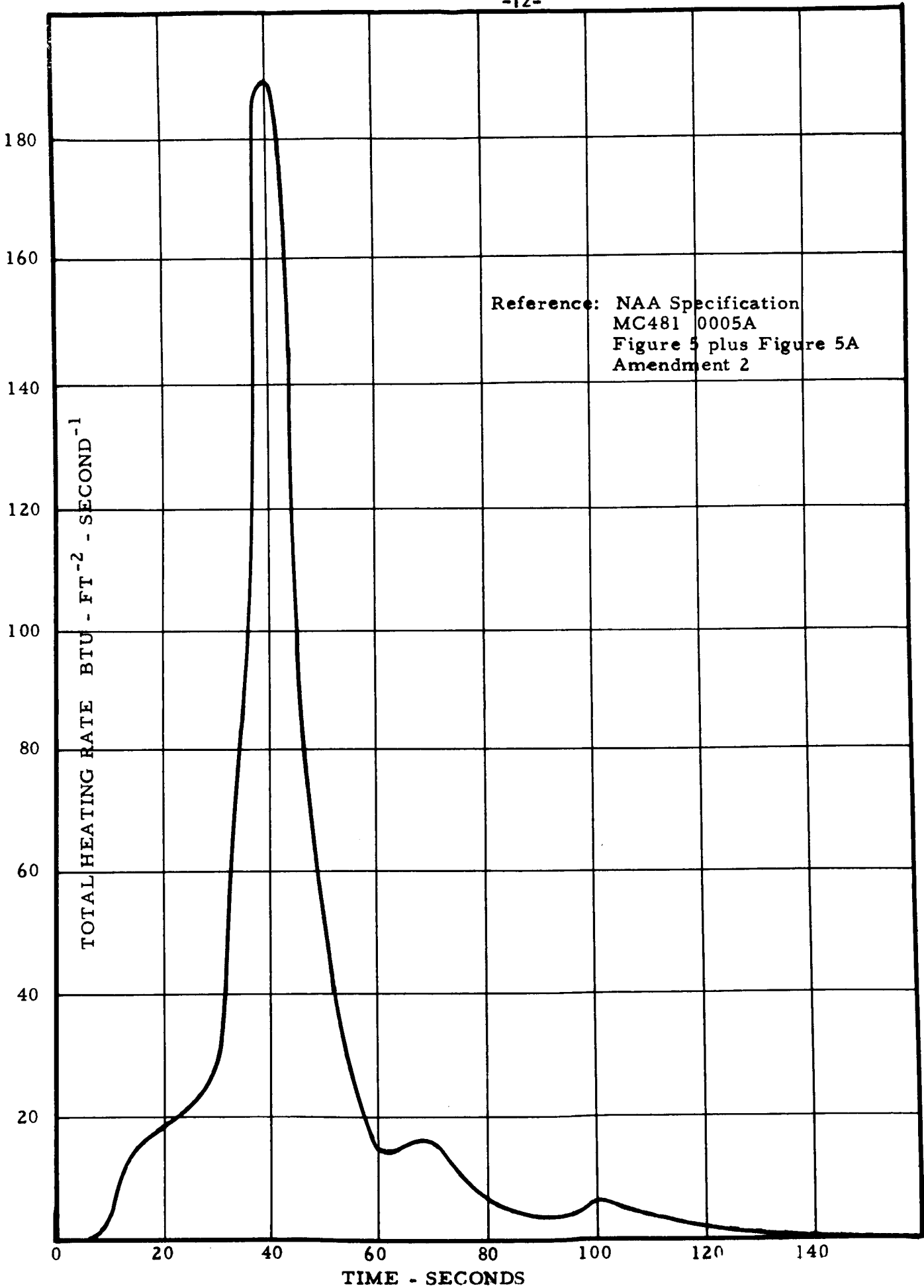


Figure 1 Undershoot Entry, Total Heating Rate For Antennas Located Near +Y_c, -Z_c, -Y_c Meridians At Maximum Capsule Diameter

The ablative covering of the spacecraft is designed to be sacrificed uniformly as heat is absorbed and carried away with the sloughed-off material, thus affording the required protection to the spacecraft outer heat shield structure. It is possible to design an antenna to reside beneath the ablative covering and therefore to be protected by the ablator. Such an antenna would have three problems:

(1) The ablator is not controlled for its electrical characteristics. It is too lossy for high efficiency performance of the C-band and S-band designs, and the losses will also reduce performance of the UHF and VHF designs to some extent. Further, the dielectric constant of the ablator will vary during the wide range of temperatures to be experienced during the space flight portion of the mission. These variations will tend to shift the operating bands of the antennas requiring that these operating bands be widened which, as discussed later, can only be offset by an increase of antenna size.

(2) The ablator may char during the earth exit phase of space flight. If this happens, C-band and S-band performance will be reduced unacceptably. Consideration is being given to

a protective covering for the spacecraft during launch, but the antenna design would be nullified if the design were made dependent upon the existence of the protective covering and such covering were then cancelled in a later project decision.

The ablator will char during earth entry. It is not a requirement that the antennas function during descent through the earth's atmosphere, but such operation would enhance the mission. Even if no charring occurs on exit, the C-band and S-band antennas would be disabled by the char covering which would form on entry.

(3) The usable space beneath the ablator is limited to 1.5 inches in depth over most of the spacecraft surface. Mechanical designs which utilize the ablator for protection must perform their electrical functions within the remaining 1.5 inches. These designs tend to get unacceptably large for the VHF and UHF functions.

When the antenna is designed to penetrate into the ablator or replace a portion of the ablator in order to minimize or eliminate the problems described above, the choice of dielectric materials is limited to those which would function well electrically as well as resist the high temperature of entry. Most of the ablative materials which have been designed for resistance to a high temperature environment have high loss tangents or char-forming tendencies since they have not been designed for optimum electrical characteristics.

2.2 The Design Approach

Although the weight of the S-band and C-band antennas are by no means negligible, by far the major part of the weight will be contributed by the VHF and UHF antennas. As noted earlier, these antennas must function at the following six frequencies: 237.8, 243, 247.3, 259.7, 296.8 and 450 mc. It is to be expected that antenna locations which would be good for operation at any one of these frequencies would also be good at the others. This suggests the use of broadband antennas, each serving several or perhaps even all of the bands from 237.8 to 450 mc. The possibility of utilizing such antennas was rejected early in the program because the first examination of the problem showed that a set of narrow band antennas, even though it comprised more antennas, would weigh less than a set of broadband antennas of equal efficiency and inherent stability. The underlying reasons for the weight advantage being with the narrow band antennas are twofold. First, with small antennas (i.e., those that are substantially less than a half wavelength in their largest dimension, as are any that would be used in this application) the maximum obtainable bandwidth is a direct function of the Q of the radiating structure and; second, the Q of small antennas varies inversely as the cube of the dimensions in wavelengths (or in effect with the volume of the antenna).

A numerical example will show that from these facts it can readily be deduced in a particular instance which will have the smaller volume (and, therefore, weight). Suppose that a 250 mc signal and a 260 mc signal are to be radiated, and that a choice is to be made between a single broadband antenna or a pair of narrow band ones of similar design. In both cases a guard band

of 1 mc is assumed on each side of each operating frequency. If separate antennas are used, one antenna must therefore cover from 249 to 251 mc and the other from 259 to 261 mc. If one antenna is used the required band would be from 249 to 261 mc. Let the 250 mc antenna have a volume V_1 . The unit to operate at 260 mc, because of the two facts cited above would need a volume V_2 and V_2 would equal abV_1 where a is the ratio of the two relative bandwidths and b is the cube of the ratio of the two operating frequencies. The relative bandwidth of the first antenna is $\frac{251 - 249}{250} = .008$ and the relative bandwidth of the second antenna is $\frac{261 - 259}{260} = .0077$. Therefore, a is equal to .96. The inverse of the cube of the frequencies, $(250/260)^3 = .887$ is the value of b . Therefore, $V_2 = .96 \times .887 V_1 = .85 V_1$ and the total volume of both together is $1.85 V_1$. Application of the same procedure shows that the 249 to 261 mc antenna would require a volume 5.5 times that of the first antenna

or 2.97 times the combined volumes of the two narrow band ones. In essence, because to cover a 12 mc band in the 250 mc region requires an antenna with approximately six times the volume that is required for an antenna with a 2 mc bandwidth in the same frequency region, two separate antennas to cover two 2 mc bands each will require only 1/3 the volume (approximately) of a single antenna in the same frequency region covering 12 mc. Obviously, as the separation between the operating frequencies decreases, the two cases approach each other. Clearly, unless the separation between the operating frequencies is less than twice the guard bands the volume advantage (and, therefore, weight) will be with the separate antennas.

As was pointed out in the beginning of this section, the above argument was based upon two characteristics of small antennas; with large antennas it would not apply. The inherent Q of large antennas is usually low enough so that in most cases it is not the characteristic limiting bandwidth. Consequently, the size is determined by the lowest operating frequency, the directivity requirements and the design techniques employed.

Returning to the present case and applying the above argument, it was seen that a substantial weight advantage would accrue if the antennas were made narrow band. The ultimate extent of the advantage

could not be accurately determined at the outset of the program because the bandwidth requirements for the narrow band antennas were not known and could not be until they had been designed and their stability and their size versus efficiency characteristics examined. It was therefore necessary to assume a bandwidth. It was taken to be two megacycles. This is a conservative estimate. Quite possibly one and a half or even one megacycle bands would be sufficient, in which case the advantage of the narrow band antennas would be greater.

Numerically, it turns out that a set of six* narrow band antennas, each having the assumed 2 mc bandwidth would offer a weight ratio advantage of 5.3 over a broadband antenna of equivalent design. In making the above calculation, one additional fact not previously mentioned was taken into consideration. It tends to reduce the advantage of the broadband antenna and is the fact that with broadband antennas more complex impedance matching techniques are applicable. In consequence for a given Q about 30% more bandwidth can be obtained in practice.

The core then of the basic electrical design approach was to design a set of narrow band antennas that would provide satis-

* It will be noted that the advantage will be somewhat smaller if the comparison is made with the 450 mc frequency excluded. In that case the weight ratio advantage is only 3.5.

factory efficiency and stability, with the smallest possible installed weight. Ninety percent was taken as an efficiency target and a bandwidth of approximately two megacycles was assumed necessary to achieve both this and satisfactory stability.

As discussed in detail in Section 3.0 two types of narrow band antennas were studied. One was of the cavity type; the other consisted of an assembly for insertion in the ablative heat shield, and will be referred to in this report as ablative shield antennas. The approach to the mechanical-thermal problem was essentially the same in both cases and is described in the following paragraphs in terms of the non-cavity approach, because this is the preferable one for the Apollo capsule.

One of the fundamental design choices is that of the type of window material. There is one general class comprising those which are readily ablated. Such a material would be sacrificed on entry and would inherently tend to maintain low inner surface temperatures. The other class consists of those which have such high melting points that they would store and re-radiate the heat input with very little sacrifice of surface material. They would tend to become hot at their inner surfaces. Examples of the former class of materials are Teflon, reinforced Teflon such as "Duroid

5650", silica reinforced phenolics such as "Refrasil" and nylon reinforced phenolics. Examples of the latter group are clear fused silica such as Corning 7940, multiform fused silica such as Corning 7941 and (possibly) alumina ceramics. For all but the C-band antenna the choice was made in favor of the latter, the refractory type of material, for the following reasons:

1. It was desired to obtain the best utilization of the space occupied by the window by having active antenna elements in the window itself rather than using the window only as a cover. It was found that variations of electrical properties of the better ablative type of materials such as Duroid 5650 with temperature were sufficient to have adverse effects on the tuning of high Q antennas within the operating temperature range of -250 F to +250 F.

2. The thermal expansion of the ablative type of materials in the temperature range of normal operation would be sufficient to detune the antennas by varying the mechanical spacing of the elements in the window. Even if a material were found which had electrical properties which remained constant, the thermal expansion would preclude its use.

Given the utilization of a ceramic material, the design approach is limited to one of three possibilities.

1. Isolate the antenna from the spacecraft as completely as possible so that the antenna effectively has no heat sink but must either store or re-radiate all heat energy received.

2. Allow the antenna to be coupled solidly to a good heat sink such as aluminum or beryllium or carbon such that all of the heat received is insufficient to raise the local spacecraft temperature over either of the two critical temperatures; that is, 600°F at the metallic support structure of the spacecraft heat shield, or 200°F at the inner structural wall, which is the pressure vessel of the manned compartment.

3. Combinations of the above two approaches.

The first approach, if carried out successfully, offers the minimum size and weight antennas because no heat sinking material need be added. It also permits the antenna to be located entirely within its window with no space occupied below the spacecraft heat shield where the heat sink would otherwise have to be located.

The heat sink approach is necessarily inefficient in its utilization of material in that the allowable temperature rise is limited to about 250°F . (The antenna may be soaked at 250°F before beginning the entry maneuver and the maximum temperature to which the heat shield structure may be exposed is 600°F . This high initial temperature also makes it difficult to protect the inner wall from temperatures above 200°F using only the heat sink approach, if any of the antenna or heat sink parts are located near the inner wall.)

The design approach chosen uses a multiform fused silica window thermally isolated from the spacecraft heat shield structure by its mounting means. The antenna radiating structure is entirely disposed within the window and no part of the antenna extends below the spacecraft heat shield except the connector. The details of the mounting arrangement are shown in Figures 3 and 4. The peak temperature reached by the block of fused silica under any of the conditions studied is 2720°R (2260°F). This occurs at its outer surface two minutes after the start of an overshoot entry. At this temperature heat re-radiation plus conduction inward exceeds the heat accepted per unit time and the temperature at the surface drops, reaching 1760°R (1300°F) after 12 minutes and 1460°F (1000°F) after 23 minutes. The heat conducted inward soaks into the

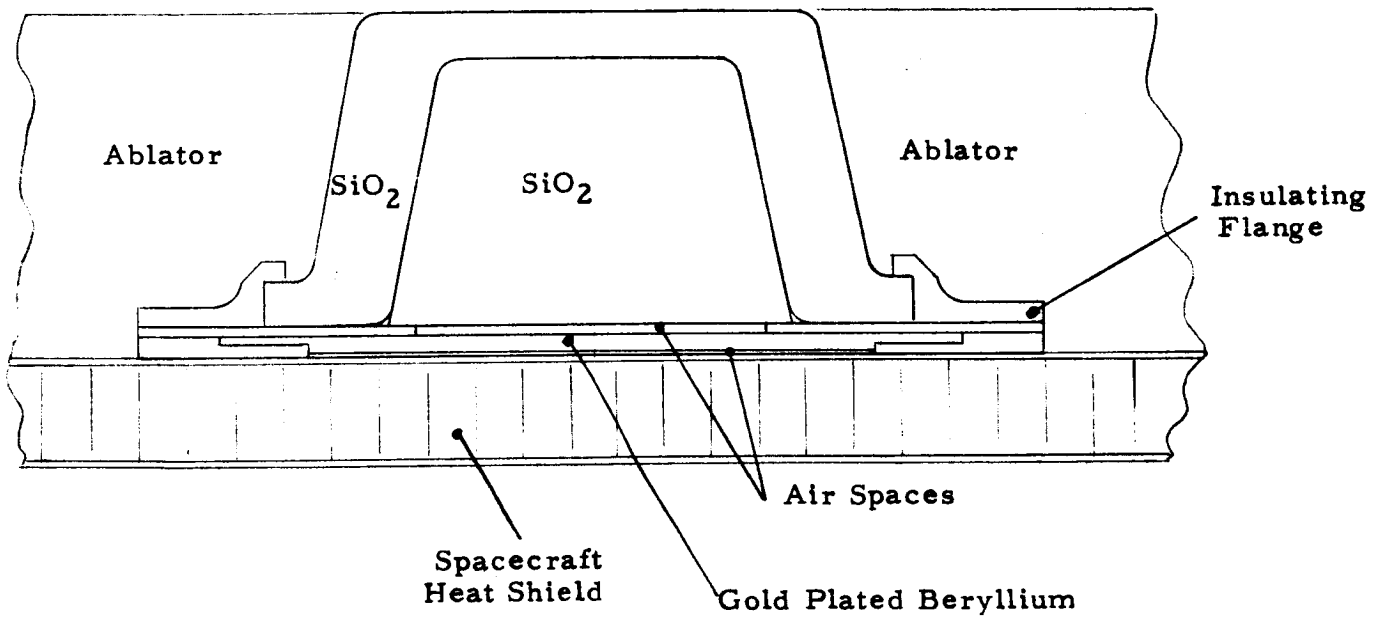


Figure 3 General Construction Of Antennas (Except C Band)

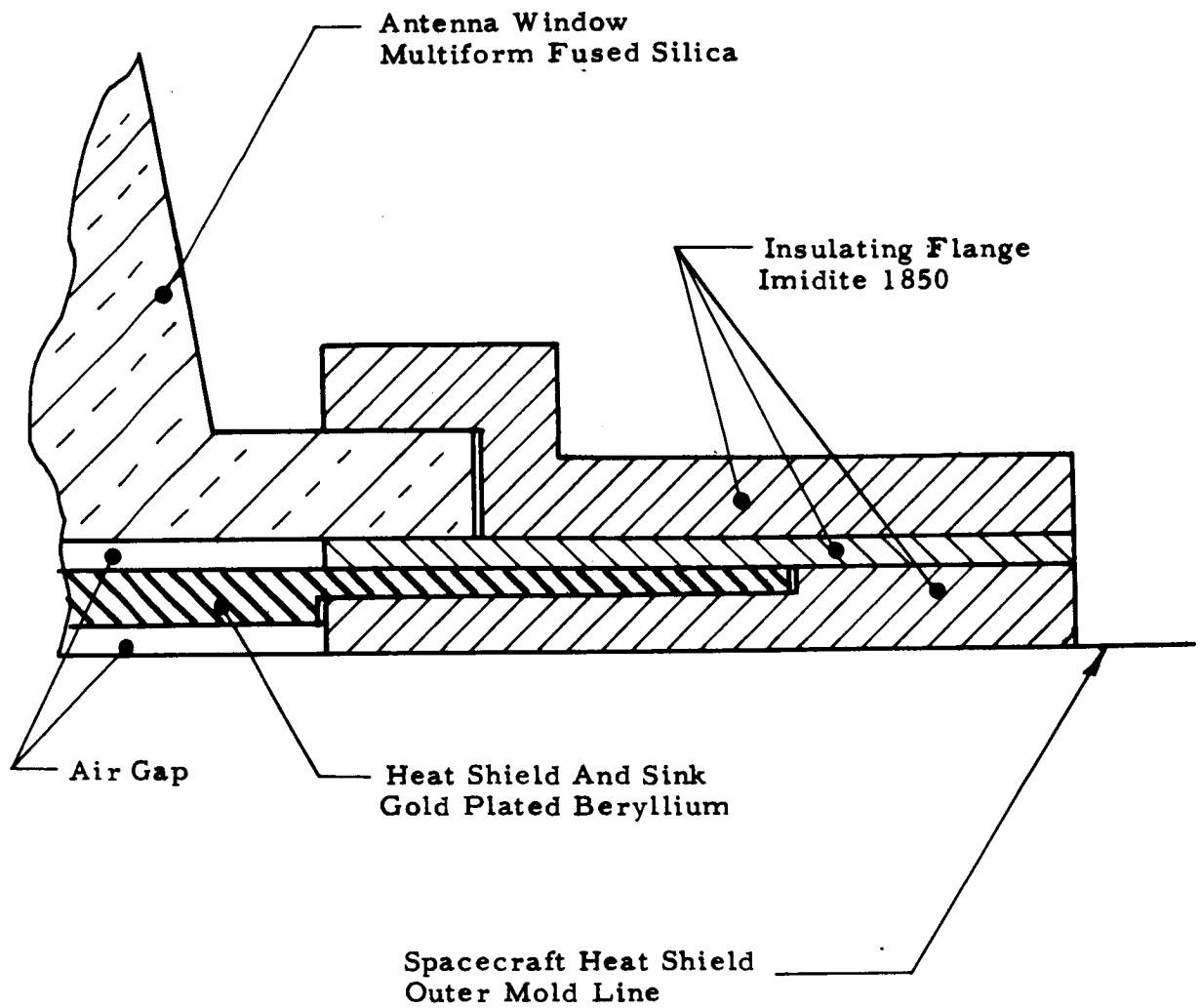


Figure 4 Detail Of Antenna Retaining And Insulating Flange

block which gradually rises in temperature at its inner surface starting at 710°R (250°F) at the beginning of the entry and reaching a maximum of 1420°F (960°F) 26 minutes later. During a portion of the entry maneuver from 9.5 minutes after start, the temperature of the lower surface of the fused silica block exceeds the allowable temperature of 600°F specified for the heat shield support structure to which it is mounted. A metal shield reflects radiant heat back into the antenna, and the low conductivity fiberglass mounting flange and isolating spacers delay the temperature rise at the spacecraft heat shield structure for an additional thirty minutes.

The approach to the C-band antenna, because it operates at much shorter wavelengths was considerably different. Because the antenna is necessarily small, weight reduction is not the dominating consideration. On the other hand, the antenna must be elliptically polarized. Accomplishing this in a stable way requires a Q that is substantially less than ten. In consequence the extreme thermal stability of fused silica through the antenna is not necessary. As shown in Figure 5 the C-band antenna approach involved an open-ended fused silica filled waveguide covered with a protective cap of Duroid 5650. This cap dissipates about half of the heat pulse before the fused silica block is exposed.

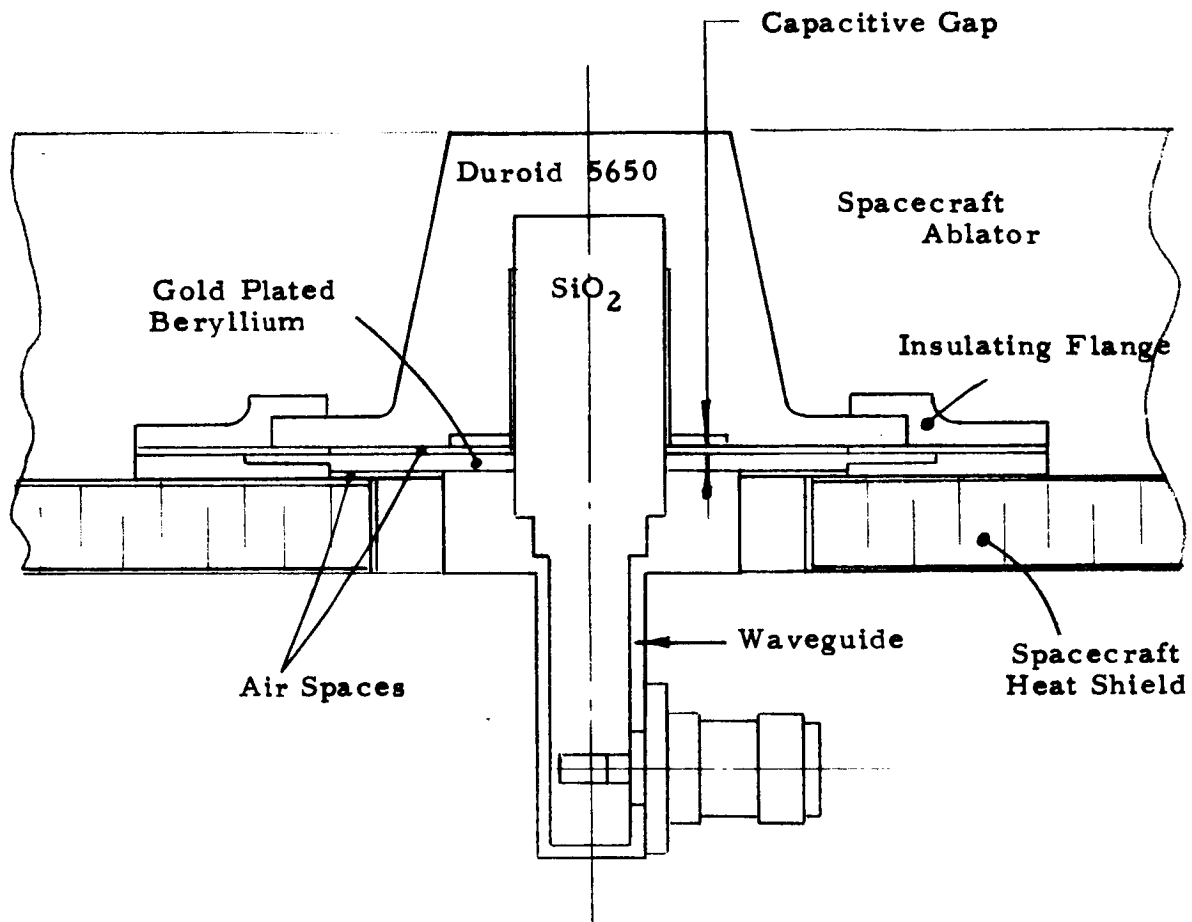


Figure 5 General Construction Of C Band Antenna

3.0 THE ANTENNA DESIGN STUDY

Two closely related but nevertheless completely distinct types of antennas were investigated and carried through preliminary design. The first of these consisted of a series of shallow cavity antennas designed to be installed in holes cut in the outer metal skin of the vehicle. These antennas extended into the space between the two skins of the capsule and had integral fused quartz covers (or windows) which replaced the ablative material which would otherwise have covered them. This window was included for the reasons discussed earlier to provide a region in the ablator having satisfactory electrical properties. Because a slight size reduction was thereby accomplished, part of the radiating structure protruded slightly into the cover.

At the outset of the work it was believed that cavity antennas were the only type of flush antennas which it was possible to design that would neither jeopardize the integrity of the vehicle during entry nor themselves be rendered inoperative by the high temperatures encountered then. As previously implied, it was found as the work progressed that it would also be possible to design antennas which would meet the applicable requirements and yet be entirely in the ablative region, thereby avoiding the need to cut holes in the outer skin except for that required for the

connecting cable. Two key points permitted this change of approach. One was learning as the calculation of the temperature gradients in the quartz covers were made that the peak temperatures within the antennas would be somewhat lower than had been anticipated. The other was the development, in the course of the design of the cavity antennas, of a technique for exciting the principal radiating element by means of a capacitance. This eliminated the need in ablative shield antennas for conductors which ran continuously from the outer surface of the ablator into the metal heat shield, and thereby eased the thermal design problem.

This second type of antenna was studied after the preliminary design of the cavity antennas was completed. Ablative shield antennas were found to be superior for the Apollo Mission. The laboratory prototypes furnished under the contract were therefore made of the ablative shield type.

3.1 The Electrical Portion of the Design Study

It was mentioned earlier that with a given antenna design the Q (when the antenna is small with respect to a wavelength) varies inversely as the cube of the dimension in wavelength* or, in other words,

* See, for example, H. Jasik: Antenna Engineering Handbook, McGraw Hill, 1960, Page 8-13.

inversely with the volume. This does not mean, however, that all antennas of the same volume have precisely the same Q . The Q also varies with the design of the antenna. With a cavity antenna of a given volume in cubic wavelengths, the Q depends both upon the shape of the cavity and the means by which it is excited*.

In the present case, with the maximum cavity depth fixed at 1.5 inches and with the skin stressed, thereby making the maximum linear dimension of the aperture, rather than its area, the major size determinant of installed weight, the optimum shape for the cavity is flat and circular.

Experience as well as heuristic reasoning show that the maximum bandwidth with a small cavity cannot be obtained if the exciting element is located below the aperture. Accordingly, the experimental work of the project was started with the investigation of a flat round aperture excited cavity for use at the lowest frequencies, (which are all in the 250 mc region). Numerous tests were run upon it to determine the best excitation scheme; i.e., the scheme that yields the lowest Q and highest efficiency for a given cavity size. Neither dielectric nor magnetic loading was used. The reasons for this were twofold. First, that at the present state of the art it

* An extensive treatment of this topic is given by A. Vassiliadis and R. L. Tanner: Theoretical Limitations on the Broadbanding Potential of Antennas, with Application to Cavity Backed Slots and Other Antennas, Stanford Research Institute Report 71, August 1960.

appears that this type of approach is not capable of producing a significant size reduction (to the authors' knowledge, none has ever been accomplished). Second, dielectric loading would add weight and magnetic loading would add both weight and temperature problems.

Typical of the antennas* measured during this phase of the work are those illustrated in Figure 6. With the first three of these (6 a) the exciting element was a flat strip of metal grounded at one end and fed at the other through a series capacitance, used for partial matching of the antenna, thereby enhancing the accuracy of the measurements. The second one (6 b) was similar, having both ends grounded and being fed in the middle. The third one (6 c) was made like the second except that the grounded ends of the strap were narrowed to provide series inductance. Although for convenience these, as well as many of the other measurements of the project, were made at scale frequencies (in this case by a factor of 1.6) the following discussion as well as all figures show full scale dimensions and corresponding frequencies. Figure 7 shows the measured input impedances of these antennas in the frequency range of

* At the time this work was performed it was understood that 1.6 inches rather than the actual 1.5 inches of depth was available. It will be noted from the figures that this is their depth.

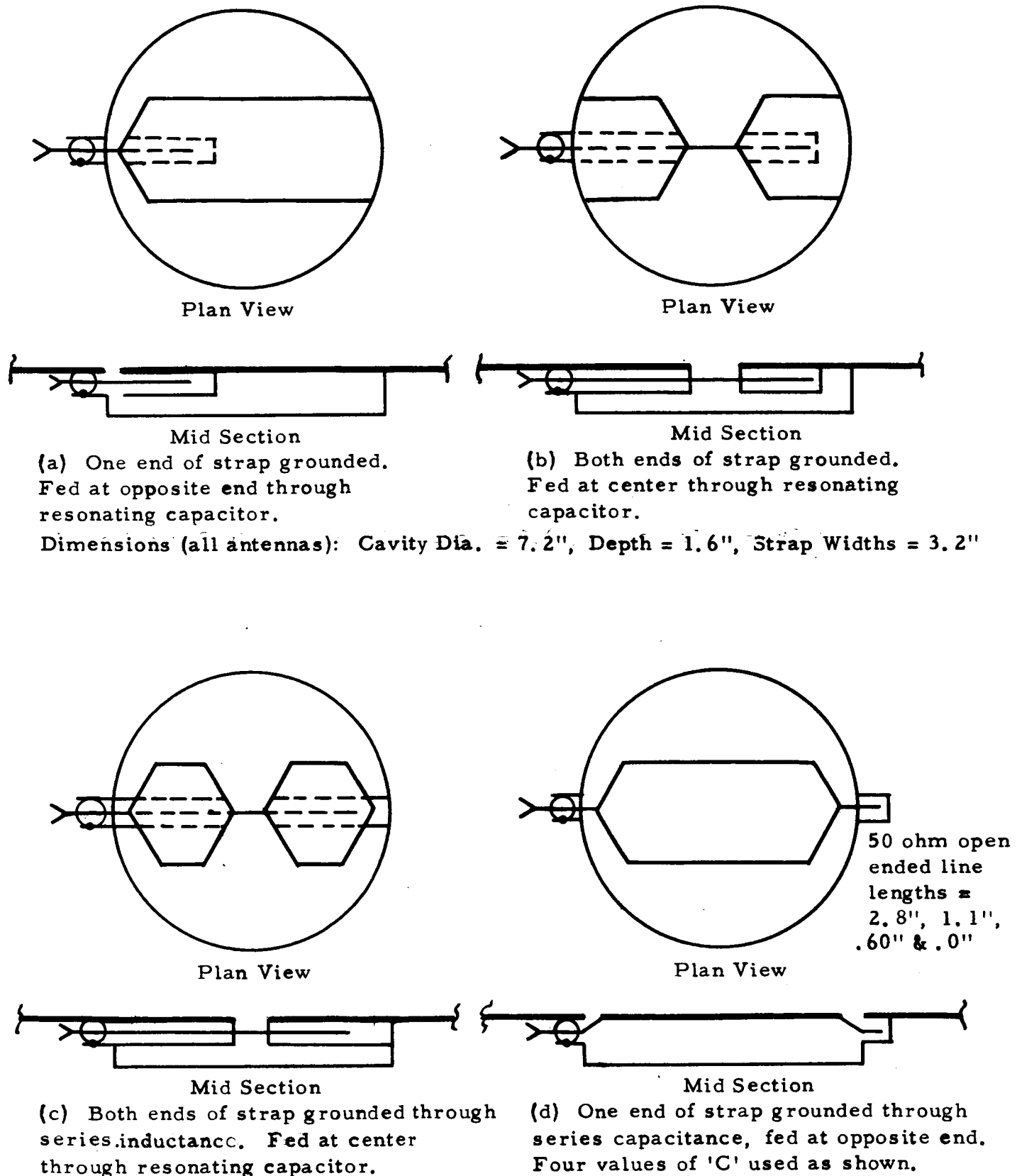
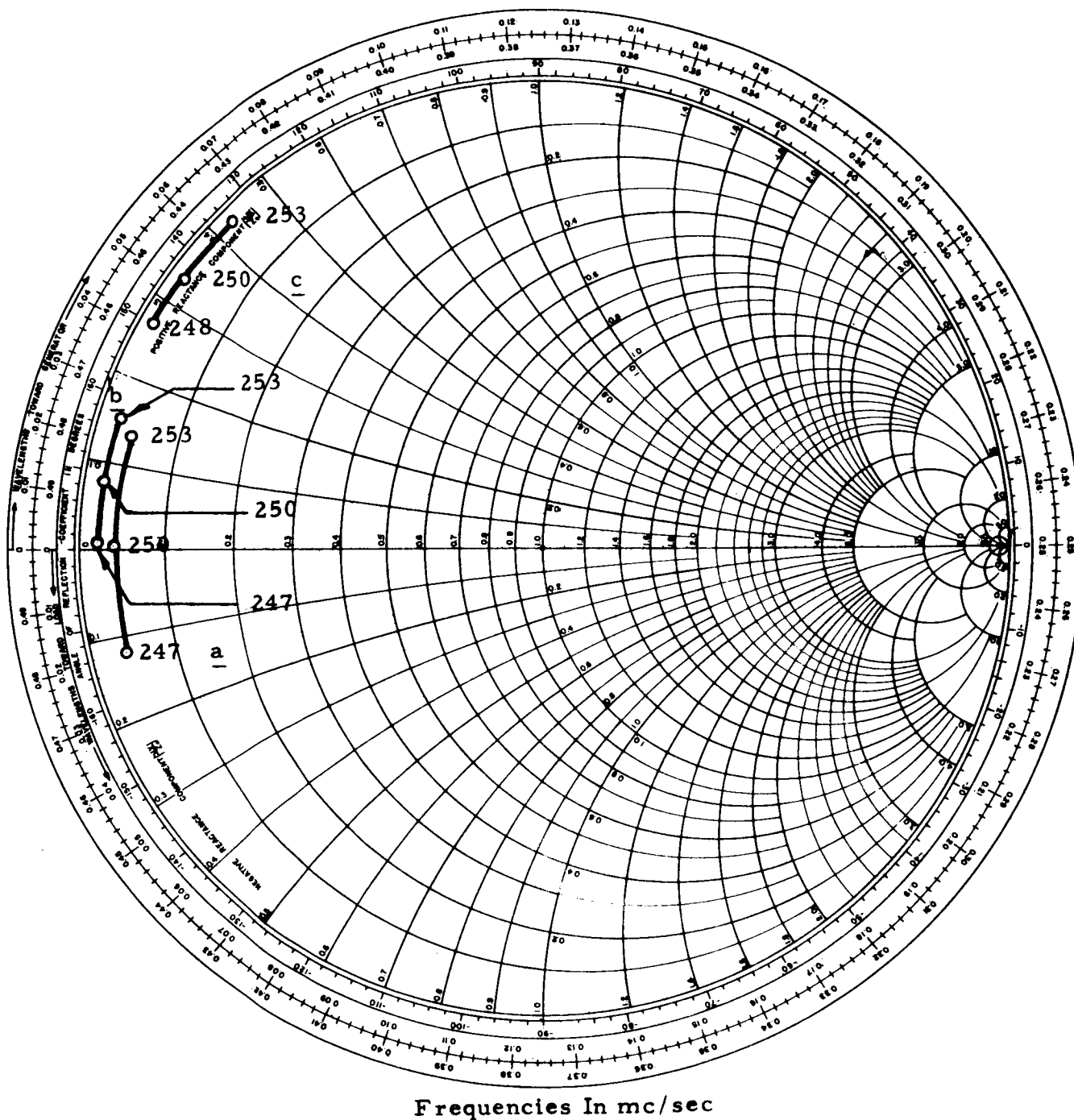


Figure 6 Diagrammatic Representations Of Flat, Round Cavity Antennas With Flush Strap Feed, Excited In Various Ways To Determine Effect Upon Input Impedance



- a. Impedance Of Antenna Of Figure 6 a
- b. Impedance Of Antenna Of Figure 6 b
- c. Impedance Of Antenna Of Figure 6 c

Figure 7 Measured Impedance Of Flat Round Cavity Antennas With Various Flush Feeds Shown In Figure 6

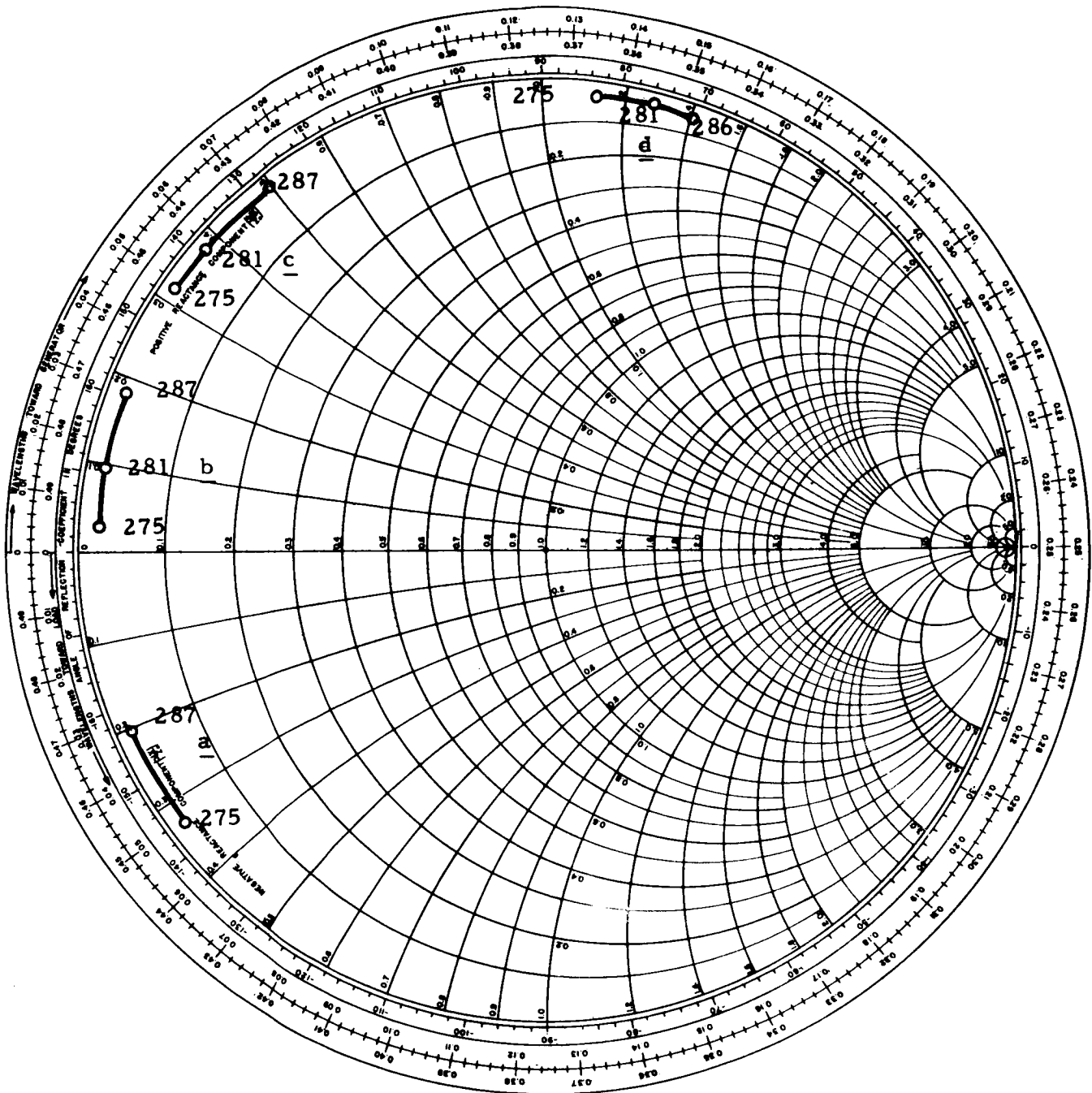
interest. Although the impedance shown by curve a has about twice the resistance level of the other two, its reactance spread is also about double, hence its Q^* is about the same as that of the others, namely, about 140. (The actual calculated values were 147.5, 145 and 130, but the differences between them are comparable to the error in this kind of measurement.) This Q is sufficiently low to provide adequate bandwidth; however, obviously, if a lower Q were obtainable with a different feed the cavity could be made smaller, provided that there were either a similar situation or a margin of safety with respect to efficiency.

Figure 6d shows the best of the other types of flush feeds that were investigated with this cavity. It was similar to that of 6a except that the unfed end was coupled to ground through a

*Throughout this project Q was computed by means of the following expression:

$$Q = \frac{1}{2R} \left(\frac{\sqrt{f_1 f_2}}{f_2 - f_1} \left| X_1 - X_2 \right| + \left| \frac{X_1 + X_2}{2} \right| \right)$$

The Q obtained with this expression is the average for the frequency interval from frequency f_1 to frequency f_2 when R is the average value of the real part of the impedance in the interval and X_1 and X_2 are the reactances at f_1 and f_2 . This expression gives the same result as more familiar but less general expressions. For example, if the device is resonant at the center of the band and the frequency interval is such that the power into the load is 3 db less at the ends of the band than at the middle, the last term will vanish and $(X_1 - X_2)$ will equal $2R$ and Q equals the relative bandwidth. The advantage of the expression used is that it permits the calculation of Q from input impedance regardless of the frequency interval or whether or not the device is resonant in that interval.



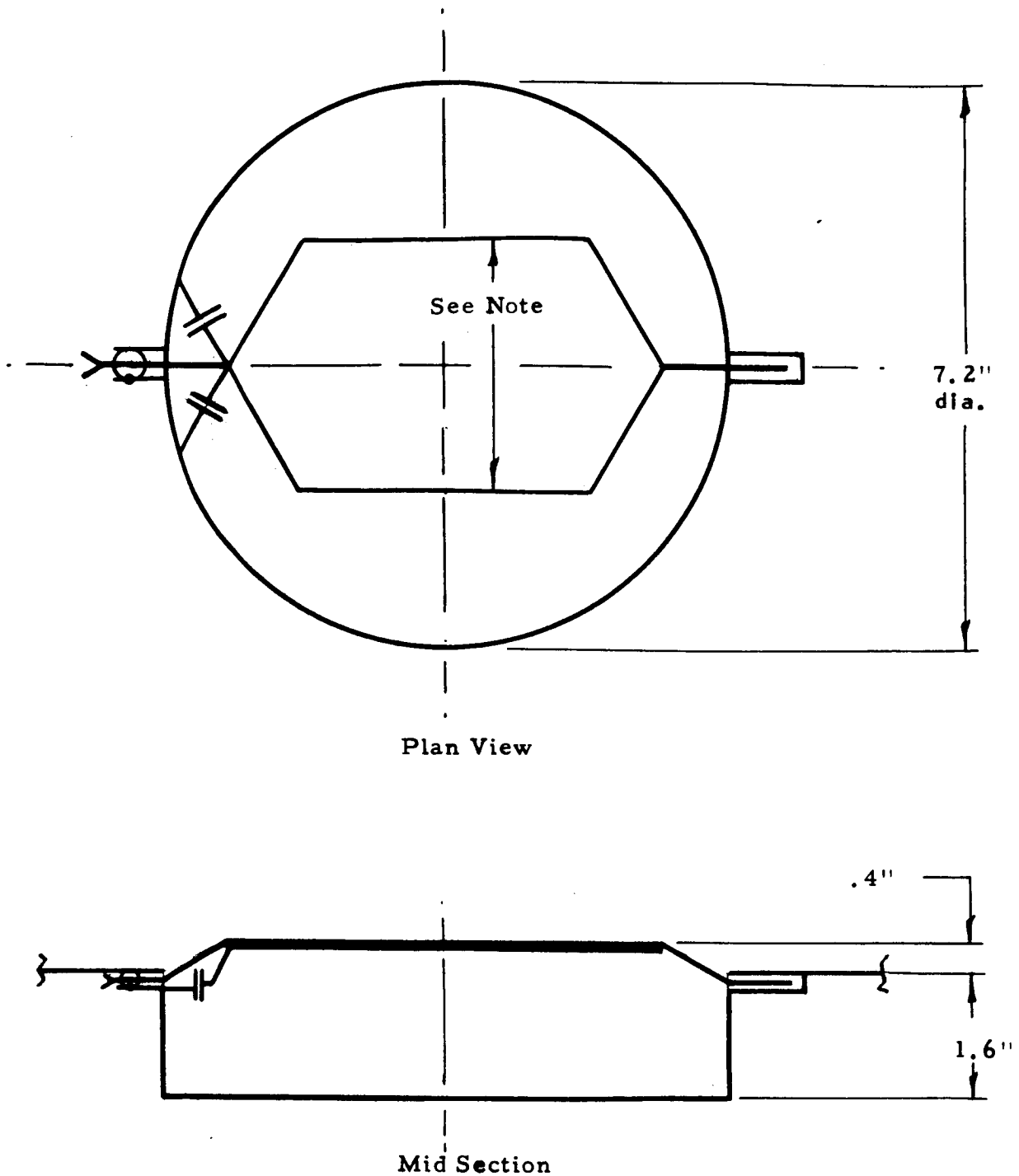
Frequencies In mc/sec.

- a. Terminating Capacitor Length Equals Zero
- b. Terminating Capacitor Length Equals .6"
- c. Terminating Capacitor Length Equals 1.1"
- d. Terminating Capacitor Length Equals 2.8"

Figure 8 Measured Impedances Of Flat Round Cavity Antenna With Flush Feed With Various Terminating Capacitors As Shown In Figure 6d

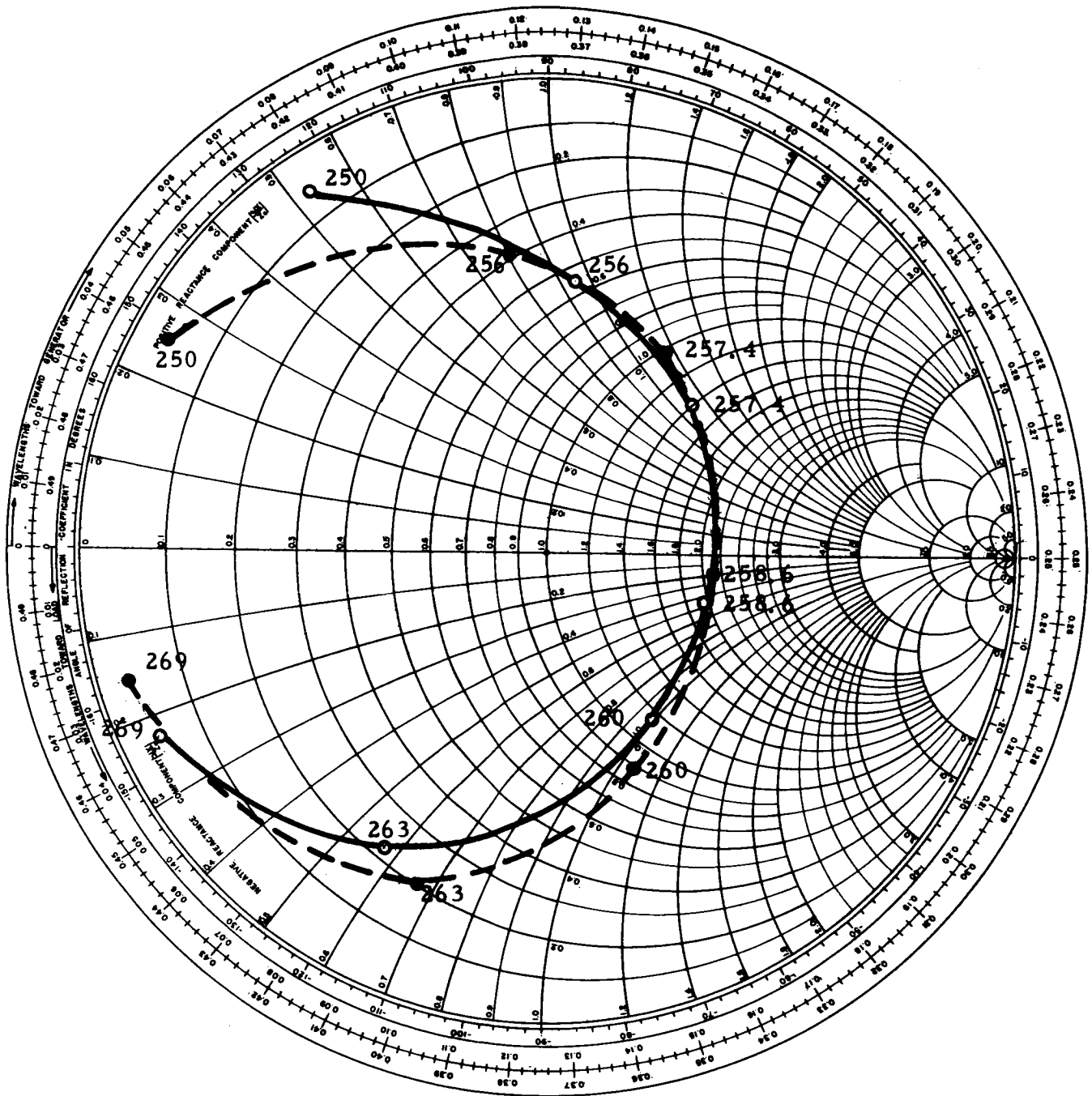
capacitance consisting of a short section of coaxial line. Measurements were made with four values of this capacitance. The results are given on Figure 8. These impedance characteristics are superior to those of the first three antennas in that the Q for each of these was about 100.

The Q of curve 8d was no higher than that of the others. Further, this curve had the interesting property that its reactance was about 60 ohms inductive. Such an antenna would normally be matched by means of a circuit using a capacitance as its first element. It was apparent that it would therefore be possible to elevate the feed strap without the need for metal elements running normal to the surface of the cavity by the use of parallel plate capacitors both to terminate and to feed it. Because this would improve the radiating properties of the antenna, the next step was to test a model (see Figure 9) incorporating what was judged to be the maximum practical amount of elevation (.4") to determine the amount of improvement. The antenna shown in this figure with the 3.2 inches wide radiating strap (which was identical to one of the antennas of Figure 6d, except for the elevation of the strap and the addition of a shunt capacitor) yielded the impedance curve shown by the solid line on Figure 10. The corresponding Q was 80. Because it was intended later to multiplex additional higher frequency antennas into the same cavity, and this would be easier if the radiating strap were narrower, additional data were obtained with



NOTE: Tested with
radiator widths of
1.6" and 3.2".

Figure 9 Diagrammatic Representation Of Flat, Round Cavity Antennas
With Elevated Feed Straps Showing Basic Configuration



Frequencies In mc/sec.

- Antenna With 3.2" Wide Radiator
- Antenna With 1.6" Wide Radiator

Figure 10 Measured Input Impedance Of Flat Round Cavity Antennas With Elevated Feed Straps Shown In Figure 9

the strap of half the width. The resultant impedance characteristic (after the capacitors were adjusted to produce the same resistance level and resonant frequency) is given by the dashed curve on Figure 10. Although it is superficially much the same as the one for the wider strap the Q was found to be higher by about 30%.

Any actual antenna would incorporate a suitable cover (or window). For reasons explained elsewhere in this report it was intended to use fused quartz. The next check made upon this antenna was that of the effect upon the Q of the addition of such a window. It was found to be negligible. The two models tested are shown by Figures 11a and 11b, and the corresponding impedance curves by curves a and b of Figure 12. Next a model incorporating the parallel plate input and load condensers shown in Figure 11c was tested. The resultant impedance characteristic is shown by curve c of Figure 12. (It should be pointed out that the antennas of Figure 11 do not include the shunt capacity across the feed point that was used for the antenna of Figure 9 because without this shunt it is possible to see more clearly the effects of the quartz and of the input capacitance.)

In Figure 13 curves obtained by applying shunt capacitance to the antennas of Figures 11a and 11c are shown. It will be seen that the two curves are very similar. The Q of the uncovered antenna was 78 and that of the covered one 89. It was thus learned that this

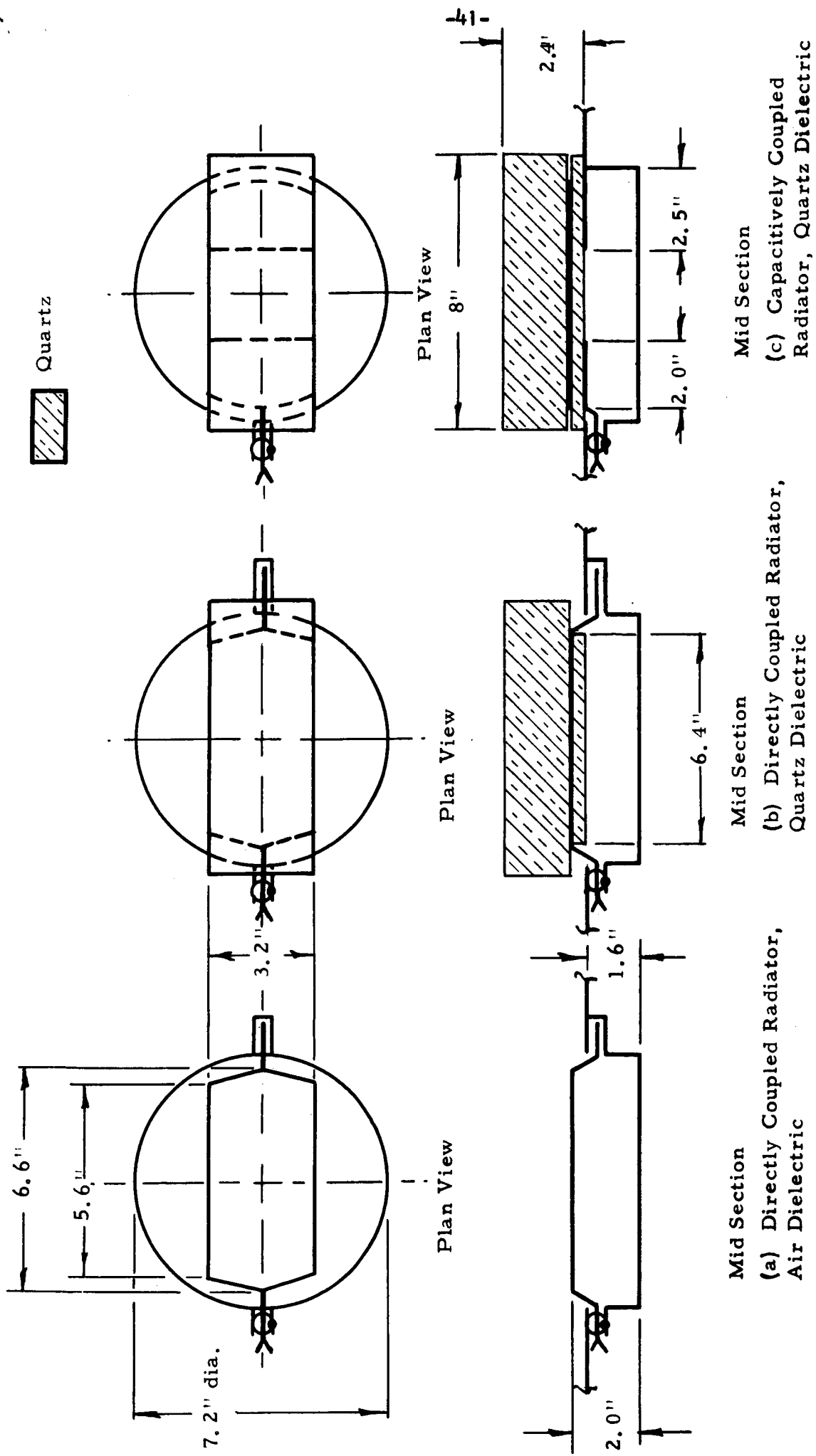
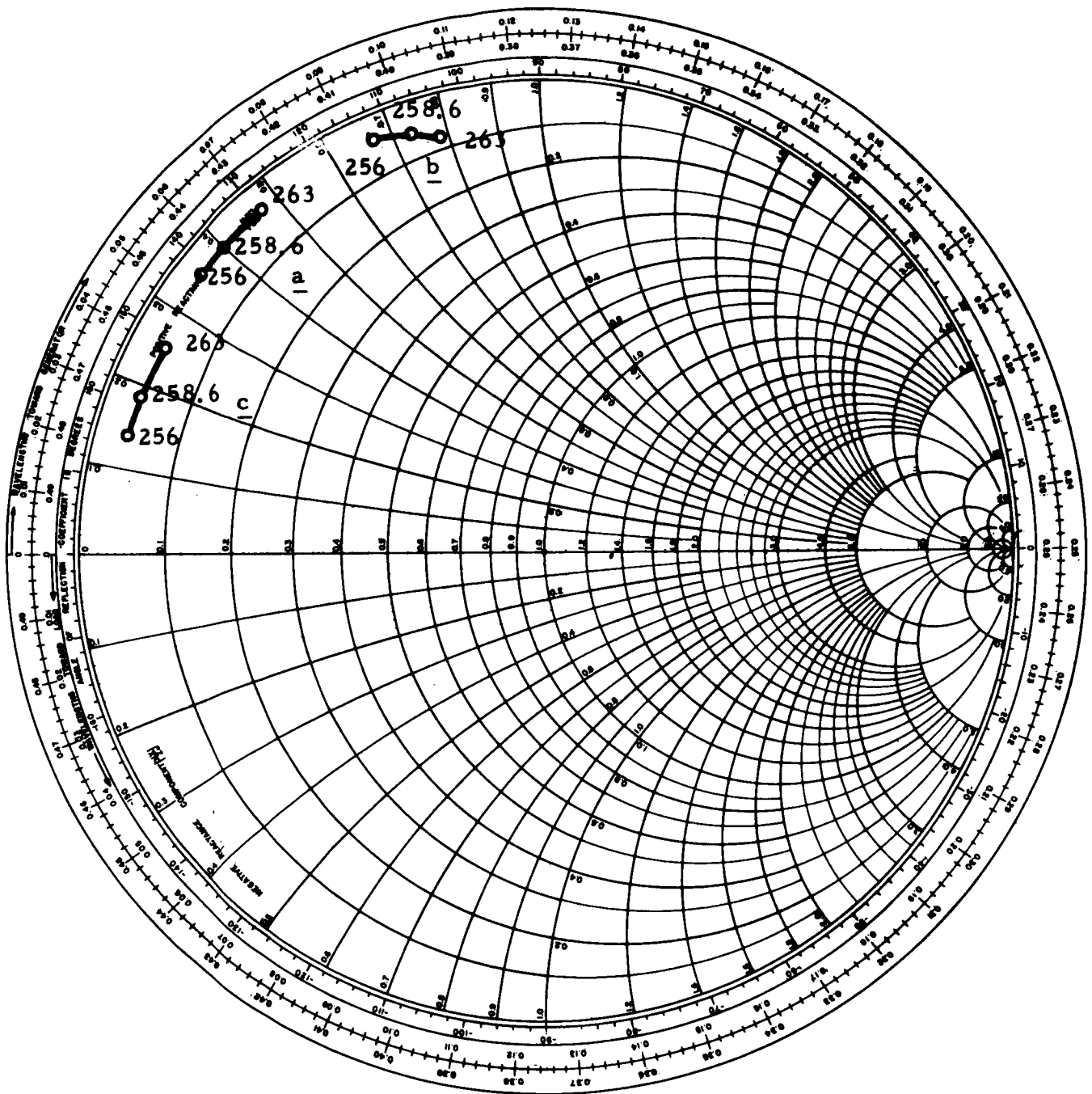


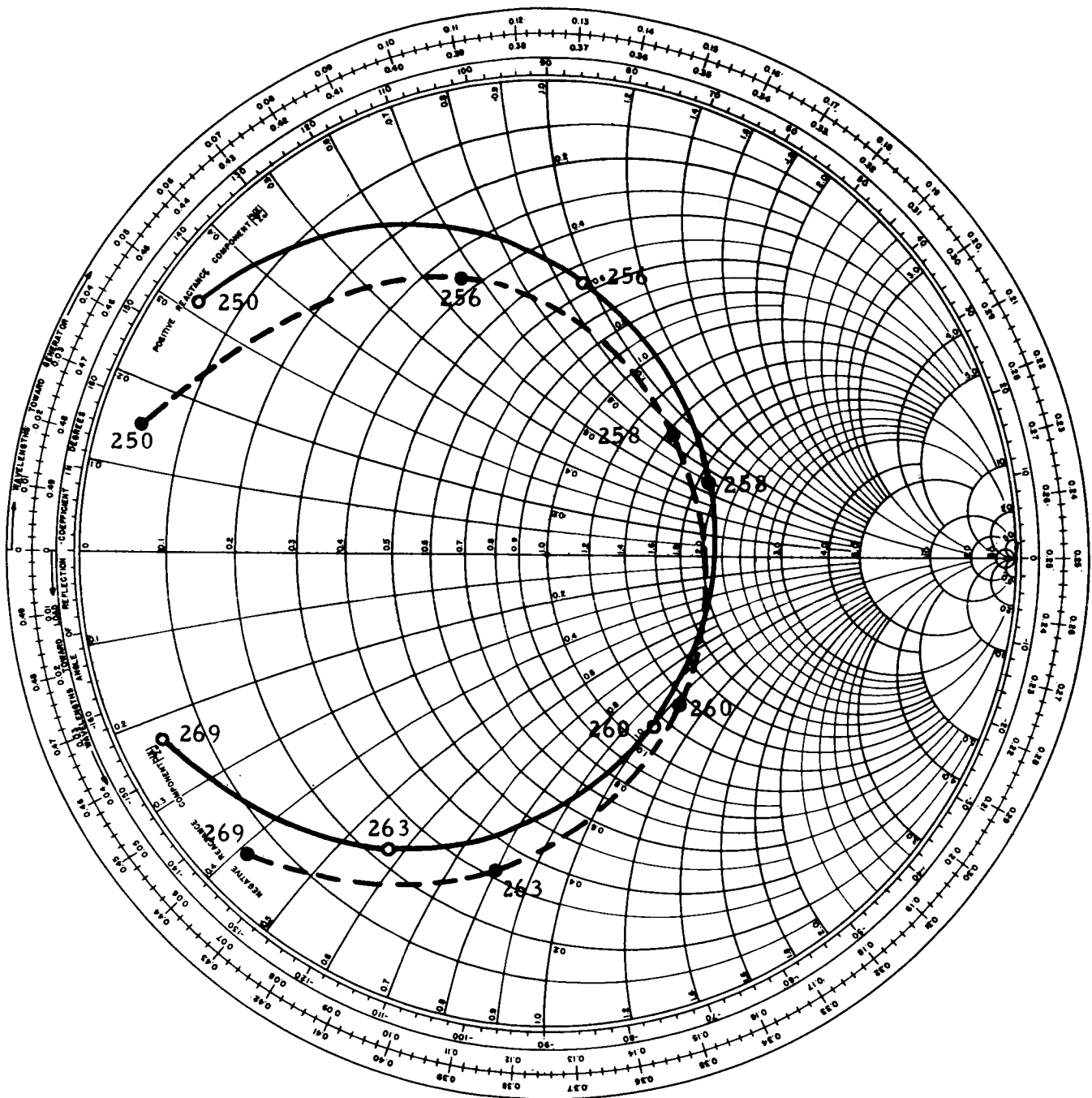
Figure 11 Diagrammatic Representations Of Flat Cavity Antennas Showing Progression To Capacitively Excited Radiator Embedded In Fused Quartz



Frequencies In mc/sec.

- a. Impedance Of Antenna Of Figure 11 a
- b. Impedance Of Antenna Of Figure 11 b
- c. Impedance Of Antenna Of Figure 11 c

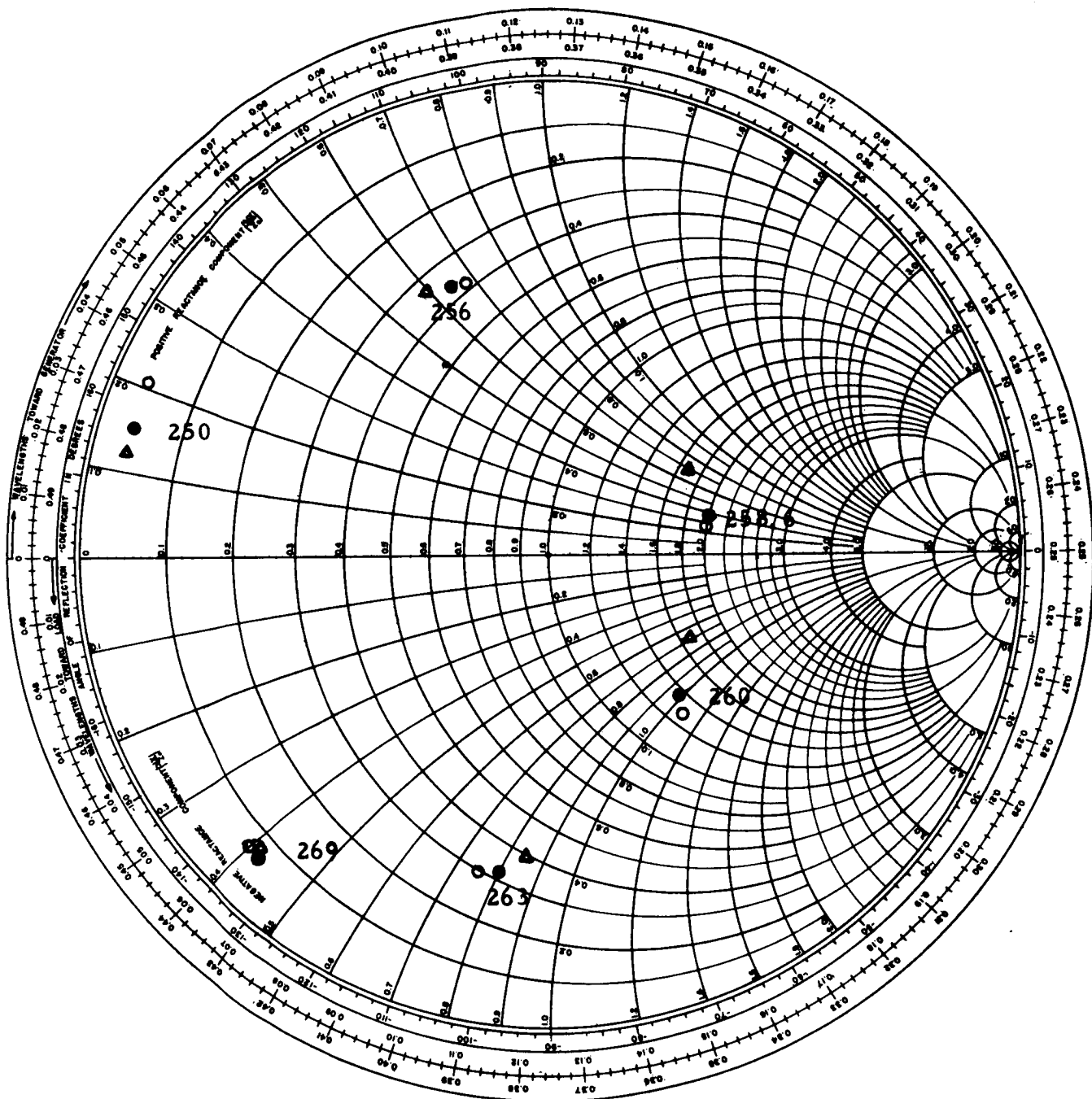
Figure 12 Measured Input Impedances Of Flat Cavity Antennas Shown In Figure 11



Frequencies In mc/sec.

- Antenna With No Quartz
- - -●- - Antenna With Quartz Cover Over Radiator

Figure 13 Measured Input Impedance Of Flat Round Cavity Antennas With Elevated Feed Strap After Matching, Both With And Without Quartz Cover As Shown In Figure 9 (With Strap 3.2" Wide) And Figure 11c (With Shunt Matching Capacitor Added)



Frequencies In mc/sec

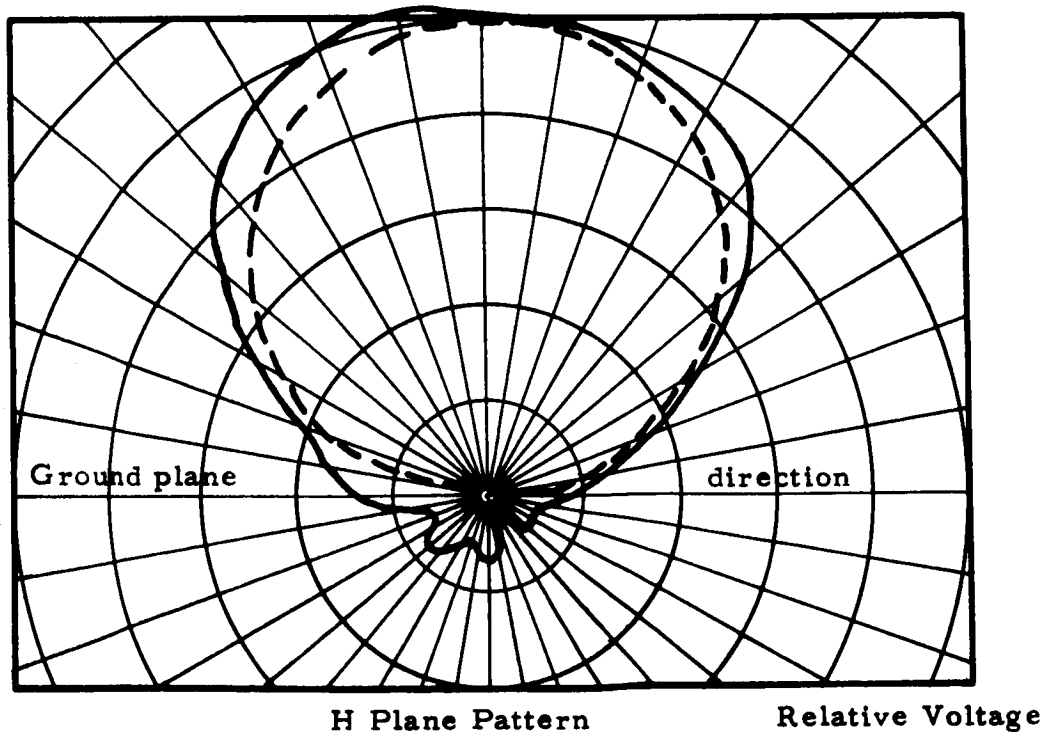
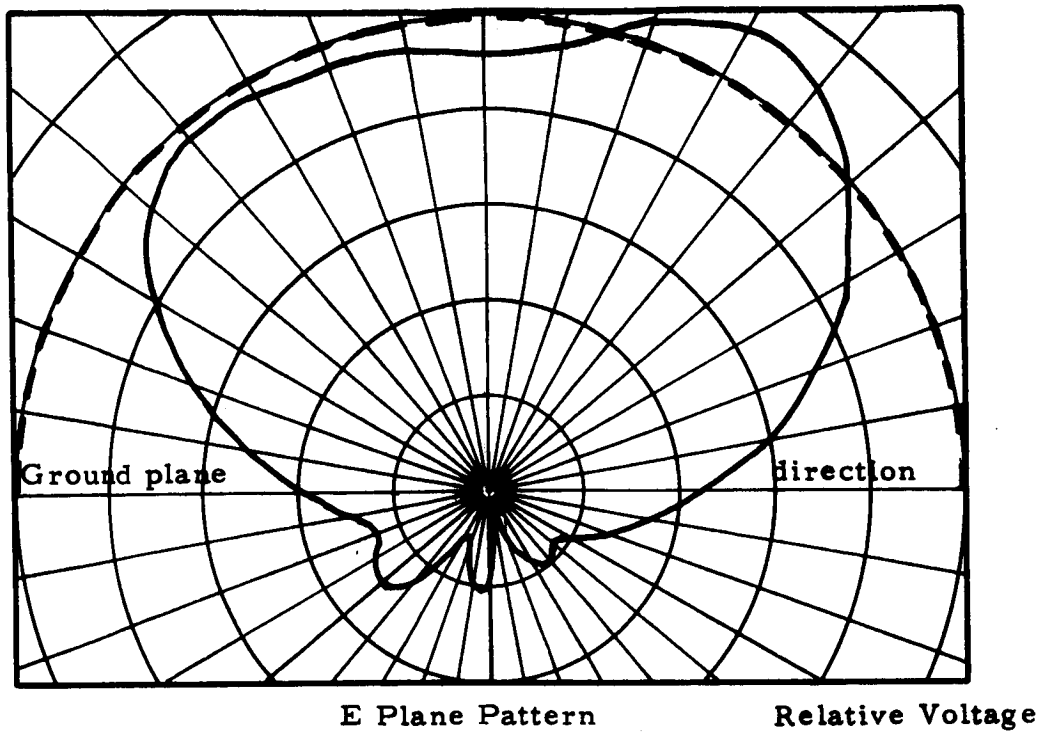
- — Quartz Thickness Equal 2.8"
- — Quartz Thickness Equal 2.4"
- ▲ — Quartz Thickness Equal 2.0"

Figure 14 Measured Input Impedances Of Flat Round Cavity With Elevated Strap Radiator Covered With Three Different Thicknesses Of Quartz

design is, as was hoped, such that bandwidth is not seriously degraded by a dielectric cover. With slight adjustments of the antennas, both curves could have been brought through the center of the Smith Chart. This was evidently a promising design.

The quartz for these measurements was 2.4 inches thick, the dimension which at that time the contractor understood to be the most probable one for the thickness of the ablative cover in the vicinity of the antennas. In order to determine how sensitive an antenna of this type would be to changes in the thickness of this cover the impedance of the antenna was measured with this cover both .4 inch thicker and .4 inch thinner. As these changes were made no adjustments were made to the matching capacitances. It was found that the effect was secondary as shown by Figure 14. This is a strong indication that an antenna of this kind would, if properly designed, be stable.

Next pattern and efficiency measurements were made. The antenna and a $7\frac{1}{2}$ inch diameter half loop antenna were mounted successively in the center of a flat 5 foot square ground plane, and their patterns were measured with equal power being fed into each antenna. The patterns were then integrated to obtain the radiated power in each case. The cavity antenna was found to have an efficiency 80% that of the loop, which in turn was known to have an efficiency of close



Note: Dashed lines show ideal patterns of magnetic dipole antenna on infinite ground plane.

Figure 15 Principal Plane Patterns Of Quartz Covered Cavity Antenna
Shown In Figure 11c, Mounted In Center Of Flat Five Foot
Square Ground Plane, Measured At 258 mc

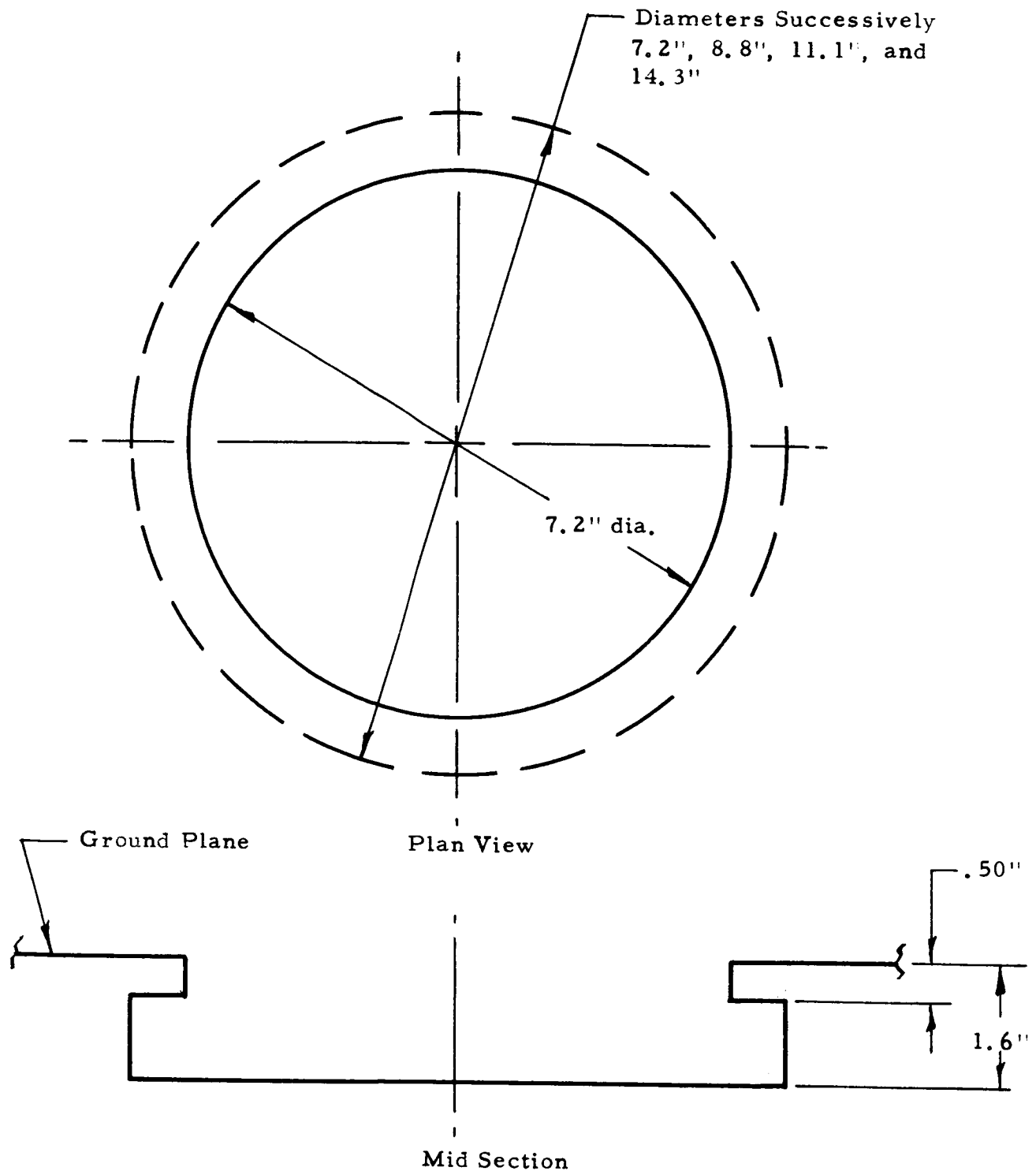


Figure 16 Cavity Shapes Tested To Determine Effect Of Enlarging Diameter Of Backing Cavity While Holding Radiating Aperture And Feed Configuration Constant

to 100%. The patterns were similar. The principal plane patterns of the cavity are shown in Figure 15.

The model tested consisted of copper soldered together and did not necessarily have the same efficiency that one of final construction would have. It was silver plated and remeasured with no perceptible increase of efficiency.

The aperture diameter for the cavities tested was 7.2 inches. Clearly, it would be desirable to decrease this aperture size without loss of efficiency. One possible way of accomplishing this is to make the backing cavity larger than the hole in the skin itself. A series of measurements were then performed to determine how much improvement could be effected by these means. The cavities tested are shown by Figure 16; all had feeds like those of Figure 9. Figure 17 summarizes the results obtained. It shows clearly that this is an inefficient way of utilizing volume. Bandwidth increased only 20% for an approximately three-fold volume increase. With an effective utilization of volume it would have increased by a factor of three.

In order to explore the feasibility of duplexing a second feed for a slightly higher frequency into the cavity the model represented in Figure 18 was built and tested. It was found that when the frequency separation between the two feeds was as small as 10%, that the

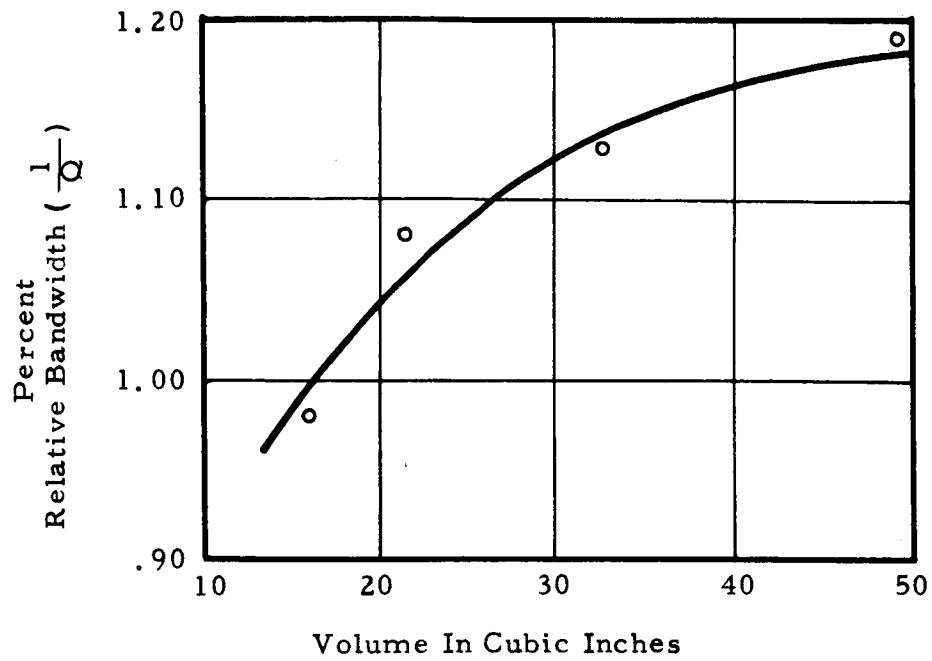


Figure 17 Relative Bandwidth Versus Volume Of Backing Cavity For Antennas Like That Shown In Figure 9 , But With Backing Cavity As Shown In Figure 15

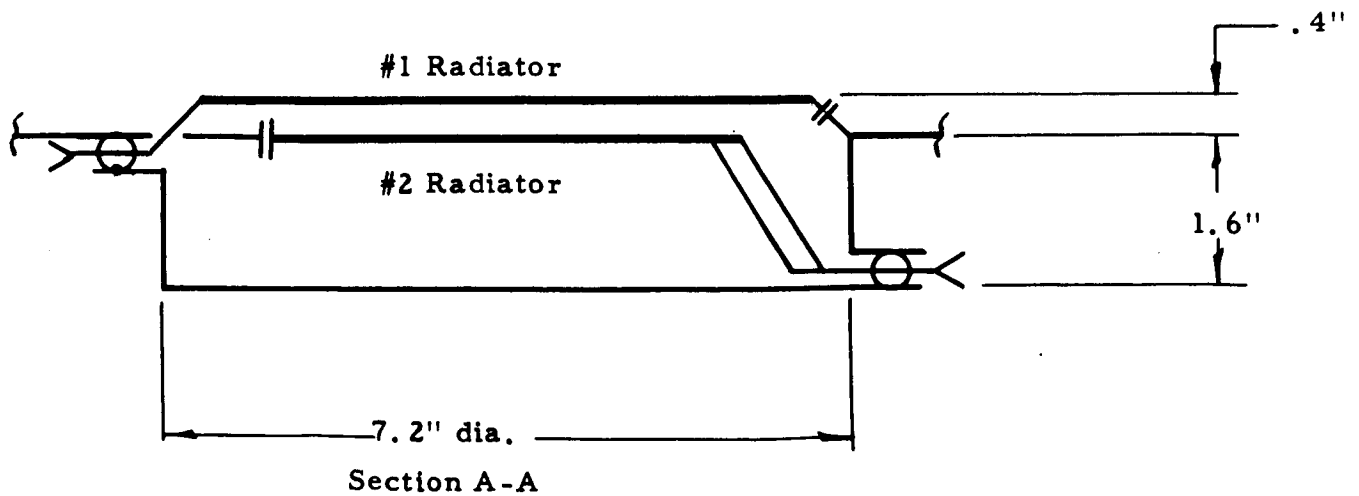
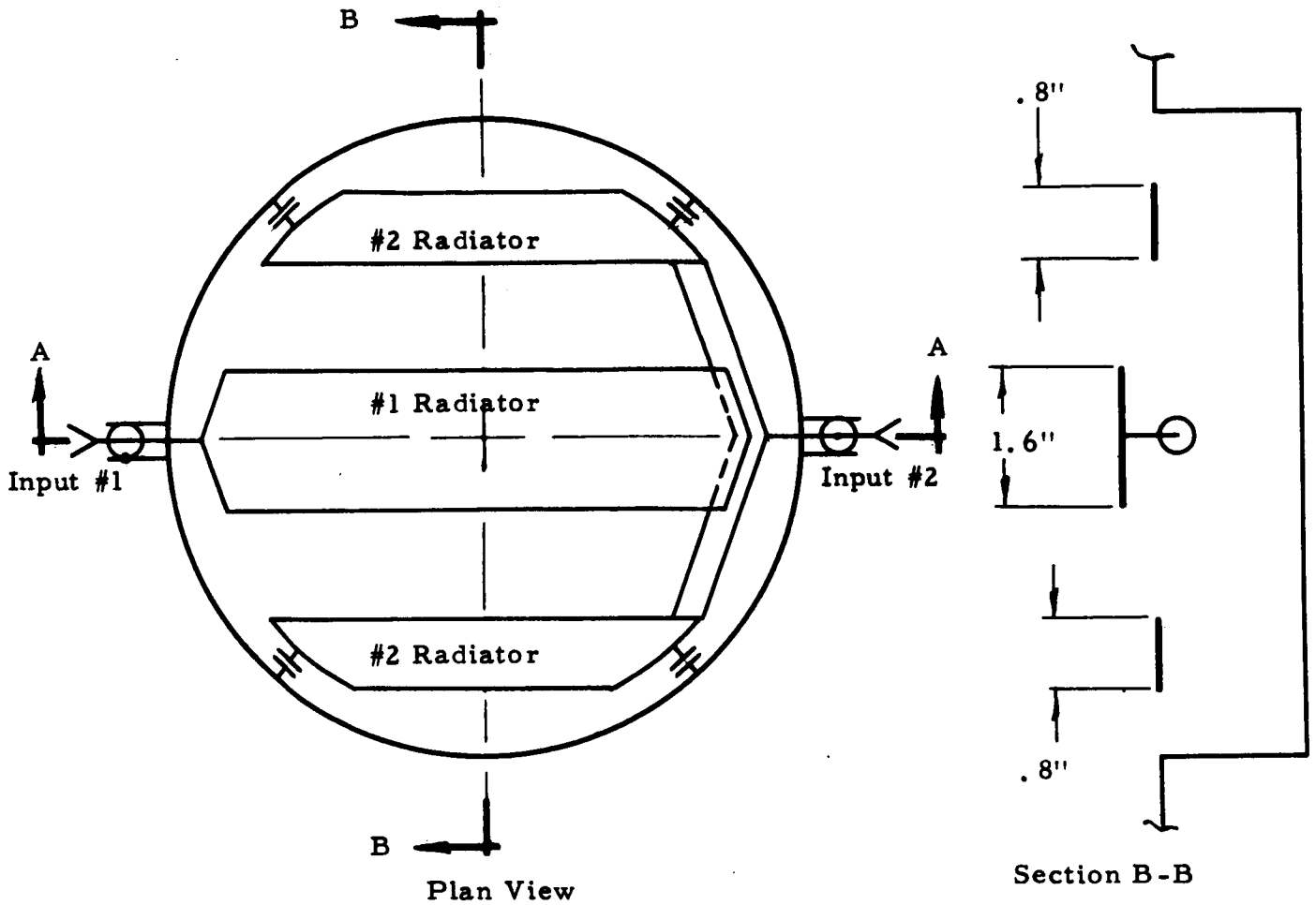


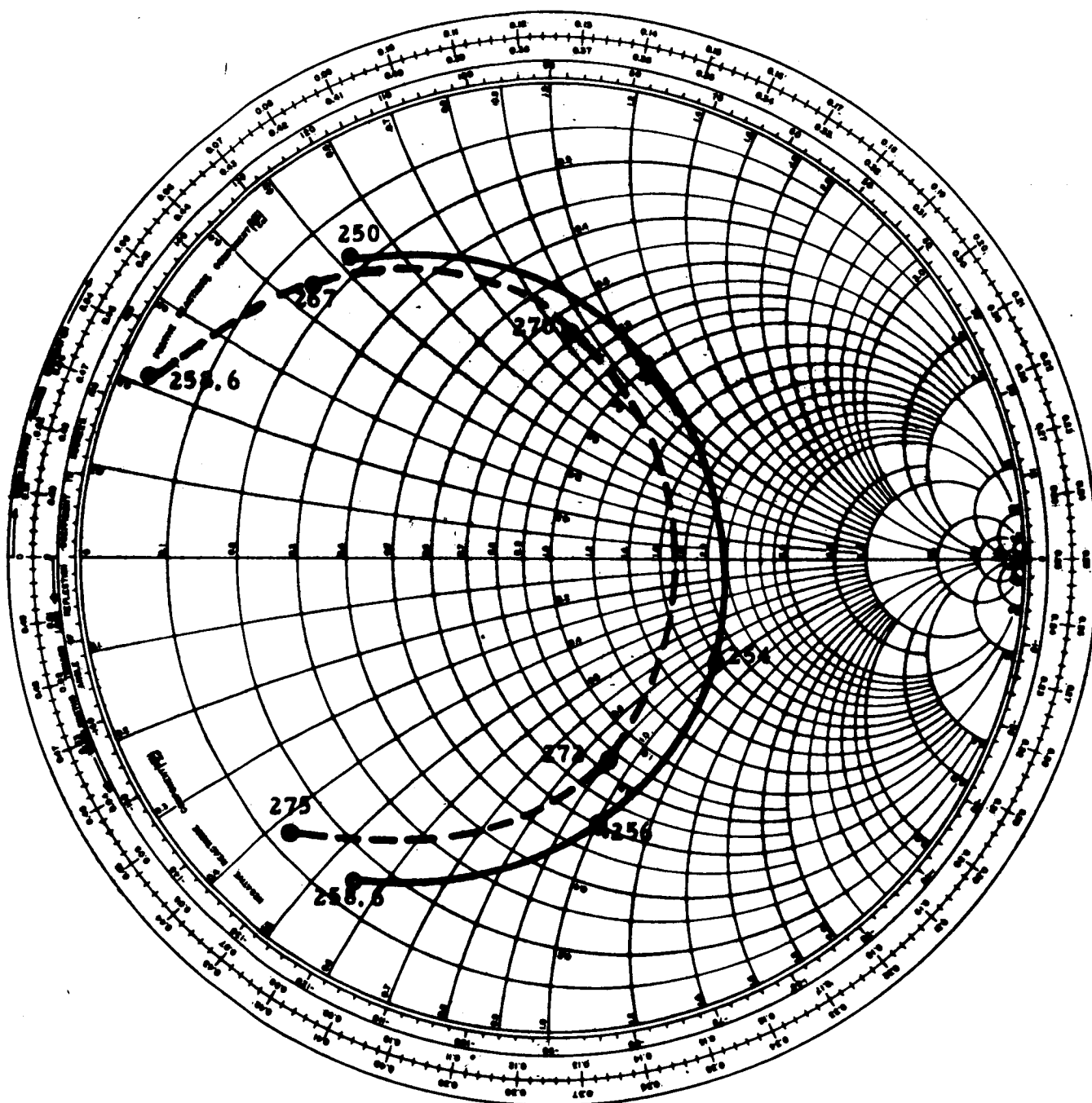
Figure 18 Diagrammatic Representation Of Flat Round Duplexed Cavity Antenna With Radiators For Two Different Frequencies

coupling between feeds was too close for satisfactory operation. This is illustrated by the impedance curves of Figure 19.

For these curves feed number one was adjusted for operation at 259 mc and feed number two was adjusted for operation at 283 mc, in each case the other input being open circuited. As the curves show, the frequency of the operating band of input number one was shifted about 7 megacycles when input number two was short circuited. A similar effect was obtained with measurements made at the other input. Satisfactory operation with such close coupling would not be possible. However, when the frequencies were separated by 28%, satisfactory isolation was obtained. This can be seen from the data of Figures 20 and 21.

Experiments were next performed to determine the feasibility of installing microwave feeds into the same cavity. For this purpose, a model incorporating a VHF radiator and an S-band slot was constructed as indicated by the sketch of Figure 22.

From this sketch it can be noted that the S-band slot is in a small ground plane that covers half the open portion of the aperture on one side of the VHF strap radiator and that this ground plane is coupled by a quarter wave open ended choke joint to the adjacent portions of the flange of the principal cavity. The S-band feed was



Frequencies In mc/sec.

—○—○— Input #2 Open Circuited
 -●- -●- - Input #2 Short Circuited

Figure 19 Measured Input Impedance At Input Number 1 Of Duplexed Antenna Like That Shown In Figure 18 But With Radiator Number 1 Matched At 259 mc And Radiator Number 2 Matched At 283 mc

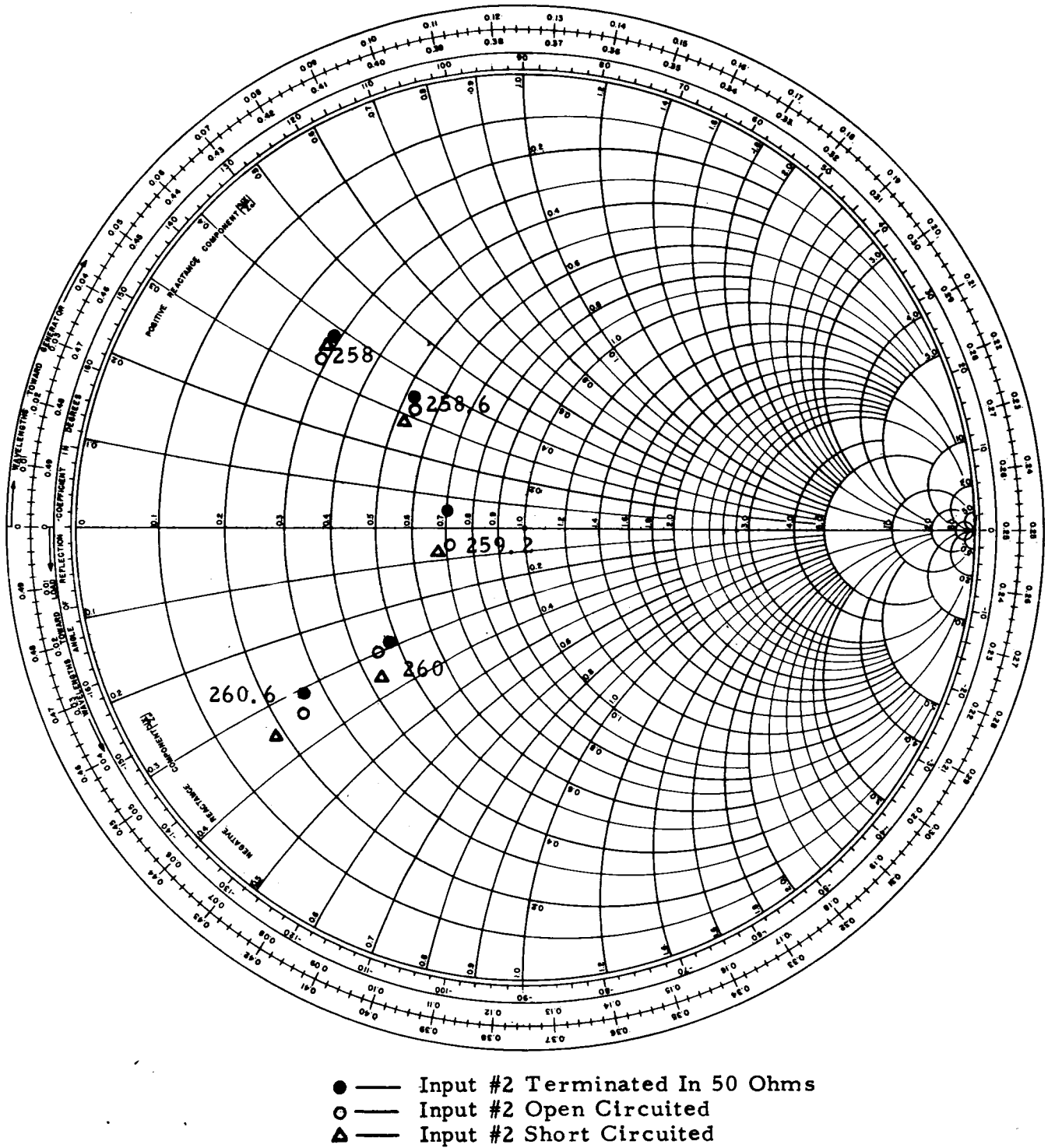


Figure 20 Measured Input Impedance Of Input Number 1 Of Duplexed Antenna Shown In Figure 18 For Various Terminations Of Input Number 2.

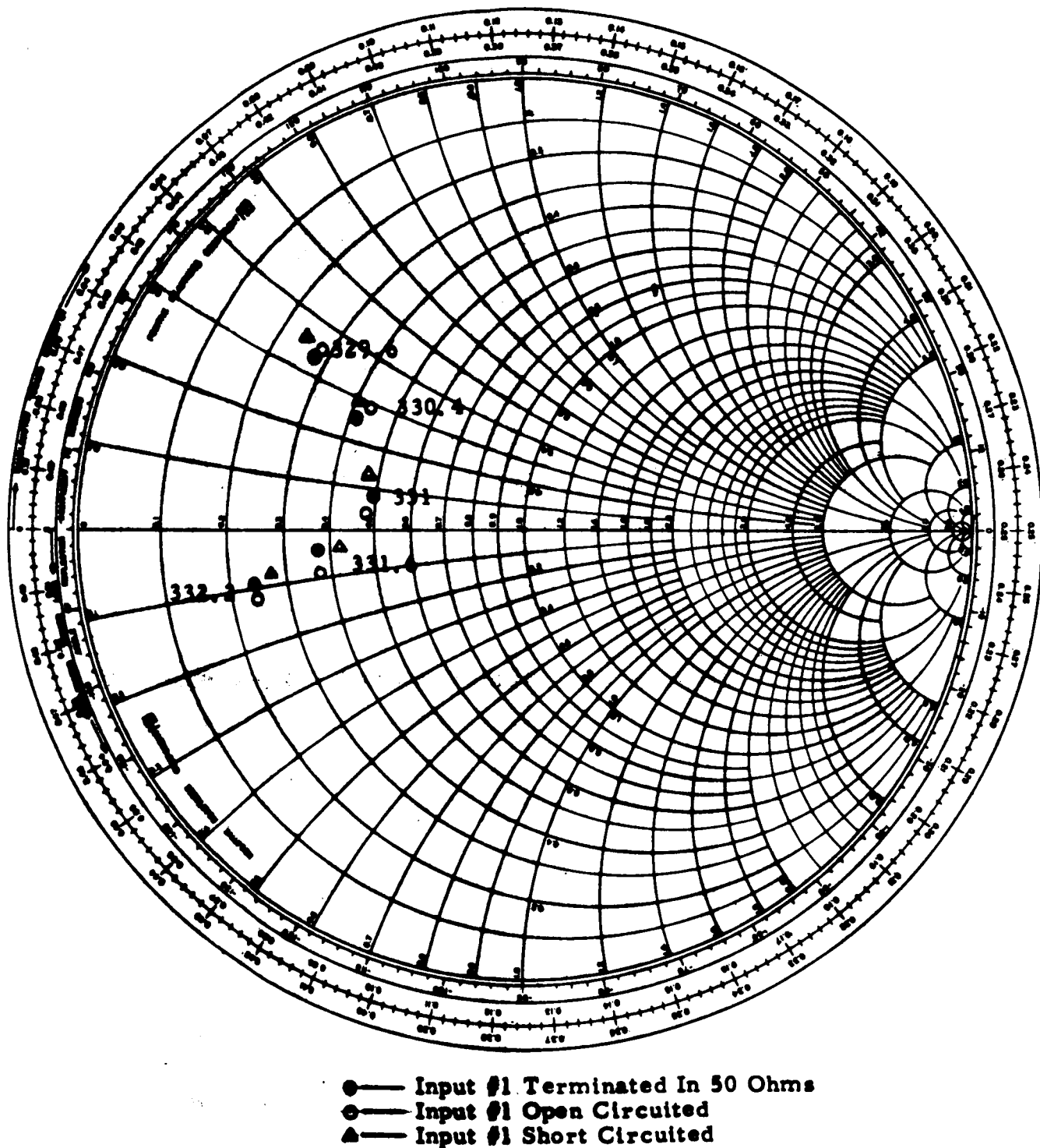


Figure 21 Measured Input Impedance Of Input Number 2 Of Duplexed Antenna Shown In Figure 18 For Various Terminations Of Input Number 1.

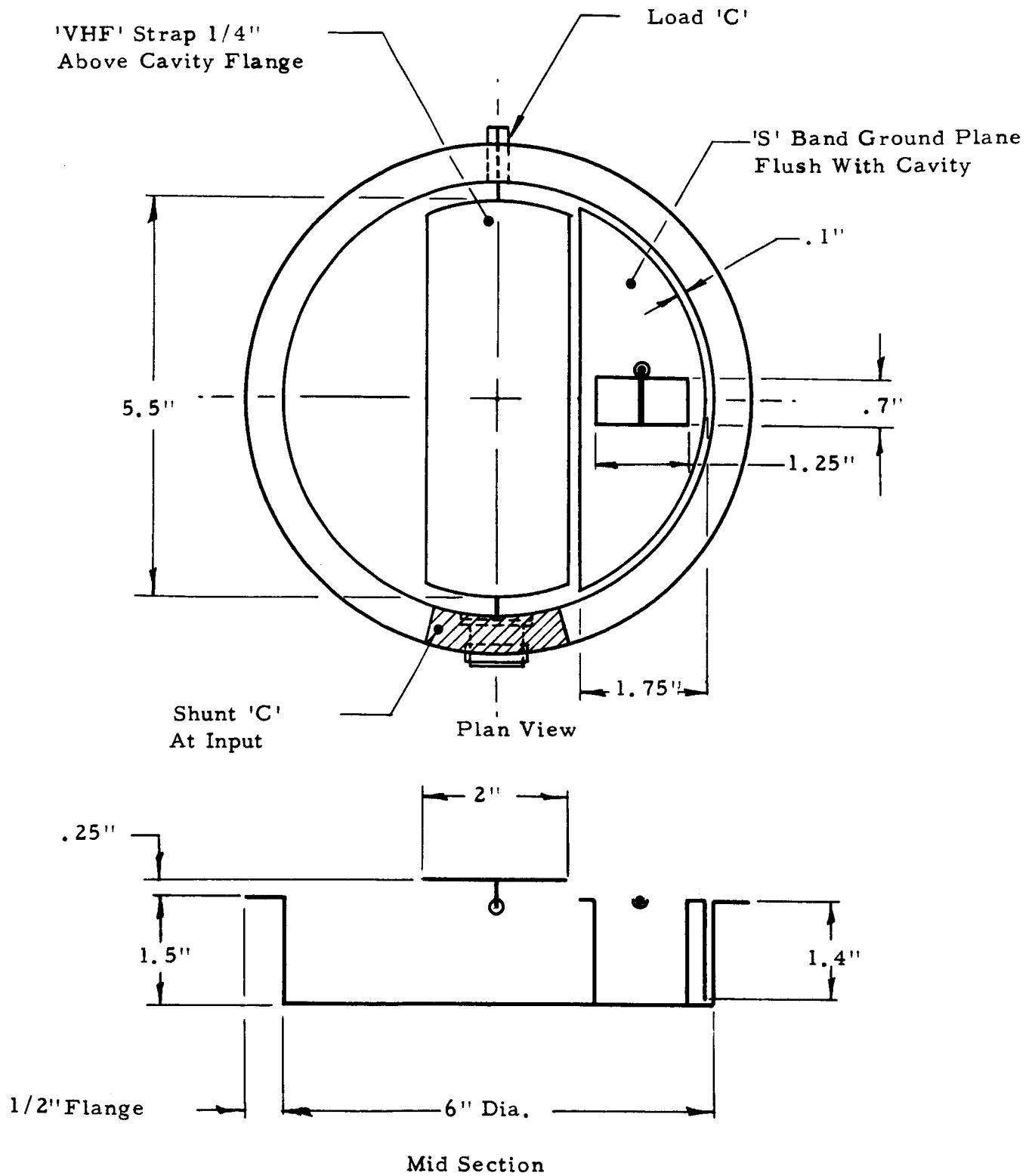


Figure 22 Sketch Of Duplexed 'VHF' And 'S' Band Cavity Antenna

run up from the back wall of the cavity to the small ground plane. With this antenna (which utilized a cavity which was slightly smaller than those previously described) there were two principal objectives. One was to find out if the performance of the VHF antenna was deteriorated by the presence of the S-band antenna. The other was to see if the S-band antenna had E plane patterns like those normally obtained from a slot radiator. There was no need to check the H plane patterns because it could be seen from the geometry that they would be less affected than the E plane, and that if the patterns were satisfactory in the E plane, they would also be in the H plane.

It was found that the VHF performance was not different from that which previous work had indicated should be obtained from a cavity of the size selected. It was also found that the E plane pattern at S-band (2200 mc) were normal. Figure 23 shows the pattern obtained with the antenna installed in a 30 inch diameter ground plane. Both the general shape and the ripples are typical of a slot in a ground plane of this size.

From these data it was judged that a C-band beacon antenna could be designed along conventional lines and similarly installed in a small choke connected ground plane.

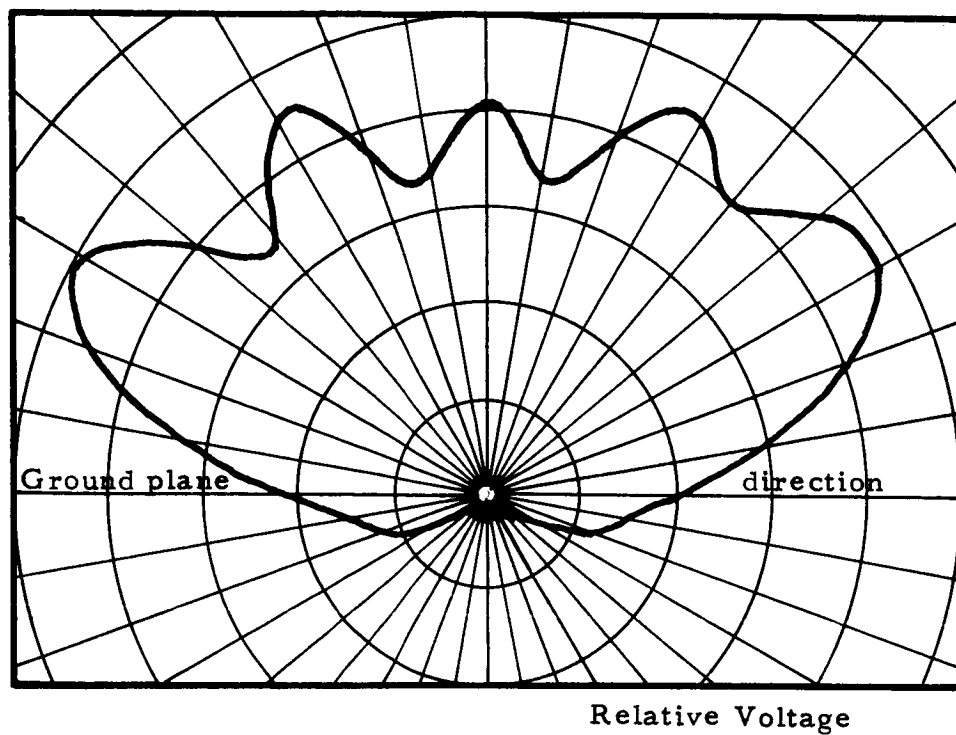


Figure 23 Radiation Pattern (E Plane) Of 'S' Band Portion Of Duplexed Antenna Shown In Figure 22 In A 30 Inch Circular Ground Plane

On the basis of the work summarized in the foregoing discussion, as well as the concurrent thermal design study that was being conducted and that is discussed in Section 3.2, it was concluded that the necessary design information had been obtained to proceed with the preliminary design of complete antennas. These were planned to consist of four basic types. Each was to have a central elevated strap feed of the general design shown by Figure 11c. These feeds were to be adjusted for operation at the four lowest operating frequencies: 237.8 mc, 243.0 mc, 247.3 mc and 259.7 mc. In addition, each cavity was to have an additional radiator duplexed into it. The 237.8 mc cavity was to have a second feed operating at 296.8 mc. The 243.0 mc cavity was to contain a second feed operating at 450 mc. The necessary S and C-band antennas were to be duplexed into the 247.3 and 259.7 mc antennas.

A number of study layouts was made. One of these, entitled "Study Layout of Cavity Antenna" is shown in Figure 24. The diameter of the antenna is not given in the sketch because the minimum possible had not yet been determined and was dependent upon the results of further work. However, it was anticipated that the apertures would be in the neighborhood of 7 inches as was the case with the models described and that the overall diameters including flanges would be at least an inch greater than this.

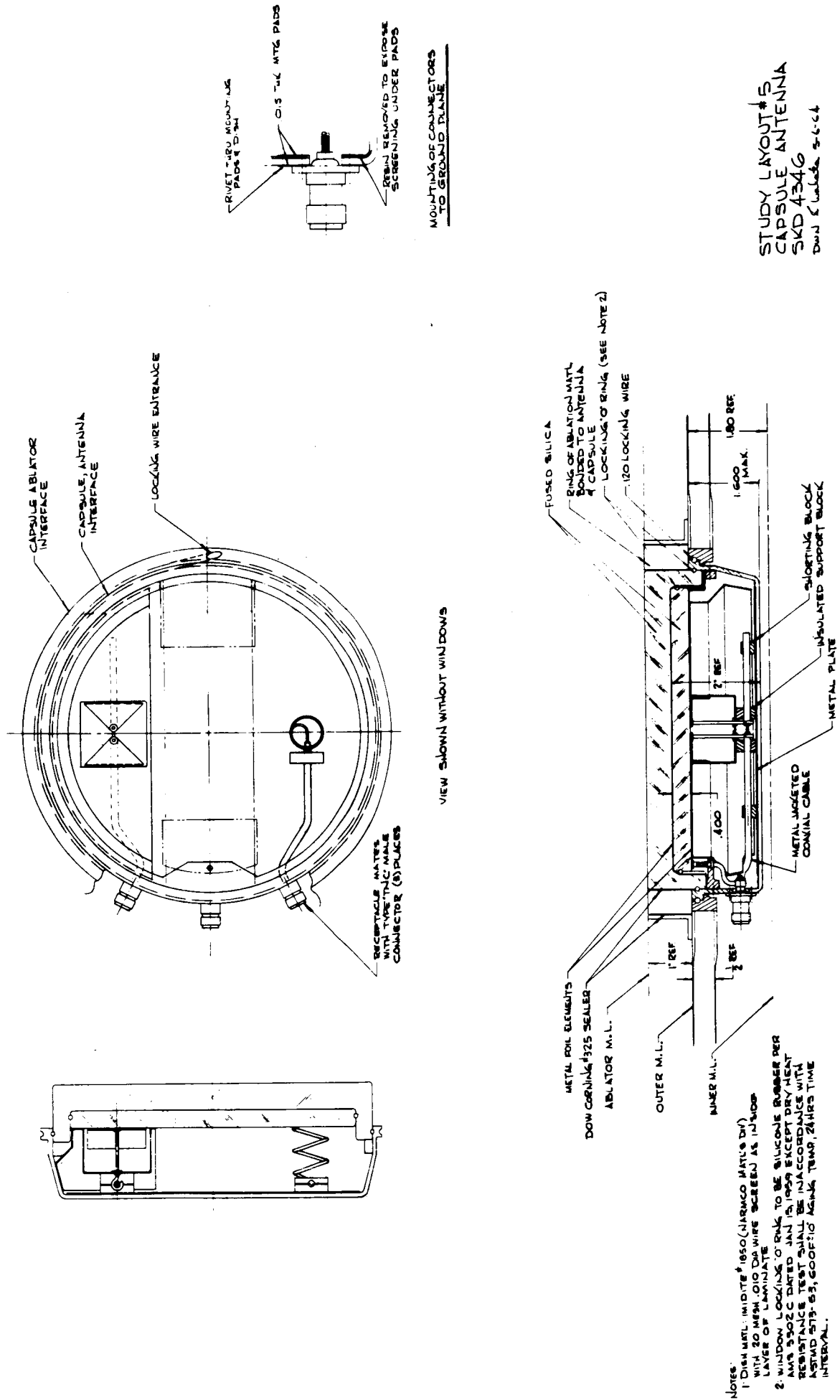
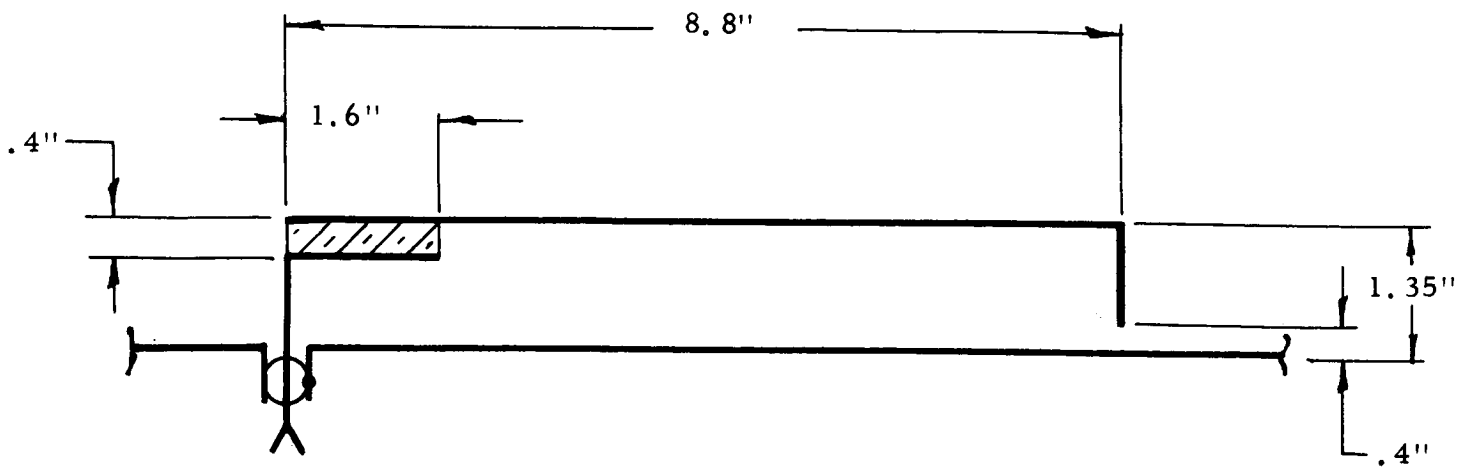


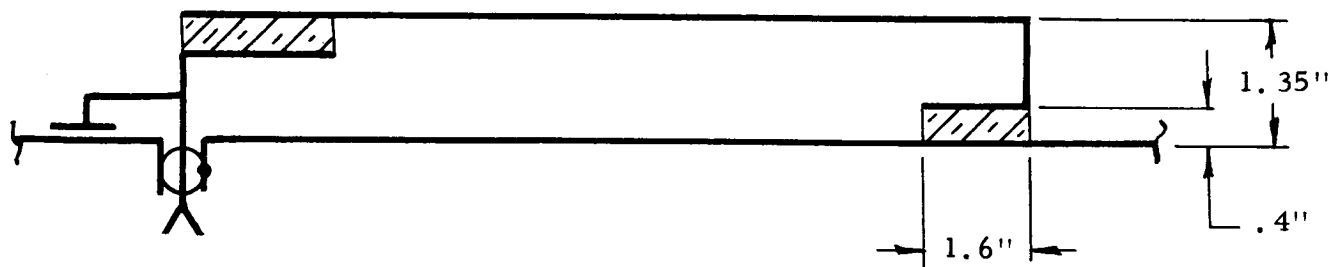
Figure 24 Study Layout Of Cavity Antenna

At this point it was apparent that the antennas being contemplated, although very small for cavity antennas, were nevertheless so large as to present a formidable and in fact, perhaps, even unacceptable installed weight penalty. Accordingly, the design approach was re-examined. By this time, as a result of the thermal design study substantial information on the temperatures within a quartz insert in the ablative cover were available. From these it could be seen that most and possibly all of the quartz would remain intact during entry and further that the temperatures even slightly below the surface were below the melting points of metals suitable for antenna construction. Further, it was clear from these calculations that if done appropriately small amounts of metal running in the direction of the heat flow could be embedded in the quartz without either jeopardizing the thermal protection of the capsule or necessitating massive heat sinks. From the electrical work done with the cavity with the elevated strap it had been learned that it was possible to excite a radiator embedded in the quartz without making direct connection with it and yet achieve essentially as effective radiation as could be obtained with a similarly located radiator conductively excited and in free space.

In view of these facts, a program was started to investigate the properties of radiators for installation in the ablative covering itself.



(a) Unmatched

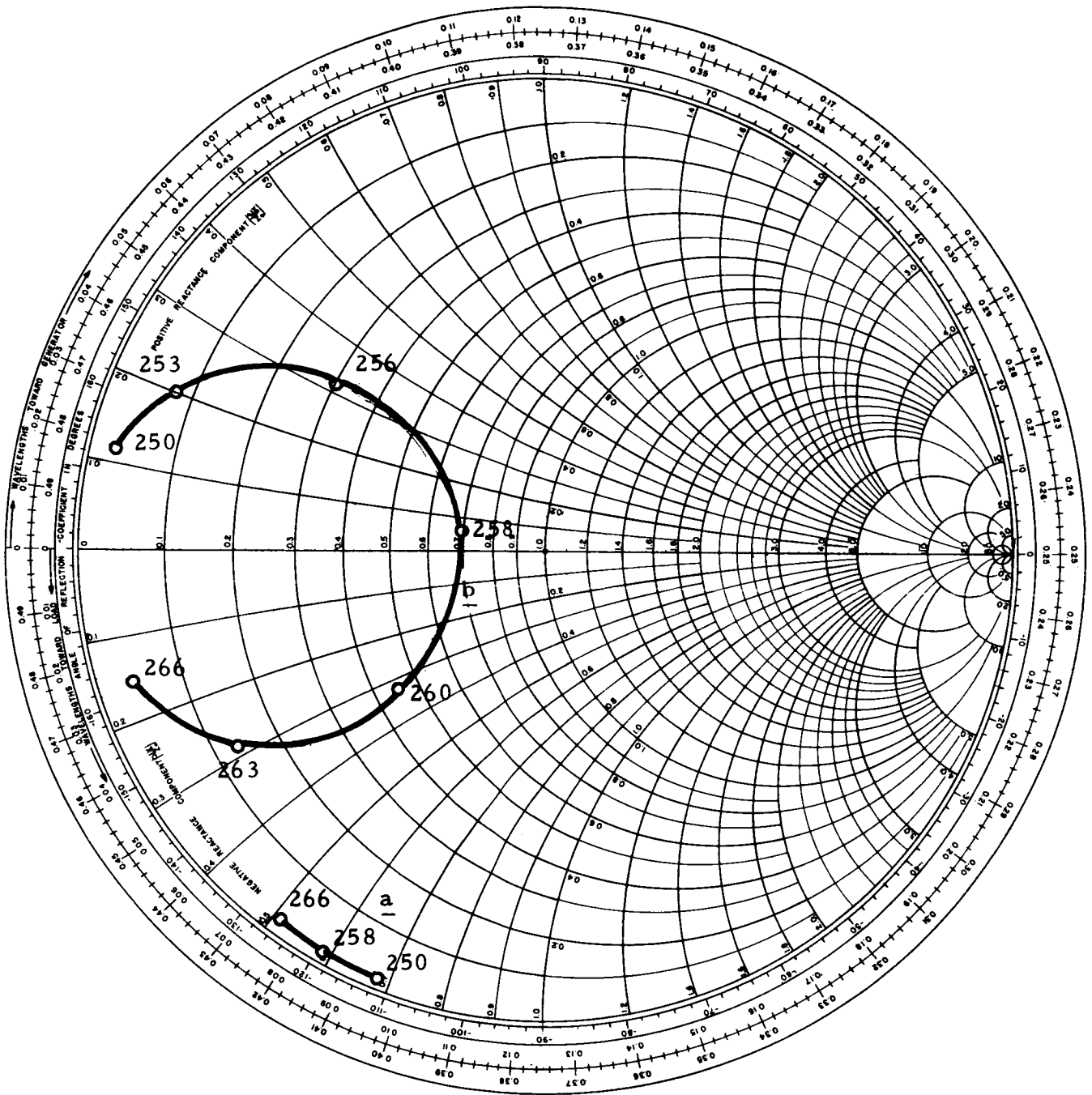


(b) Matched

Note: All straps 3.2" wide.

Figure 25 Diagramatic Representations Of Strap Radiators

As a starting point, the antenna shown by Figure 25a was built and tested. Its impedance was found to have the characteristic shown by curve a of Figure 26. The Q of this curve was reasonably low, and it was evident from the previous work that with the addition of a terminating capacitor that the curve could be displaced clockwise to a position suitable for matching with a shunt capacitor. Figure 25b illustrates these changes and curve b of Figure 26 shows the impedance characteristic which they yielded. This curve showed the antenna to have a Q of 61. The radiation patterns of this antenna mounted on a flat five foot diameter ground plane were then measured and compared for gain and shape with those of the half-loop antenna previously used. The patterns were essentially the same for both, and also like those previously obtained with the cavity. The principal plane patterns are shown in Figure 27. This result was expected but not counted upon. Because of the geometry of the antenna, it was possible that the radiation from the flat strap itself might so exceed the radiation from the rods which are part of the structure that the radiation pattern would have been like that of a small dipole parallel to a ground plane. In that case there would have been complete nulls in the E plane pattern in the directions of the ground plane (i.e., plus and minus 90 degrees) and the patterns would have been too directional for the intended application.



Frequencies In mc/sec.

- a. Impedance Of Antenna Before Matching
- b. Impedance Of Antenna After Matching

Figure 26 Measured Impedances Of Strap Radiators Shown In Figure 25

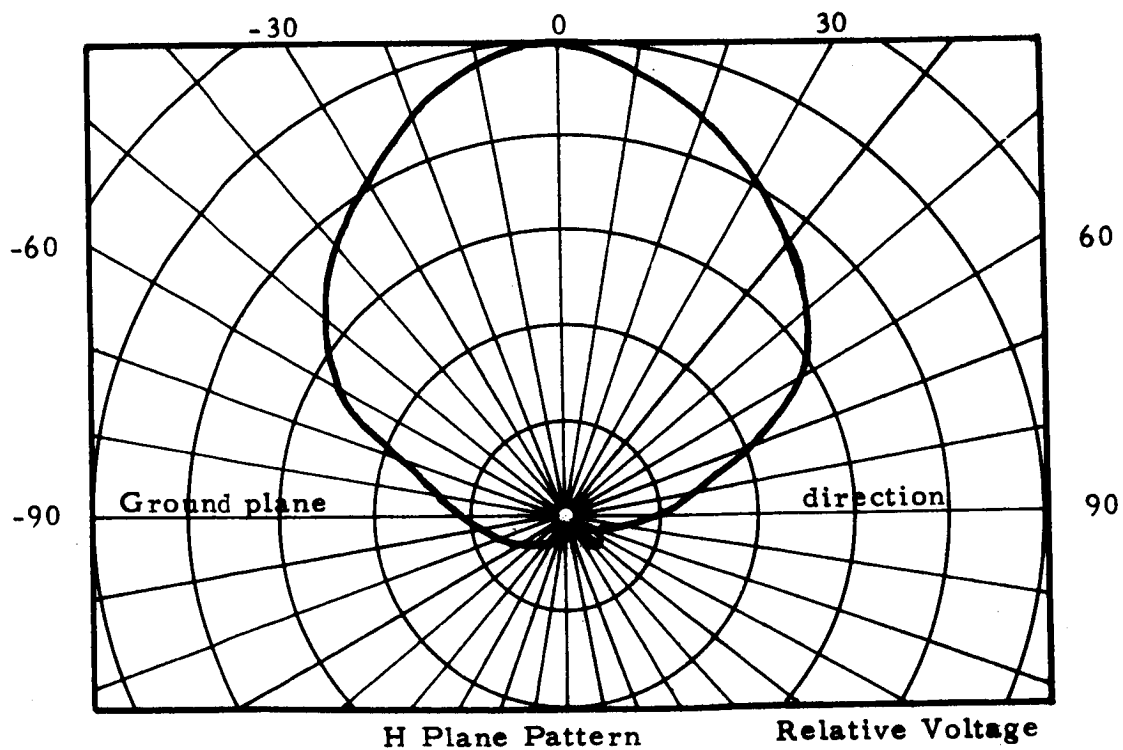
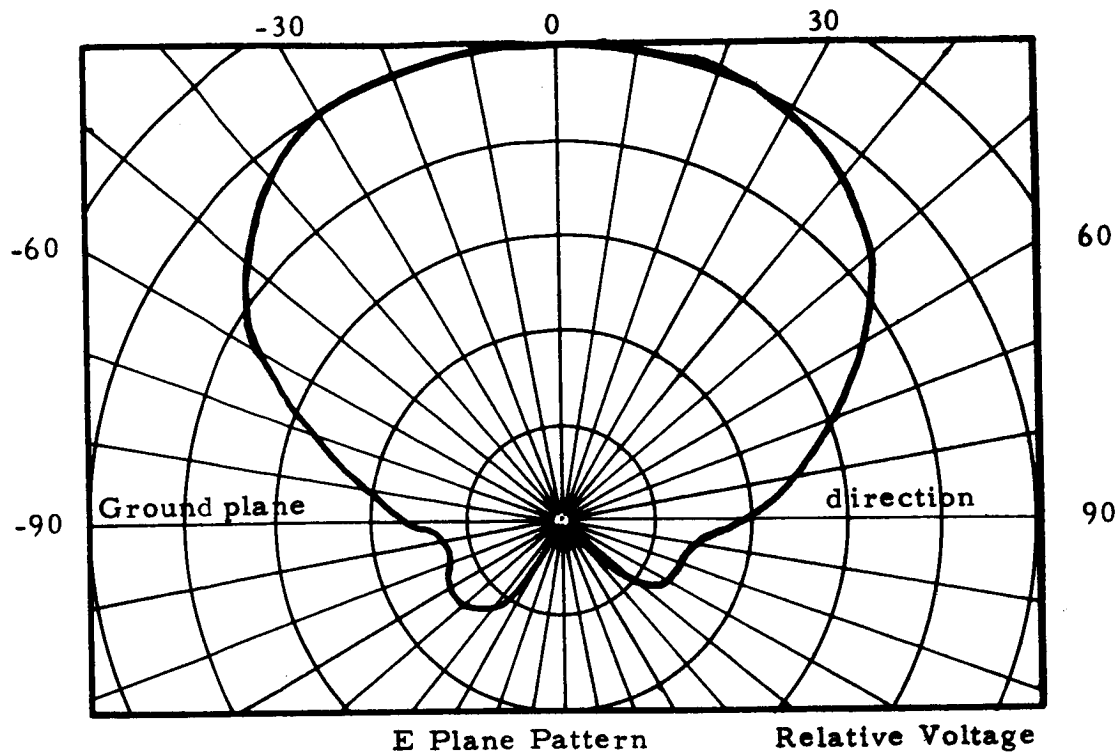


Figure 27 **Principal Plane Patterns Of Strap Antenna Shown In Figure 25b**
Mounted In Center Of Flat Five Foot Diameter Ground Plane
Measured At 258 mc

The gain data showed this antenna to be about 10% more efficient than the loop. This was seen as a measurement error, but nevertheless a definite indication of high efficiency. Rather than take time to repeat the measurements it was decided to proceed with the development and to check the efficiency of the next model as early as feasible.

A model of the antenna in which the elements were embedded in fused quartz was then constructed and adjusted for operation at 258 mc. A sketch of this antenna is given in Figure 28 from which it can be seen that the metal structure of the antenna consists of four flat sheets of metal which lie at right angles to the direction of heat flow, and therefore will not affect the thermal flow and two rod-shaped conductors running in the direction of heat flow, but that neither of these extends to the outer surface of the antenna and that the longer length is only about six tenths the thickness of the ablative cover.

Figure 29 shows the impedance characteristic of this antenna. It is of course quite similar to that of the cavity antennas. The Q calculated from it is 107, considerably higher than the 61 of the previous antenna that was not embedded in the quartz. The major portion of this increase is to be attributed to size reduction. The Q of 61 was lower than required; therefore, the radiator was

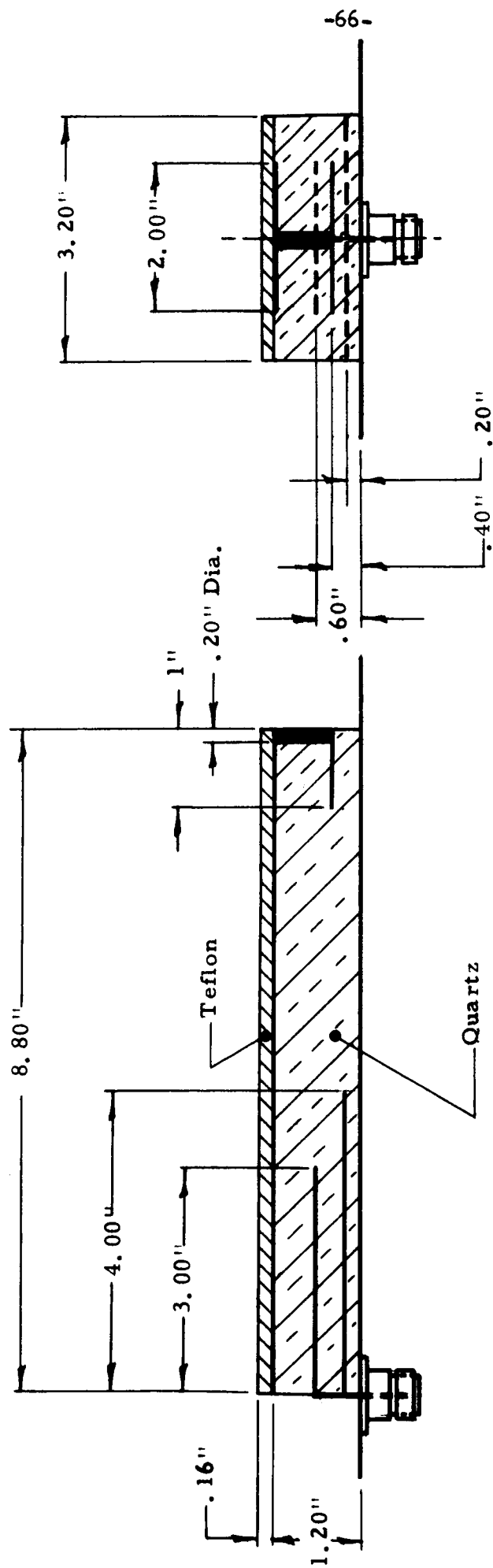
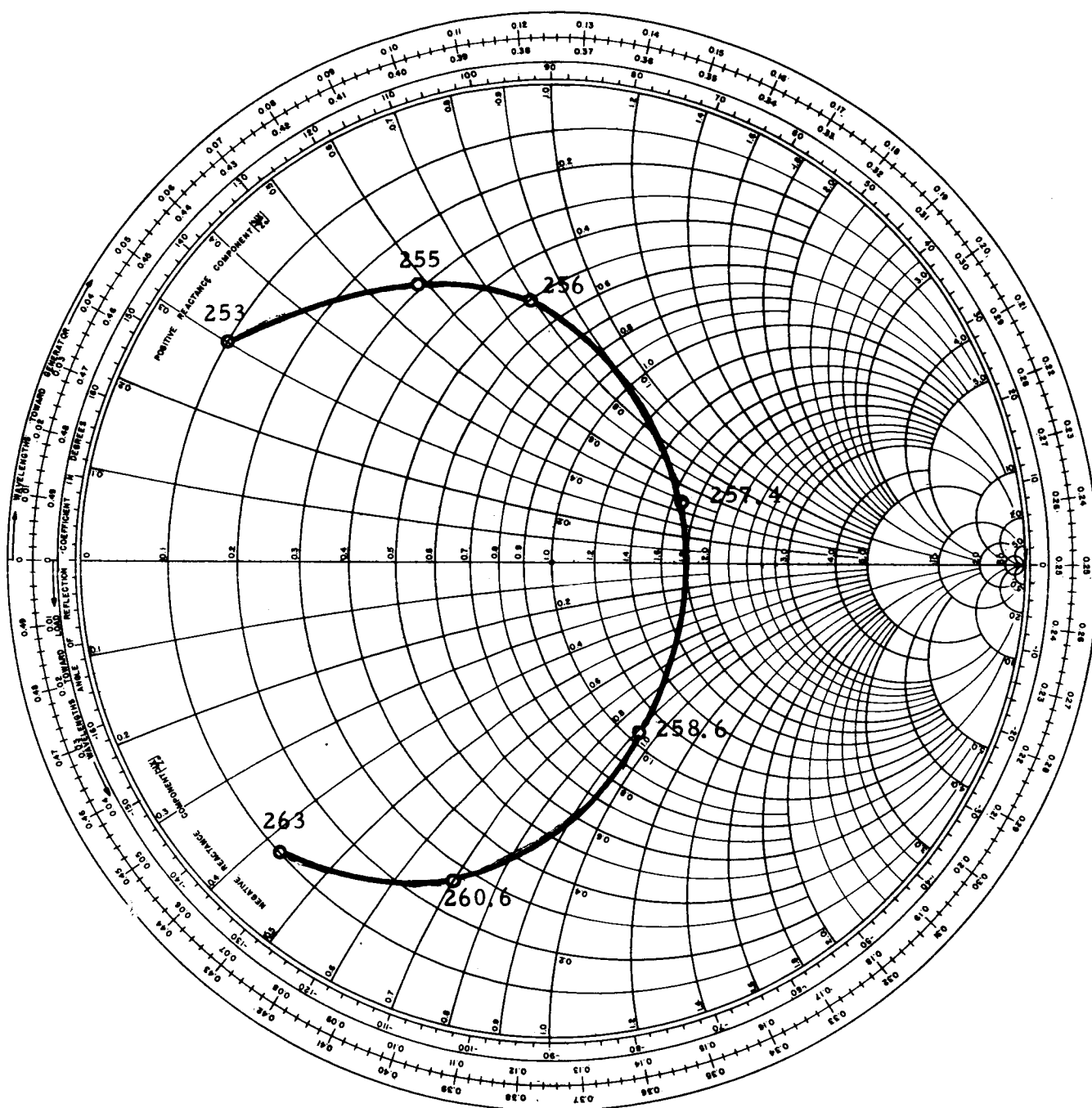


Figure 28 Sketch Of First Quartz Laboratory Model Of VHF Strap Antenna



Frequencies In mc/sec.

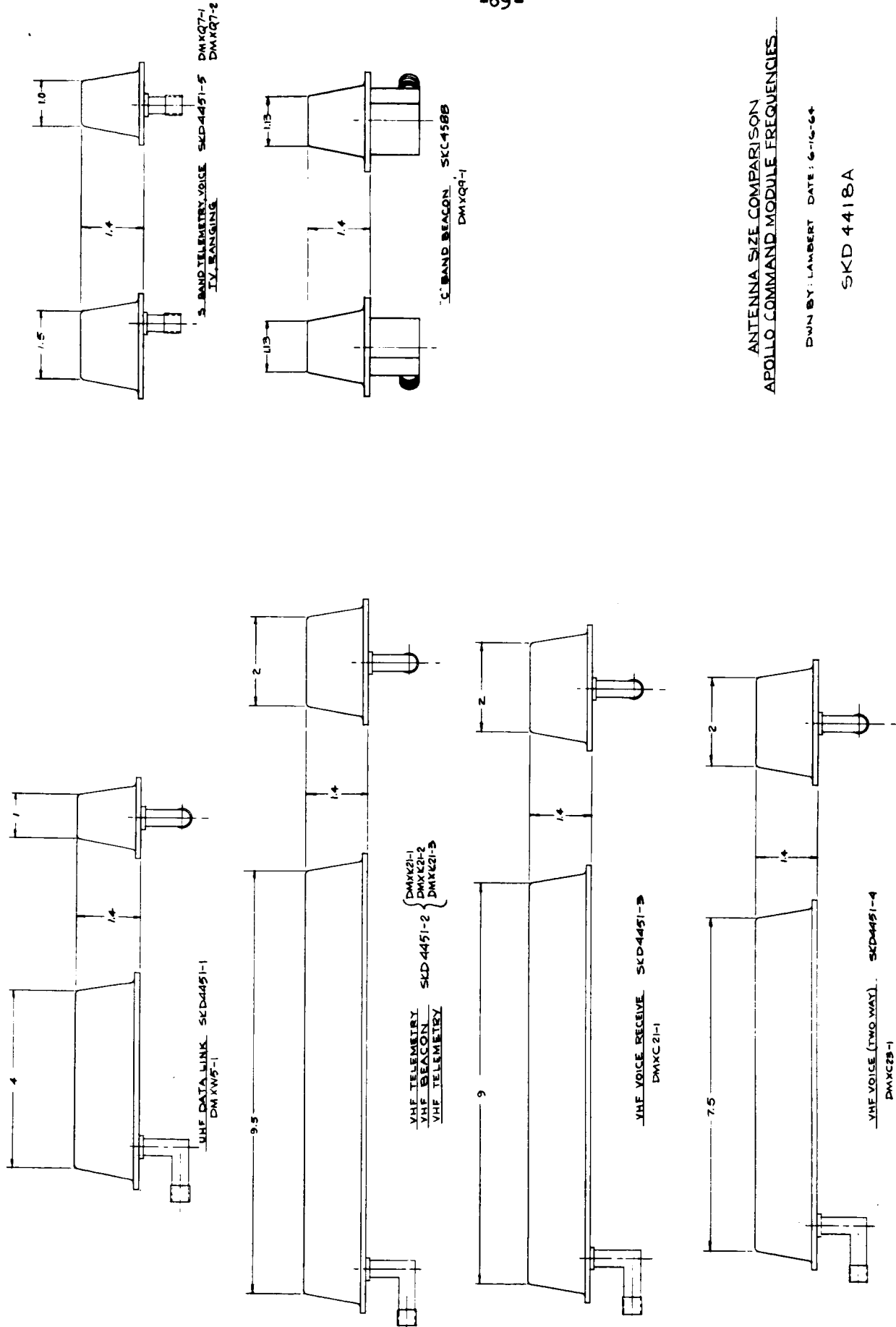
Figure 29 Measured Impedance Of Final Laboratory Model Of VHF Strap Antenna Shown In Figure 26

narrowed from 3.2 to 2.0 inches. The quartz itself was made substantially wider than the radiator, as it would have to be with the operational antenna, so that there would not be any of the capsule ablative covering material immediately adjacent to it because the variation of the dielectric constant of that material with temperature changes would change the tuning of the antenna.

Pattern and gain measurements showed the patterns to be insignificantly different from those of the previous model and the efficiency to be 97% of that of the reference antenna.

It appeared that this type of design should be satisfactory not only for the lowest frequency antenna, but for all the others as well except for the C-band (which, as previously discussed, is required to be circularly polarized). Extrapolating from the data the envelope dimensions of each of the antennas required for a complete set were then estimated and are shown on Figure 30. (This figure also shows the outline of the C-band antenna; however, it was separately determined.)

It was estimated that a complete set of one each of these antennas would weigh about 14.5 pounds, whereas a set of the cavity antennas would weigh about 29 pounds. After discussion with cognizant NASA personnel it was decided to carry forward the design of these units for the laboratory prototypes to be furnished.



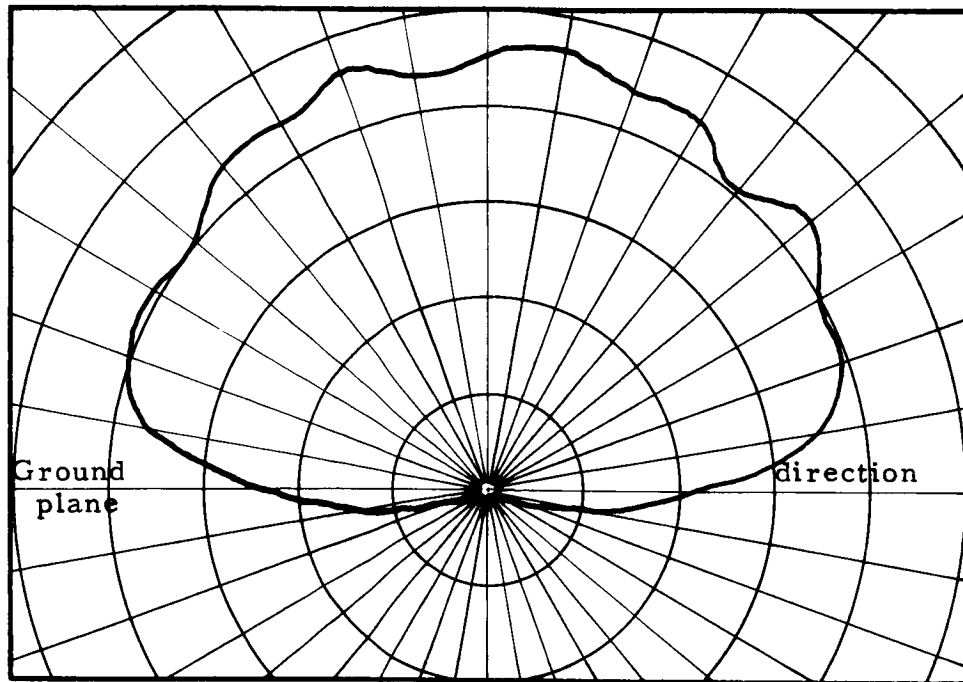
ANTENNA SIZE COMPARISON
APOLLO COMMAND MODULE FREQUENCIES

DUN BY: LAMBERT DATE: 6-16-64

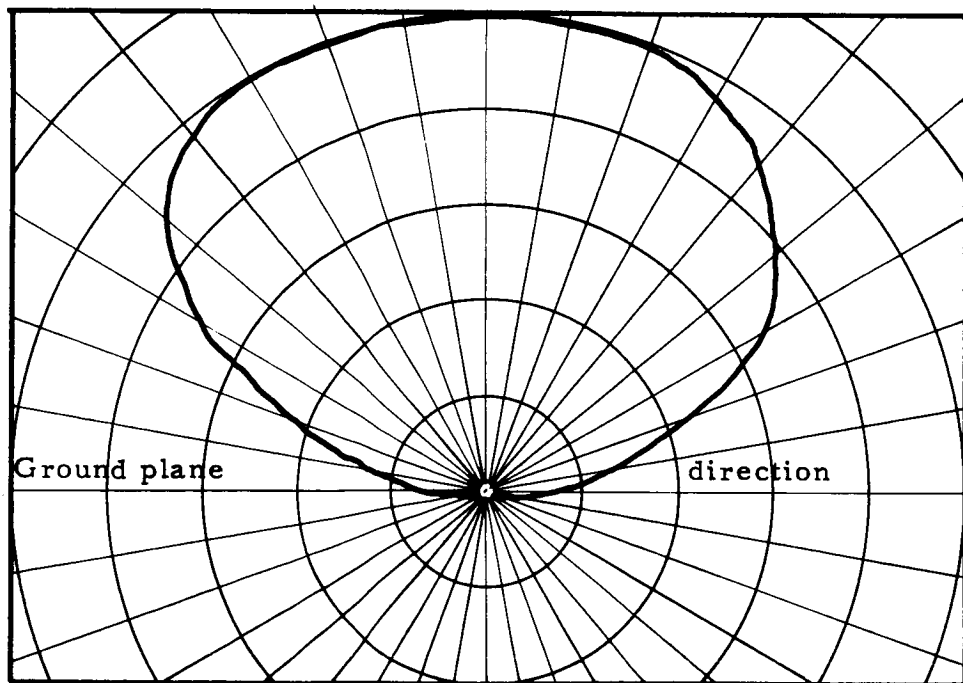
SKD 4418A

Figure 30 Outline Drawings Of Ablative Shield Antennas

There remained the design of the C-band antenna. Because a wavelength at its frequency of operation is only slightly more than two inches, this antenna will necessarily be small and there is not a significant weight advantage directly obtained by locating it within the ablative shield. As with the other antennas, it is desirable that the patterns that will lie in planes parallel to the Z axis of the capsule be as broad as possible and that patterns at right angles to this be in the range of 90 to 120 degrees wide. Accomplishing this while meeting the other requirements poses a number of problems. Nevertheless it appears that many design approaches could be successfully applied to the problem. However, it is to be noted that the ablative cover severely attenuates the signal where its direction of propagation is such that it has a long path through the cover as it does when the angle of elevation of the radiation above the surface of the vehicle is in the region of 15 degrees or less. This is illustrated by the two patterns on Figure 31. The upper pattern is the E plane pattern of a C-band slot radiator in a four foot square ground plane. The lower pattern is that obtained when the antenna and the entire ground plane are covered by a 1.1 inch thick layer of simulated ablative material (mahogany wood was used). It is seen that the radiation at 90 degrees from the normal is almost completely eliminated, and that radiation 75 degrees from the normal is attenuated by 10 db. This



Relative Voltage



Relative Voltage

Figure 31 E Plane Patterns Of Small S Lot In 3 Foot Square Ground Plane

effect cannot be eliminated; even if the antenna aperture were at the outer ablative surface, the electromagnetic field would spread into the ablative material and the effect would still be present. As a result, it is desirable to install the antennas on the broadest part of the capsule, where the surface is curved away from the normal in both planes.

The design that was performed comprises a rectangular aperture located about one third of the way in from the outer surface of the ablator. It is excited by a quartz-filled rectangular waveguide section, which in turn is excited in two orthogonal lowest order TE modes. By selection of the guide dimensions one mode is advanced 90 degrees with respect to the other.

The quartz guide is embedded in a Duroid covering block as explained and illustrated elsewhere in this report.

The approach was selected because it was judged that it was less critical dimensionally than would be a design using a helical type radiator. As the work progressed, it appeared that the resulting antenna would be sufficiently non-critical to be satisfactory. Therefore, other approaches were not pursued.

3.2 Mechanical Design

The core of the mechanical design is comprised in the selection of materials and the solution of the thermal design problems. These topics are discussed in this section.

3.2.1 Materials

Several dielectric materials were investigated for use as antenna windows or as structural portions of the antennas. These were:

Clear Fused Silica	Corning Glass Company	Code 7940
Multiform Fused Silica	Corning Glass Company	Code 7941
Reinforced Teflon	Rogers Corporation	Duroid 5650
Polyaromatic Resin Laminate	Narmco Materials Division	Imidite 1850

The first three listed were considered for use in the window itself. For the form of antenna recommended as a result of this study, certain combinations of characteristics are required which tend to exclude many materials which might otherwise be considered. Among the class of materials capable of surviving earth entry trajectories, only those which exhibit low loss tangent and stable dielectric constant over a wide temperature range can be considered in order to degrade neither the thermal stability nor the electrical efficiency of the antennas.

Clear Fused Silica

The following curves are characteristic of this material in the temperature range of interest:

Thermal Conductivity	Figure 32
Specific Heat	Figure 33
Thermal Diffusivity	Figure 34
Dielectric Constant	Figure 35
Los Tangent	Figure 36
Emissivity	Figure 37

The sharp rise in thermal conductivity and thermal diffusivity shown above about 1100°F is to be noted. Clear fused silica is transparent to radiant heat, and this latter mechanism begins to become a significant mode of energy transport above this temperature. Heat transfer experiments concerned only with heat transferred between two surfaces in a given period of time show the operation of the radiation mechanism as an apparent increase in conductivity. When appropriately designed experiments isolate the two effects (for example by measuring heat transfer between source and sink, both before and after the test sample is inserted) the conduction mechanism alone is shown to be reasonably constant with temperature. This is illustrated by the curve of Figure 38.

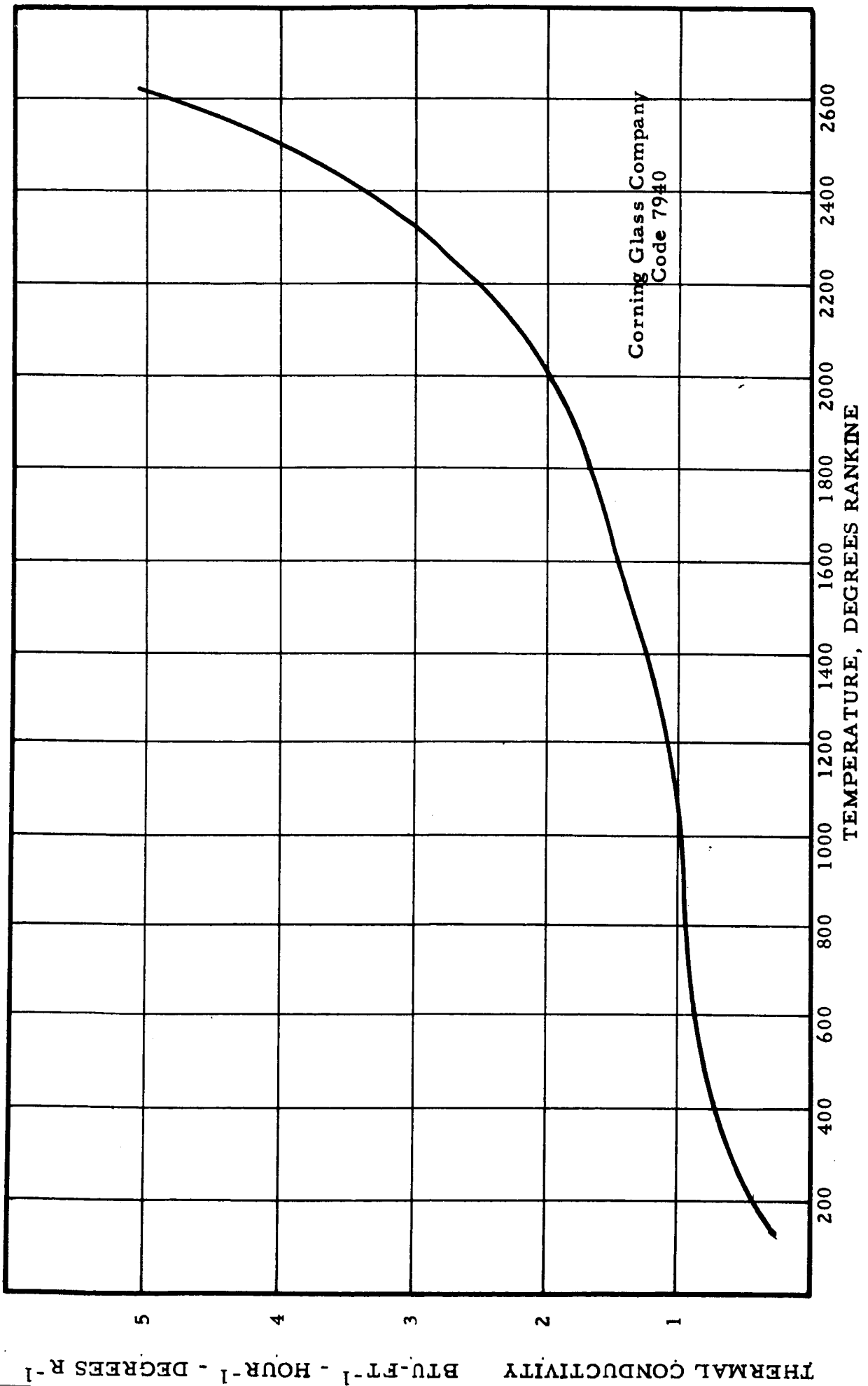


Figure 32 Thermal Conductivity Of Clear Fused Silica

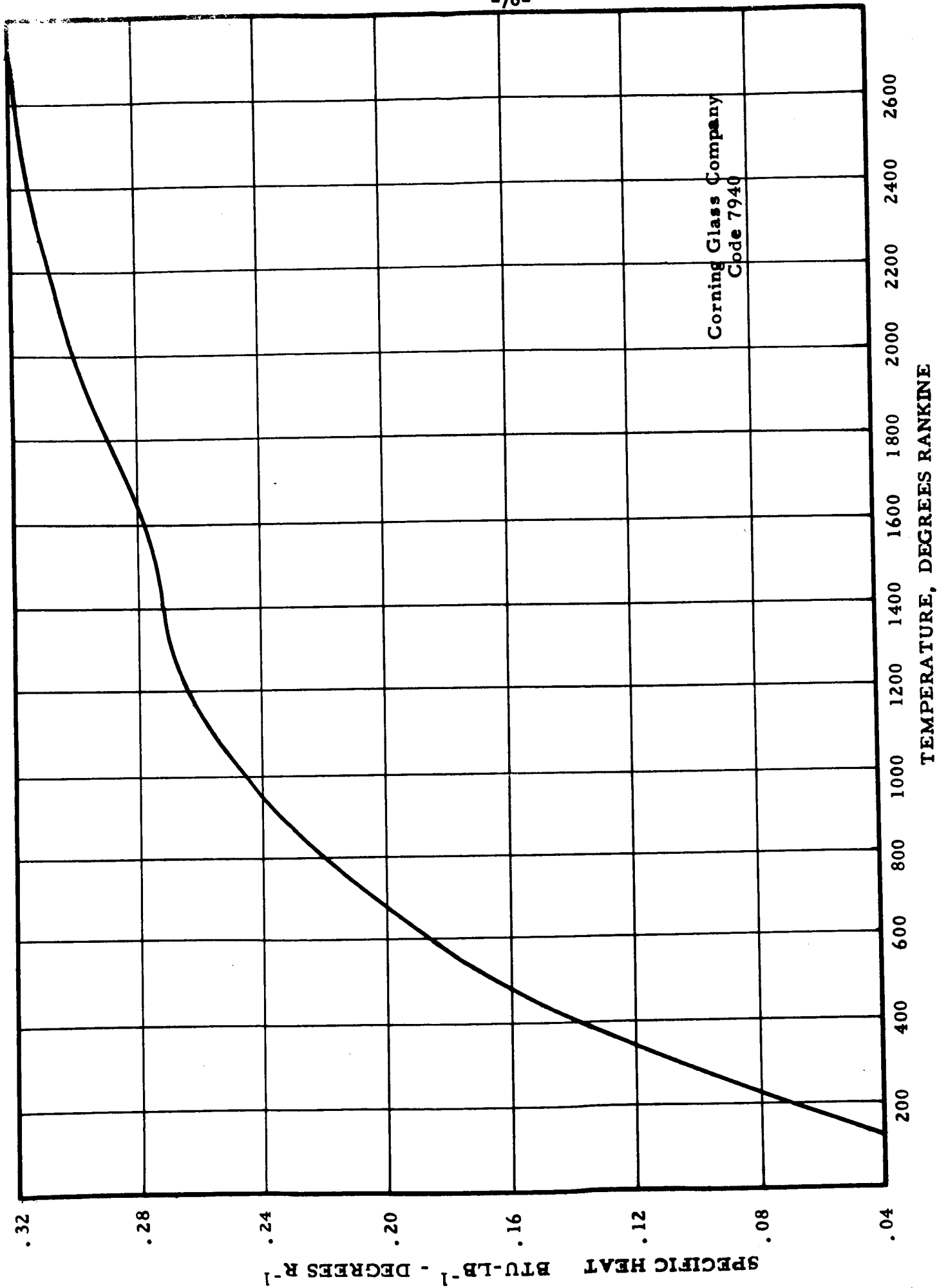


Figure 33 Specific Heat Of Clear Fused Silica

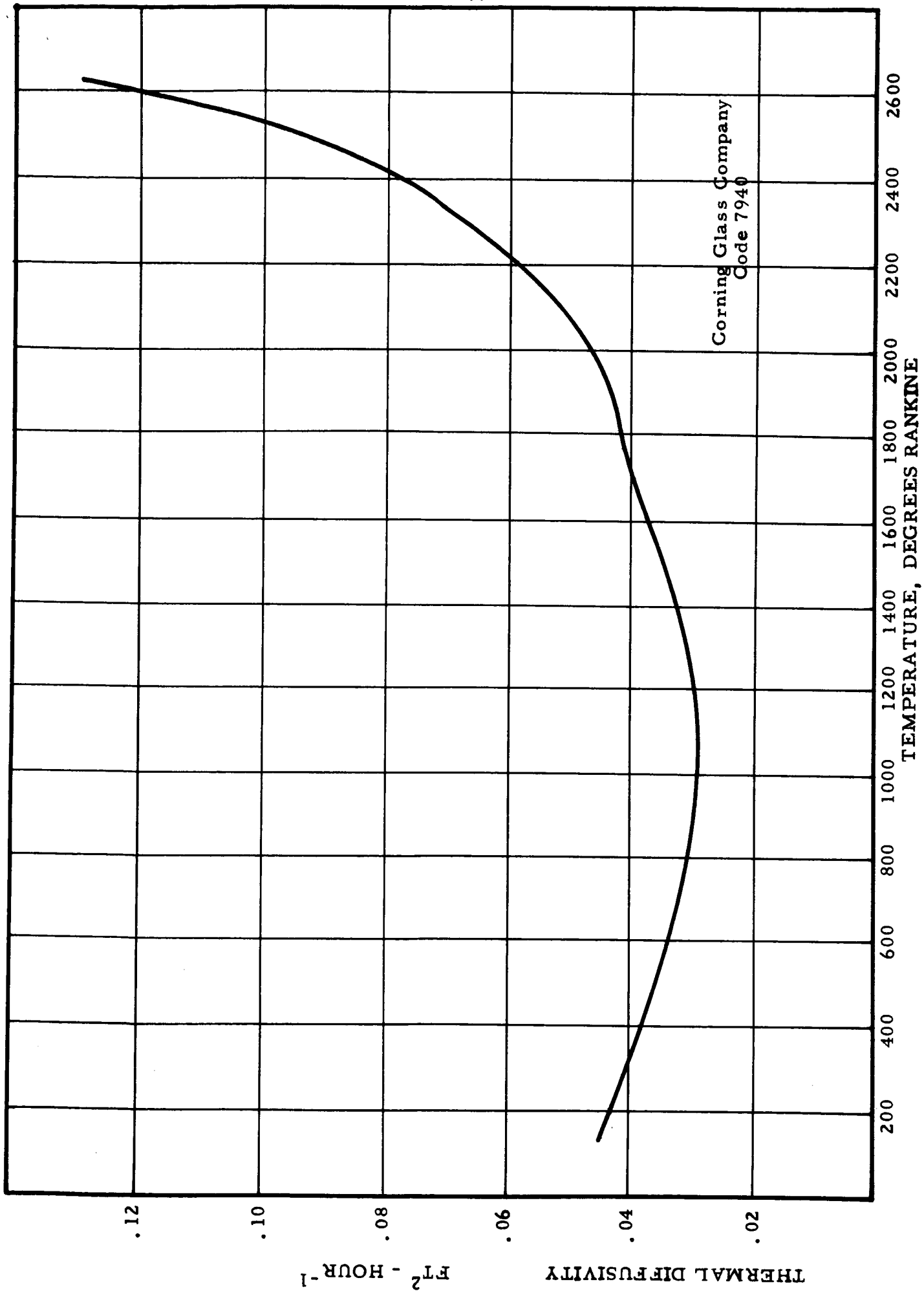


Figure 34 Thermal Diffusivity Of Clear Fused Silica

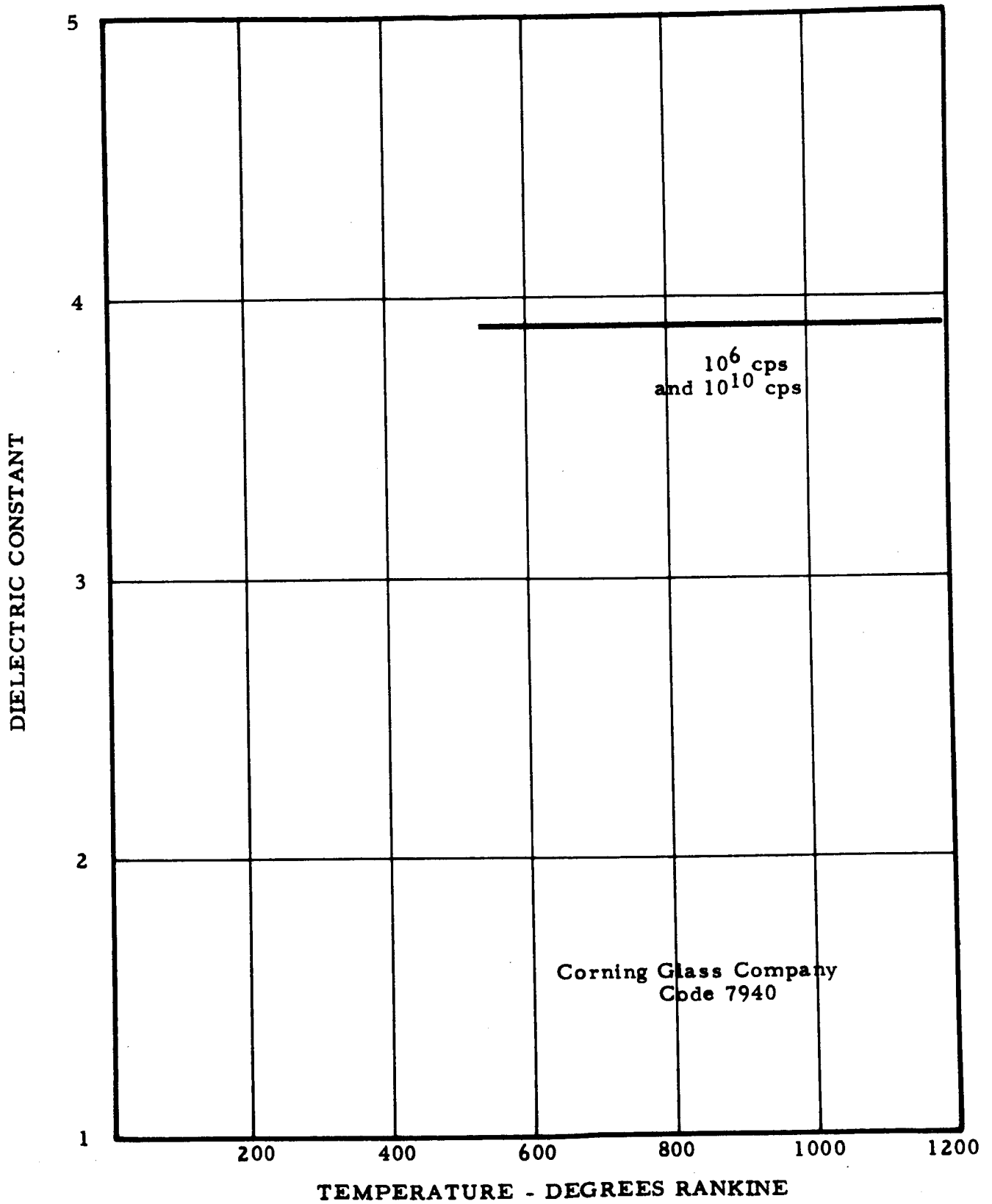


Figure 35 Dielectric Constant Of Clear Fused Silica

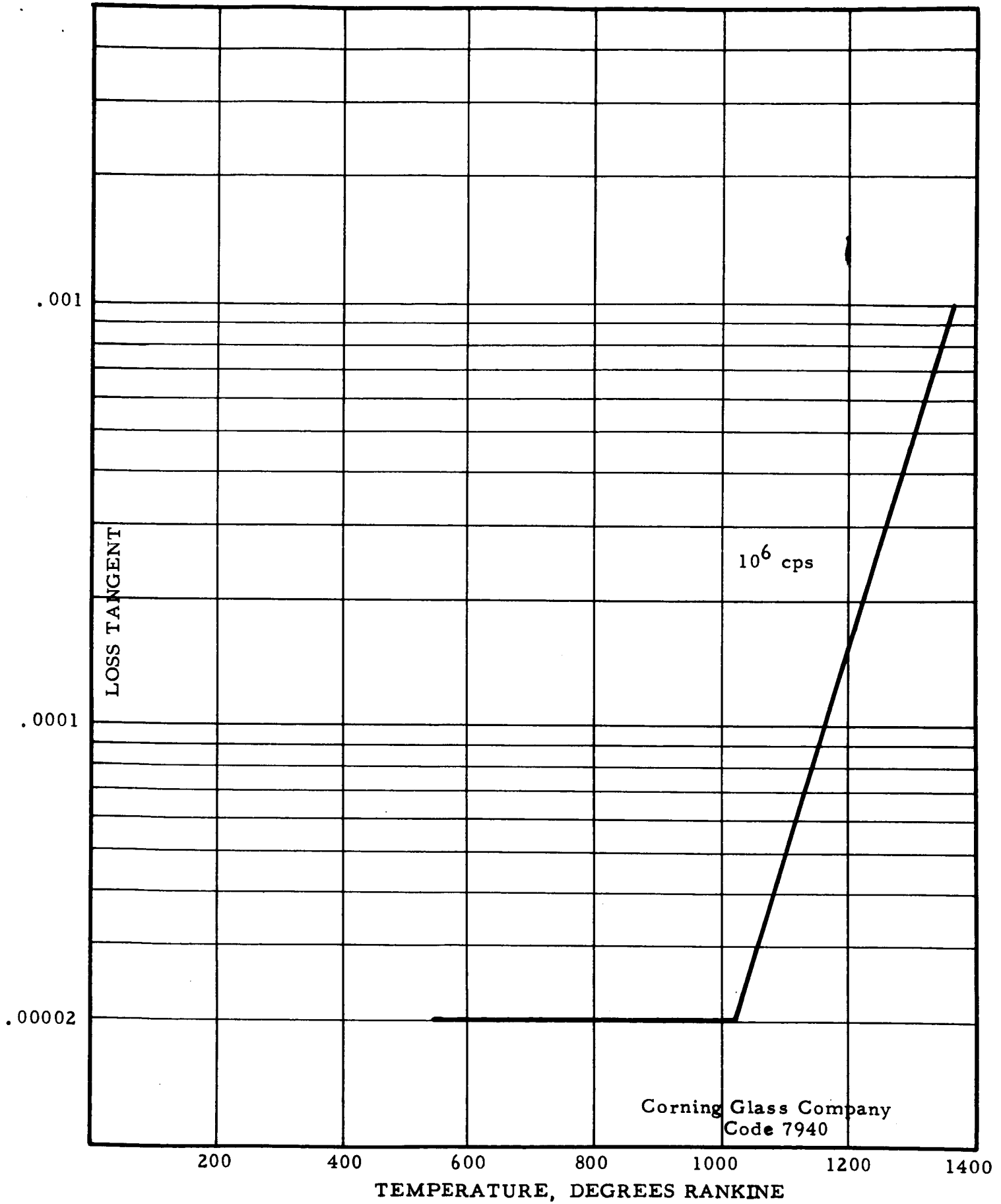


Figure 36 Loss Tangent Of Clear Fused Silica

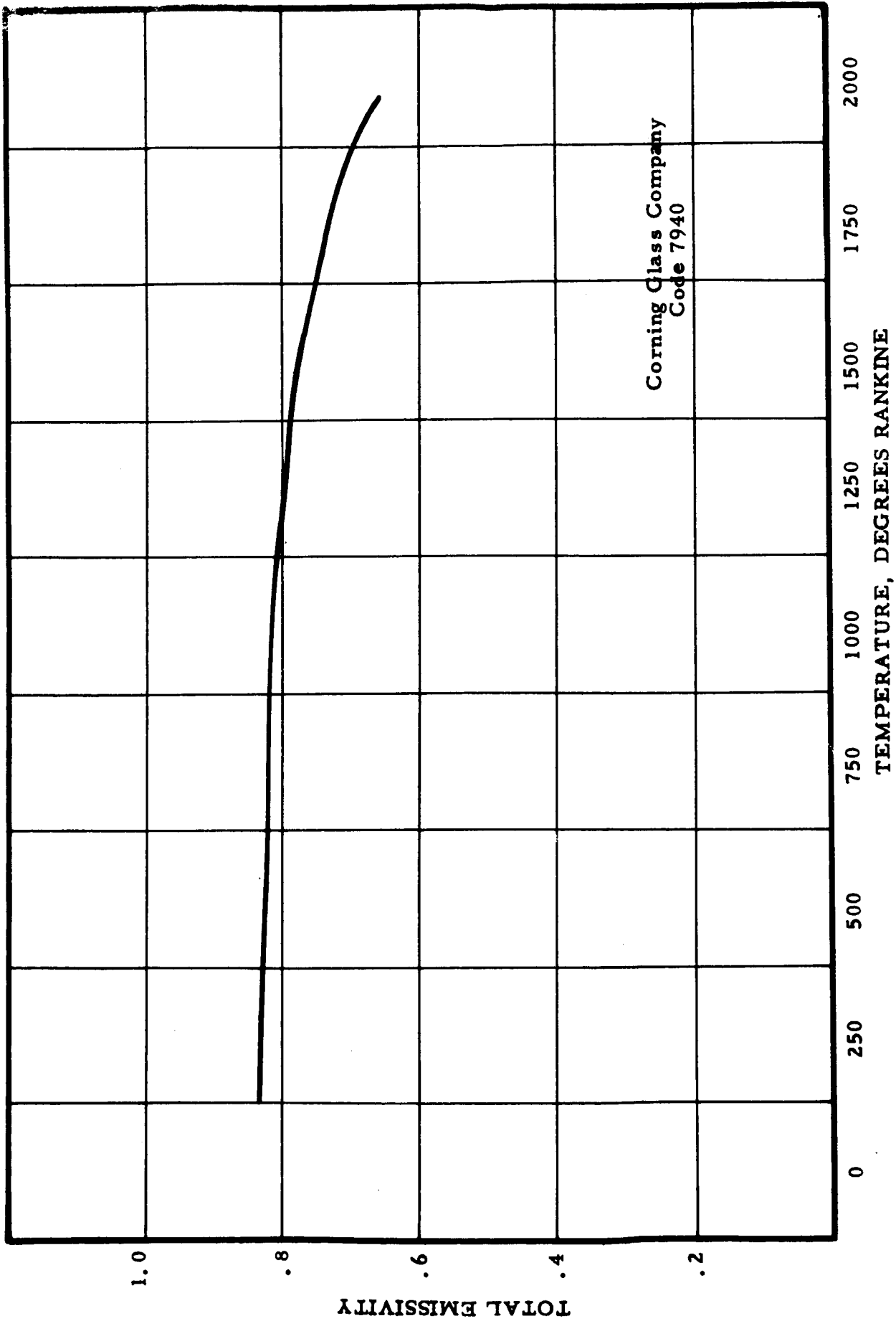


Figure 37 Emissivity Of Clear Fused Silica

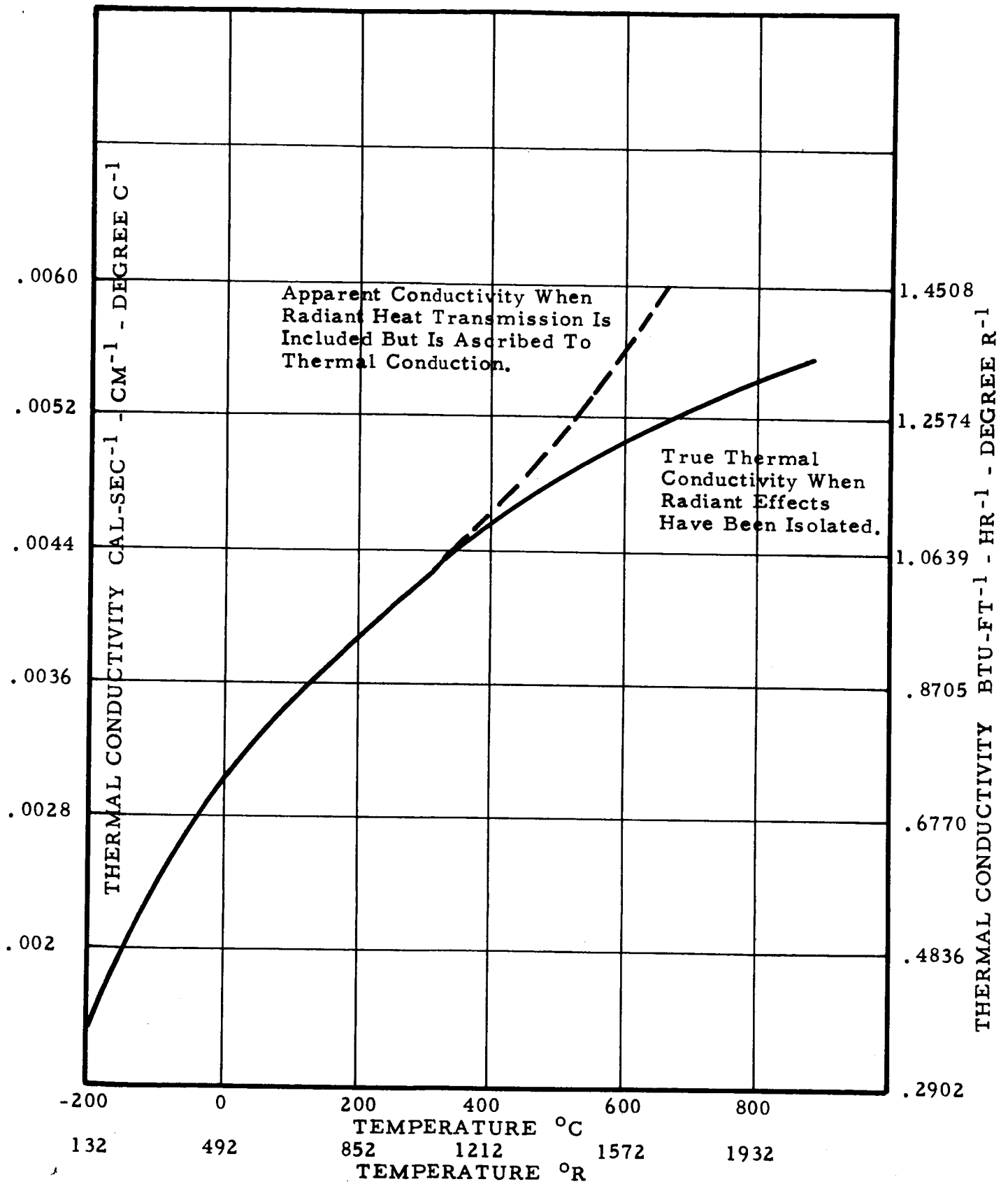


Figure 38 Conductivity Of Clear Fused Silica Showing Operation Of Radiant Heat Transfer Mechanism

The high heat transport rate through clear fused silica makes it unsuitable for use as an antenna window for Apollo earth entry conditions.

Multiform Fused Silica

The following curves are characteristic of this material in the temperature range of interest:

Thermal Conductivity	Figure 39
Specific Heat	Figure 40
Thermal Diffusivity	Figure 41
Dielectric Constant	Figure 42
Loss Tangent	Figure 43
Emissivity	Figure 44

This material exhibits much the same electrical characteristics as clear fused silica but with superior thermal properties. The material is opaque to radiant heat transfer, hence does not exhibit the sharp rise in conductivity characteristic of the clear form. The material exhibits a lower conductivity than clear fused silica even in the absence of the radiant heat transport effect in the latter, probably because it is slightly porous and granular in nature.

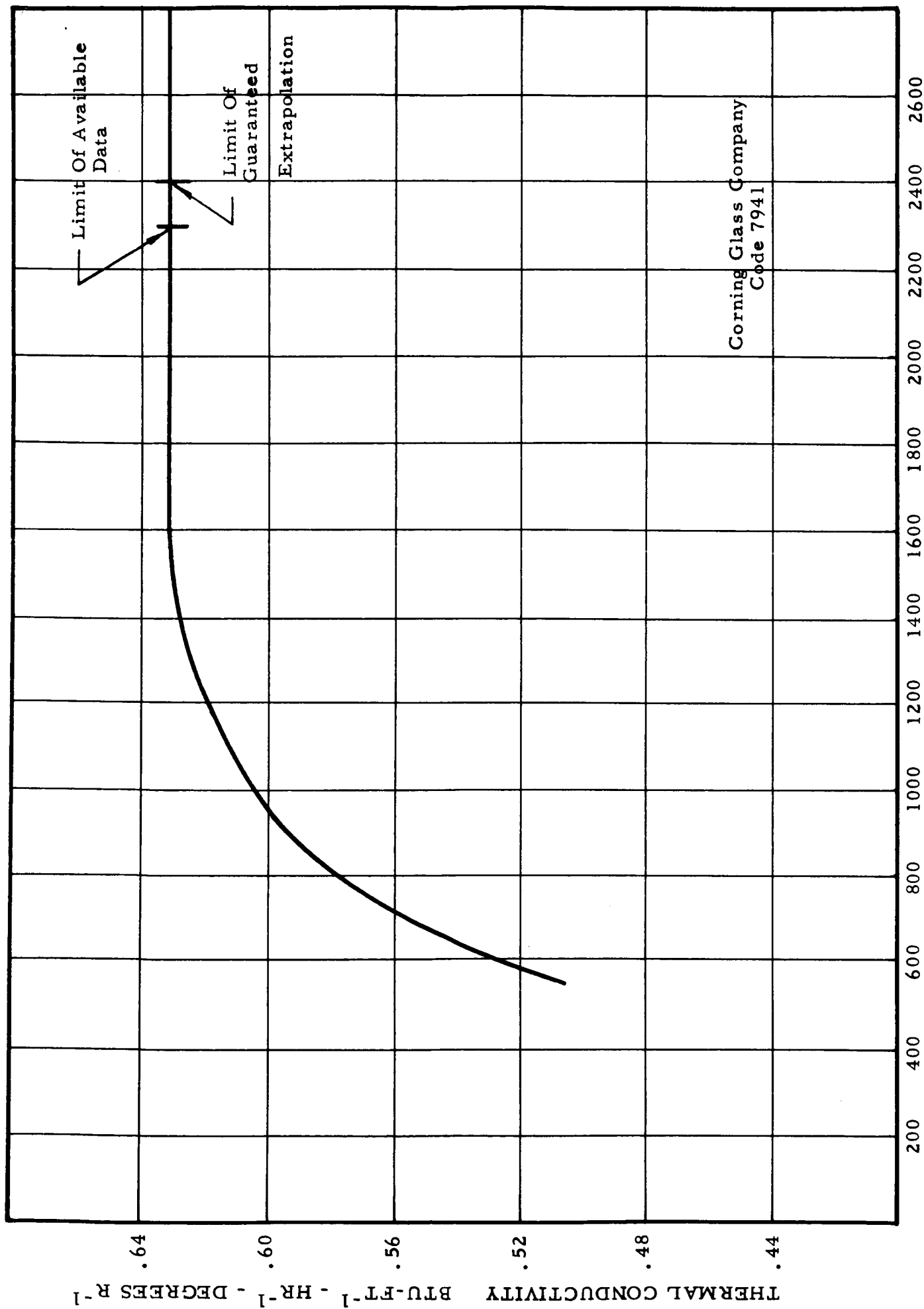


Figure 39 Thermal Conductivity Of Multiform Fused Silica

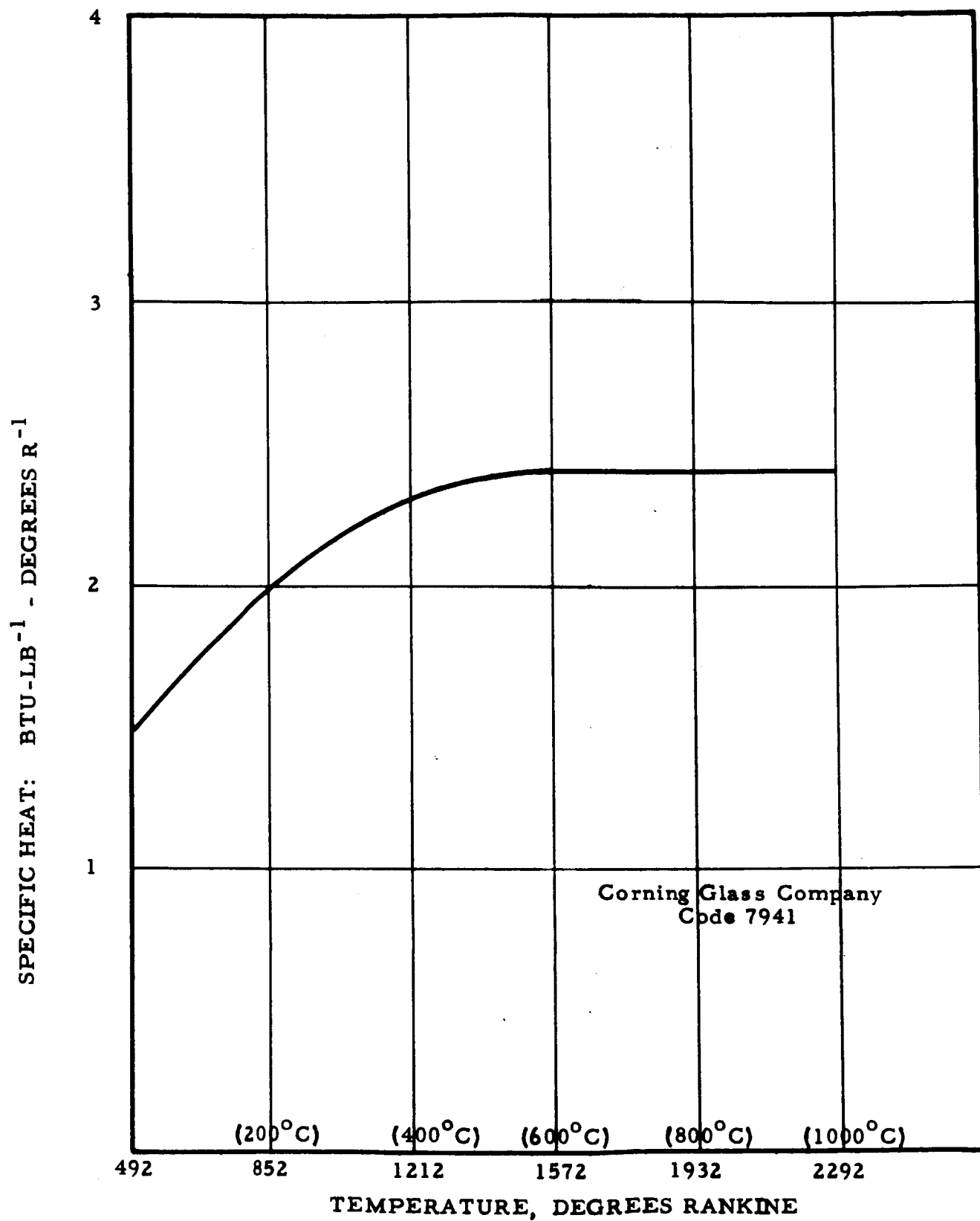


Figure 40 Specific Heat Of Multi-form Fused Silica

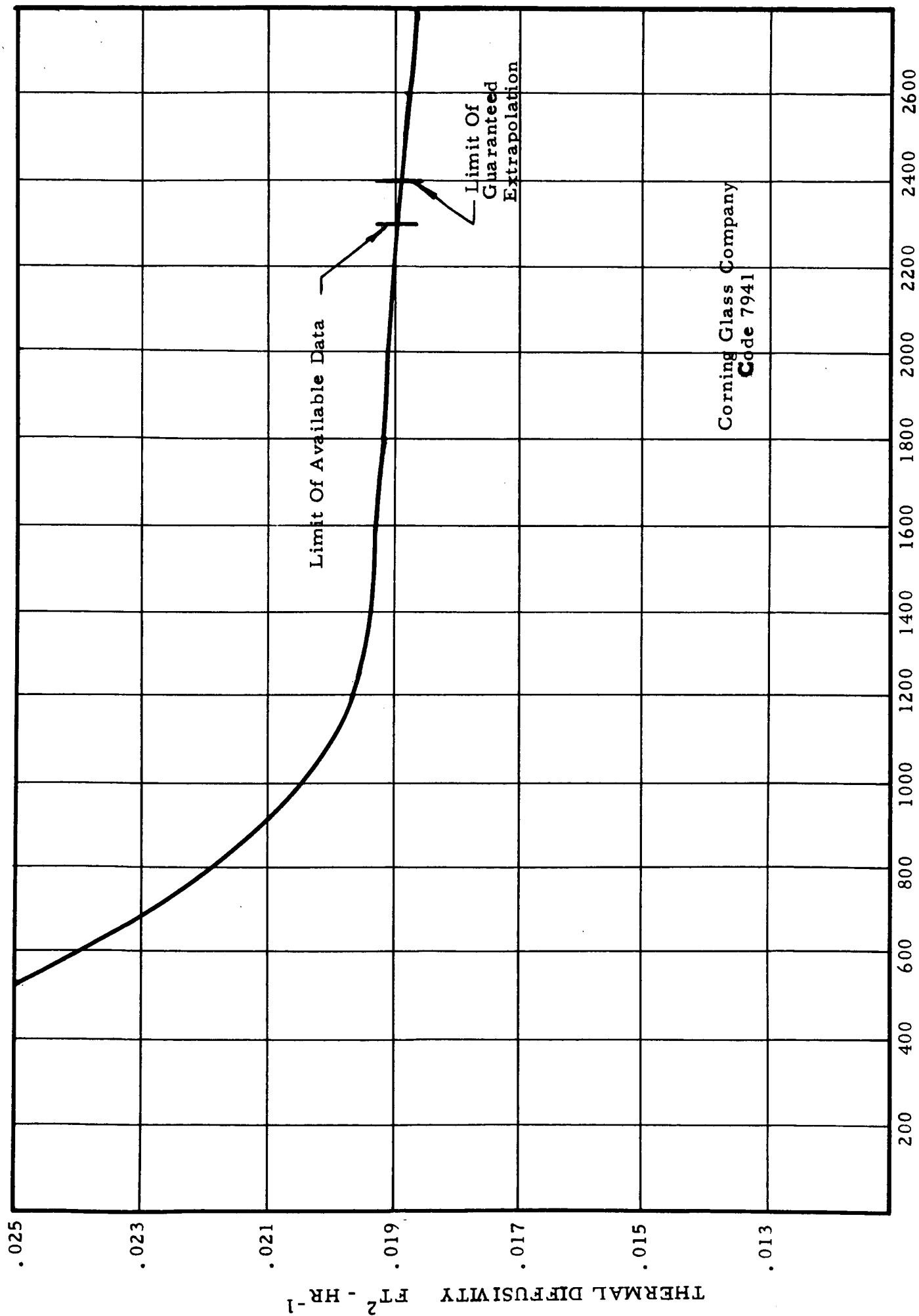


Figure 41 Thermal Diffusivity Of Multiform Fused Silica

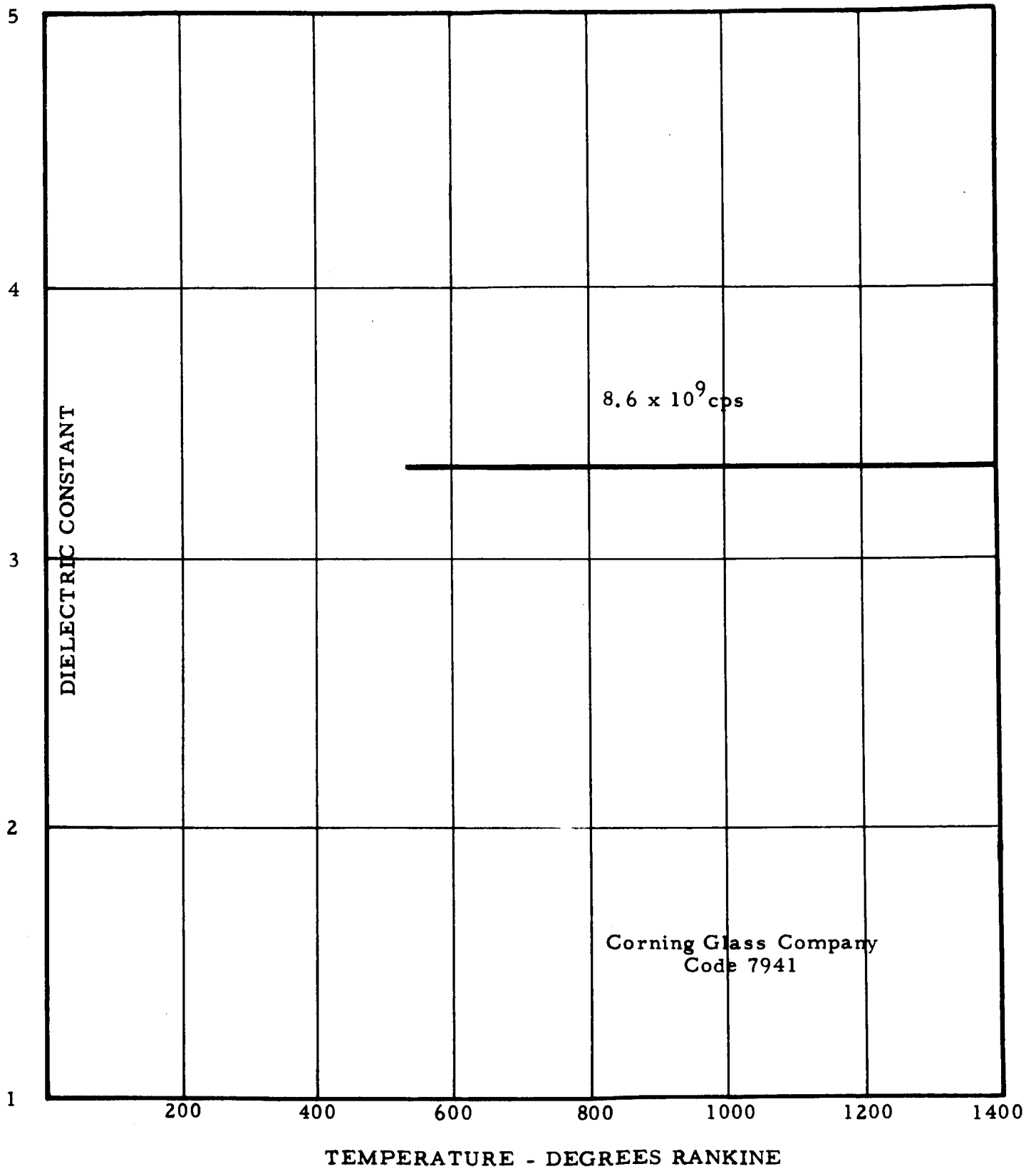


Figure 42 Dielectric Constant Of Multifom Fused Silica

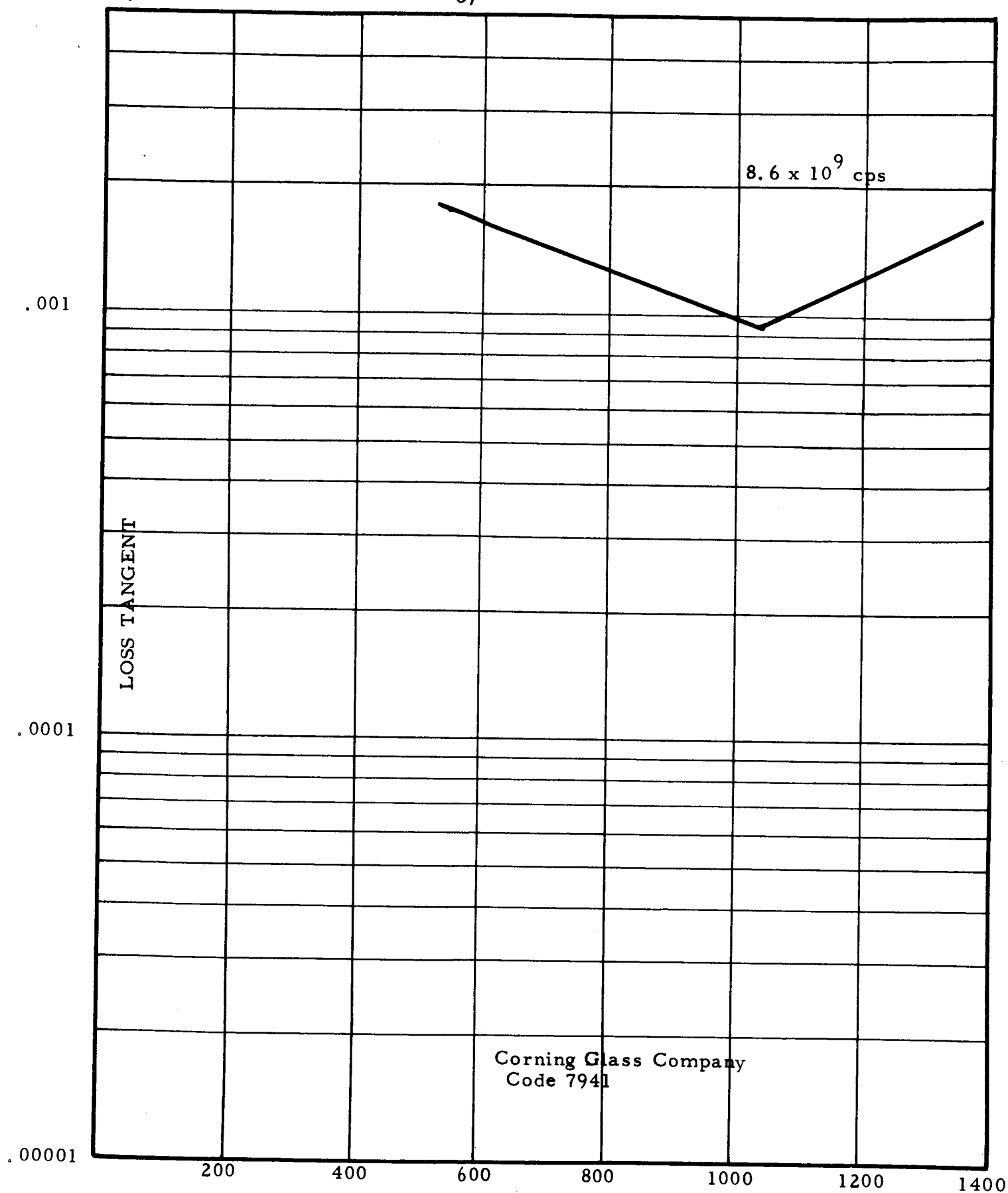


Figure 43 Loss Tangent Of Multiflow Fused Silica

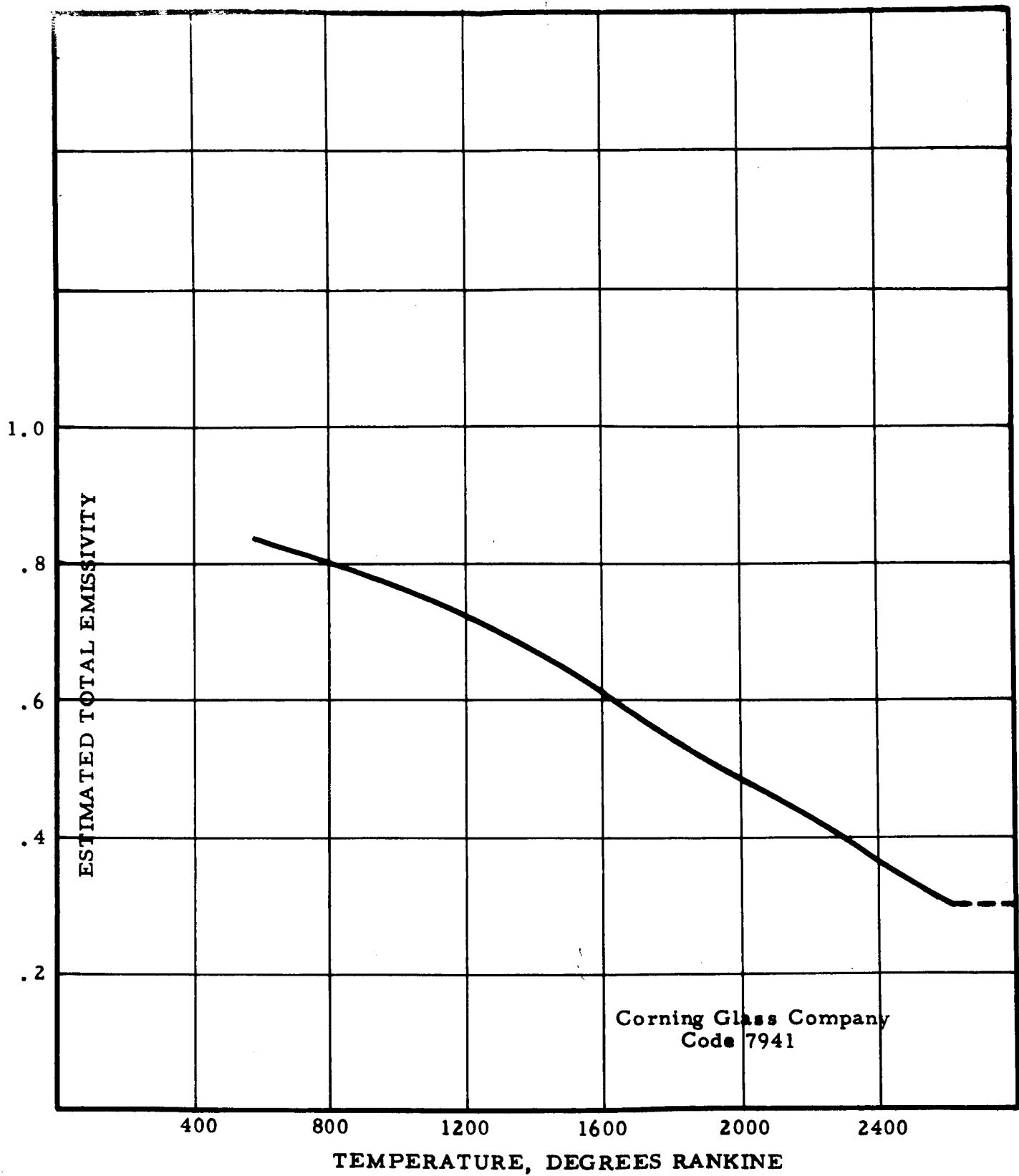


Figure 44 Estimated Emissivity For Multi-form Fused Silica

Reinforced Teflon (Duroid 5650)

The properties of Duroid 5650 are shown in Table 1.

TABLE 1

Specific Heat	$\frac{\text{BTU}}{\text{LB} \cdot ^\circ \text{F}}$.24																		
Thermal Conductivity	$\frac{\text{BTU} \cdot \text{FT}}{\text{FT}^2 \cdot ^\circ \text{F} \cdot \text{HR}}$.165																		
Loss Tangent	1 MC	.0016																		
Dielectric Constant	1 MC	2.6																		
Specific Gravity		2.15																		
Emissivity		.85																		
Heat of Ablation	$\frac{\text{BTU}}{\text{LB}}$	<u>Depending on Entry Conditions:</u>																		
		<table><tr><td>Heat Flux BTU/SQ.FT- SEC.</td><td>Heat of Ablation</td></tr><tr><td>60</td><td>1200</td></tr><tr><td>90</td><td>1400</td></tr><tr><td>130</td><td>700</td></tr><tr><td>470</td><td>1000</td></tr><tr><td colspan="2">Stagnation Point Enthalpy</td></tr><tr><td colspan="2">$\frac{\text{BTU}}{\text{LB}}$</td></tr><tr><td>1000</td><td>1200</td></tr><tr><td>10000</td><td>4700</td></tr></table>	Heat Flux BTU/SQ.FT- SEC.	Heat of Ablation	60	1200	90	1400	130	700	470	1000	Stagnation Point Enthalpy		$\frac{\text{BTU}}{\text{LB}}$		1000	1200	10000	4700
Heat Flux BTU/SQ.FT- SEC.	Heat of Ablation																			
60	1200																			
90	1400																			
130	700																			
470	1000																			
Stagnation Point Enthalpy																				
$\frac{\text{BTU}}{\text{LB}}$																				
1000	1200																			
10000	4700																			

Data are not available on this material sufficient to draw continuous curves as a function of temperature. In general, the conductivity of this material is about one-quarter that of the multiform fused silica, but the density and specific heat are about the same.

In order to obtain a comparison between the thermal characteristics of antenna windows made with and without a Duroid cap, calculations were made setting emissivity 0.85 constant with temperature, and setting all other thermal properties equal to those of multiform fused silica except thermal conductivity and thermal diffusivity which were multiplied by 0.25, in the top inch of a 1.4 inch thick window.

The calculation showed a peak cold side temperature in the quartz slab of 1240°R occurring at 40 minutes. The peak is 280°R lower and 10 minutes later than if the cap had not been enplaced. This computation was not precise in that the lower temperature ablation characteristics of the Duroid were not taken into account, but it served to illustrate the effect of changes in the conductivity parameter.

Despite the substantial thermal advantage offered by Duroid it was possible, as previously mentioned, to utilize it only for the smallest antenna (C-band) because of the following characteristics:

1. The coefficient of thermal expansion is anisotropic, and is very high.

2. The basic constituent is teflon which can be cemented only after a sodium ammonia etch. The resulting bond is weak. Evidence exists that the bond strength is reduced considerably in strong ultraviolet light radiation.

Duroid is manufactured in paper-thin layers using about 40% aluminum silicate fibers in a teflon matrix. Because of the nature of the process, the reinforcements lie entirely within each layer and do not cross between plies if one or more layers are bonded together. The fibers contribute a large amount to the erosion resistance, hence Duroid to be used as a re-entry antenna window must have its end-grain only exposed. (Exposure parallel to the thin plies results in delamination without significant endurance.)

This is accomplished by first bonding plies together under heat and pressure, into blocks about $\frac{1}{4}$ inch thick, and then by building the blocks up into larger structures by etching and cementing. The finished product, viewed at the ablation face, has the appearance of a "butchers block".

Unfortunately, the coefficient of expansion at right angles to the plies, or in the only unreinforced direction, is high. The following table shows typical values.

TABLE II

Temperature °F	Thickness of Laminate at Right Angle to Plies $\text{IN/IN-}^\circ\text{F} \times 10^{-6}$	Parallel to Laminate in the "Machine" Direction $\text{IN/IN-}^\circ\text{F} \times 10^{-6}$	Parallel to Laminate in the Cross Machine Direction $\text{IN/IN-}^\circ\text{F} \times 10^{-6}$
-40 to +30	69.9	10.0	18.6
30 to 60	90.0	10.2	21.8
60 to 75	422.7	9.0	32.3
75 to 90	124.5	9.9	28.1
90 to 120	101.2	7.2	16.4
120 to 170	125.8	5.1	10.7
170 to 200	156.1	3.6	5.8
<hr/>			
0 to 100	120	19	22
100 to 350	120	5	11
75 to 250*	73.2		

In a test run at Dorne and Margolin, Inc., a sample 13 inches long at room temperature was heated to 250°F and expanded to a total overall length of 13.187 inches.

* Measured at Dorne and Margolin, Inc. (Uncertainty $\pm 7\%$).

Retention with the reliability required for the Apollo Mission of a large sized window over a temperature range -250°F to 250°F and through re-entry was judged impractical. One solution, which is satisfactory in some applications, involves the use of a heel piece at right angles to the ply direction, to restrain against expansion. Although one such sample, approximately 6.7 x 4.6 inches, warped .093 out of flat after exposure to 250°F for four hours. In a Dorne and Margolin test, it was judged that the method would be satisfactory with much smaller pieces of material. It was used in the C-band design.

Polyaromatic Resin Laminate (Imidite 1850)

Imidite* 1850 was considered because it is a fiberglass laminate which is capable of withstanding very high temperatures for moderate periods of time. This material is rated for 15 minutes exposure to 1250 F or for continuous exposure in the range 750° to 1000°F if protected against long-term oxidation. Mechanical properties of this material are shown in Figure 45 and in Table III.

* This material is described and discussed in WPAFB classified report ASD-TDR-63-498 by Harold Levine: Research and Development of High Temperature Resins for Structural Laminates and Adhesives, dated May 1963. (U)

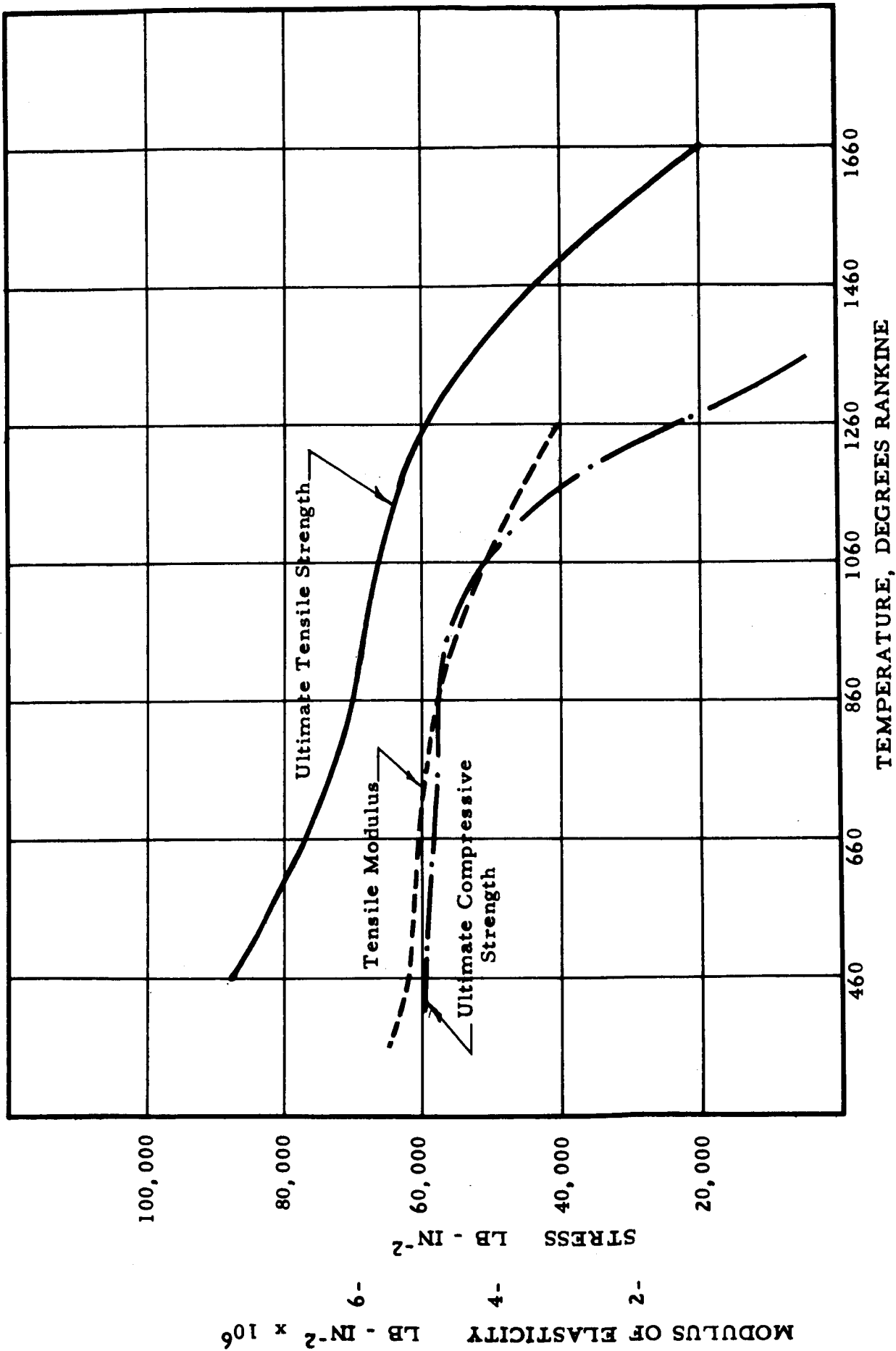


Figure 45 Mechanical Properties Of Imidite 1850

TABLE III

Dielectric Constant		4.8
Loss Tangent		.005
Coefficient of Thermal Conductivity	$\frac{\text{BTU}}{\text{FT-HR-}^\circ\text{R}}$.083*

The material was judged the best available for the cavity pan of the slot-type antennas; the necessary electrical conductivity being obtained through the use of embedded wires. The thermal conductivity of the composite material would be sufficiently low to protect the inner compartments of the spacecraft against excessive heat flow through the antennas.

With the ablative shield type antennas the material is recommended for the antenna retaining flange and the thermally insulating sheet between the antenna and the spacecraft.

Other Materials Investigated

Other materials about which information was obtained in the course of the program were:

Beryllium Oxide
Pyrolytic Graphite

* Estimated. Theoretical values based on glass-resin ratios are higher than this, but the material is porous and test values as low as .067 have been observed.

Beryllium Oxide - Beryllium Oxide has an unusual heat conduction mechanism such that although electrically an insulator, it is an excellent conductor of heat. Thermal conductivity at room temperature is equivalent to aluminum. This material would be useful if heat had to be conducted to a sink through an electrically active area which would be disturbed by conductive elements.

The antenna design recommended for Apollo requires no such heat sinking techniques. Therefore, no use of Beryllium Oxide is foreseen in this program.

Pyrolytic Graphite - This material has an anisotropic heat conduction mechanism. In the two directions, thermal conductivity is 175 times its value in the third direction of the crystalline structure. It would prove useful as a combination insulator and heat pipe if heat were to be conducted from a source to a sink without leakage into the structure.

No requirement for these properties exists in the antenna design recommended for Apollo, hence no use for Pyrolytic Graphite is foreseen in this program.

*

At 500°F the value along the axes having the higher conductivity is:

$$\frac{175 \text{ BTU-FT}}{\text{FT}^2\text{-HR-}^\circ\text{F}}$$

3.2.2 Heat Transfer Calculations

The heat transfer problem was treated as one of unsteady state conduction and radiation. Ablation was regarded as insignificant unless temperature rose over a certain threshold, and it was then treated in a simplified manner. No attempt was made to evaluate the interaction between the window and the ablator surrounding it, nor to assess the effects of shear and enthalpy on the effective heat of ablation.

The essence of the approach lay in dividing the window into a number of elements for purposes of analysis and then programming the problem for an IBM 1620 computer. With the program set up, each element may be conductively coupled to as many as six other elements, and may be coupled to exchange heat by radiation with as many as five other elements. Although the program was set up with provision for heat reception or rejection from several external sources and sinks, or from internal sources and sinks, these provisions were not used during the solution to the problem.

The choice of element definition depends on the configuration being analyzed. For antennas of the design recommended herein, the problem is essentially one dimensional except under some special circumstances which will be described later. Hence, the elements chosen take the form of layers, each exchanging heat with the element above

and below, the first element accepting the heat pulse and being allowed to re-radiate to space as well as to conduct to the second element. The last element can reject heat only to a radiative heat sink which was designed to have very low emissivity so that very little heat is accepted by the spacecraft from the antenna. (In the simple one dimensional case 20 elements are used to describe a window 1.4 inches thick.)

Four different heat input pulses were programmed. They were obtained from NAA Specification MC481-0005A (including the amendments). The first two of these were shown in Figures 1 and 2, and represent undershoot and overshoot conditions respectively at locations possible for antennas at which heating would be comparatively great*. The second two heat pulses are given by the curves of Figures 46 and 47 and show the undershoot and overshoot conditions at a spot on the capsule that would be aft of the maximum temperature zone** at a typical possible antenna location during earth entry.

* $x_c = 20.766$ inches upward from blunt end of capsule at diameter of maximum girth at meridians $-y_c$ to $-z_c$ to $+y_c$, $\theta = 270^\circ$ to 360° , 0° to 90° .

** $x_c = 59$ inches, $+z_c$ axis in vicinity $\theta = 180^\circ$ to 195° . On the side of the spacecraft which will experience the most heating, the antennas probably will have to be withdrawn aft of the point of maximum girth to be located to this zone where earth entry heating is somewhat lower.

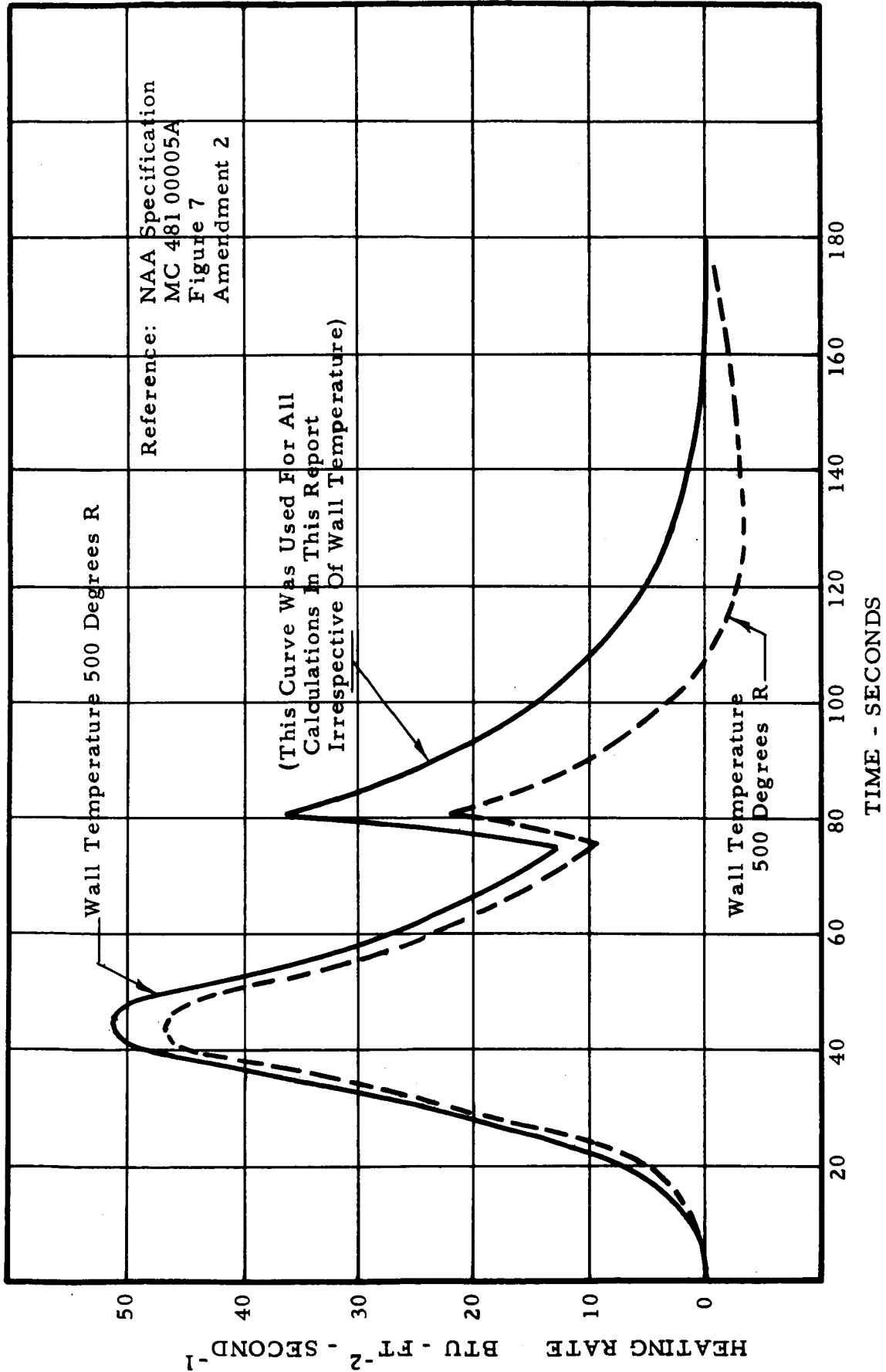


Figure 46 Antenna, Convective Heating Rate Aft Of Maximum Heating Zone.
 $X_c = 59.0$ at $+Z_c$ Axis

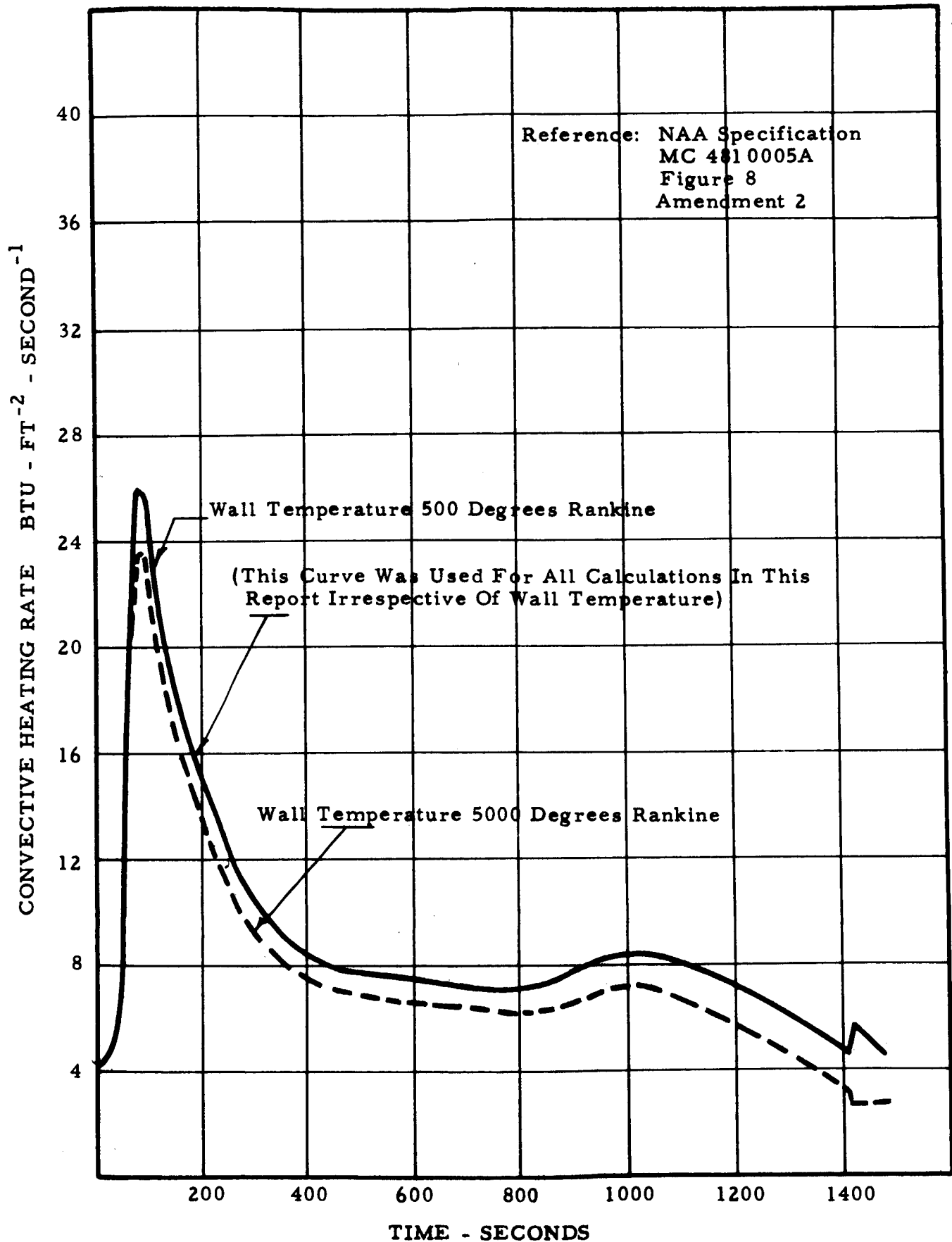
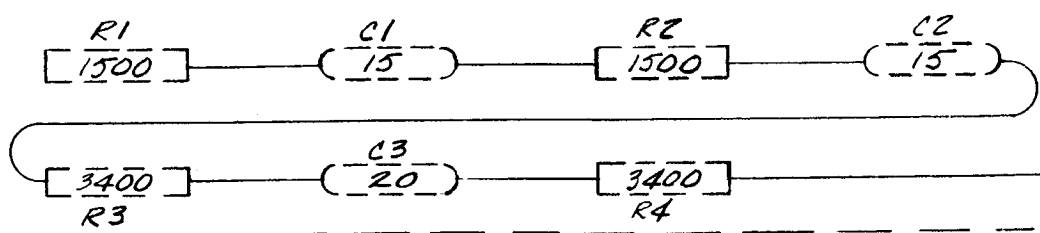
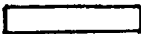


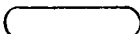
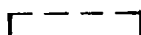
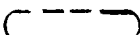

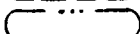
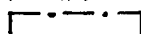
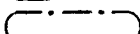


Figure 47 Antenna Convective Heating Rate Aft Of Maximum Heating Zone. $X_c = 59.0$ At $+Z_c$ Axis. Overshoot Entry.



NOTES:

- 1-  - INDICATES RESISTOR.
 - INDICATES CAPACITOR.
- 2- DIFFERENCES IN OUTLINE CONFIGURATIONS OF RESISTORS & CAPACITORS INDICATE COMPONENT MAT'L USED.
 OR  - PLASTIC
 OR  - QUARTZ
 OR  - BERYLLIUM
 OR  - ST. STEEL
- 3- PLUS SIDE OF CAPACITORS SOLDERED TO JUNCTION OF RESISTORS.
- 4- MINUS SIDE OF CAPACITORS GO TO GROUND.
- 5- NUMERICAL VALUES OF RESISTORS ARE IN OHMS, CAPACITORS IN MICROFARADS.
- 6- HORIZONTAL DASH LINES ACROSS SCHEMATIC INDICATE MAT'L THICKNESS USED:

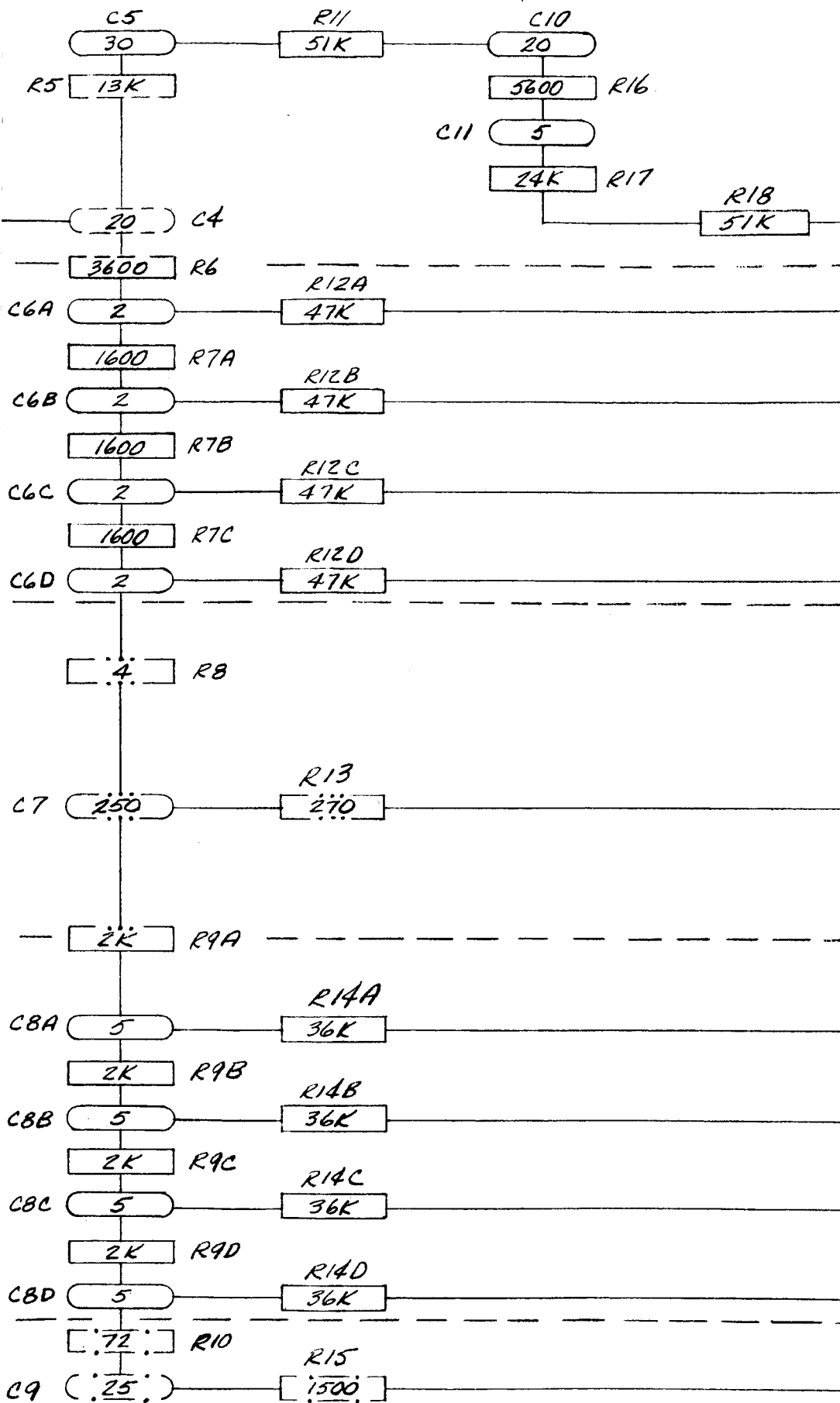
AREA 1 = .050

AREA 2 = .060

AREA 3 = .030

AREA 4 = .030

AREA 5 = .045



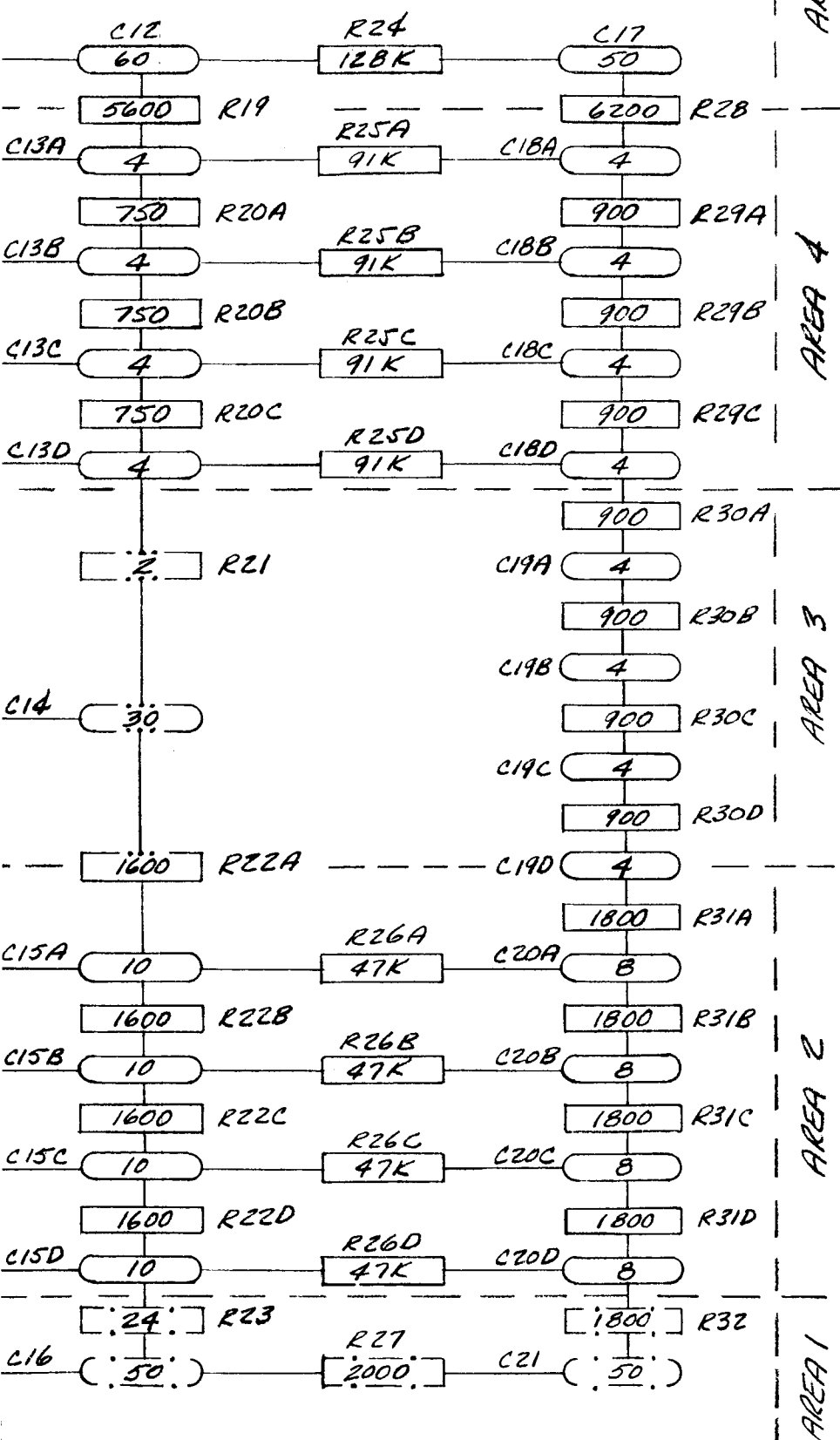
SCHEMATIC DIAGRAM OF ANAL

DRAWN BY: W. YENGER

DATE: 7-17-64

CHECKED BY:

2



OG COMPLITER SKB4523

FIGURE 57

3

The computer program proceeds by a process of numerical integration. Time is divided into periods of approximately .006 minutes. The temperature of each element and the rate of temperature change of each element is known at the start of the period. In order to save computing time, the program uses variable time intervals for the integration. When the rate of change of temperature is small the intervals used are larger, and conversely when the rate of change of temperature is large the integration interval is cut down.

During the interval, heat is accepted from the source and is conducted into the window. Heat is also radiated to space. The temperatures of each element are assumed based on previous internal temperature and previous rate of temperature change. The assumed temperatures permit a computation of net heat flow into each element, and a calculation of the temperature rise of each element as a result of this balance. The solutions to all 20 temperatures are computed simultaneously and are compared to the 20 assumed temperatures. If the solutions differ by more than a certain amount (experience with the program has shown .01 degrees R or better to be necessary to avoid large stability problems in the iteration) the assumed temperatures are adjusted and the interval is iterated again. On obtaining agreement within the test gate tolerances on all 20 temperatures, the program proceeds to the next time interval.

At every computation, the thermal properties of each element are read from the appropriate curve versus temperature. Thus the program has the ability to take into account the wide range through which material properties will vary when temperatures change over a range as great as 3500°R. For multiform fused silica the curves used were:

Thermal Conductivity given by Figure 39,

Thermal Diffusivity given by Figure 41, and

Emissivity given by Figure 44.

Specific heat was computed as needed by dividing the value of the conductivity curve by the density times the diffusivity. Density was treated as a constant (137.6 lb/ft³) throughout the problem.

The design of the antenna, disposed entirely within the window itself, creates a few unusual problems because most of the conductive elements lie along isothermal lines. The electrical design of the antenna requires that highly conductive elements cross through the window in several places. The cross conductors were made very thin so as to carry as little heat as possible. The designs analyzed used these as thin walled cylinders to minimize the electrical inductance of the elements.

To account for these short circuits, additional elements were added to the program, coupled conductively to appropriate points in the window. The analysis showed a rapid decay in the local hot spot, which has a maximum value at the metal of 1330°R above the undisturbed portion of the window, decaying to 58°R above the undisturbed portion .001 inch away and to 0°R above the undisturbed portion .003 inch away from the metal.

In effect, the thermal short circuits, which are necessary for proper electrical function of the antenna, have a negligible effect on the antenna as a whole when properly designed.

In the space vehicle it may not be sufficient to assume that the heat input is accepted only through the face which is initially flush with the ablator. As the ablator wears away, some surface of the antenna window (which experiences little or no ablation) becomes exposed to heat input. The effect is smaller than might be anticipated because although additional heating is picked up on the windward surfaces, additional heat rejection area is created for radiation to space. Compensation for this effect is made by assuming the recession of the ablator to half its initial thickness in proportion to the

* See Figures 50 and 51.

integral of the heat pulse from the start of the problem, and allowing all elements so exposed to exchange heat with the source and with space. Space was taken at 560°R to account for the fact that the heat sink might be some part of the earth.

The results of this calculation procedure on a typical prism-like window are shown as follows:

Figure 48 shows temperature distribution at outer surface, mid-plane and inner surface for overshoot entry of an antenna subjected to pulse shown by Figure 2.

The antenna was presumed to be flush with the ablator; hence, 1.4 inches thick. No compensation, as described above, was made for exposure of additional surface as the ablator was worn away, nor were the thermal short circuits taken into account.

Figures 49, 50 and 51 show the same problem as reported in Figure 48, rerun with compensation for the ablator recession and for local thermal short circuits.

Differences exist between this case and the previous one, but they are very small. From Figure 49 it can be seen that the inner surface temperature in the undisturbed window remote from the thermal short reaches 1420°R after compensation, at 26 minutes from the start of the problem whereas it had been 1400°R in the noncompensated case. The maximum difference noticed in the outer surface temperature occurs after about 14 minutes when the outer surface is at 1760°R compared to 1640°R in the uncompensated case.

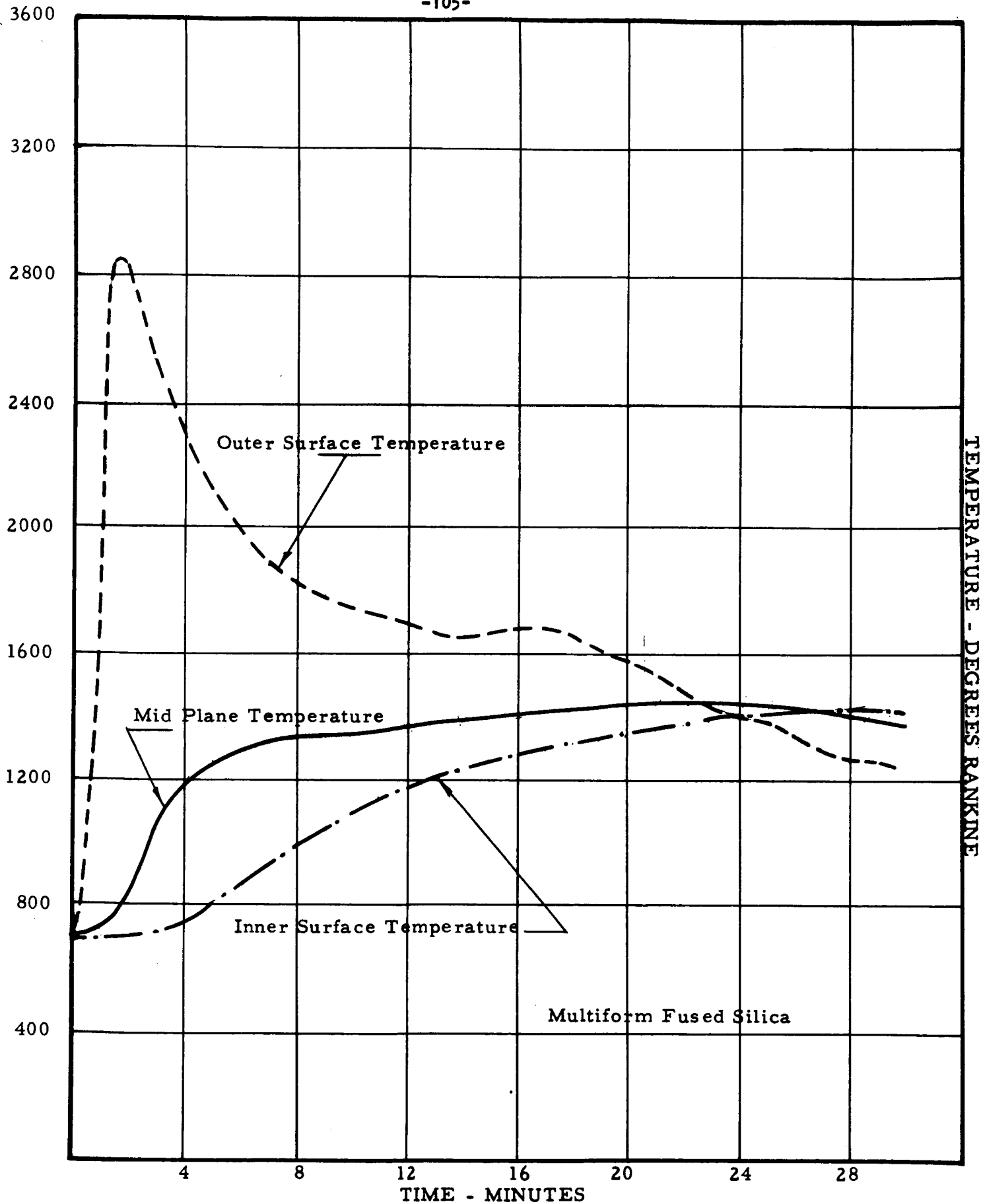


Figure 48 Temperature Distribution In Prism Shaped Window. Simplified Problem Statement. Surrounding Ablator Does Not Change In Thickness. Antenna 1.4 Inches Thick Exposed To Overshoot Entry Per Figure 2

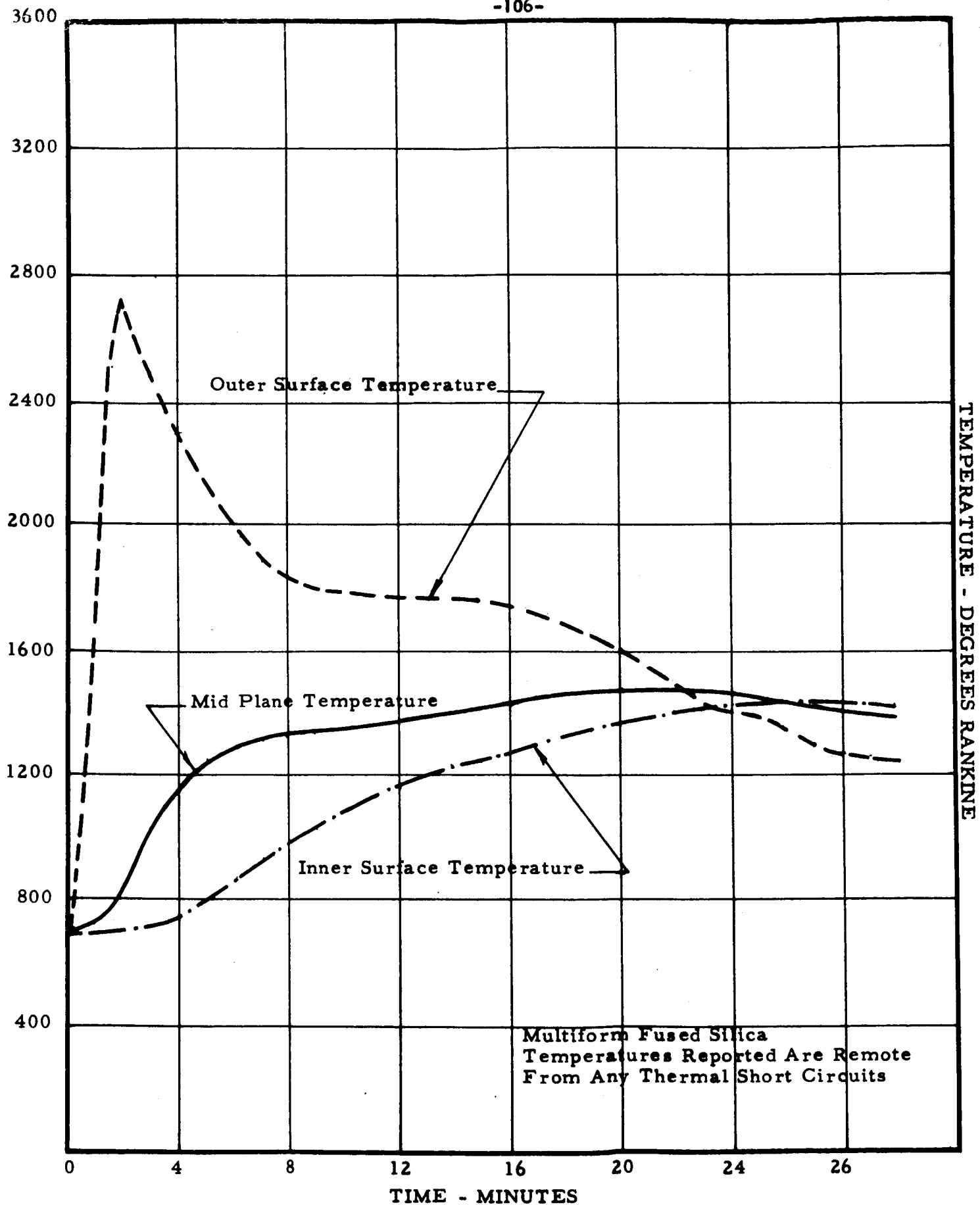


Figure 49 Temperature Distribution In Prism Shaped Window. Ablator Recedes 0.7 Inch During Heat Pulse. Antenna Exposed To Overshoot Entry Per Figure 2

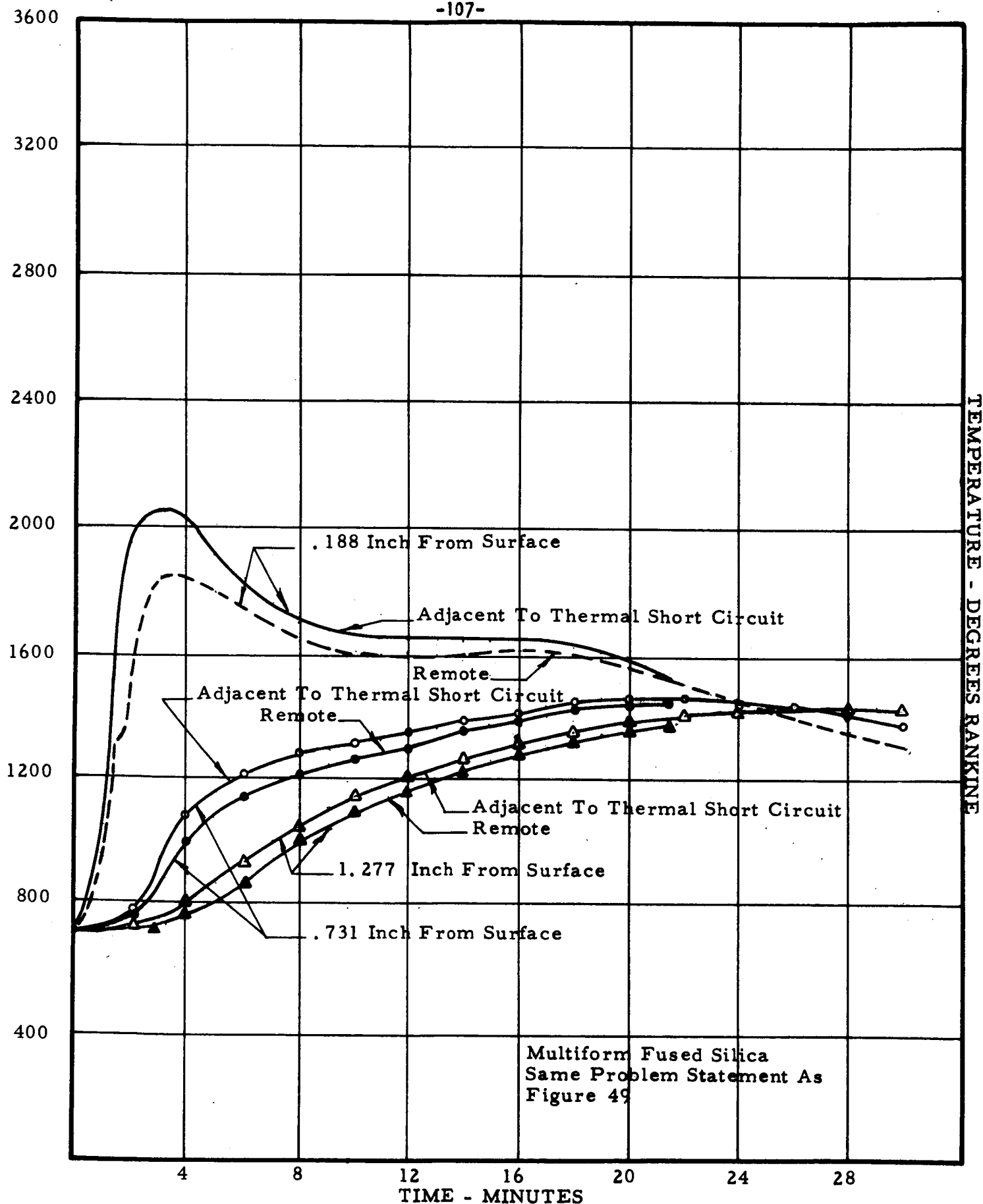


Figure 50 Temperature Distribution In Prism Shaped Window As Influenced By Local Thermal Short Circuits. Antenna Exposed To Overshoot Entry Per Figure 2

Figure 50 shows the effect of the thermal short in a small area adjacent to a platinum conductor extending from .188 to 1.277 inches below the surface. For the reader's convenience, temperatures in the undisturbed window at similar locations are also given. It is to be noted that these do not coincide with the locations in the window (hot side or mid-plane, or cold side) chosen as standard reporting points for previous curves such as those of Figure 49.

Figure 51 shows the effect of the thermal short in a small area adjacent to a copper conductor extending from .588 to 1.275 inches below the surface. Again, to facilitate reading, temperatures in the undisturbed window at similar locations are also given.

Because the heat flow is nearly one-dimensional, small changes in slab form factor do not have much effect. This is brought out by Figure 52 which shows the effects of the same input as for Figure 48, but applied to a 3 inch round specimen rather than the 2.5 x 9.5 inch one. The round antenna has slightly lower temperatures (about 40°R lower at the inner surface compared to the prism shape) because it offers a slightly more favorable volume for diffusion of heat energy compared to available surface for heat input.

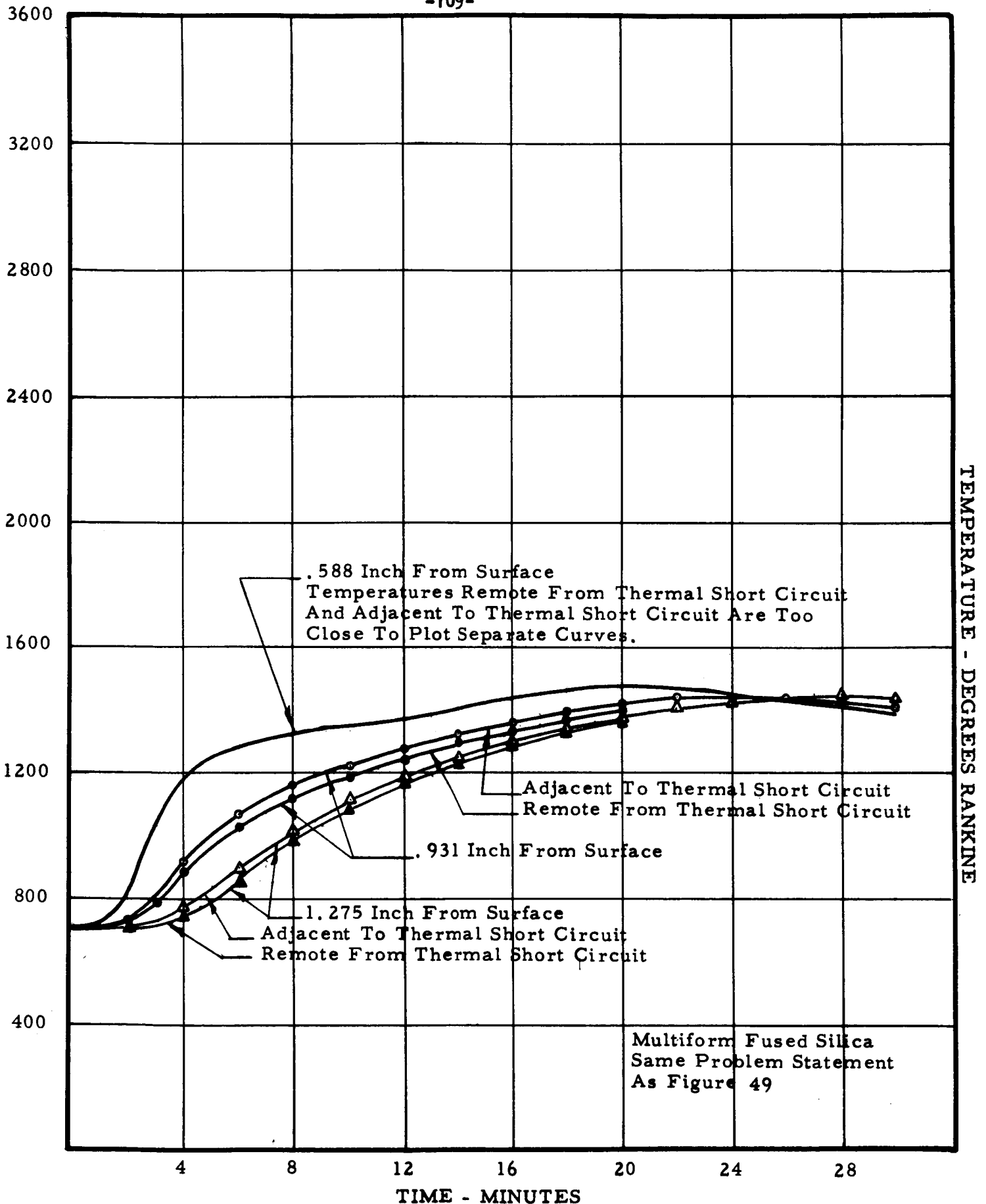


Figure 51 Temperature In Prism Shaped Window As Influenced By Local Thermal Short Circuits. Antenna Exposed To Overshoot Entry Per Figure 2

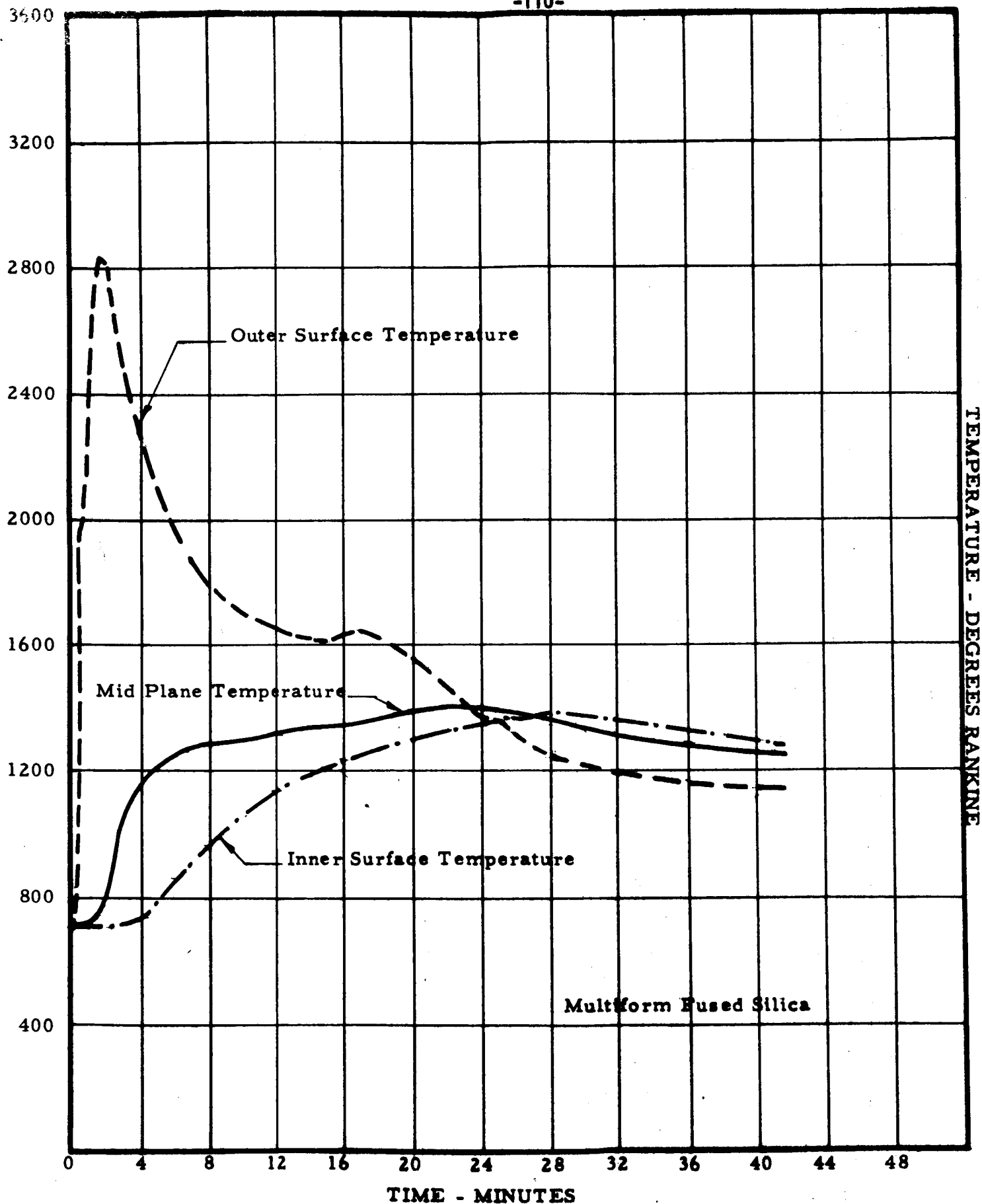


Figure 52 Temperature Distribution In Conical Frustrum Window. 3 Inch Top Diameter. 60° Included Angle. 1.4 Inches Thick. Antenna Exposed To Overshoot Entry Per Figure 2

Because this difference was trivial, it was concluded that any results obtained by further study of the elongated prism shape would apply sufficiently well to the other form factors (shorter prism, conical frustrum) that were likely to be used for this type of antenna.

In the course of the study, it was observed that the most severe thermal problem occurred on overshoot-type entries. The heat pulse, although lower in peak value, exists for so much longer a time (30 minutes) that much more heat diffuses to the inner surface where it can affect the spacecraft.

The following comparison of the various heat pulses on similar slabs* illustrates this point:

Figure 53 shows the temperature reached during an overshoot entry as a result of the application of a heat pulse as shown by Figure 2. It is to be noted that a maximum inner surface temperature of 1510°R is reached in 28 minutes.

Figure 54 shows the temperature reached during an undershoot entry as a result of the application of a heat pulse as shown by Figure 1. Note that the maximum inner surface temperature is 1470°R and that it

*

These slabs are semi-infinite slabs 1.4 inches thick. This analysis was made early in the program when interest was centered on cavity type structures. However, the information is pertinent to prism shaped and conical windows and other configurations of interest.

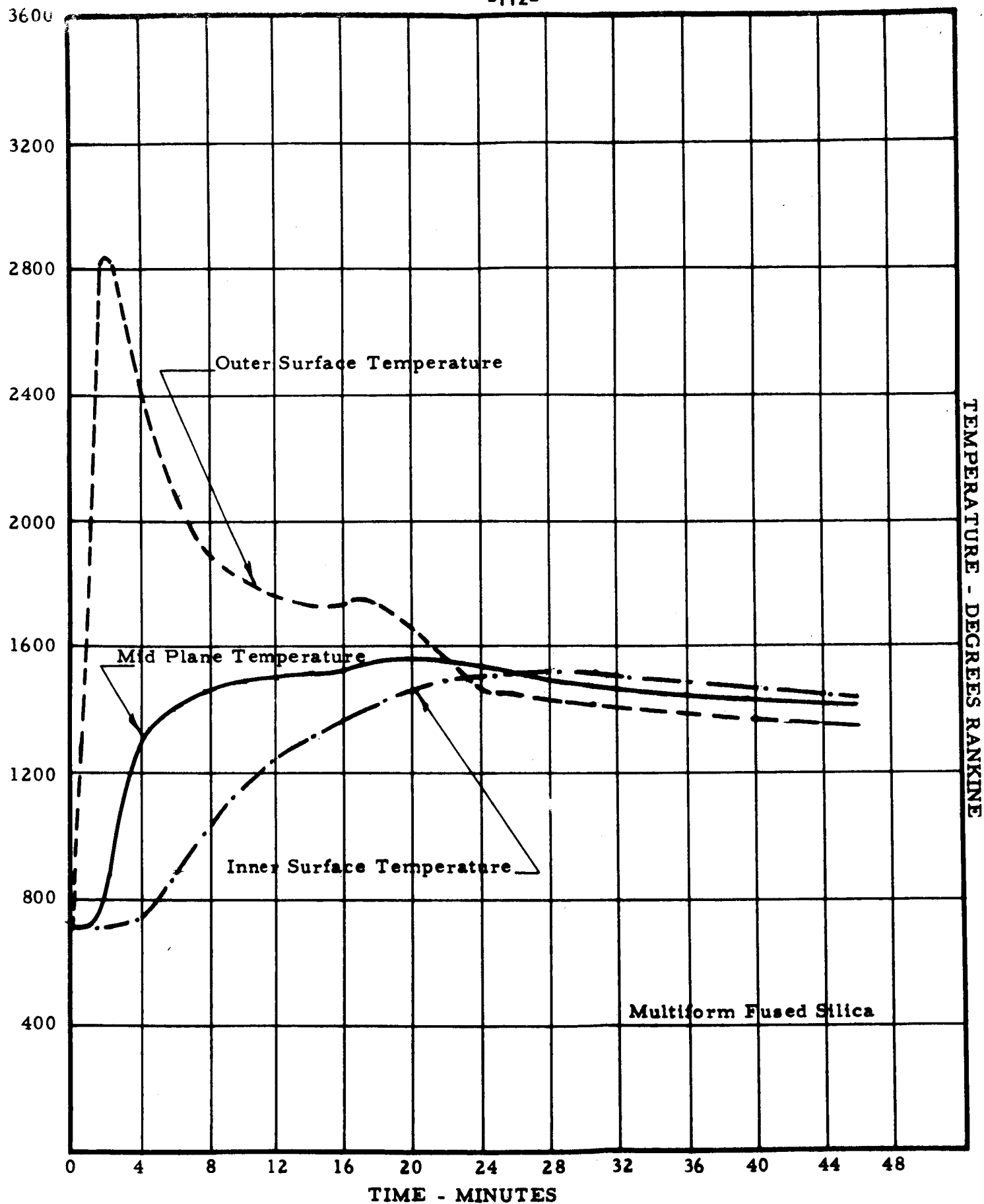


Figure 53 Temperature Distribution In Semi Infinite Slab Window 1.4 Inches Thick.
Antenna Exposed To Overshoot Entry Per Figure 2

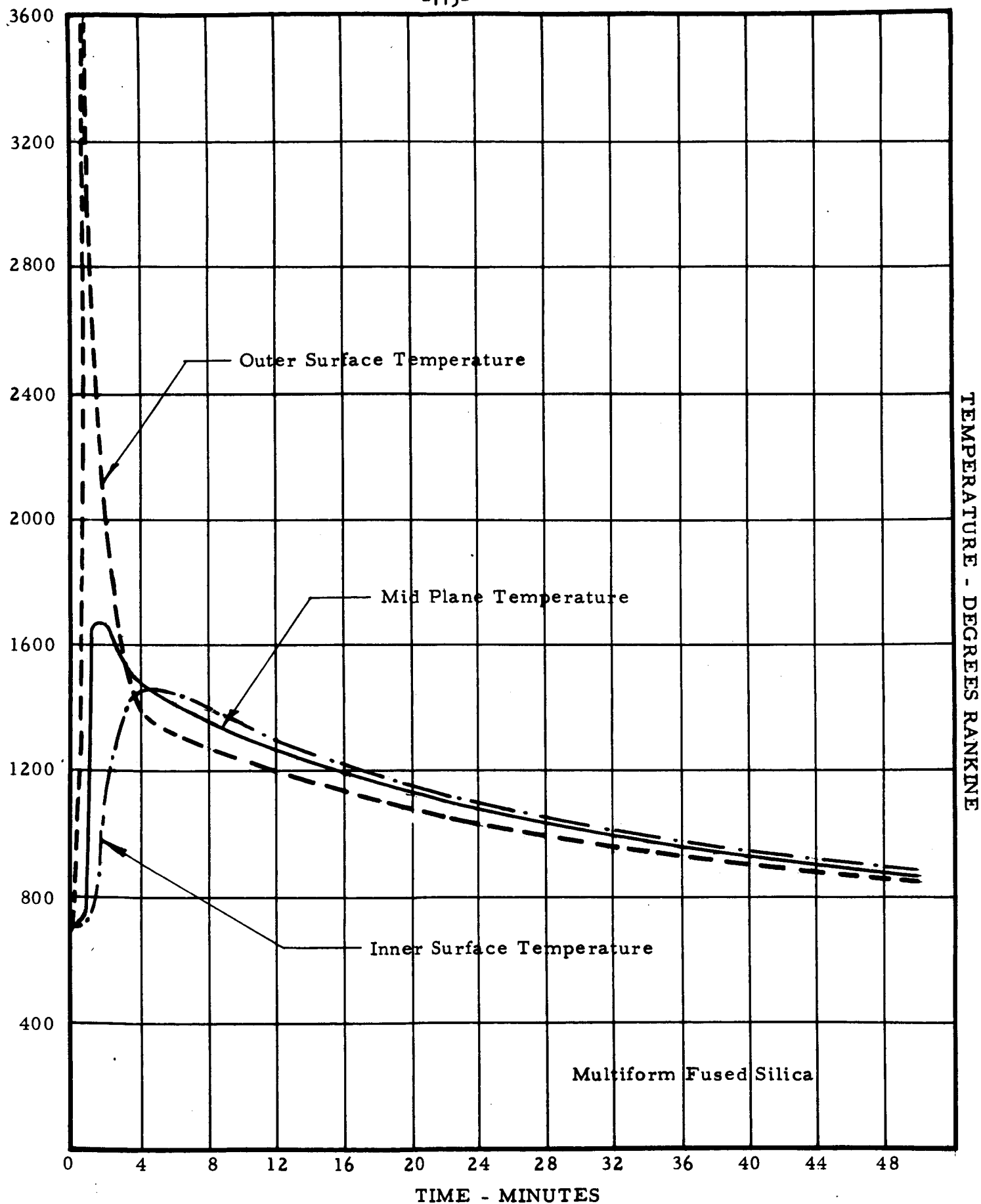


Figure 54 Temperature Distribution In Semi Infinite Slab Window 1.4 Inches Thick. Antenna Exposed To Undershoot Entry Per Figure 1

is reached in five minutes.

Figure 55 shows the temperatures reached during an overshoot entry by a 1.3 inch thick window subjected to the heat pulse of Figure 47. Note that the maximum inner surface temperature is 1560°R after 28 minutes.

Finally, Figure 56 shows the temperature effects of an under-shoot entry on a 1.3 inch thick window subjected to the heat pulse of Figure 46. Note that the maximum inner surface temperature is 1040°R after 16 minutes.

In all cases, the computer was programmed to assume that no ablation took place unless the temperature exceeded 3600°R . In that case, heat of ablation was to be set at 5,500 BTU/LB and a sufficient amount of material was to be sacrificed to hold temperature at 3600°R . In no case examined did this set of conditions take place. In Figure 54 the temperature of 3600°R is touched but no ablation takes place because the temperature is not exceeded.

In all cases the starting point of the program assumes a soak at 250°F (710°R). This is the highest temperature specified for steady state operation of the system and there is no reason to presume that the antennas will be at any lower temperature at the start of the entry heating pulse.

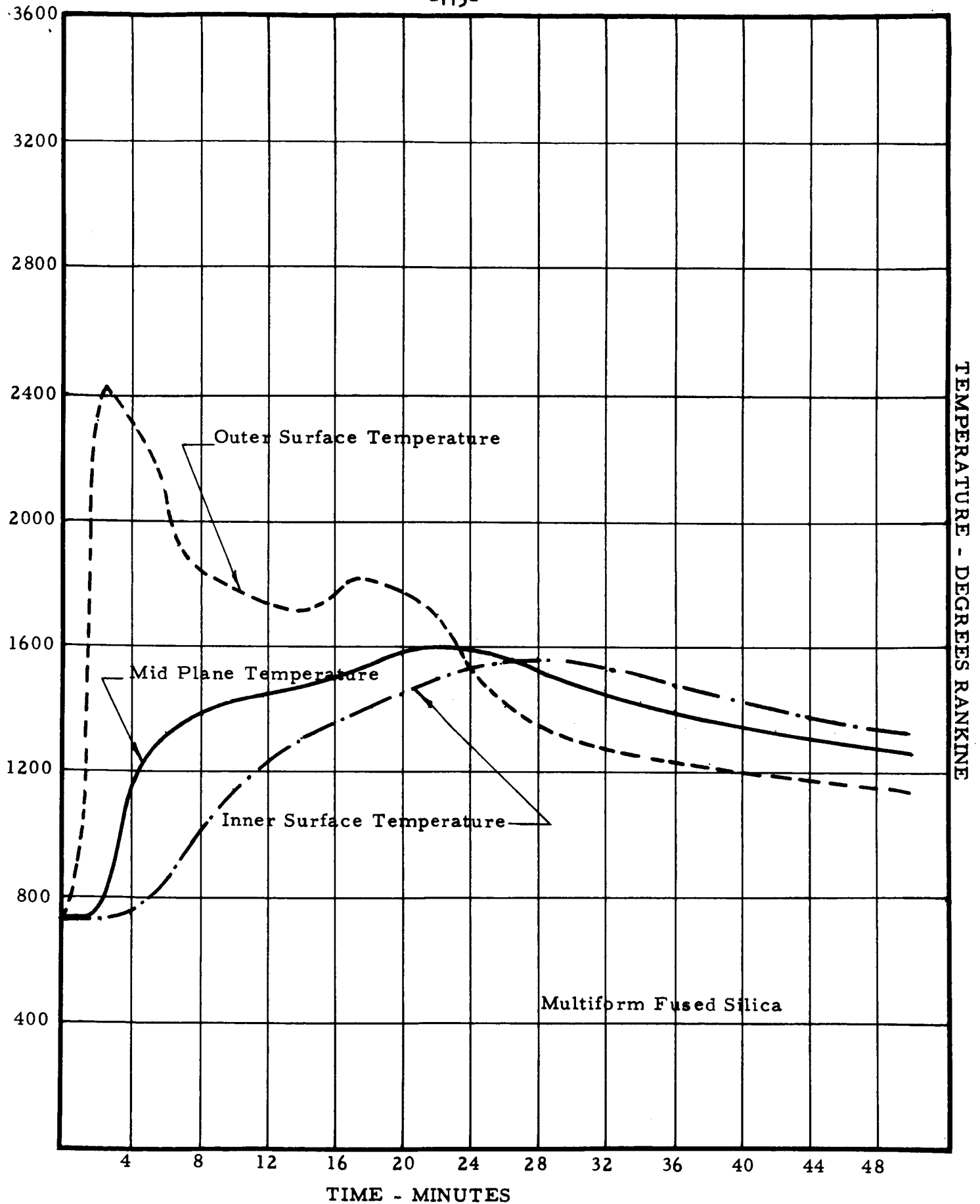


Figure 55 Temperature Distribution In Semi Infinite Slab Window 1.3 Inches Thick. Antenna Exposed To Overshoot Entry Per Figure 47

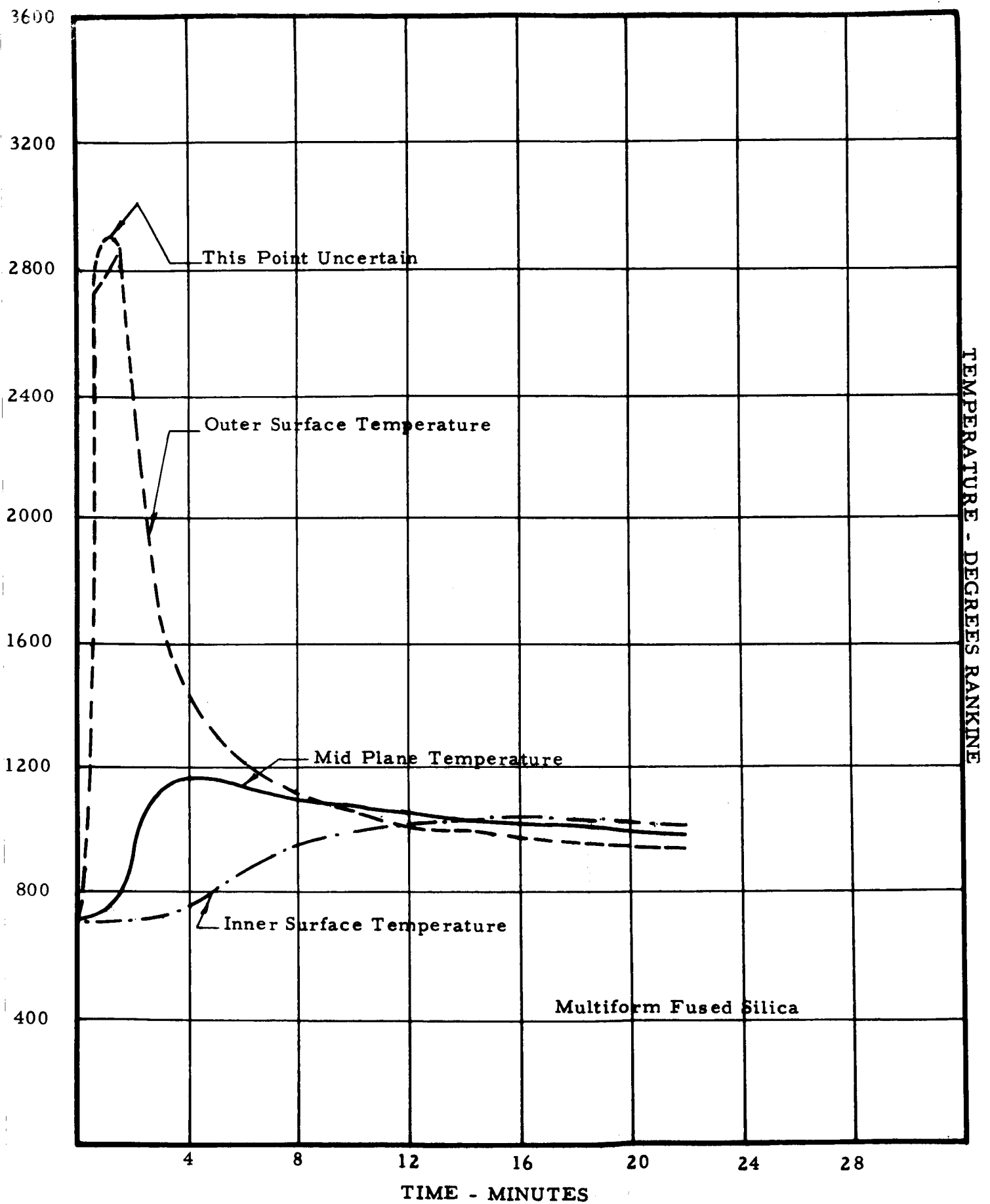


Figure 56 Temperature Distribution In Semi Infinite Slab Window 1.3 Inches Thick. Antenna Exposed To Undershoot Entry Per Figure 46

Attachment to the Spacecraft - Criteria to be met at the interface between the antenna and the spacecraft are these:

The stainless steel honeycomb forming the heat shield structure must not be heated above 600°F (1040°R) during entry while it is retaining the ablator and sharing dynamic loads. This period may be considered to end about 34 minutes after the start of entry or about 10 minutes after the heat pulse is over (about 24 minutes after start of entry).

The inner walls of the spacecraft must not be subjected to temperatures over 200°F during the same interval described above.

With the recommended design which locates the antenna entirely within the ablator, the latter condition will present no serious problem so long as the former is met.

Examination of Figure 49 shows that the maximum temperature at the underside of the window will be 1440°R, reached in 28 minutes. The spacecraft must be protected against this temperature, which is 400°R above that permissible by some combination of heat sinks and heat insulators. Figure 4 showed the design that was evolved to accomplish this, It will be seen that it comprises an insulating flange to support the antenna window and a heat shield and sink in an air gap between the inner surface of the antenna window and the spacecraft outer metal surface.

To compute the heat flow in the flange during the course of its design, a simple analogue computer was built. In the analogue, charge represented heat, voltage represented temperature, resistance represented the inverse of thermal conductivity, and capacitance represented mass times specific heat.

Figure 57 is a schematic diagram of the flange which is electrically analogous to the thermal model, for computer time running 144 times faster than real time.

Figure 58 shows the temperature in the spacecraft wall just under the antenna flange for a heat input per the "cold side" of the antenna window of Figure 49.

The limit temperature of 600°F in the spacecraft heat shield is reached about 45 minutes after the start of overshoot entry. The heat pulse is complete about 27 minutes after the start of entry at which point the spacecraft heat shield has been heated to 450°F . Since the critical temperature is not reached for 18 minutes after the heat pulse is over, it is presumed that the spacecraft will have landed and that soak-back of stored heat energy into the cooler portions will no longer be a problem. The results achieved with the analogue are conservative in that the input temperature was kept at 1440°R after 30 minutes rather than dropped to allow for the slow cooling which will take place as a result of re-radiation.

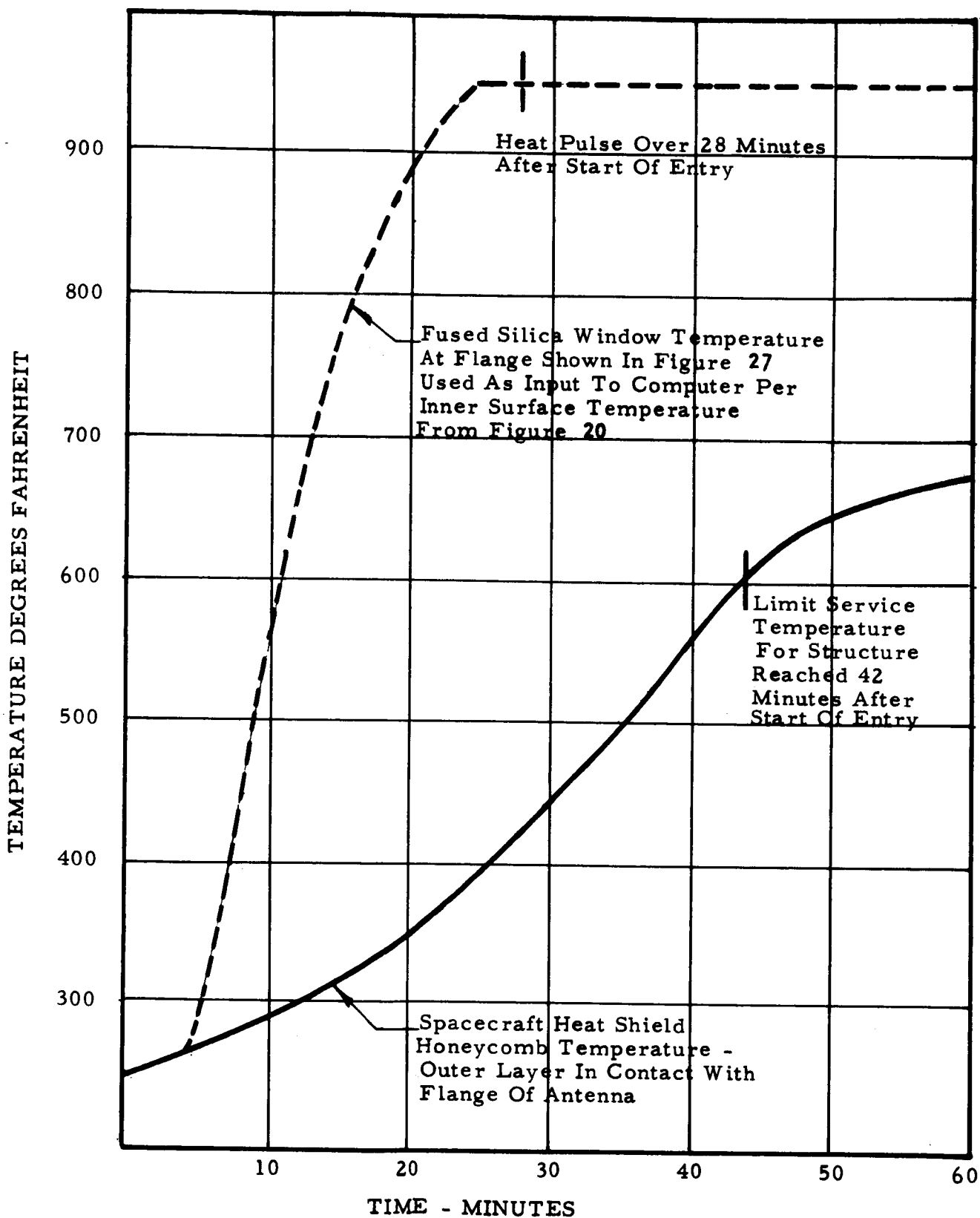


Figure 58 Temperature - Time Plot Of Spacecraft Heat Shield Wall Under Antenna. Analog Computer Output

4.0 FINAL DESIGN AND LABORATORY PROTOTYPES

4.1 Recommended Designs

The ablative shield type of antennas evolved during the work described in the preceding section are recommended as satisfactory for use on the Apollo Command Module.

The principal materials would consist of the following:

Window - Multiform fused silica such as Corning Glass Code 7941 or equivalent. This material offers very low loss, acceptable dielectric constant, low thermal diffusivity, and extremely stable properties over the temperature range of interest.

Flange - Imidite 1850 fiberglass laminate. This material offers low thermal conductivity and short time temperature resistance to 1200°F.

Conductors - Copper, silver or platinum as determined by final construction technique requirements.

Heat Shield-Sink - Gold plated beryllium.

Sealer - Dow-Corning 325 Compound or equivalent. This would be a resilient sealer to take up the space between the antenna and the ablator to absorb difference in linear dimensions between the ablator and the antenna arising from thermal and mechanical distortions of the spacecraft.

The sizes and shapes of the antennas would be approximately those shown by Figure 30. In shape, each antenna would be a frustrum of a pyramid. The height would, in general, correspond to the thickness of the ablator covering in the areas where they were located. This would

be in the neighborhood of 1.4 inches. The antennas could be made as much as 30% lower in height than this if need be, with minor loss of efficiency except at the lowest frequencies. Similarly, the quartz cover could be increased by a comparable amount without difficulty.

Length would be dependent upon the operating frequency, varying from 1.13 inches at C-band to about 9.5 inches at VHF. Width would vary from about 1.25 inches at C-band to a maximum of about 2.5 inches at VHF.

Except for C-band, the antennas would be constructed of four flat, fused-together, silica layers with metallic layers deposited on each and interconnected as described elsewhere in this report.

All the layers would be captured within a slip cast fused silica cover which would be mounted to the spacecraft by a fiberglass flange. The flange would be arranged to contact the antenna at three points only so that distortions of the spacecraft would not be transmitted to the fused silica. All non-contact points would be relieved and filled with an elastic sealer. The flange would have three layers. The upper part would capture the fused silica antenna proper; the second part would support the first and extend inward sufficiently to support and complete the capturing of the silica block; the bottom

layer would support the other two and entrap a polished metal reflecting shield located between the antenna proper and the outer metal surface of the capsule. This shield would function not only as a thermal barrier but also as an electrical ground plane for the antenna.

The entire system would be shaped to the curvature of the spacecraft at the point of installation. Installation would require four to fourteen threaded pads in the heat shield honeycomb structure, depending upon antenna size, and a clearance hole on the order of 1.5 inches in diameter for the radio frequency cable connector. A block of the spacecraft ablator would have to be removed to provide access to the antenna. This would require an edge seal for this block and a seal between the block and the antenna, probably of Dow Corning 325 ablator or equivalent resilient material. It would be feasible to cure the antennas with the spacecraft ablator should it ever prove desirable to do so.

No mention has been made thus far of the intended means of securing thermal insulation between the antenna proper and the input cable. The base region of the antenna will, of course, reach a temperature in the neighborhood of 1400°R and the input cable should be kept around 600°R maximum. This is not a difficult problem. The techniques used for designing the antenna proper are applicable here

and their straightforward application can be expected to yield a solution readily. Metal conductors would be made non-structural, consisting of thin plated coatings on insulators. Series insulators in the form of capacitors could be added if required.

4.2 Description of Laboratory Models

The scope of the study program did not require that laboratory models be made with curvature, nor be constructed in accordance with techniques that would be used for operational units. The models were fabricated of flat layers of quartz which were glued together with epoxy cement, rather than fused as shown by the two sketches on Figure 59. Metallic layers were constructed of copper foil so that adjustments could be made easily. A margin was left about each metallic layer to correspond to the material which would, in the final design, be part of the cover piece and not part of the layered structure.

Figure 60 shows the assembly of the largest of the laboratory model antennas that were furnished, corresponding to the VHF telemetry and beacon requirements. Other models, except C-band, were constructed in a similar fashion except for the length and width of the pieces. Electrical performance of these antennas is influenced by the presence of the ablator which would surround the antennas in

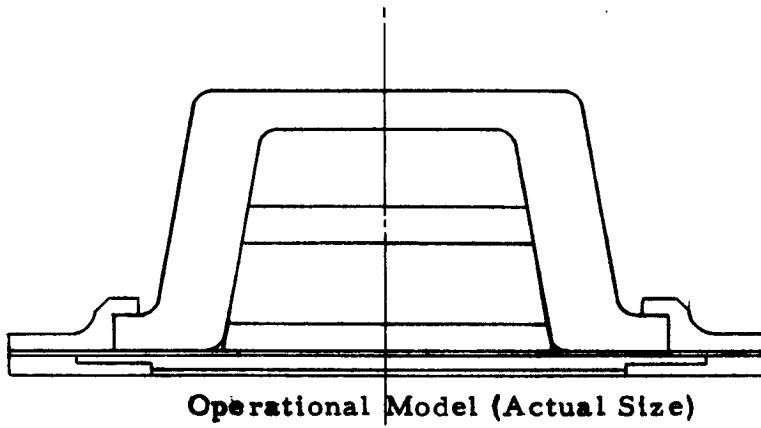
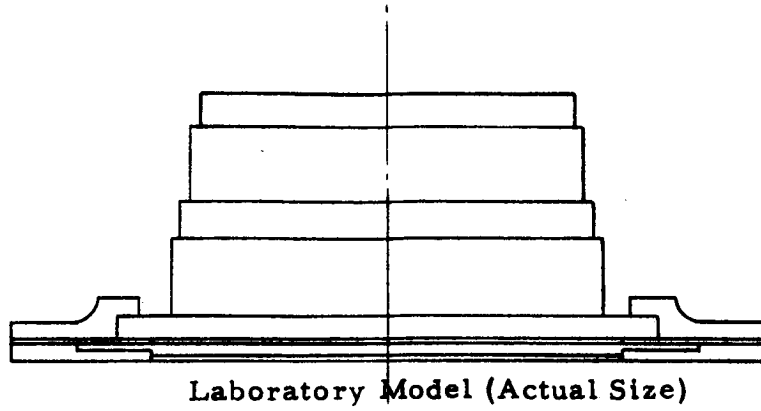
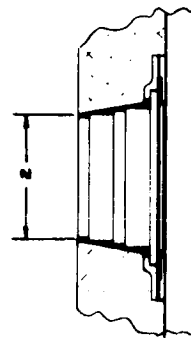


Figure 59 Comparison Between Laboratory Model Design And
Operational Model Design Of Antennas



- 1. determine absolute VAE telemetry.
- 2. size types of antennas may be assembled by using less than numbers of details should.
- 3. number of mounting holes a hole pattern will change for different retaining rings.

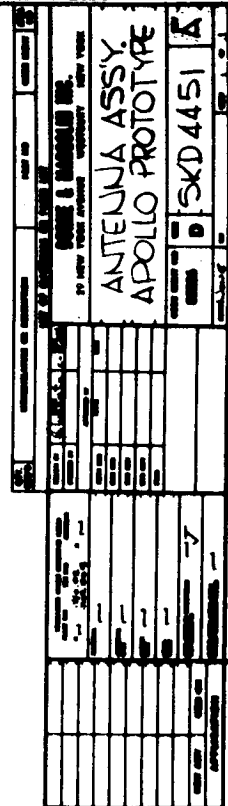
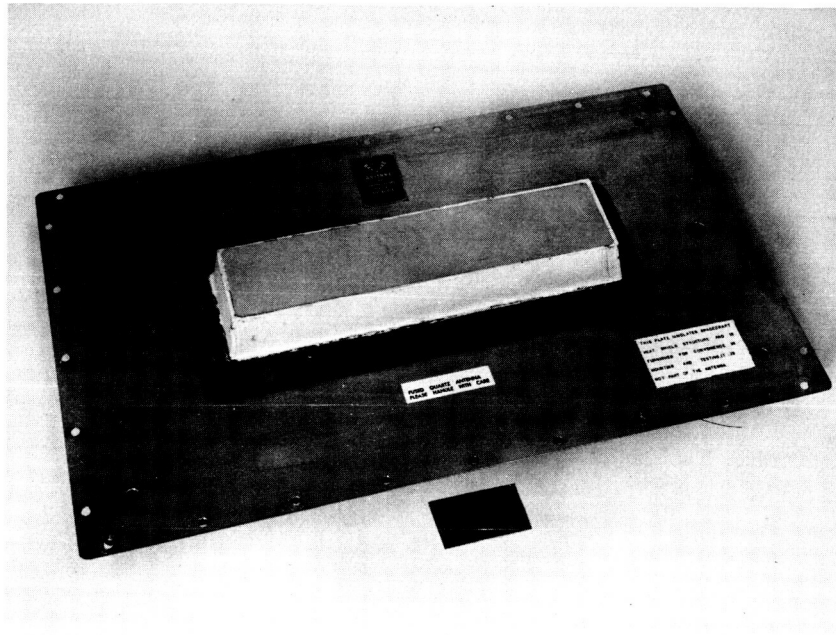


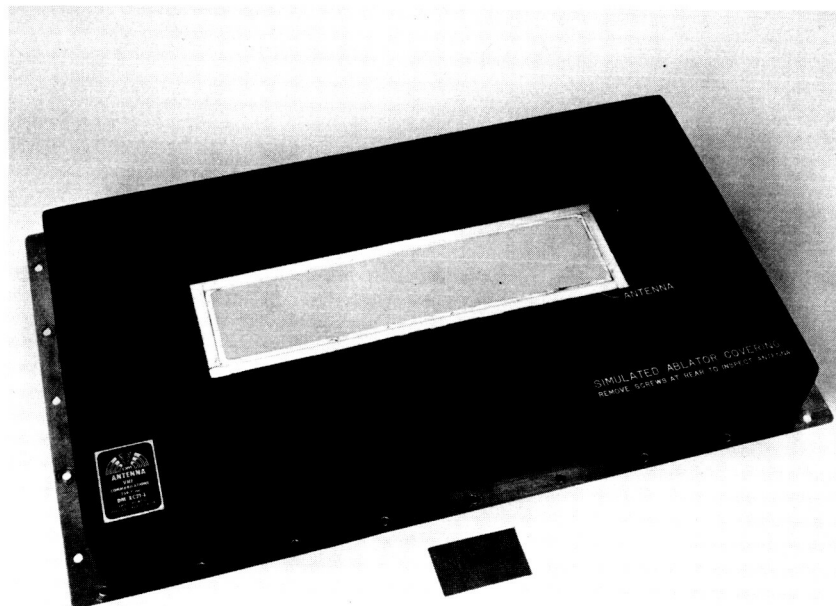
Figure 60 Assembly Drawing For Laboratory Prototypes For VHF Through S Band

actual service. So that the antennas would be adjusted for proper performance in the intended service environment, and to demonstrate this performance, a small block of material with electrical properties similar to those expected of the service ablator material (dielectric constant 1.85-1.95 loss tangent .015) was furnished with each antenna. The antenna and simulated block of ablator were mounted on a $\frac{1}{2}$ inch thick ground plane consisting of a metal clad plywood sheet simulating the spacecraft heat shield upon which operational antennas would be mounted. The antennas of the quartz sheet construction were similar in appearance except for their size. Photographs of the largest and the S-band antenna, which was similar, are shown by Figures 61 and 62, respectively.

The layers were composed of clear fused silica, because of its ready availability, rather than multiform fused silica which will be required in final units. Metallic foil elements were interleaved between the silica elements to form the electrical structure. Interconnections, required in three places, were made with solid metallic rods. These would be thin tubular metal plated material in operational models. The outermost foil is the principal radiator, and is connected to one of two separate pieces which together make up the lowest layer of the foil, by a tubular element which crosses three of the layers. The feed point is connected to the second layer which forms the series



Antenna Mounted on Ground Plane



Antenna on Ground Plane with
Ablative Surrounding Material

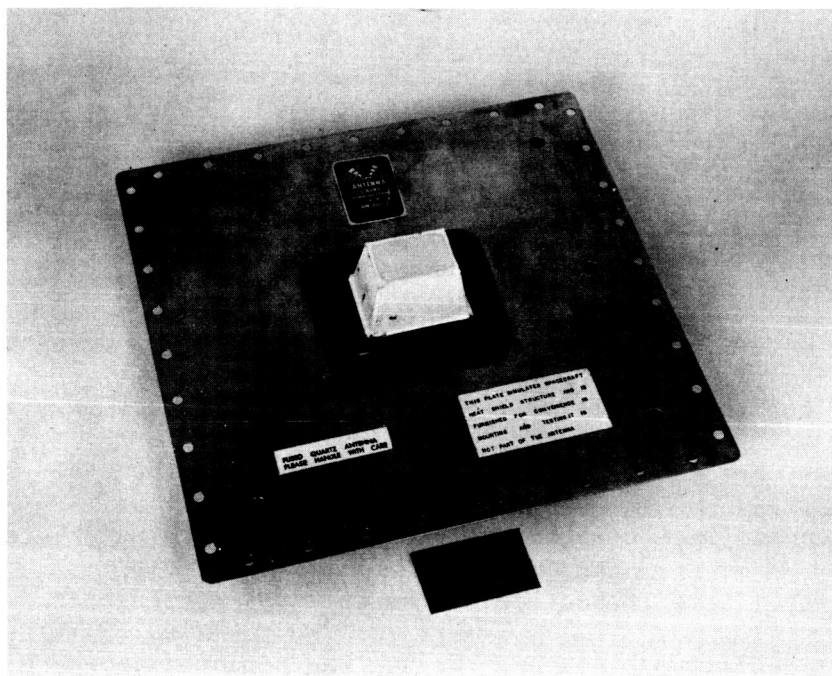
FIGURE 6/ - LABORATORY PROTOTYPE OF VHF ANTENNA

capacitor with the radiator. The thermal calculations discussed earlier show that in no entry maneuver examined will any of the fused silica be melted or vaporized. However, even if loss were to occur, so long as vaporization did not continue down to the second element some performance, although substantially reduced, will be available with the second layer functioning as the radiator.

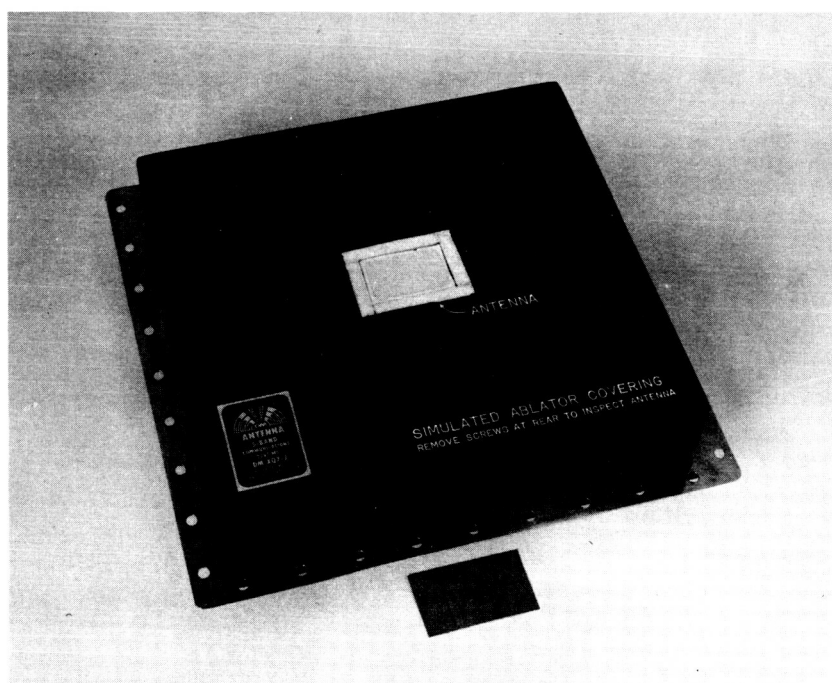
The rod which connects the feed point and the input capacitor is connected to the piece of foil at the lowest layer which forms the shunt capacitor portion of the feed network.

As mentioned previously, all layers of the laboratory model antennas were cemented together using an unfilled epoxy adhesive. In operational models such adhesive bonds would fail during the entry maneuver temperature rise, and retention would depend only upon the capturing cover layer. Additional reliability would be obtained if the antenna layers were fused together after the metallic portions were fired or plated on. This technique is believed feasible using a fused silica frit in a controlled atmosphere furnace, and it is expected that it would be used for operational models.

The thickness of the lowest layer, which in the laboratory model also serves as the flange, is .125 inch. The operational



Antenna Mounted on Ground Plane

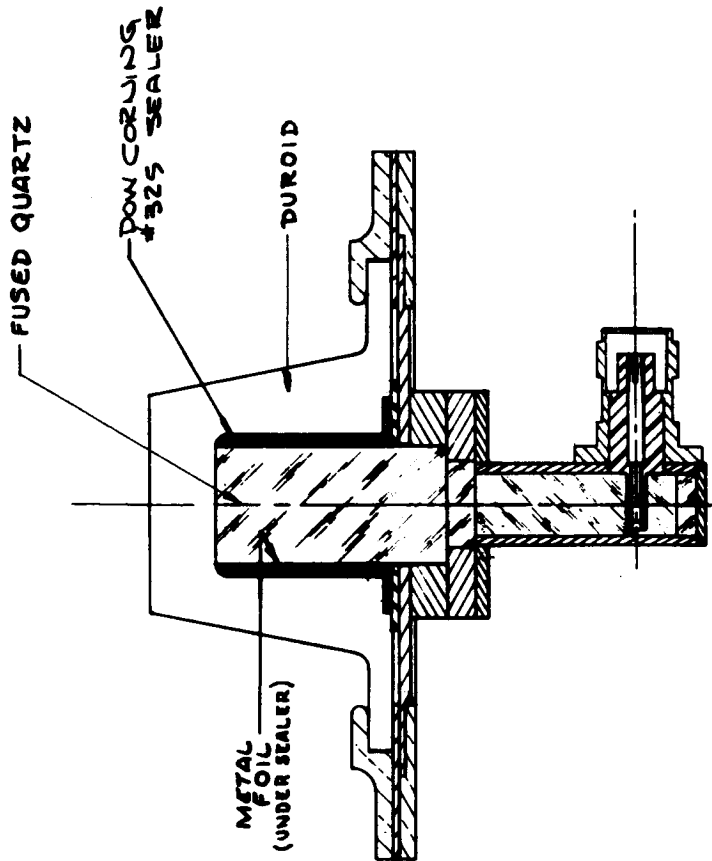


Antenna on Ground Plane with
Ablative Surrounding Material

FIGURE 62 - LABORATORY PROTOTYPE OF S BAND ANTENNA

model flange should be substantially heavier than this to make it stronger. The outer surface of each of the prototypes was covered with a 1/32nd inch thick layer of teflon for impact protection. It is intended that operational units also include this. The sides of each of the antennas were covered by a layer of Dow Corning 325 sealing compound. To facilitate inspection of the antennas a thin crack was left between the ablative block and the sealing compound on the antenna, thereby permitting the block of Stycast material to be lifted off. The holes in the Stycast blocks into which the antennas were fitted were lined with one quarter inch thick teflon. Because teflon is much less lossy electrically than the ablative material, this had the effect of reducing the dielectric loss as it would be if the antennas were slightly larger. Because the efficiency turned out to be quite good, and because the curvature of the actual spacecraft will tend to improve electrical efficiency, this size increase would probably not be required in operational models.

The basic design of these units provides for the addition of an input series resonant circuit that was omitted from the prototypes. Such a circuit would slightly increase both the bandwidth and the thermal insulation. Because it would increase the complexity, its addition may not be desirable. This matter would be resolved during a final design.



VIEW SHOWN WITH CONNECTOR
ROTATED 60° FOR CLARITY

NOTE
1. SEE L/M 24588 FOR PARTS LIST

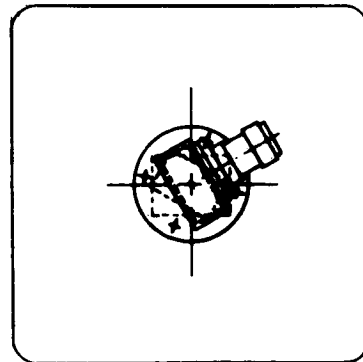
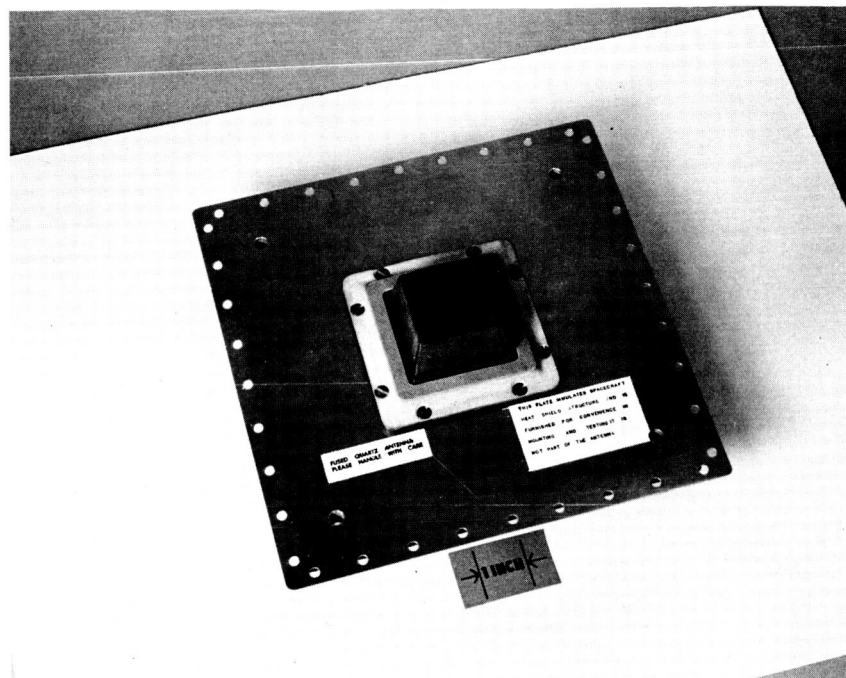
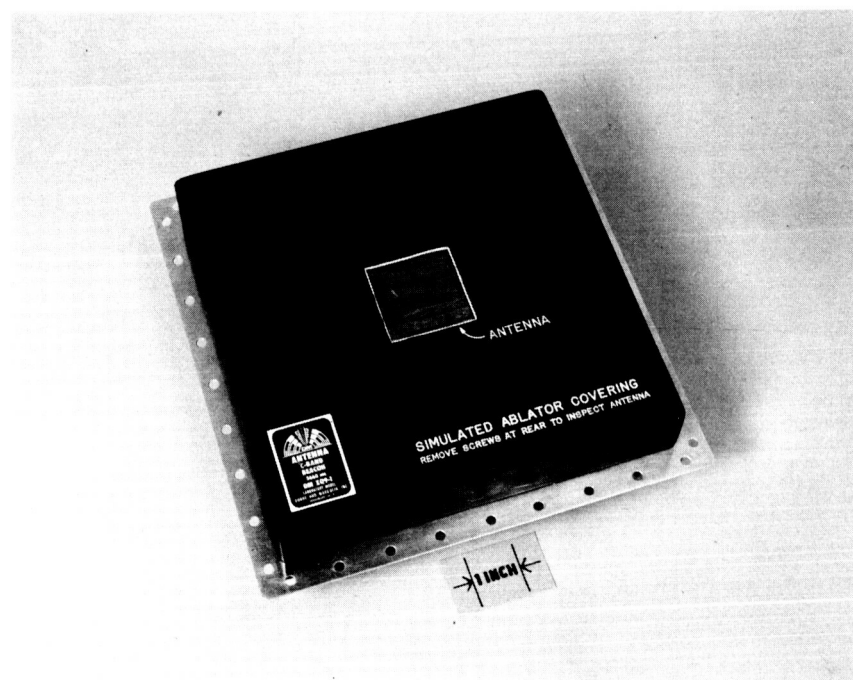


Figure 63 Layout Of C Band Antenna

LAYOUT 'C' BAND ANTENNA
SKC 4588
DWN 8-1-64 f. Wadsworth
PROS 1791
SCALE 2/1



Antenna Mounted on Ground Plane



Antenna on Ground Plane with
Ablative Surrounding Material

FIGURE 64 - LABORATORY PROTOTYPE OF C BAND ANTENNA

The C-band prototype construction can be seen in Figure 63 (photographs of the prototype are shown in Figure 64). The waveguide is sufficiently long that the temperature at the feed point does not exceed 400°F at the termination of the heat pulse. Acting as a transition between the high dielectric constant fused silica and free space is a reinforced teflon cover made of Duroid 5650. This cover has excellent low temperature ablation characteristics similar to those of teflon. The protection will recede as the heat pulse progresses and will expose the open end of the waveguide when about half of the heat pulse (in terms of BTU's per square foot) is over. During the remainder of the pulse the heat input is fairly constant at 4 BTU's/square foot-second. The outer surface of the fused silica reaches a temperature of about 2090°R, when radiative heat loss rate to space equals the heat input rate. This high temperature diffuses through the fused silica, producing the temperature after 25.8 minutes shown by Figure 65.

Two design features of the C-band antenna are required to isolate the high temperature of the silica portion of the waveguide from the mounting structure. (1) The waveguide walls are composed in the portion of the antenna extending beyond the mounting surface of metal foil. This foil is interrupted by a capacitive gap, so that high temperatures are not conducted into the mounting structure. (2) In addition, the fused silica will be relieved from contact with the

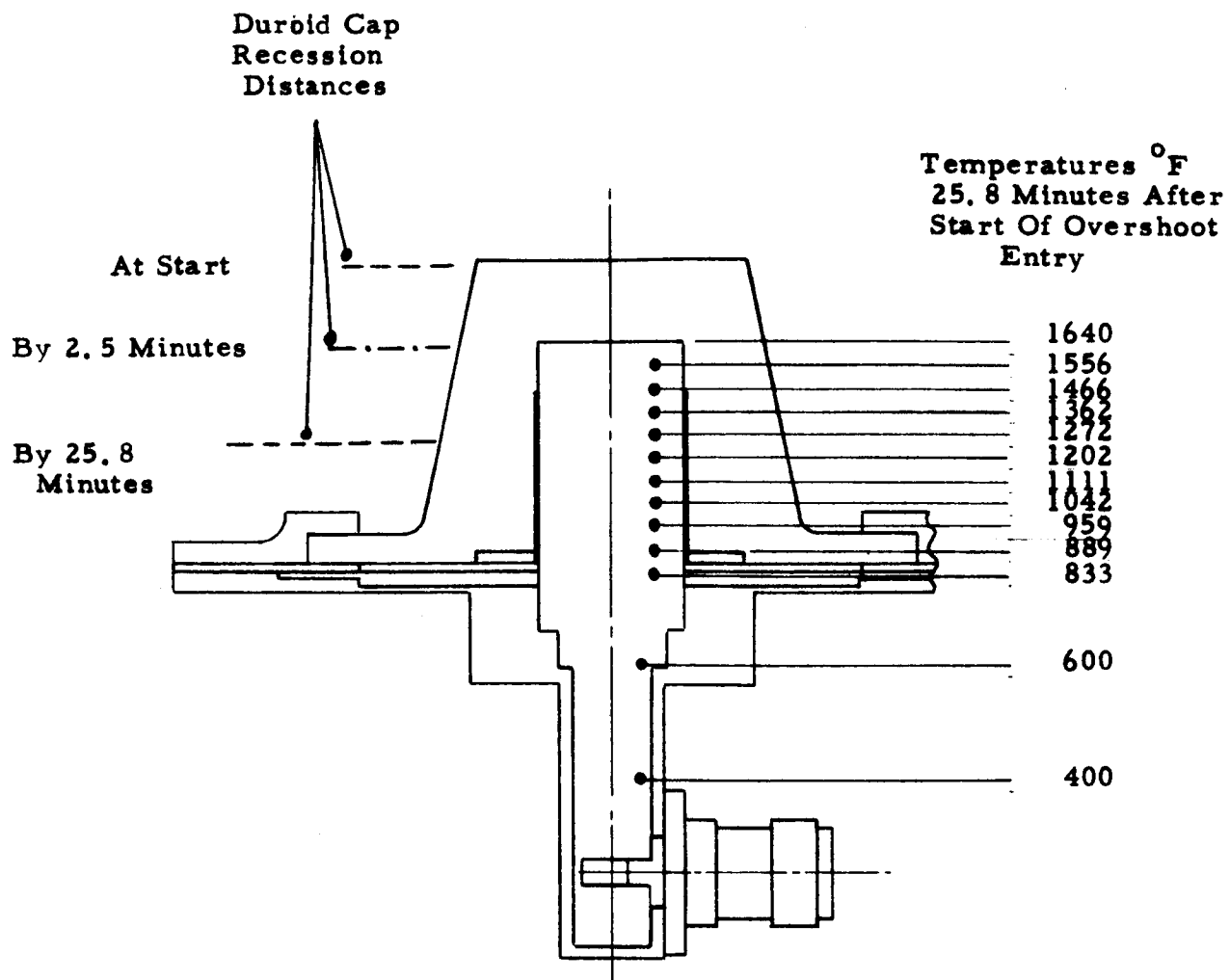


Figure 65 **Temperature Profile In C Band Antenna At Completion
Of Overshoot Entry Heat Pulse**

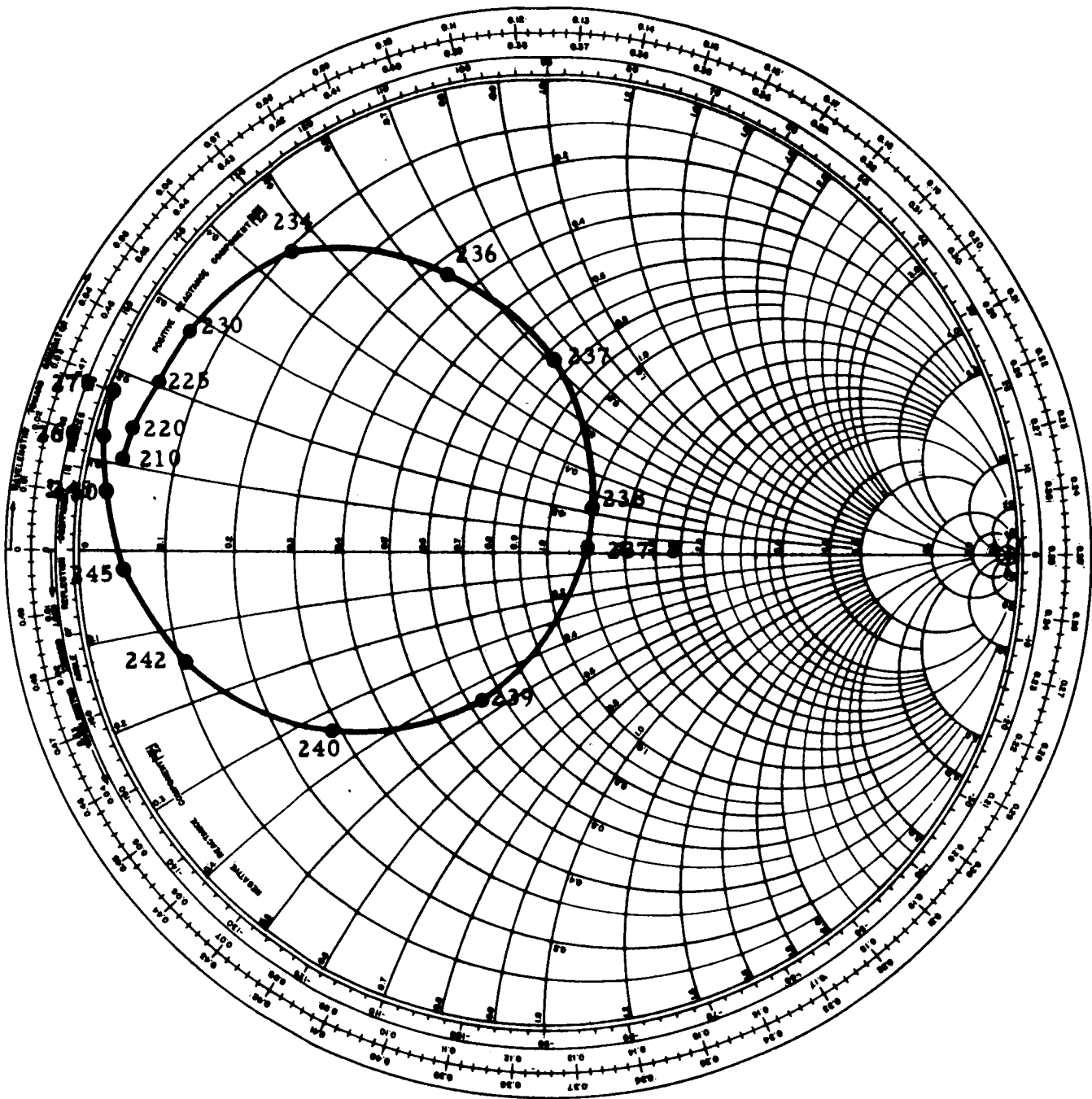
waveguide walls below the capacitive gap so that heat transfer by conduction will be inhibited except at the bottom of the guide.

4.3 Performance of Laboratory Models

Figures 66 thru 73 show the measured input impedance characteristics of the laboratory models. All of the VHF and UHF units were mounted for these measurements on a ten foot square ground plane facing into a ten foot cubical anechoic chamber.

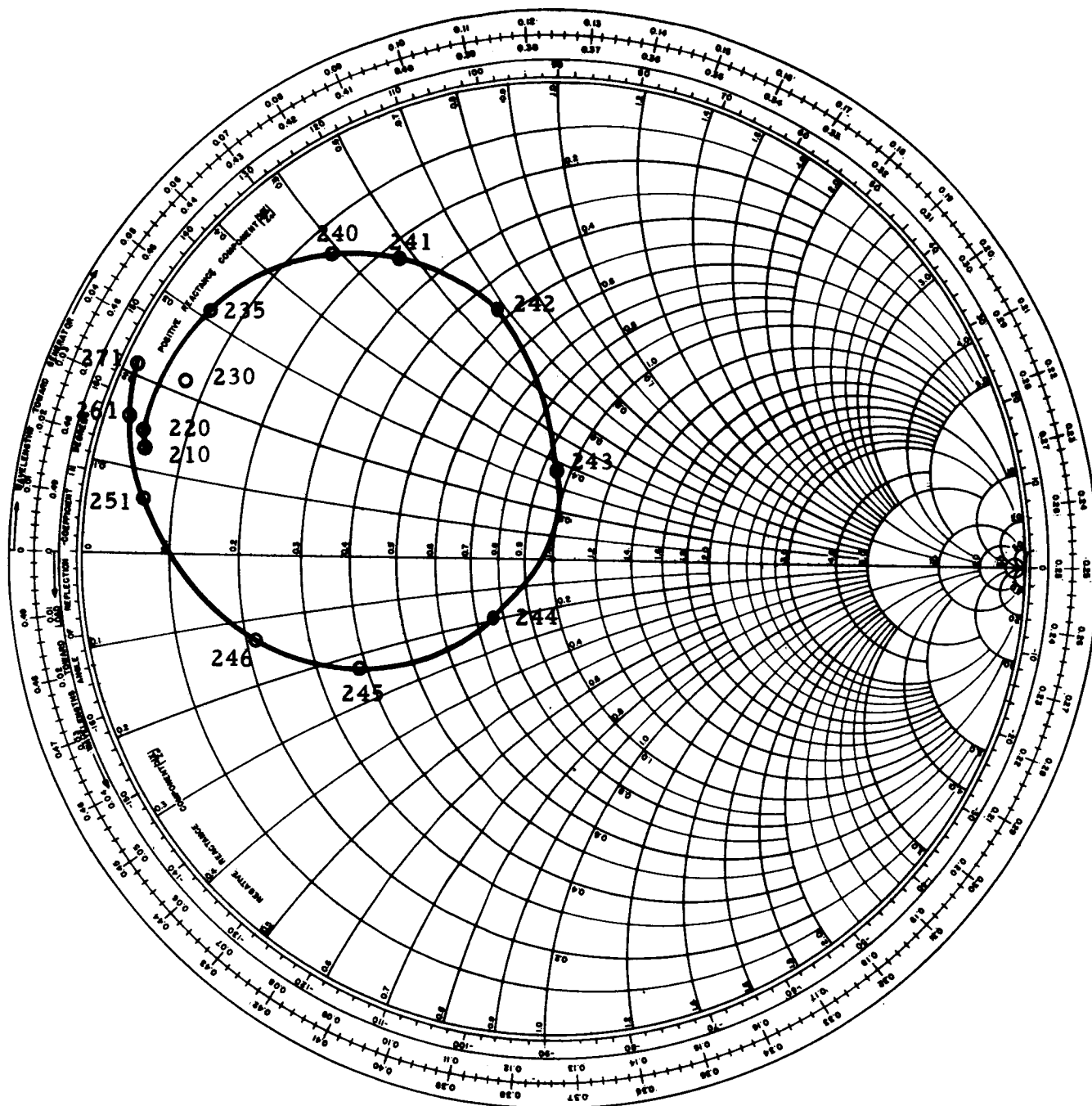
The impedance plots, each of which is referred to the load side of the input connector and normalized to 50 ohms show that the antennas have satisfactory bandwidth and impedance match. It will be noted that the bandwidth under 2:1 of the lowest frequency unit is about 1.75 mc, and that this increases from unit to unit becoming about 6 mc with the 450 mc unit. It will also be noted that in some cases the final adjustment achieved was not completely optimum; however, in later units it could readily be made so by displacing the curves slightly. Nevertheless with all these units VSWR's well below 2:1 at the operating frequency were obtained in all cases.

As can be seen from Figure 71 the VSWR of each of the S-band units was well under 1.5 to 1.0 throughout the entire operating band involved. Each of them also was susceptible to more precise adjustment. The C-band unit as shown by Figure 73 was matched under 1.5 to 1 from 5.50 gc to 5.85 gc. In later units the band from 5.60 gc to 5.815 gc could be optimized so that it would be considerably below 1.5 in this band.



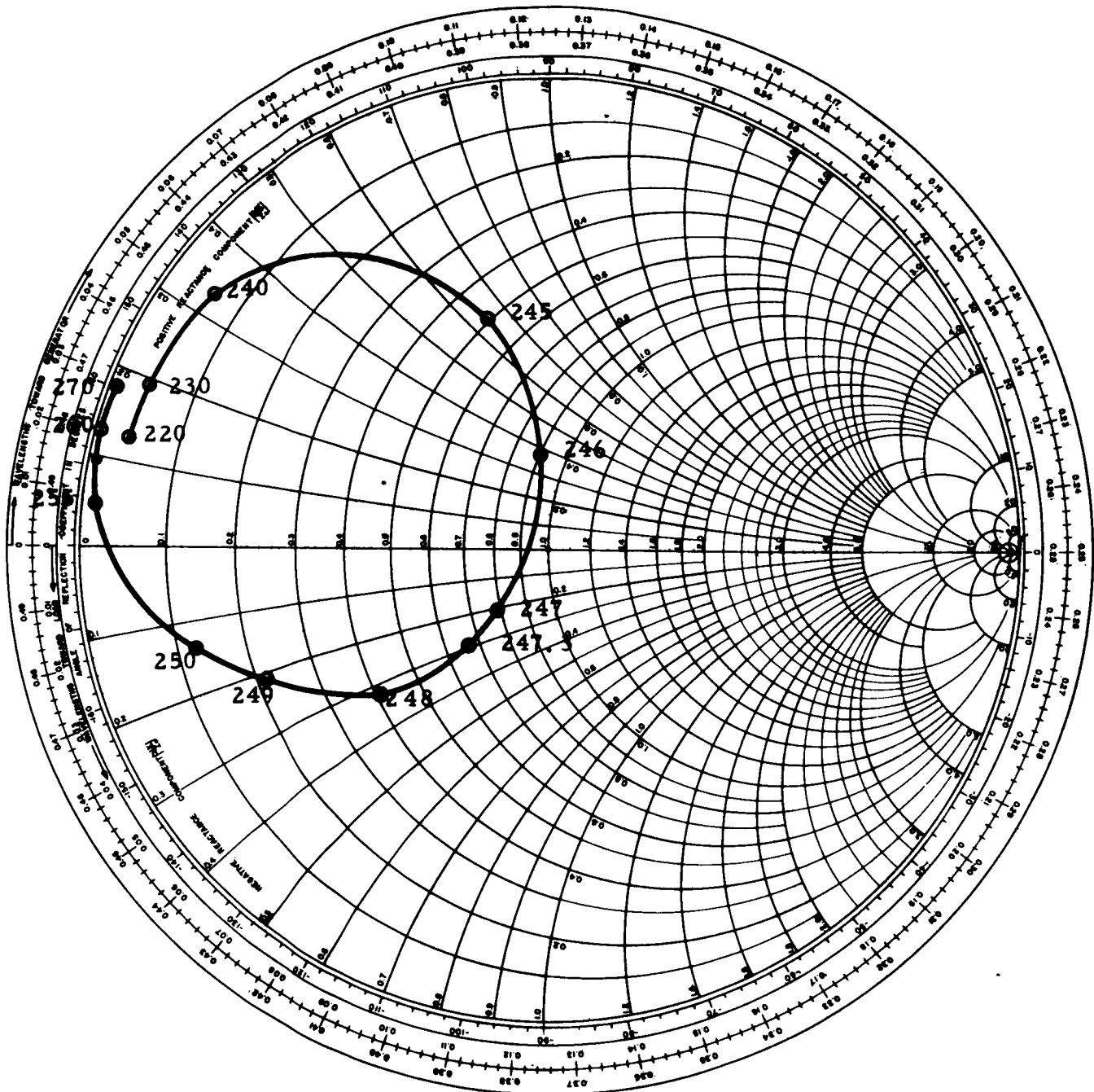
Frequencies In mc/sec.

Figure 66 Measured Input Impedance Of 237.8 MC Prototype



Frequencies In mc/sec.

Figure 67 Measured Input Impedance Of 243 MC Prototype



Frequencies In mc/sec.

Figure 68 Measured Input Impedance Of 247.3 MC Prototype

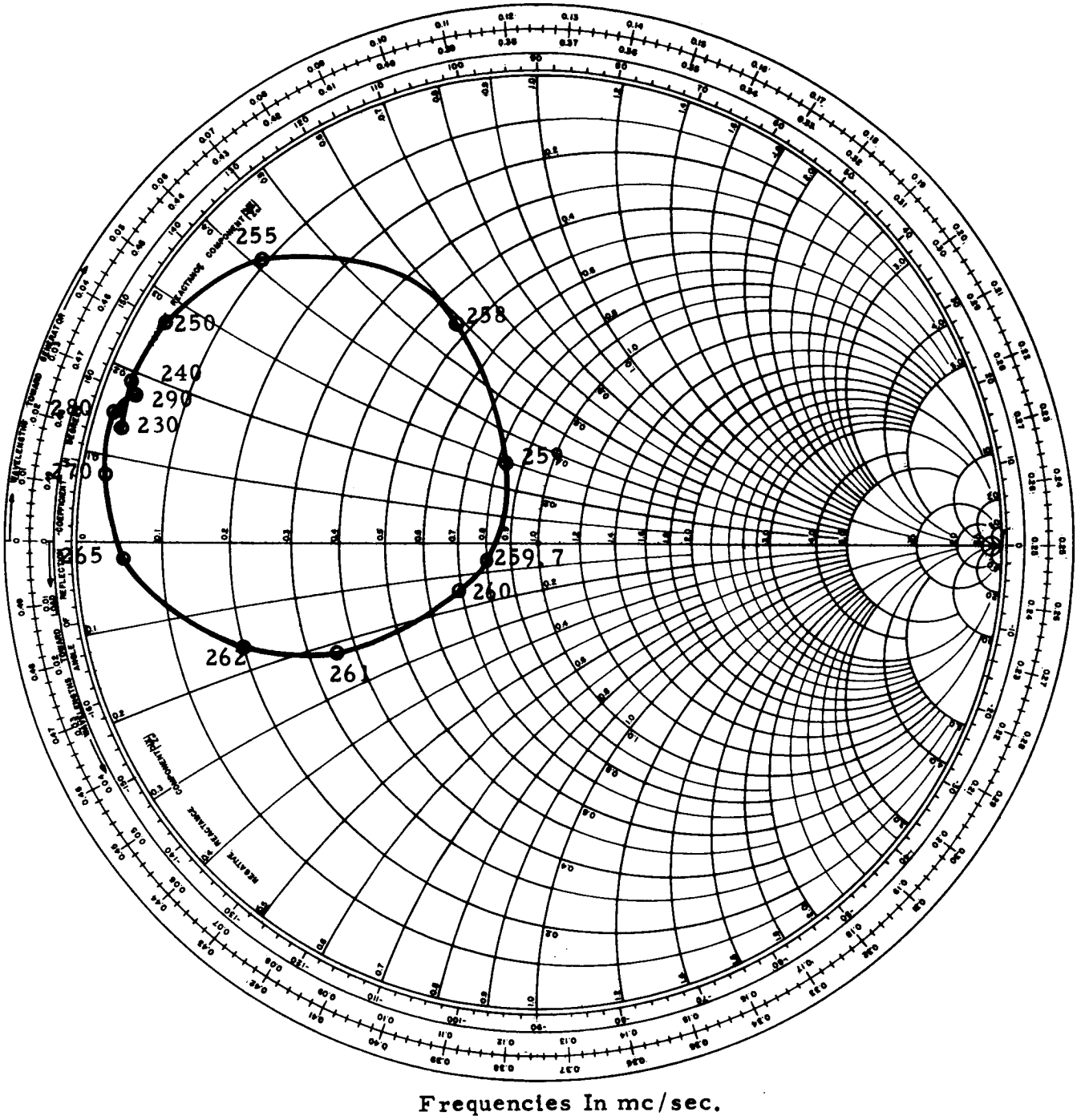
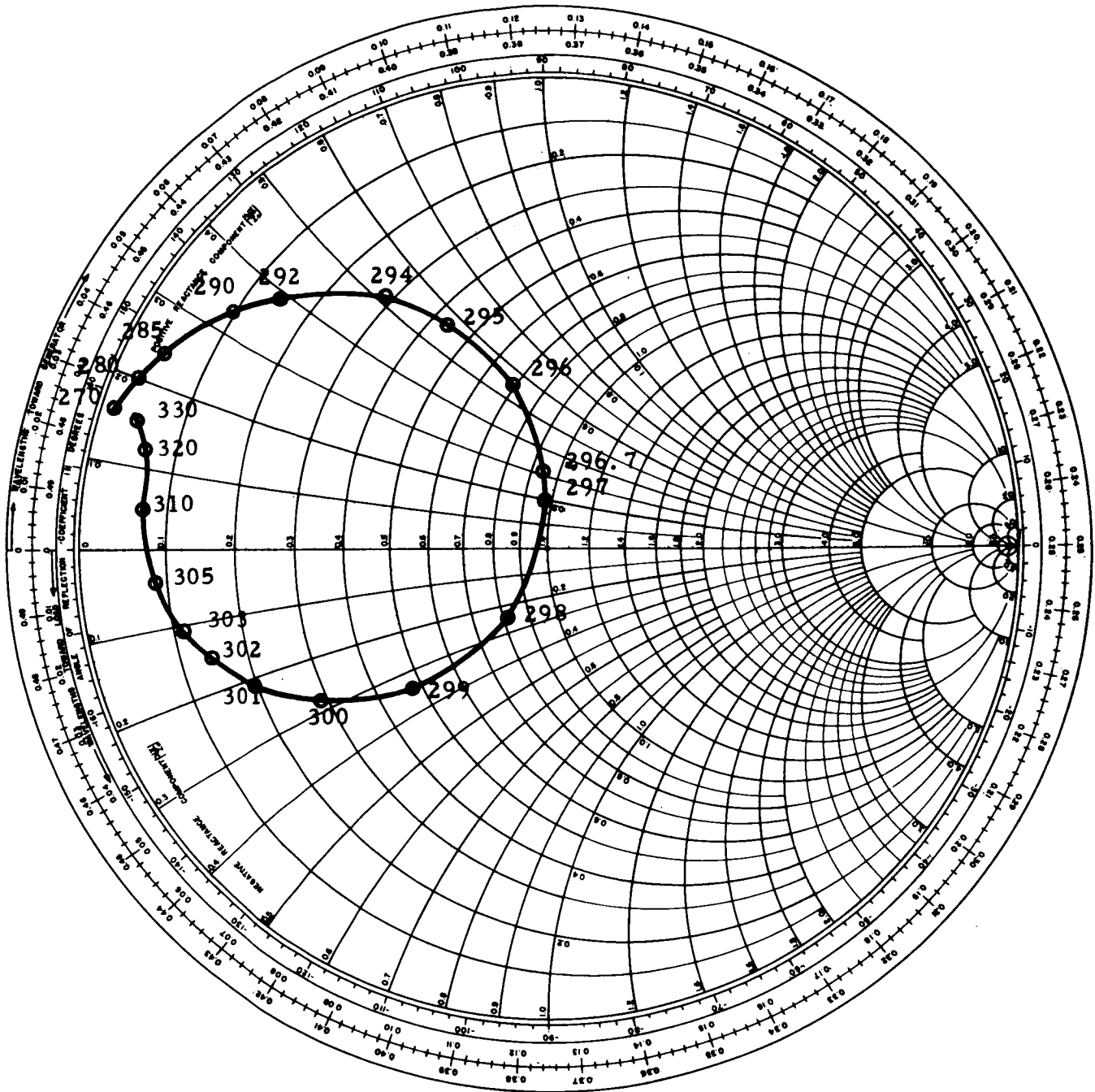
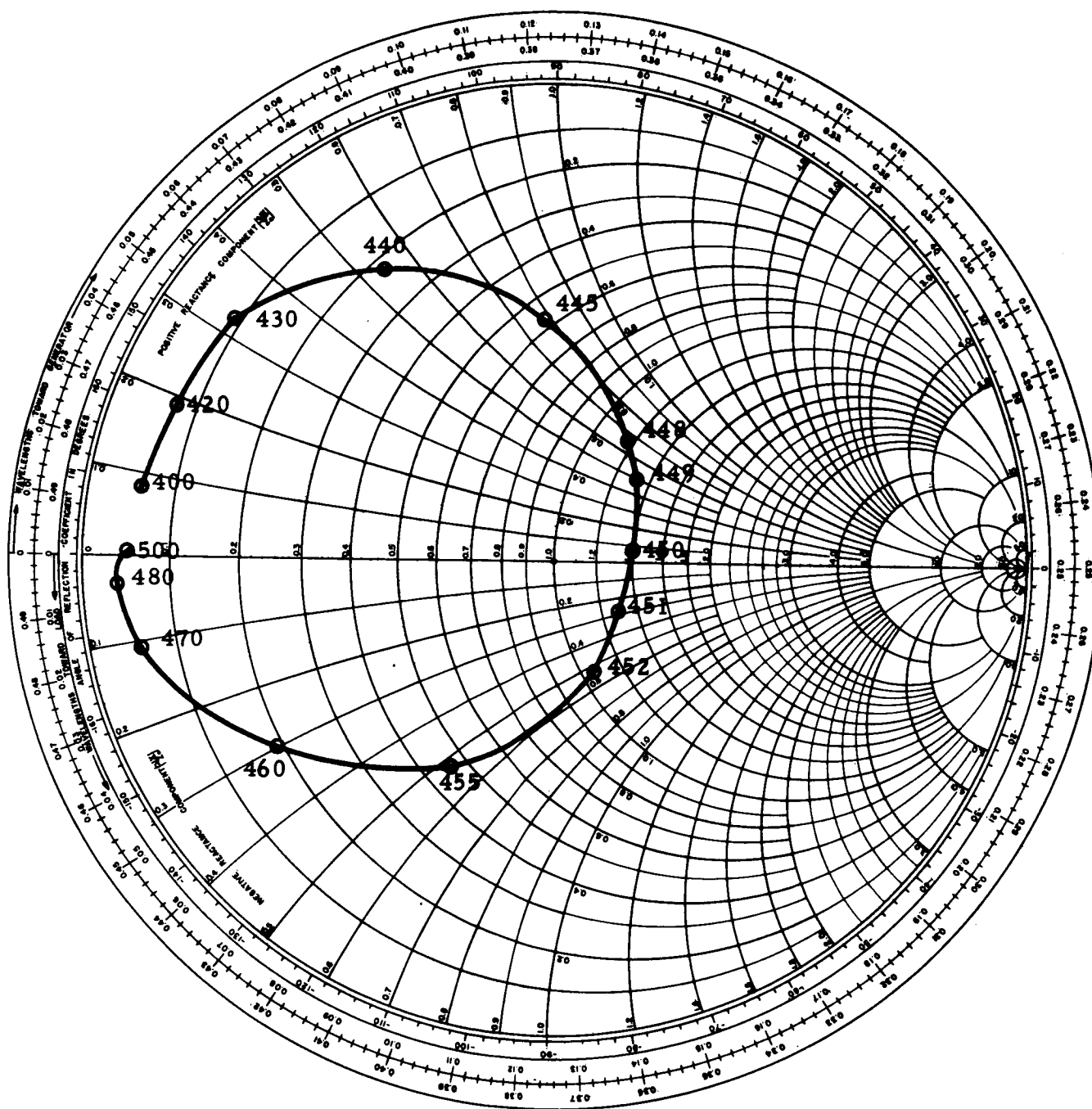


Figure 69 Measured Input Impedance Of 259.7 MC Prototype



Frequencies In mc/sec.

Figure 70 Measured Input Impedance Of 296.7 MC Prototype



Frequencies In mc/sec.

Figure 71 Measured Input Impedance Of 450 MC Prototype

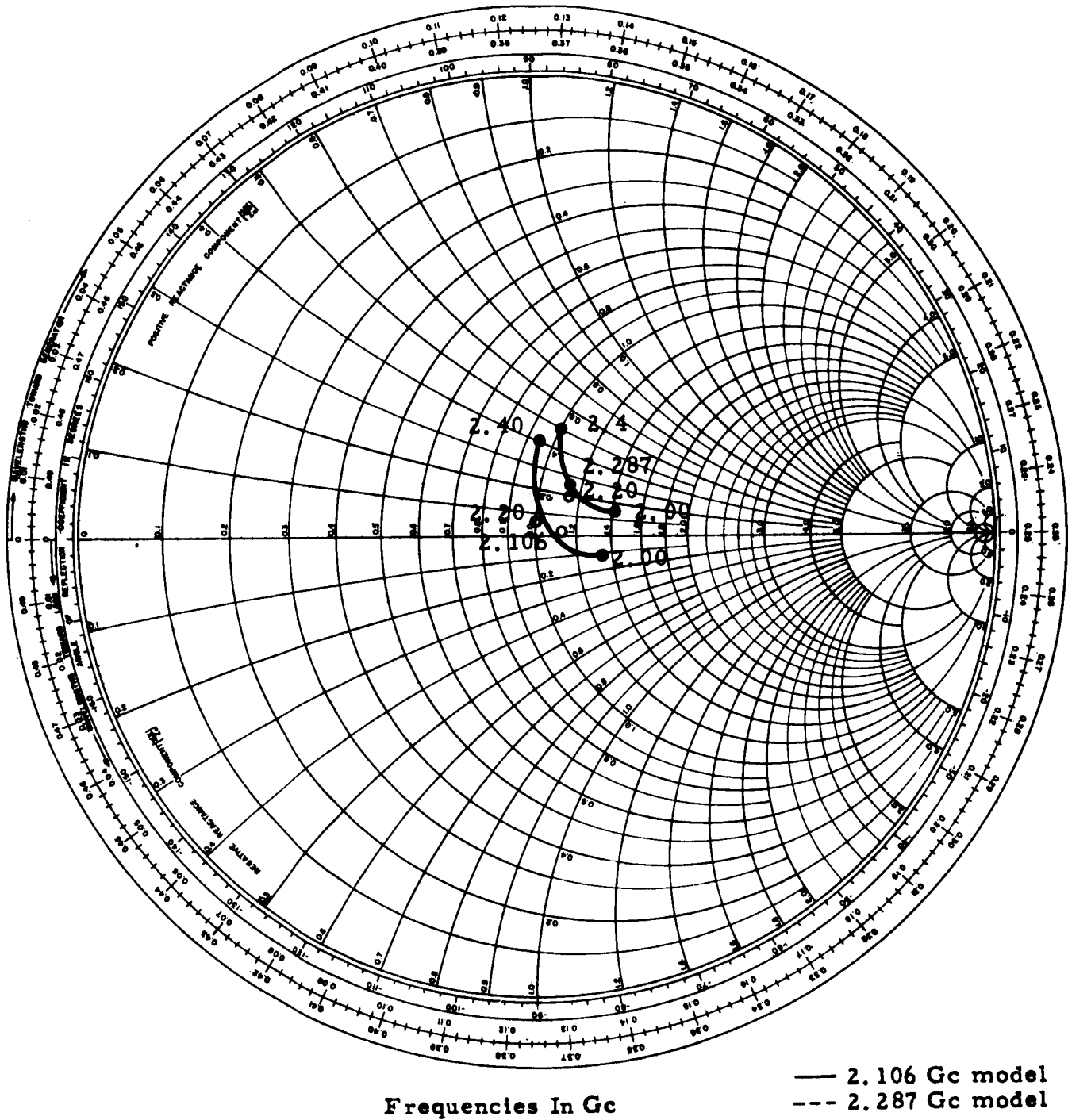
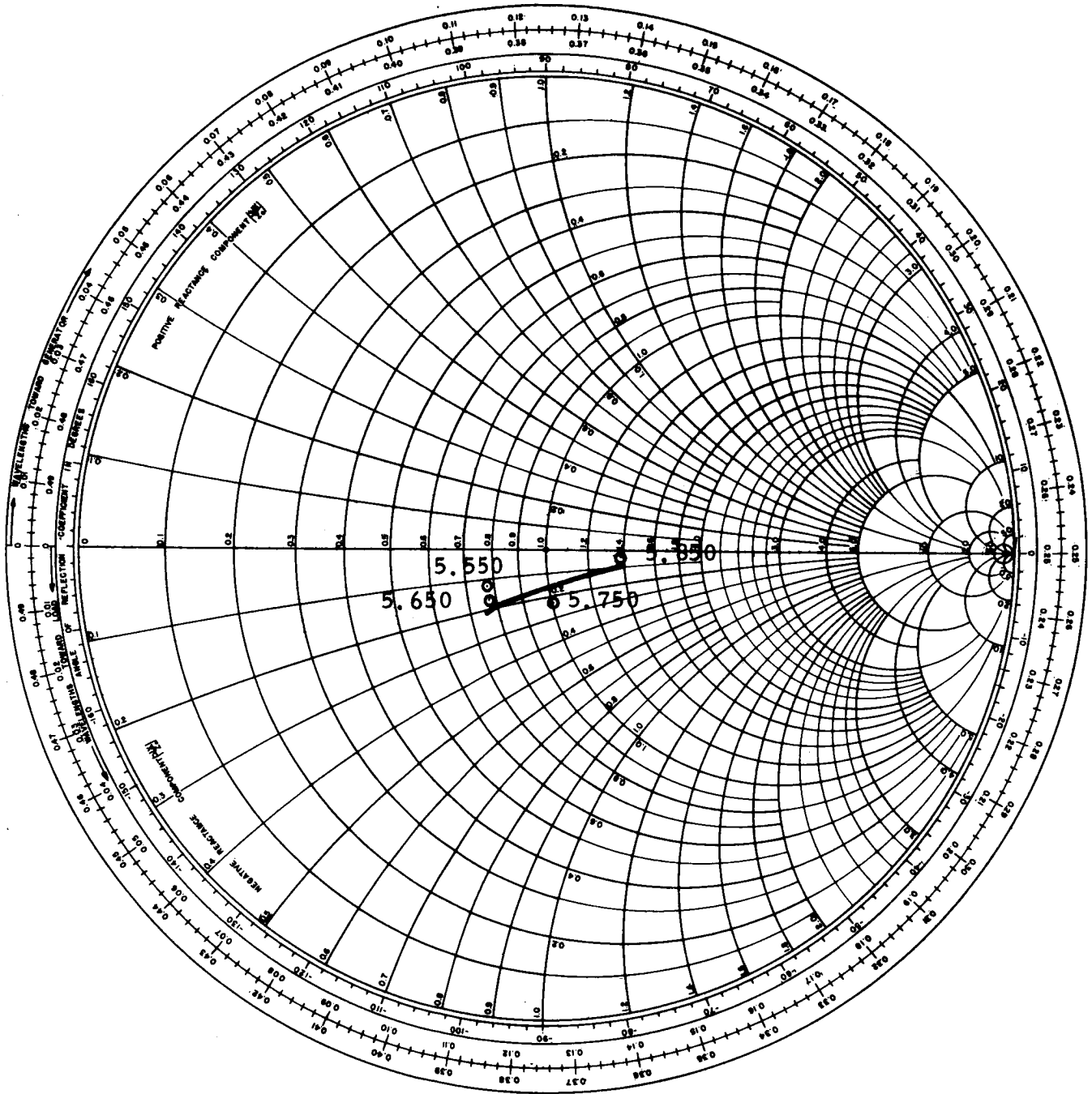


Figure 72 Measured Input Impedance Of S Band Prototypes



Frequencies in gc

Figure 73 Measured Input Impedance Of C Band Prototype

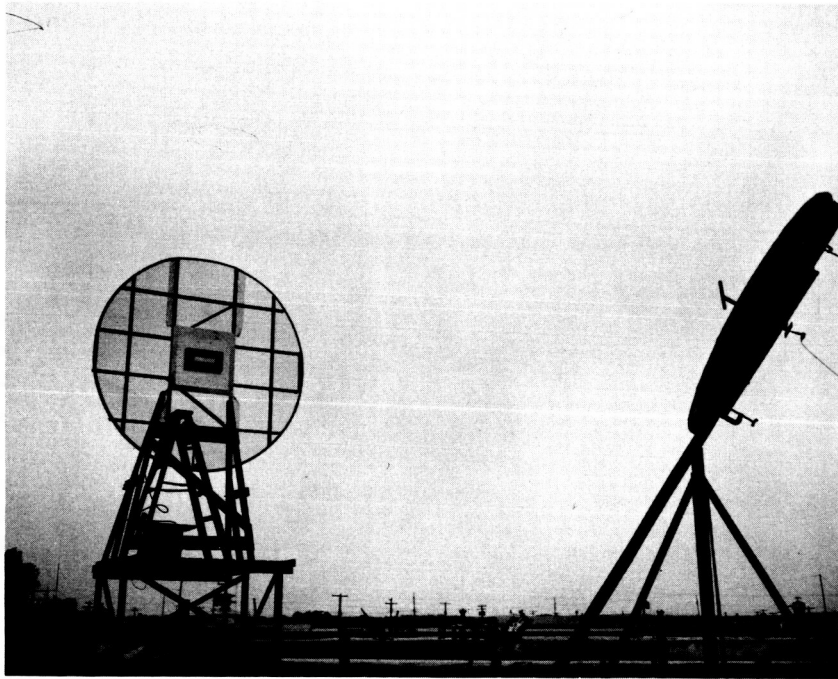
The polarization ellipticity ratios obtained with C-band antenna as measured on the normal to the ground plane through the center of the antenna had the following values:

<u>Frequency</u> gc	<u>Axial Ratio</u> db
5.55	1.0
5.60	0.8
5.65	1.0
5.70	0.6
5.75	1.4
5.80	2.0

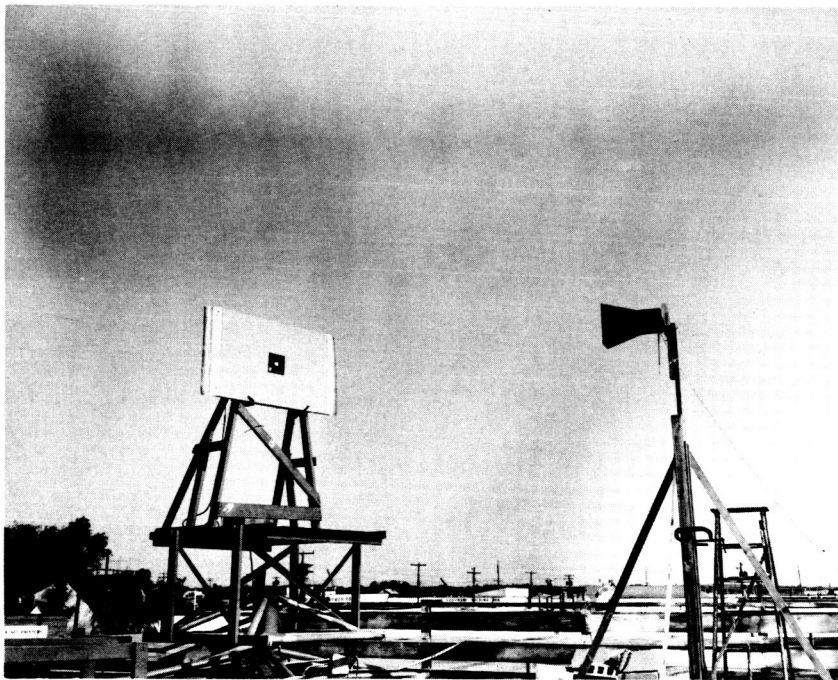
With later units it would clearly be necessary to raise the band of best performance to coincide with the operating band.

Principal plane patterns were measured on the 237.8 mc, 296.7 mc, 455 mc, S-band and C-band units.

The set-ups used are shown by Figure 74. The upper photograph shows a VHF antenna mounted on the eight foot circular ground plane used. The lower photograph shows the S-band unit mounted in a three foot by five foot rectangular ground plane used for the S and C-band units. This ground plane was covered with 1.4 inches of mahogany plywood to simulate the ablator.



VHF-UHF Set-Up



S Band - C Band Set-Up

FIGURE 74 - PROTOTYPE ANTENNAS UNDER PATTERN TEST

Figures 75 and 76 show the E plane patterns of the 237.8 and the 296.7 mc models respectively. Each figure also shows the E plane pattern of a half loop reference antenna that was substituted for it. It will be noted that in both cases the patterns of the prototype are substantially the same as those of the reference antenna.

Comparing the patterns it is noted that the prototype produce slightly more radiation in the general region normal to the ground plane, and slightly less in the region parallel to it than do the loops. This effect, which is not extreme, is greater with the lower frequency antenna. It would decrease if the antennas were curved in their long direction as they would be if they were designed for installation in the bilge area (the area recommended by pattern consideration).

Radiation efficiency of these models was approximately 70 and 90 percent for the 237.8 mc and 296.7 mc models respectively. Operational units of the same size would have higher efficiencies because they would not be glued together with epoxy and because they would be mounted on a curved surface.

If efficiencies of the lowest frequency units needed further improvement it could be obtained by raising the radiator within the quartz; in the limit, locating it on the outer surface of the unit. In the latter case, it would be at the sacrifice of good post-entry performance. Inasmuch as the latter is not an essential requirement it appears more desirable to relinquish it than to increase the size of these antennas.

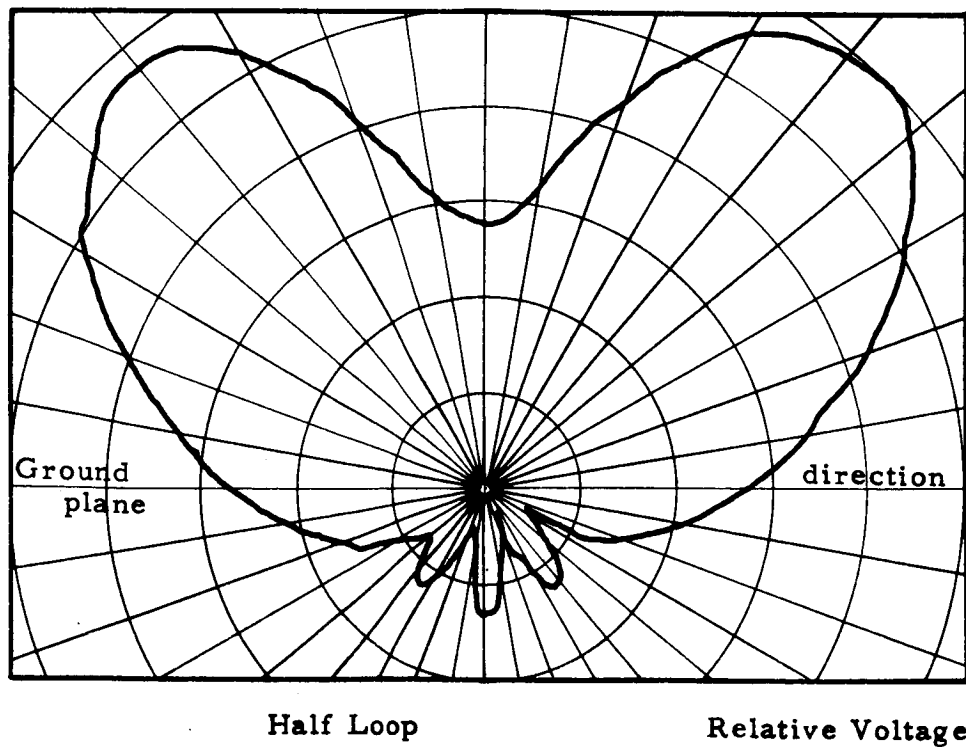
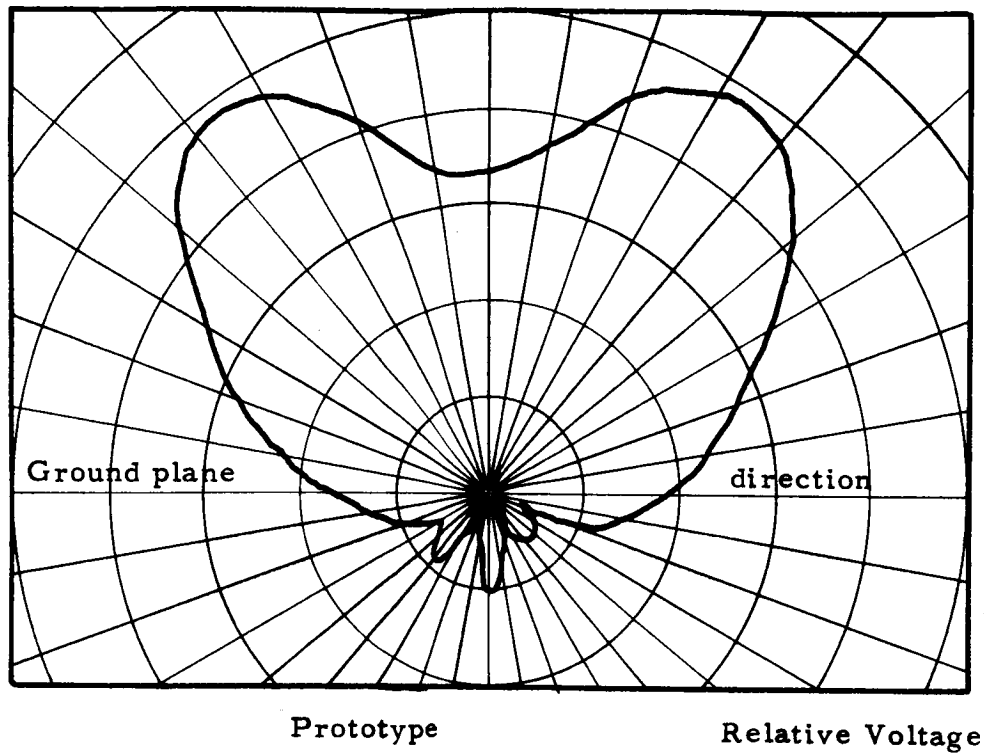


Figure 75 Measured E Plane Radiation Patterns Of 237.8 MC Prototype And Half Loop Reference Antenna

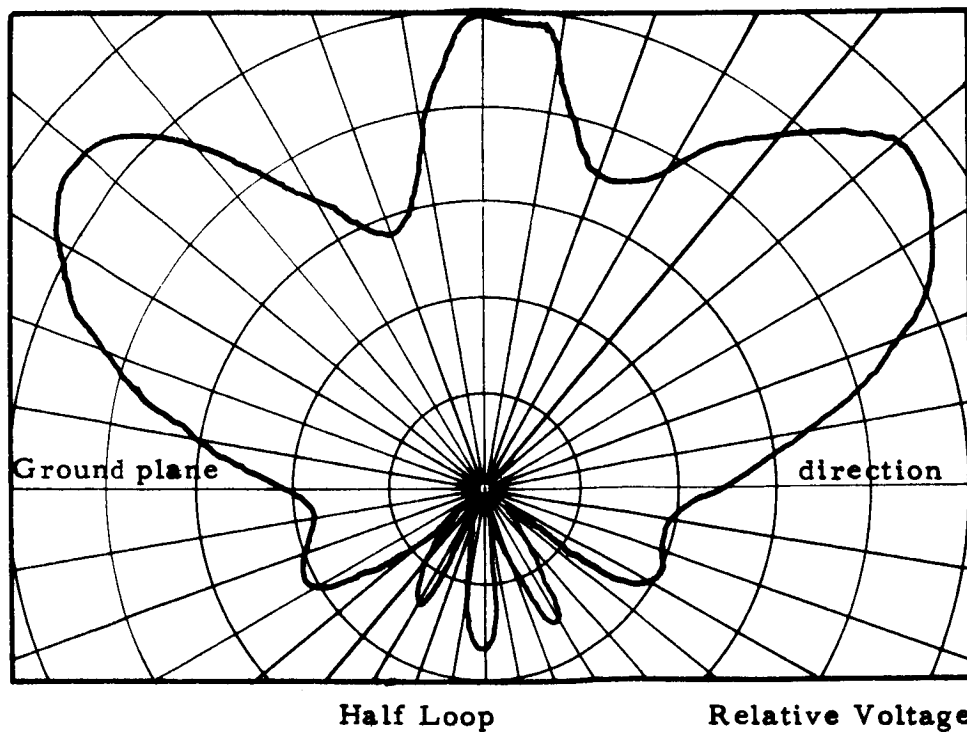
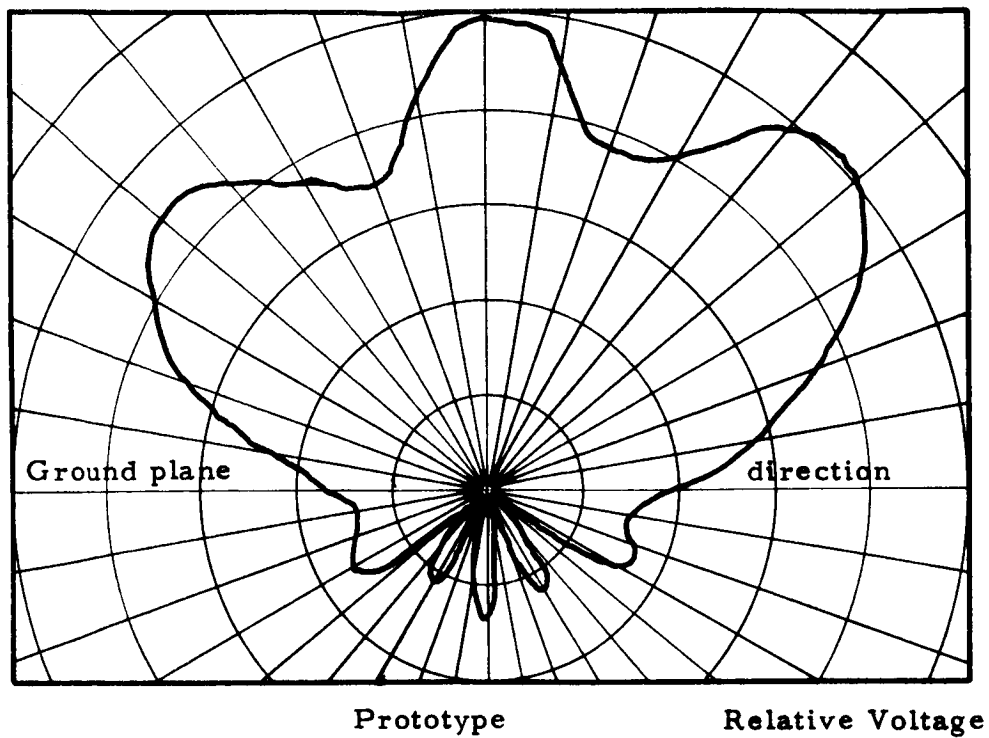


Figure 76 Measured E Plane Patterns Of 296.7 MC Prototype And Half Loop Reference Antenna

Figure 77 shows the measured patterns at S-band. In this case no comparison with a reference antenna was made because the antenna is not extremely small in wavelengths and efficiency is not a concern. From the figure it will be observed that the E plane pattern shows gain toward one side. It is intended that the lobe be pointed toward the service module to help reduce the shadow which it produces. It will be noted that in the E plane there is substantial reduction of radiation in the direction of the ground plane. As discussed earlier, this is a result of the ablator, and an effect which cannot be eliminated. It can, however, be made undamaging by location of the antennas at the widest point of the capsule. In that case because of the curvature of the surface the direction of attenuation will fall in acceptable zones.

Figures 78 through 81 show the radiation patterns of the C-band antenna from 5.5 to 5.8 gc. With the prototype the best operating band is slightly too low being from about 5.500 to 5.700 gc. Below this the patterns are a little sharp; above it severe nulls begin to appear. On final units not only could the band be shifted, but symmetry could readily be improved and the amount of lobing slightly reduced.

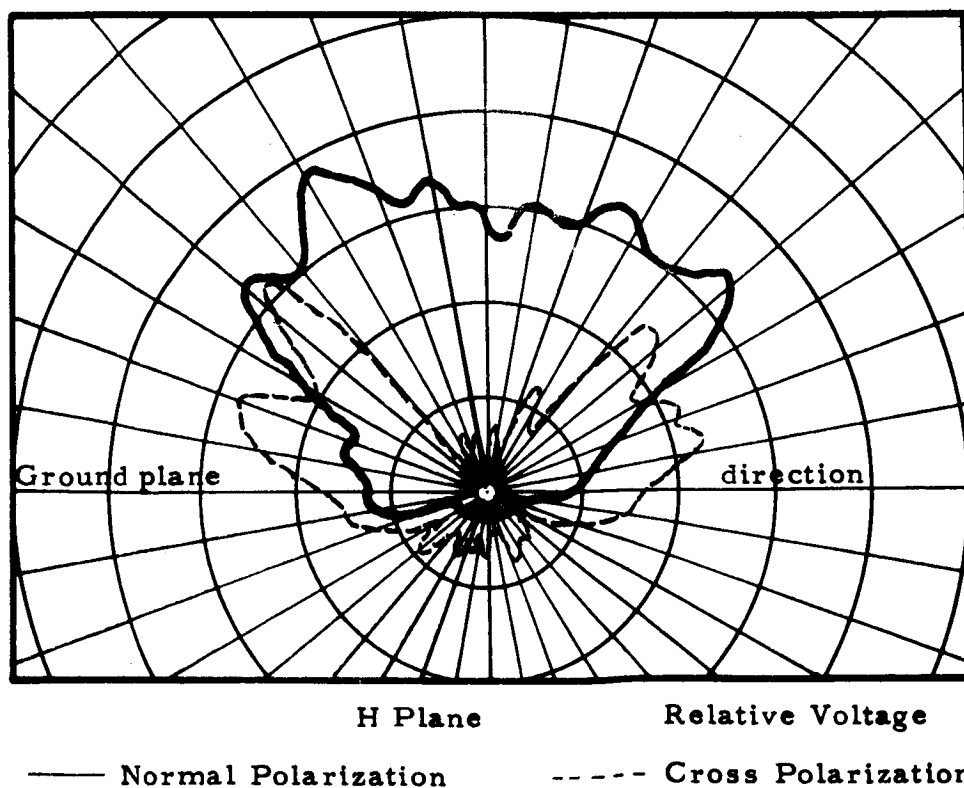
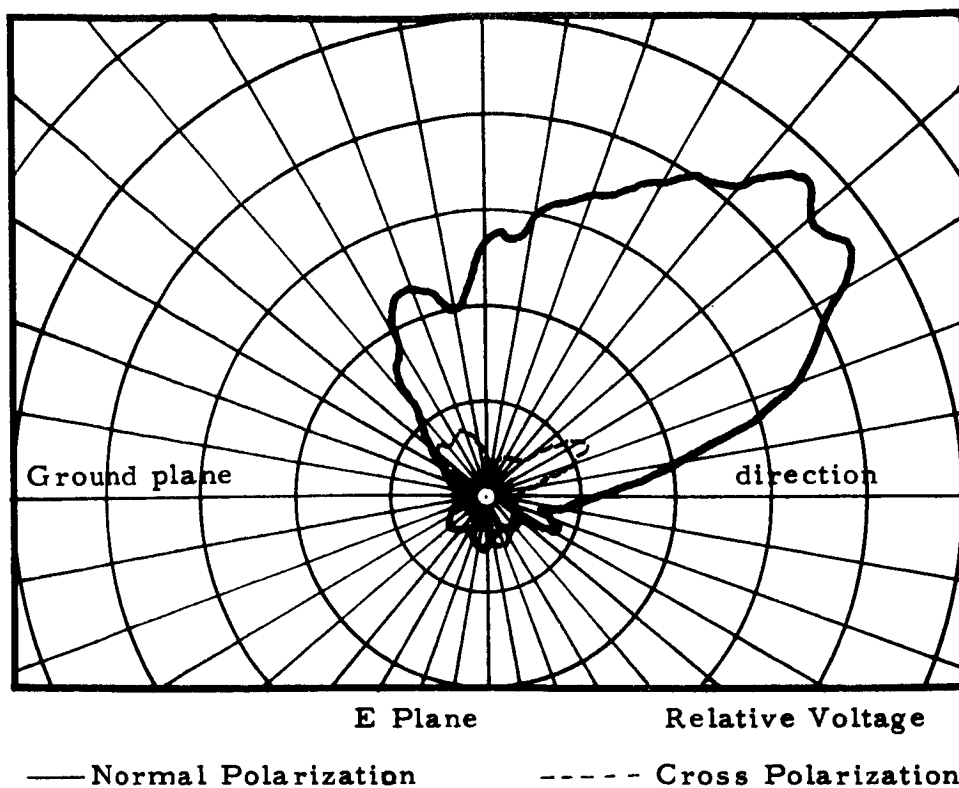
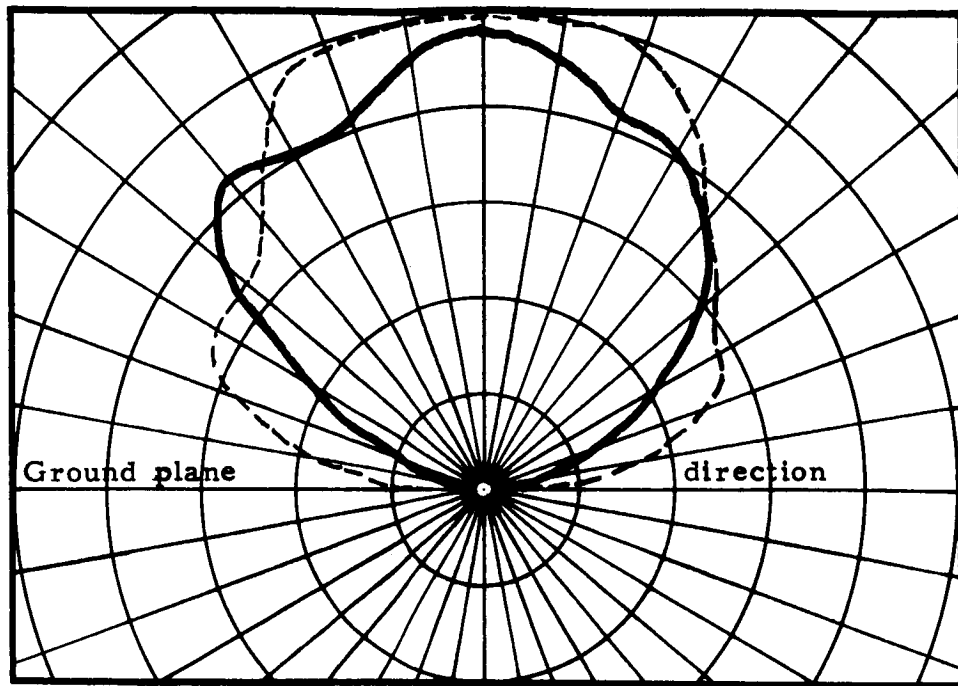
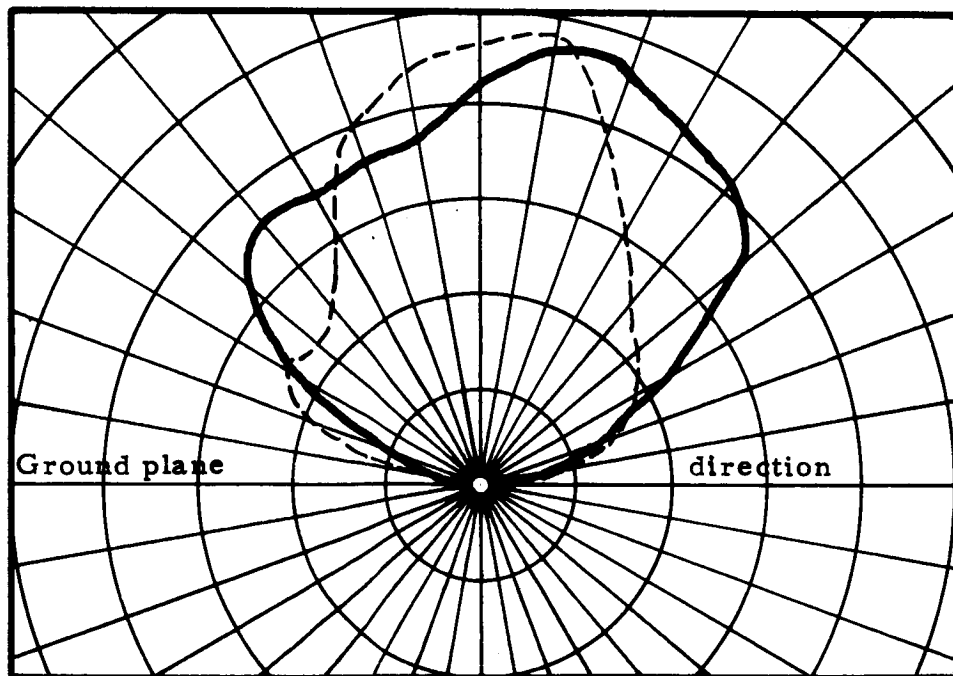


Figure 77 Radiation Patterns Of S Band Prototype Measured At
2100 MC



In Plane Parallel To Large Guide Dimension Relative Voltage

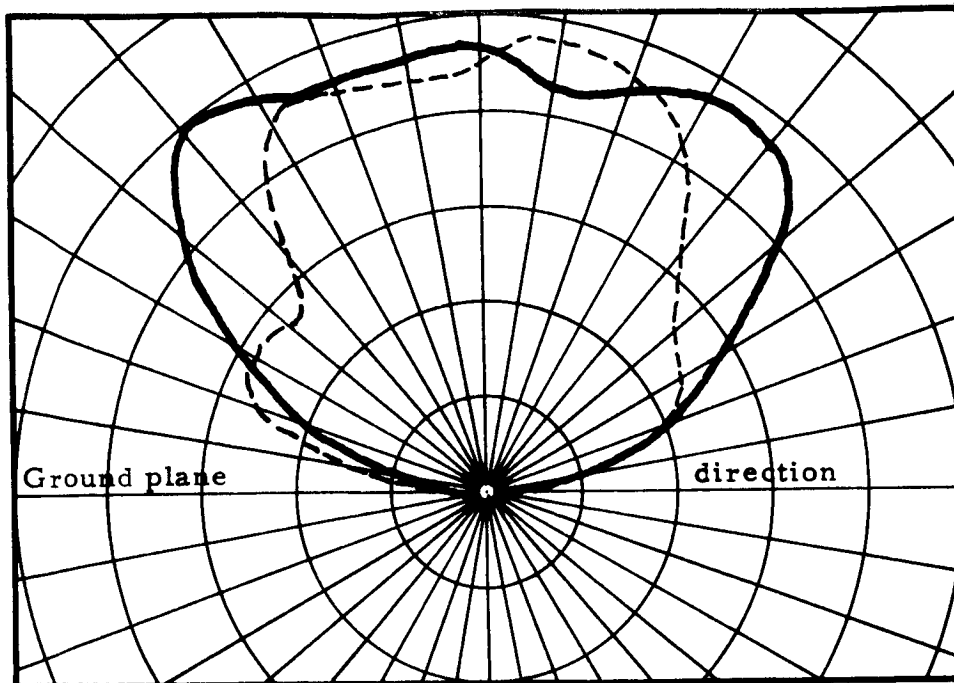
— E Component Parallel To Plane Of Pattern
--- E Component Normal To Plane Of Pattern



In Plane Parallel To Short Guide Dimensions Relative Voltage

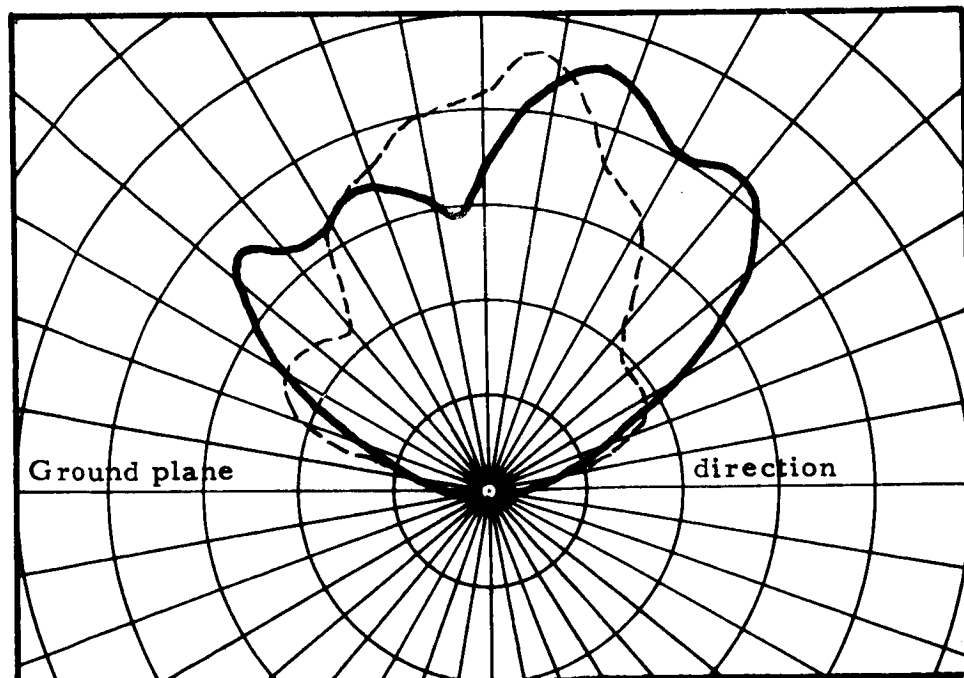
— E Component Parallel To Plane Of Pattern
--- E Component Normal To Plane Of Pattern

Figure 78 Radiation Patterns Of C Band Prototype Measured At
5500 MC



In Plane Parallel To Large Guide Dimension Relative Voltage

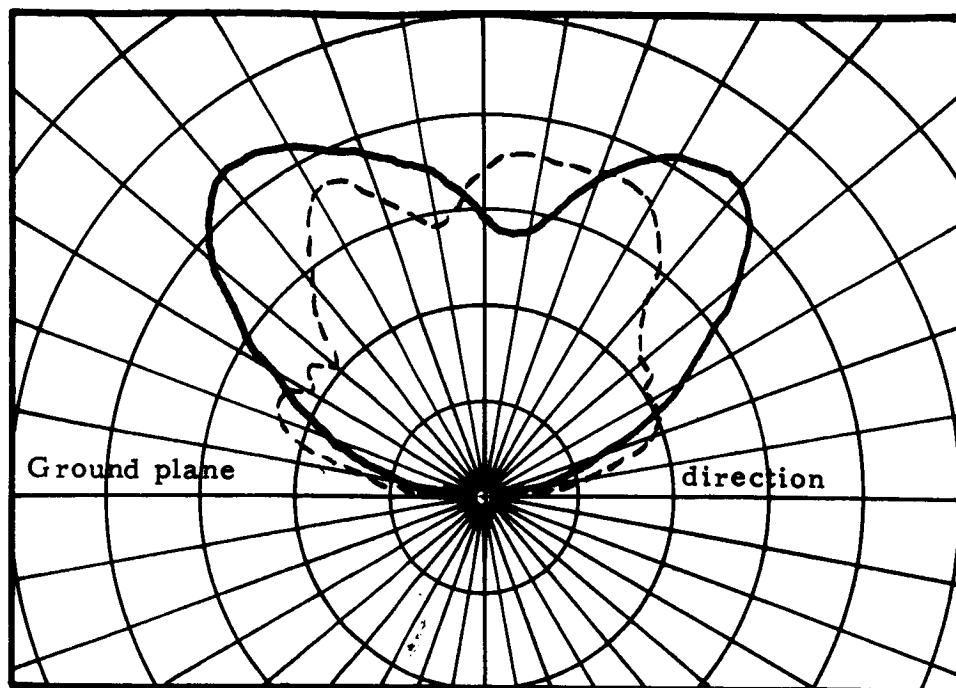
— E Component Parallel To Plane Of Pattern
--- E Component Normal To Plane Of Pattern



In Plane Parallel To Short Guide Dimensions Relative Voltage

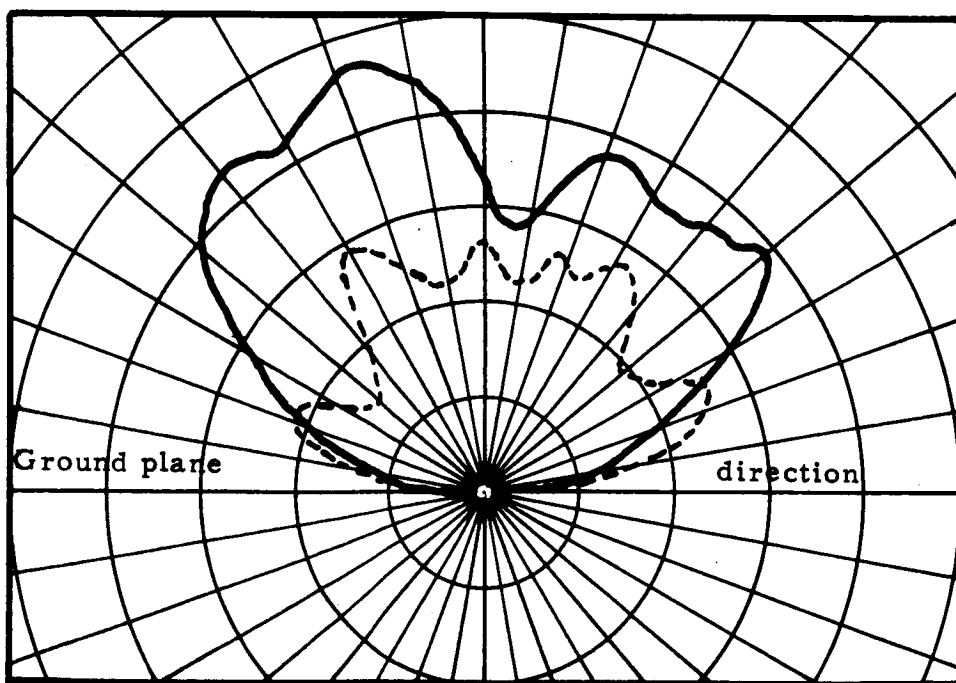
— E Component Parallel To Plane Of Pattern
--- E Component Normal To Plane Of Pattern

Figure 79 Radiation Patterns Of C Band Prototype Measured At
5600 MC



In Plane Parallel To Large Guide Dimension Relative Voltage

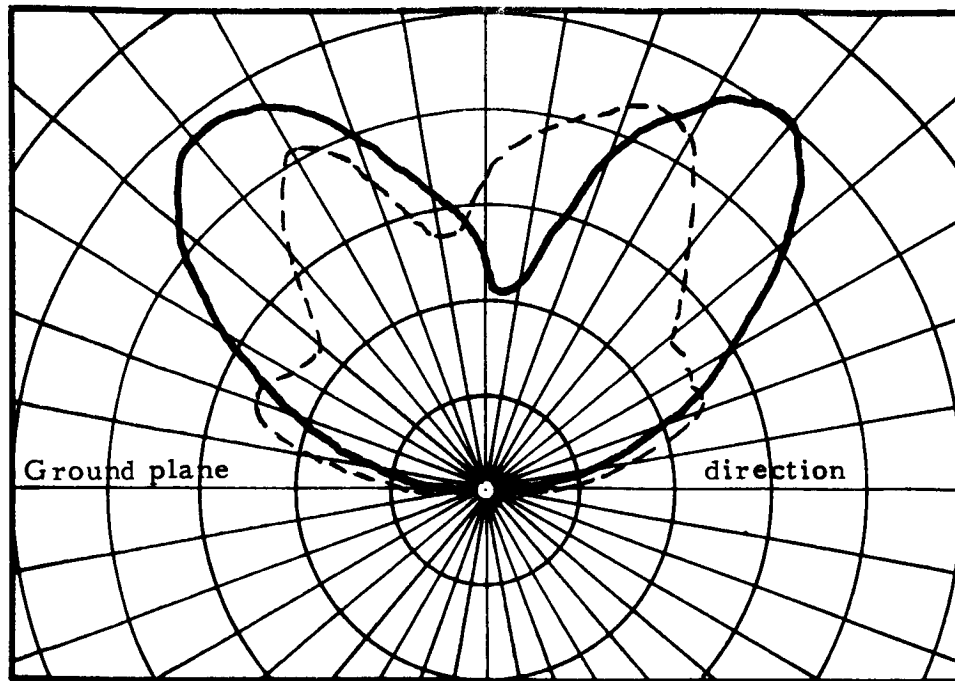
— E Component Parallel To Plane Of Pattern
 --- E Component Normal To Plane Of Pattern



In Plane Parallel To Short Guide Dimensions Relative Voltage

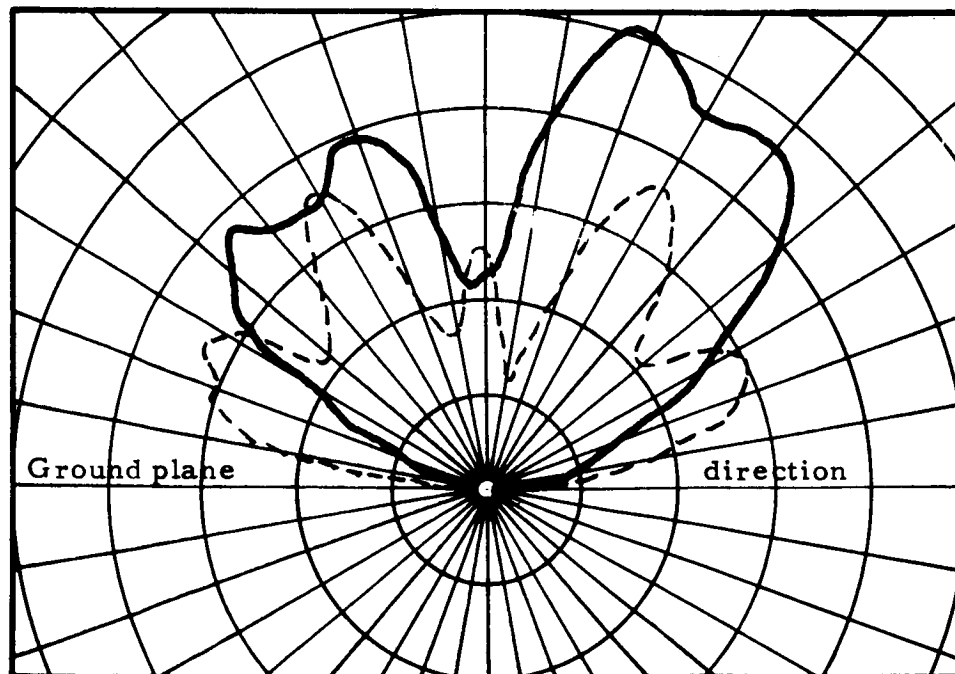
— E Component Parallel To Plane Of Pattern
 --- E Component Normal To Plane Of Pattern

Figure 80 Radiation Patterns Of C Band Prototype Measured At
 5700 MC



In Plane Parallel To Large Guide Dimension Relative Voltage

— E Component Parallel To Plane Of Pattern
--- E Component Normal To Plane Of Pattern



In Plane Parallel To Short Guide Dimensions Relative Voltage

— E Component Parallel To Plane Of Pattern
--- E Component Normal To Plane Of Pattern

Figure 81 Radiation Patterns Of C Band Prototype Measured At
5800 MC

5.0 MODEL RADIATION PATTERN STUDY

It was explained in the opening section of this report that at the outset of the work it was planned at each test frequency to measure and compare the patterns of installations utilizing sets of four, six and eight antennas dispersed about the capsule. During the earliest stages of the work this plan was followed. Early in the program it was learned that weight restrictions were so severe that it was not feasible to install such large numbers of antennas, and that, therefore, the results of such a study would not be of significant value. Accordingly, the direction of the program was shifted to explore the ways of obtaining the best performance from sets employing minimum numbers of antennas.

As the work progressed it appeared that the junction between the command and service modules might severely reduce radiation aft at S-band (and presumably also at C-band, although this was not measured). If this were true the result would be far less radiation tending to go aft than that inherently possible with the geometry of the command-service module assembly. This situation was clearly of potential importance and, therefore, it was investigated.

The overall purpose of this study was to obtain data that would permit the drawing of generalizations that would be of value as guides in the overall planning of antenna installations. Considerably more

data were measured than are presented here. What are shown was judged to comprise the part which has significant value for this purpose.

5.1 Discussion of Test Facility and Pattern Testing Procedure

A 1/4th scale model (see Figure 82) of the full scale command-service module assembly was constructed in accordance with NAA supplied drawings. The modules were so constructed as to be detachable, care being exercised to duplicate the geometry of the command-service module attach points. (It may be noted that the service module touches the command module only at three asymmetrically located tie points.) The outer skin gap (between command and service module) was so constructed as to simulate the spacing required on the actual vehicle to permit the ablative on the command module, which covers its lower surfaces completely, to pass between the two modules. For the VHF and UHF measurements the ablative was omitted from the model. For the S-band measurements it was included.

The test set-up employed is shown in Figure 83. It will be noted that the pattern range used was 50 feet in length. This distance is less than that necessary to meet the $2D^2/\lambda$ criterion. To minimize the effect of this, the centers of the antenna arrays under test were in all cases placed over the axis of rotation of the rotator. Tests have shown that the accuracy of such a set-up is satisfactory*, and that the errors

* See for example: Omnidirectional Airplane Antenna Study, J. J. Nail, W. Sichak, et al, March 1956 issued by Federal Telecommunications Laboratory under Contract NOa(s) 12212.



FIGURE 82 - ONE-FOURTH SCALE MODEL USED FOR PATTERN STUDY

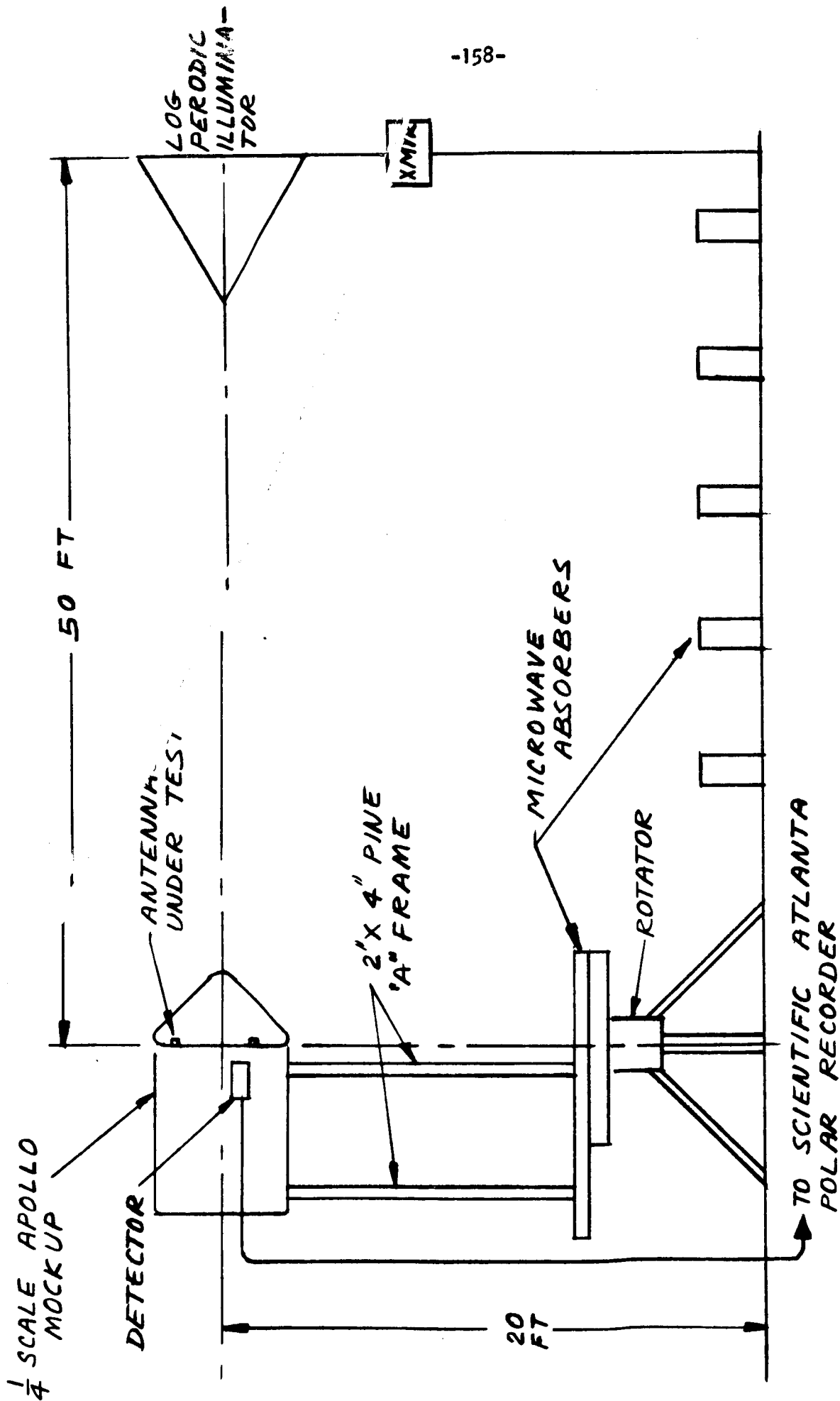


Figure 83 Sketch Of Model Pattern Test Setup

do not affect overall pattern characteristics although they do modify the apparent position of individual lobes in zones where there are many narrow lobes.

The illuminating antenna used was of the log periodic type having a half-power beamwidth of 30° independently of frequency.

Two types of radiation patterns were recorded. Pitch yaw-plane, (θ constant, ϕ varied) and roll-plane, (θ constant at 90°) ϕ varied. Figure 84 presents a sketch showing the coordinate system.

The radiation patterns were recorded using a Scientific Atlanta polar recorder and were plotted as a function of relative voltage. A bolometer was used as the detecting device in all cases.

5.2 Model Pattern Measurements

The first sets of patterns shown were obtained with arrays of small half-loop antennas (shown by Figure 85) excited at a frequency of 920 mc, corresponding to a full scale frequency of 230 mc. This antenna has approximately the same total length in wavelengths as do the prototype, but is of slightly different proportions, being somewhat higher but not so long. The effect of this difference is to increase slightly the amount of cross polarized radiation. As a result, with the antennas installed as they were for these measurements the E_ϕ component of the radiation is slightly greater in comparison to the E_θ component than it otherwise would have

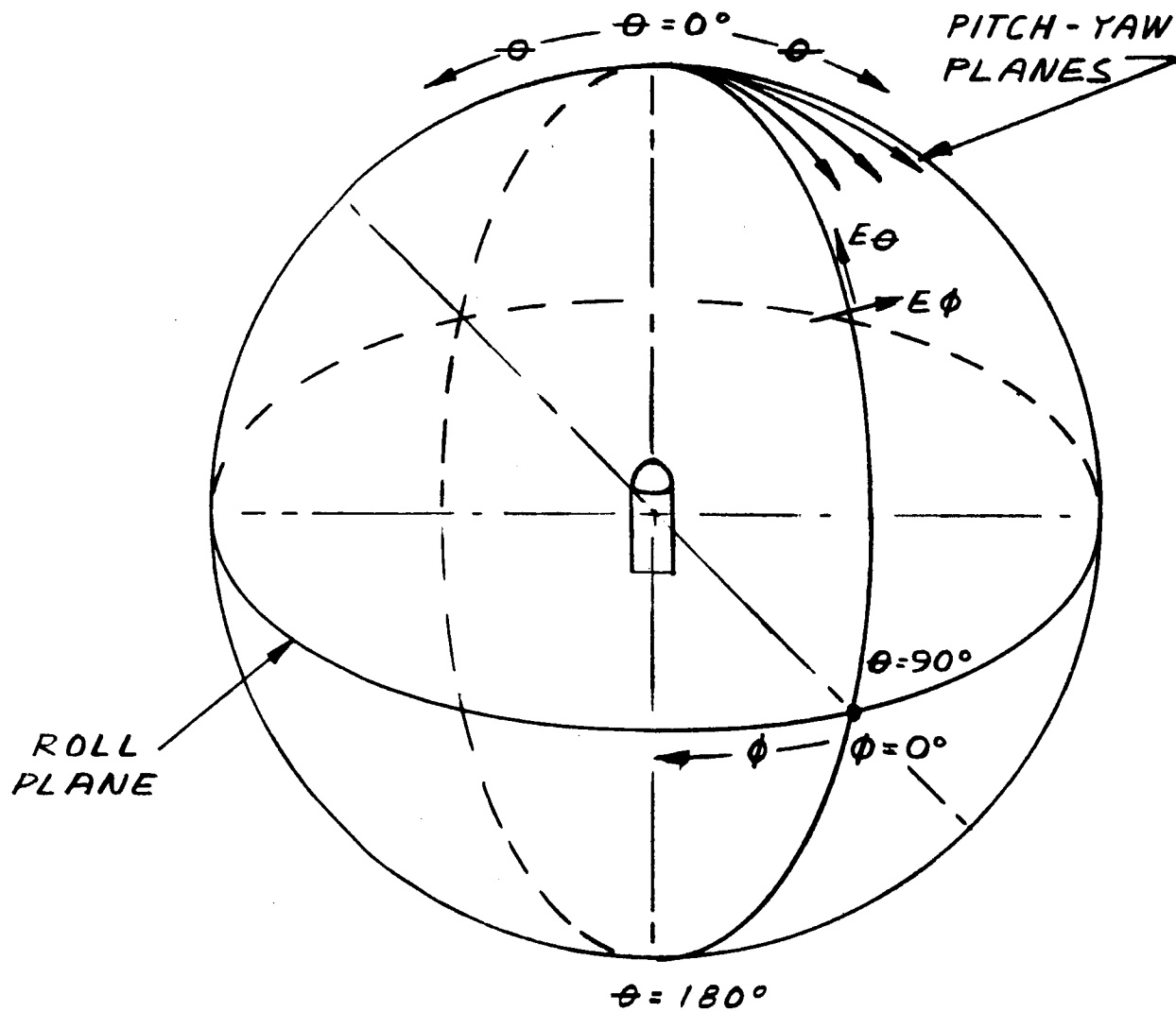


Figure 84 Radiation Pattern Coordinate System

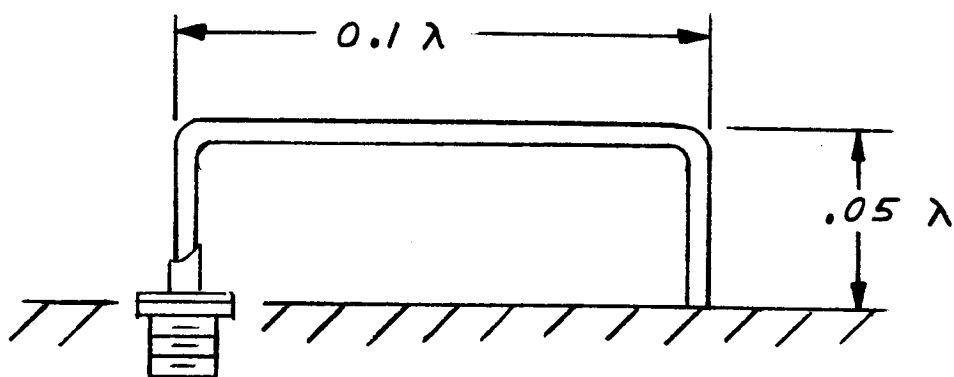


Figure 85 Sketch Of Unbalanced Half-Loop Antenna

been. This type of antenna was chosen because with installations on large structures having the shape of figures of revolution the minima in the E_θ patterns tend to occur at the same angles as the maxima of the E_ϕ patterns and vice versa. This is illustrated by Figure 86, which shows both the patterns of a pair of linear slots (corresponding to the balanced mode radiation from two loops) and a pair of annular slots (corresponding to the unbalanced mode radiation from the two loops) at the same locations on a cylinder. In the cases tested some of the E_θ radiation present results from this unbalance; the remainder is a result of the conical shape. The patterns are nevertheless representative of those that would be obtained with any small loops or linear slots similarly installed. As the balance of the antennas were increased, the E_θ component of radiation would decrease. In the limit, when the antennas were fully balanced the E_θ radiation would be three or four db less than for the patterns shown.

Figures 87, 88 and 89 show the effects as manifested in the roll plane patterns at 230 mc of varying the number of antennas in a set and of changing the locations of the sets between three different stations. The patterns of Figure 87 were all taken at the lowest of these, Station 30, and show the E_θ and E_ϕ radiation with three different arrays of the model loop antenna. In each case, the antennas were installed normal to the skin and running straight up and down (i.e., plane of loop in plane containing x axis) with the fed end down. The arrays were fed

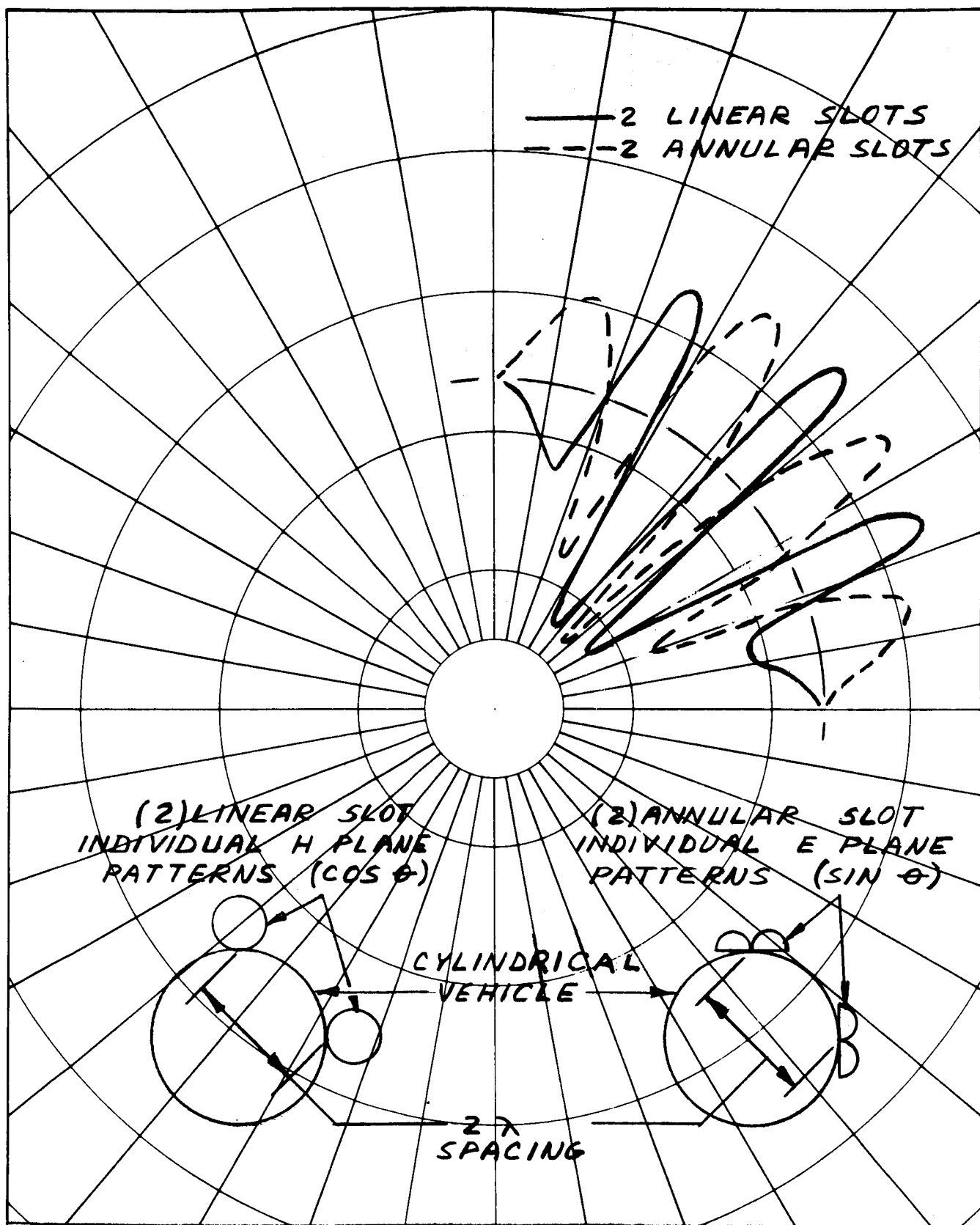
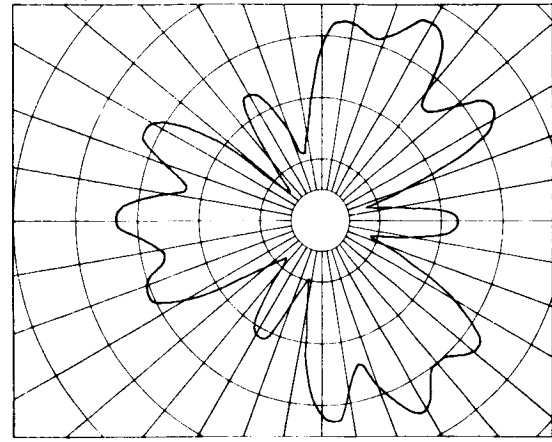
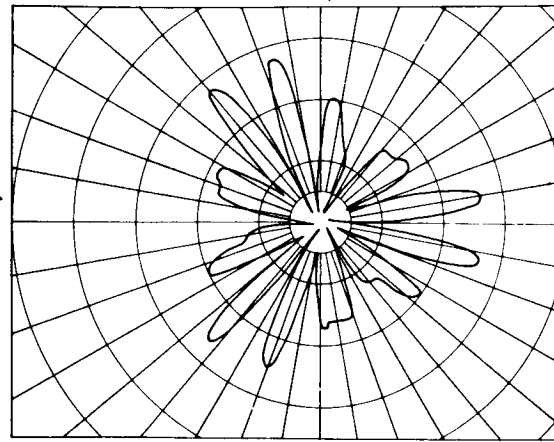


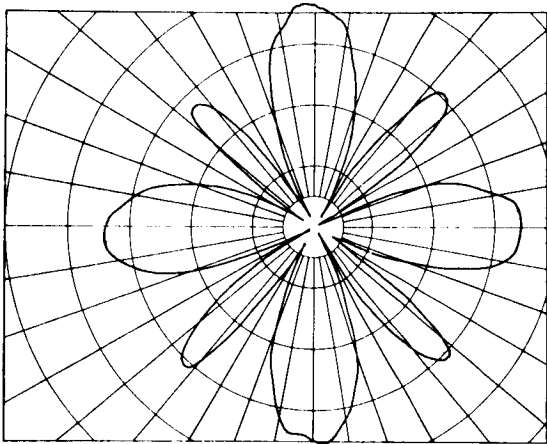
Figure 86 Computed Roll Plane Pattern For Two Sets Of Two Antennas On A Cylinder (Linear Slot And Annular Slot)



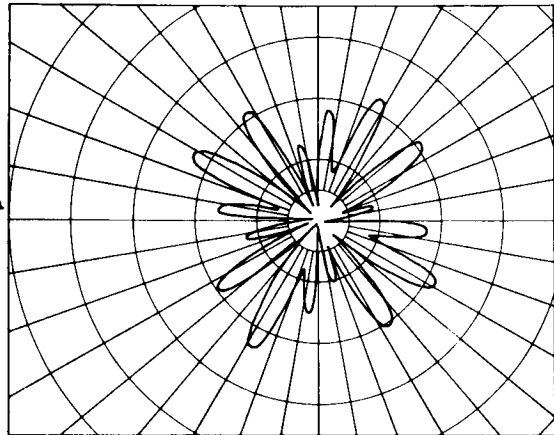
E_θ
Three Antennas



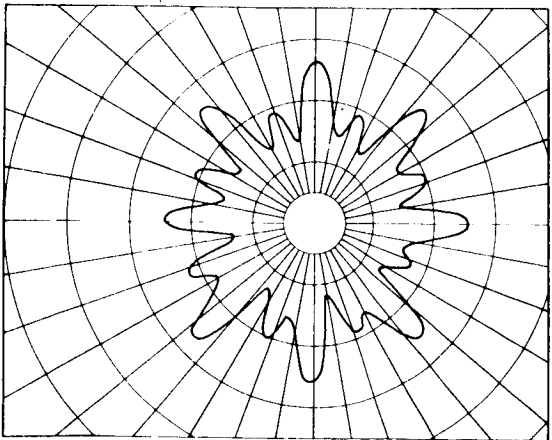
E_ϕ



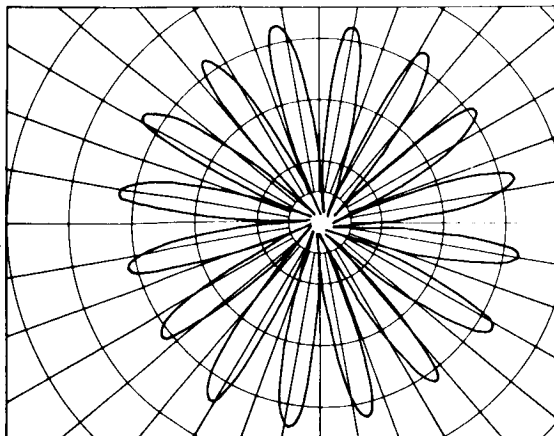
E_θ
Four Antennas



E_ϕ

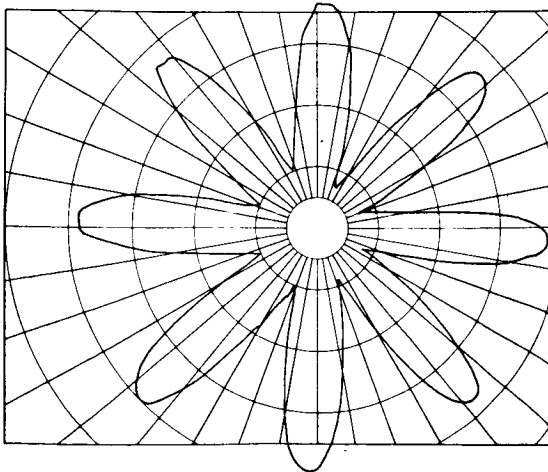


E_θ
Eight Antennas

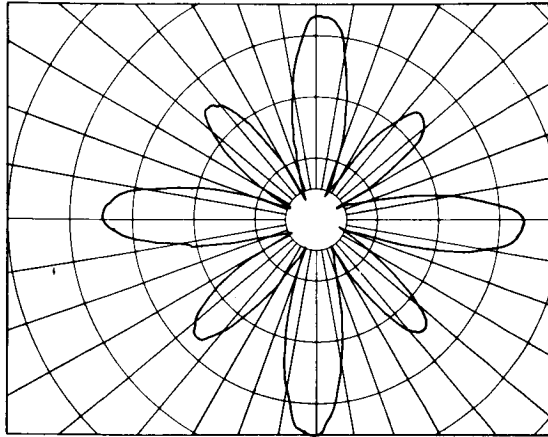


E_ϕ

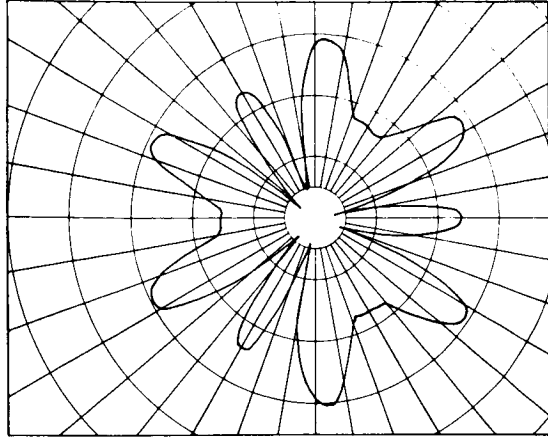
Figure 37 Relative Field Radiation Patterns In Roll Plane Of 230 MC Antennas At Station 30



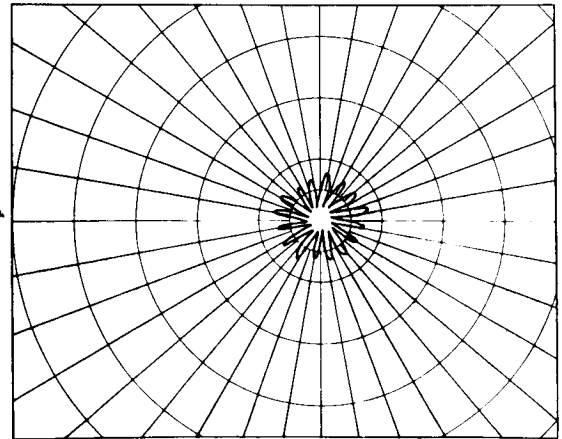
E_θ
Eight Antennas



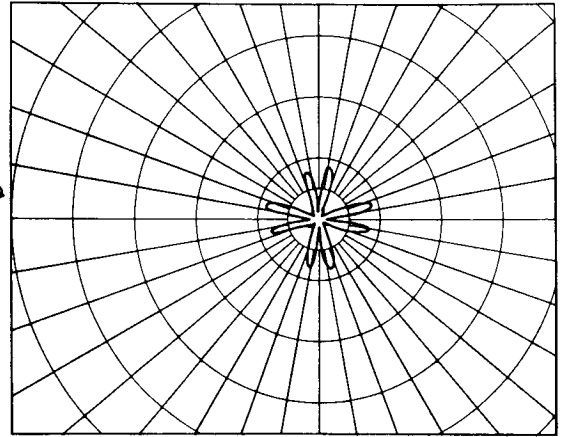
E_θ
Four Antennas



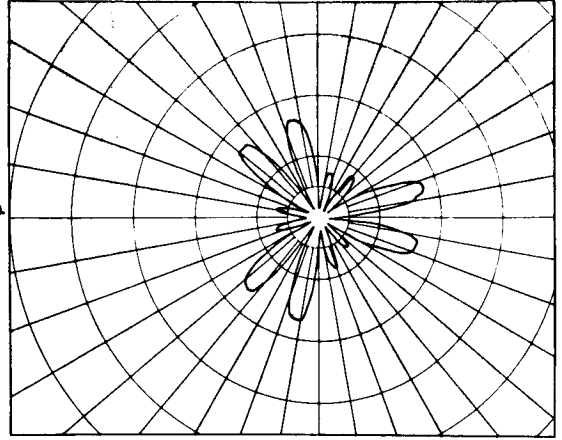
E_θ
Three Antennas



E_ϕ

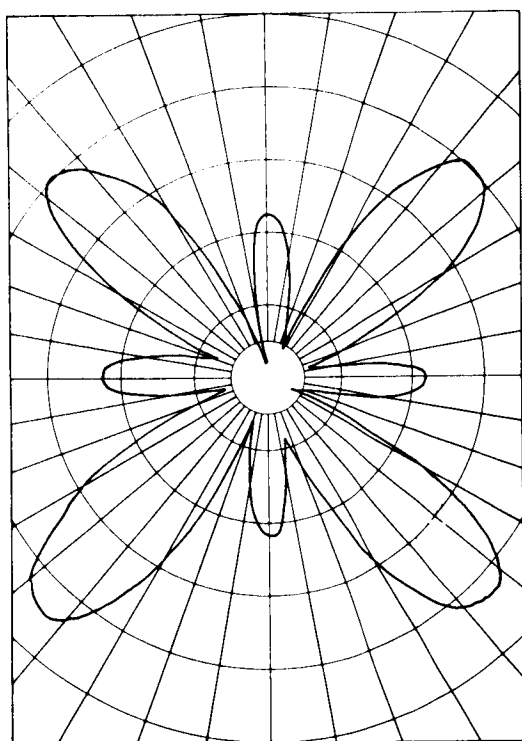


E_ϕ

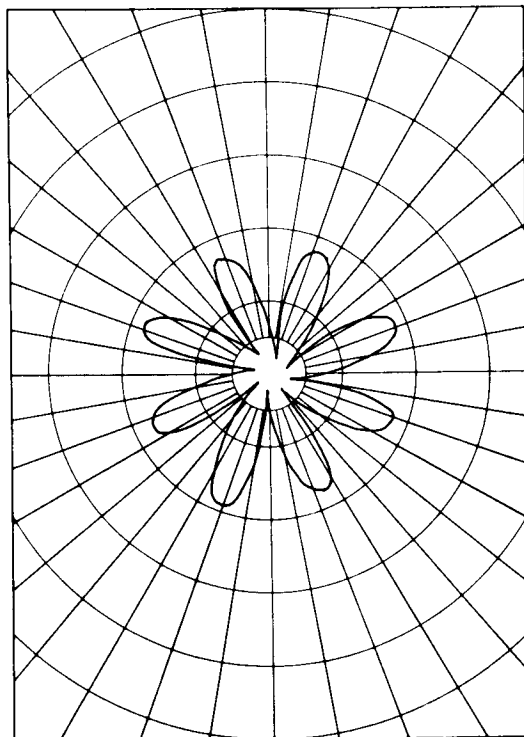


E_ϕ

Figure 88 Relative Field Radiation Patterns In Roll Plane Of 230 MC Antennas At Station 68



E_e



E_ϕ

Four Antennas

Figure 89 Relative Field Radiation Patterns In Roll Plane Of 230 MC
Antennas At Station 107

with equal in phase currents and comprised eight, four and three elements respectively. In all cases these were equally spaced circumferentially. The Station 30 locations are in the widest portion of the command module and constitute approximately the lowest location possible for antennas of this size.

The patterns of Figure 88 were taken with three similar installations at Station 68, which is about half way up the capsule. Finally, Figure 89 shows the patterns of a set of four antennas at Station 107 up near the apex of the cone. In this part of the vehicle the circumference is too small to accommodate reasonably eight antennas, therefore no test simulating such an installation was seriously contemplated. Further than this it was learned in discussion with NAA personnel that this portion of the capsule is so crowded with equipment that it became apparent that it was not practical to install antennas here. Accordingly, only limited data were taken in this region.

Pitch-yaw plane patterns, of the above installations are shown in Figure 90, 91 and 92. All of the patterns referenced in the above paragraphs were measured with the complete command-service module assembly. From these several points of interest could be noted. At Station 30, the array of eight antennas produces a much smoother yaw plane pattern than does the 4 or 3 element array. However, the yaw plane pattern of the eight element array at Station 68 is not so smooth as that at Station

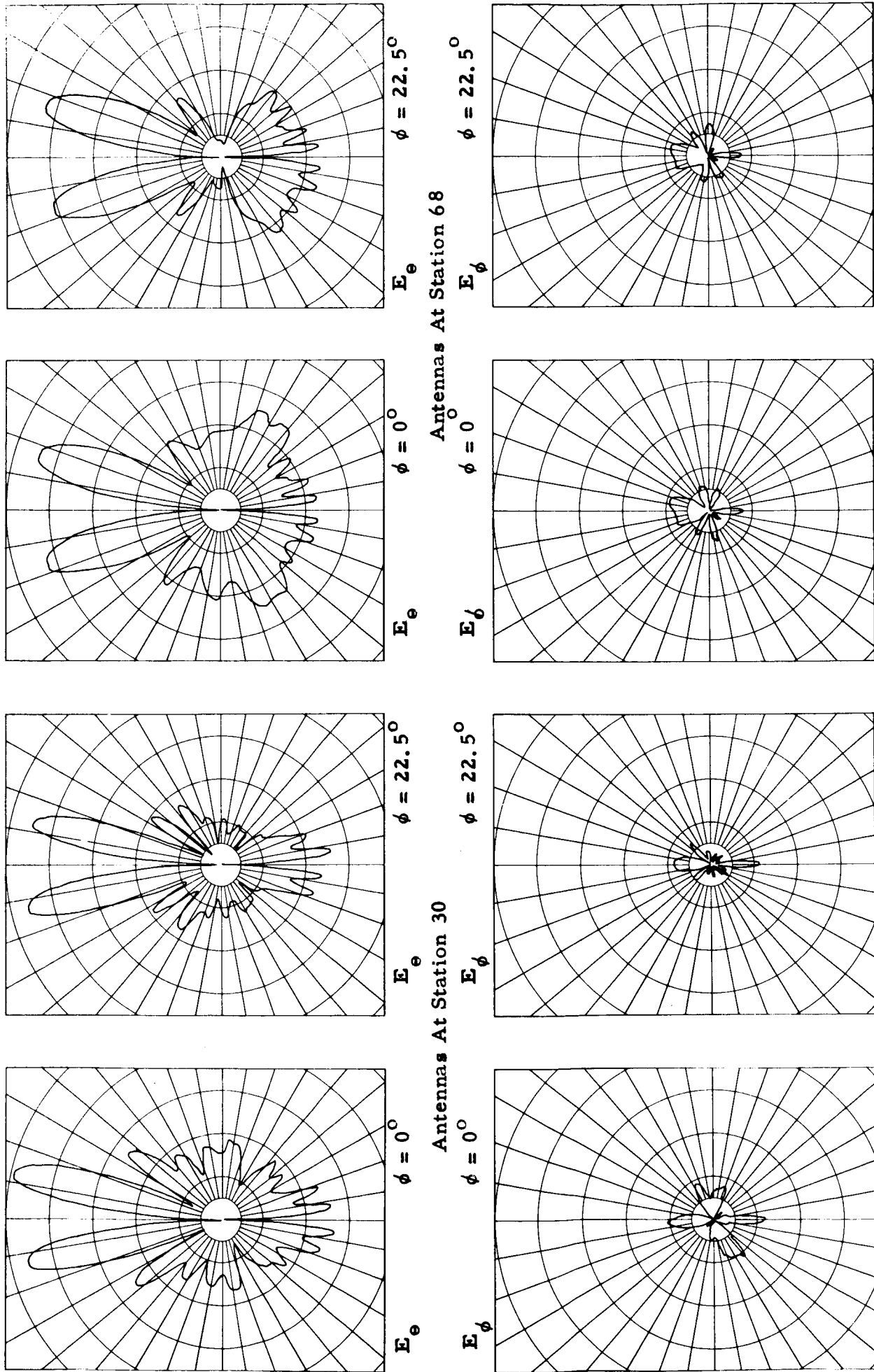


Figure 90 Relative Field Radiation Patterns in Pitch-Yaw Planes of Arrays of Eight 230 MC Antennas

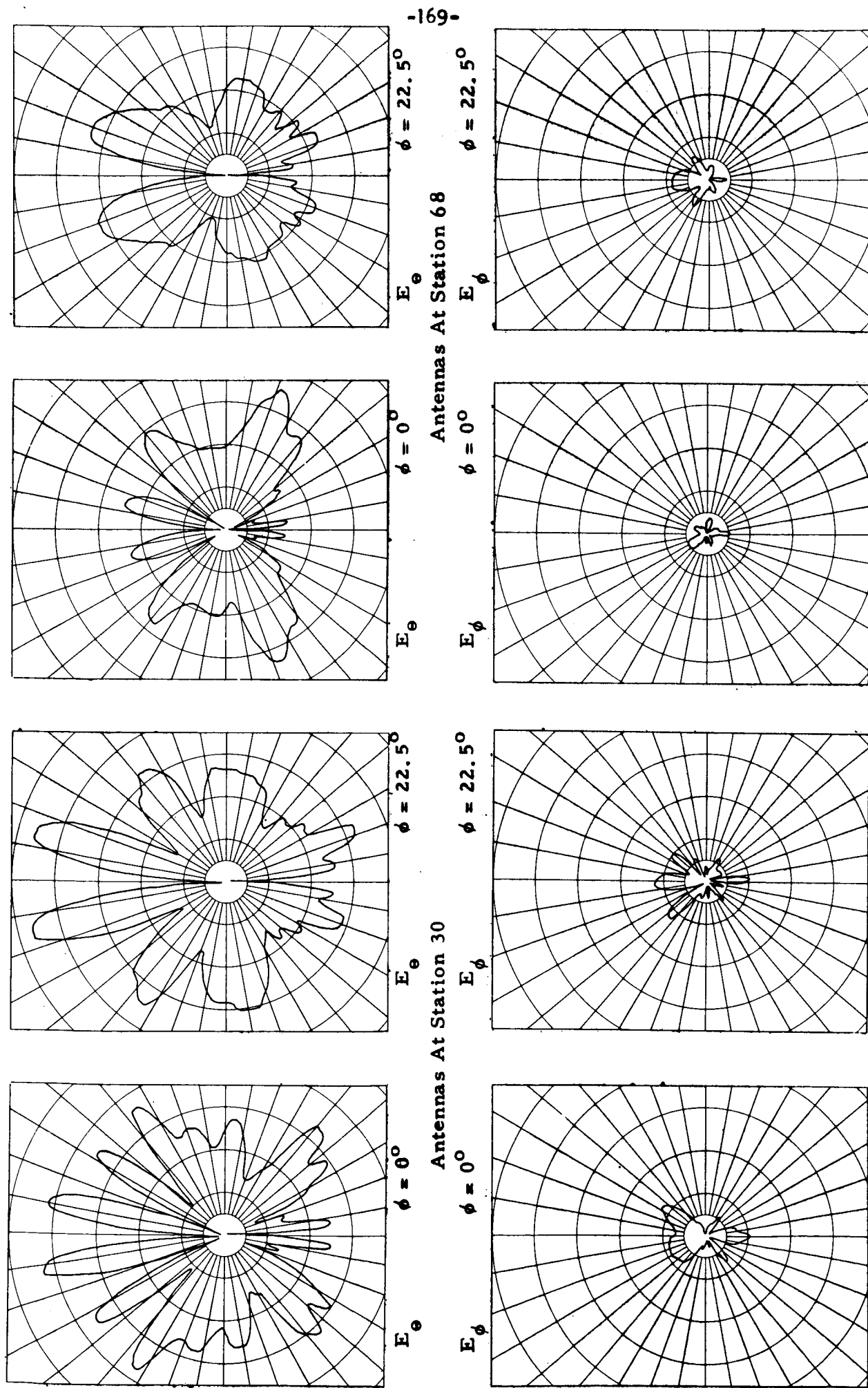


Figure 91 Relative Field Radiation Patterns In Pitch-Yaw Planes Of Arrays Of Four 230 MC Antennas

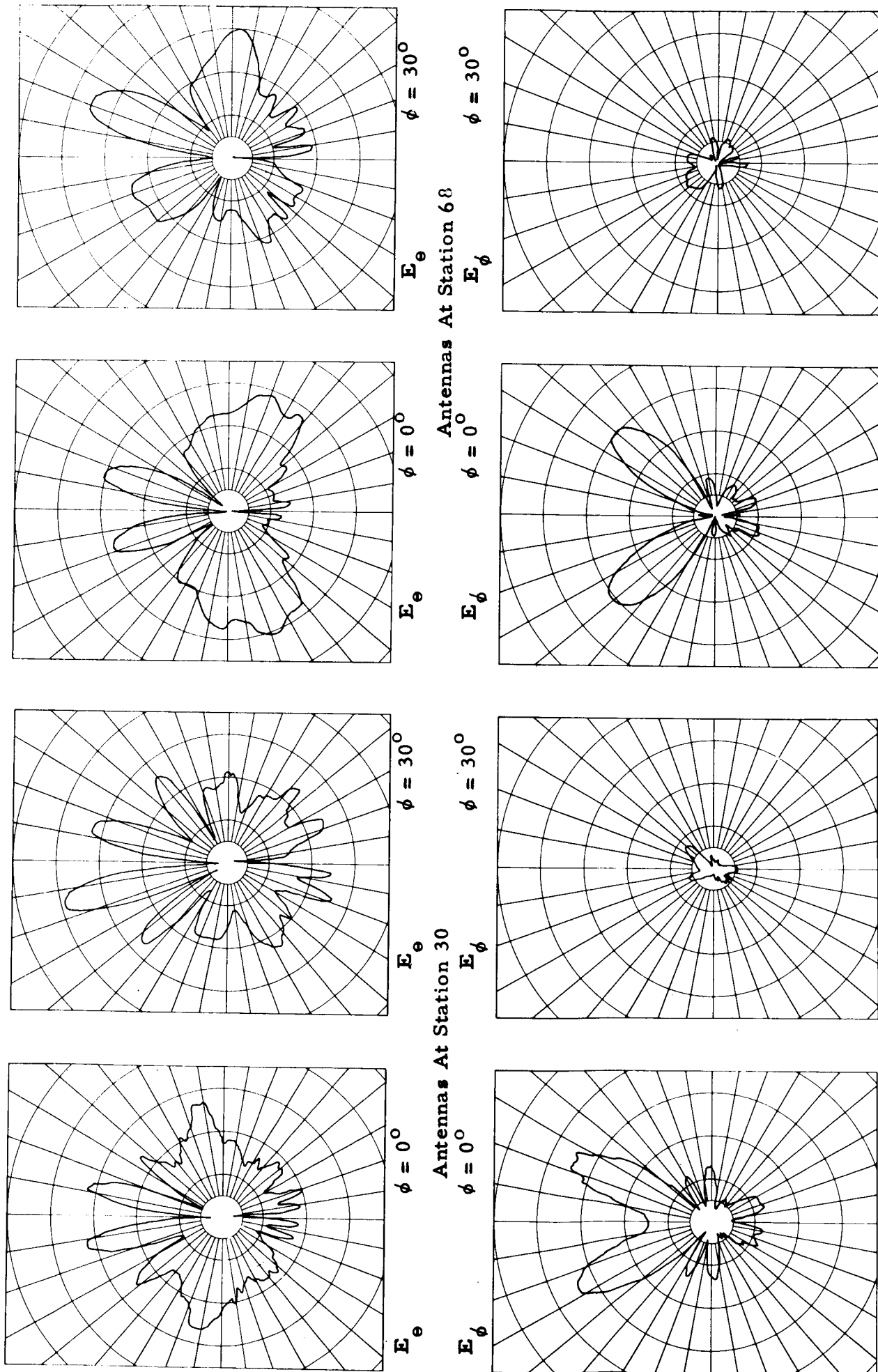
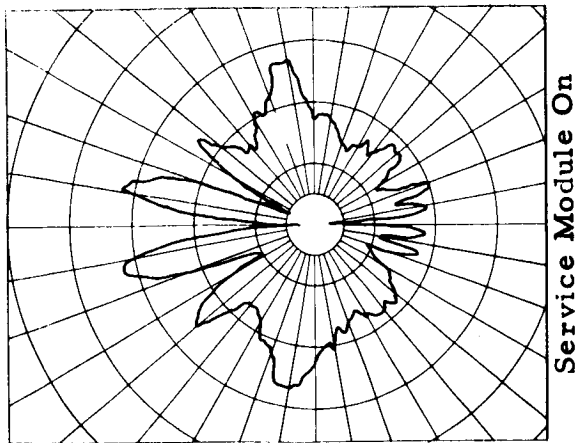


Figure 92 Relative Field Radiation Patterns in Pitch-Yaw Planes of Arrays of Three 230 MC Antennas

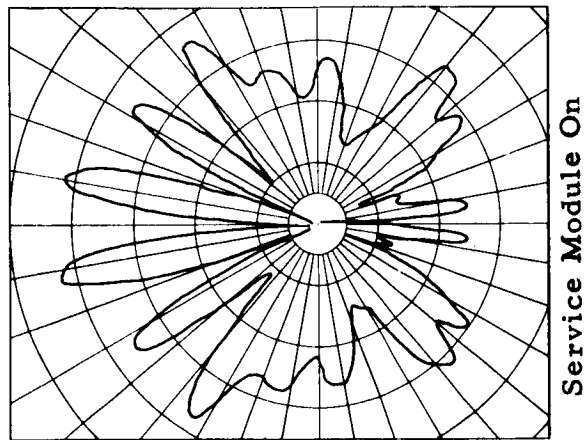
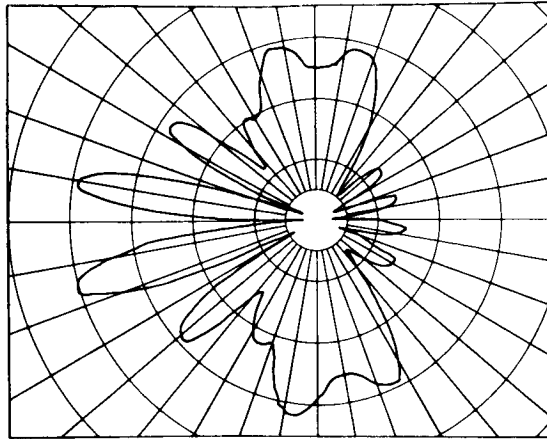
30 even though the antennas are closer together. This indicates that even with eight antennas the spacing between elements is so great that only with a particular (critical) geometry is a relatively null-free pattern obtained. The effect is apparently a result of the conical shape and is significantly different from that obtained on cylinders. It is also to be noted that at Station 68 the E_θ radiation is considerably reduced with the eight element array. On the other hand, with the three element array at this station the E_θ radiation is virtually complementary to the E_ϕ radiation. With this type of pattern and polarization diversity at earth stations a considerable reduction of effective nulls should be accomplished.

The pitch-yaw plane patterns show that radiation aft is adequate with installations at either Station 30 or Station 68, although it is slightly superior at Station 30.

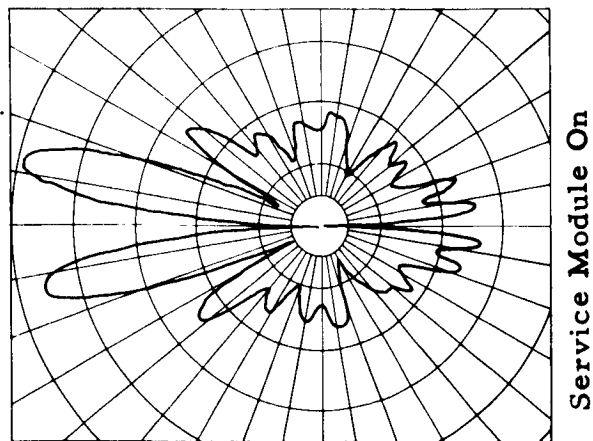
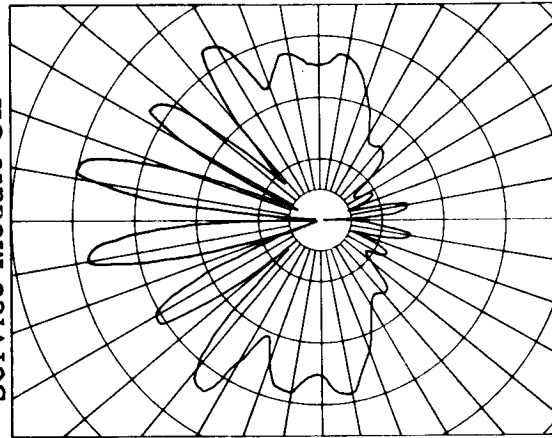
It was mentioned above that all of these patterns were obtained with the complete command-service module assembly. All of these conditions were also tested with the service module detached. No appreciable change was observed in any of the roll plane patterns. In the pitch-yaw plane a change is apparent. This can be seen from Figures 93 and 94. The first of these show comparative pitch plane patterns



Three Antennas, E_θ , $\phi = 0^\circ$
Service Module Off



Four Antennas, E_θ , $\phi = 0^\circ$
Service Module Off



Eight Antennas, E_θ , $\phi = 0^\circ$
Service Module Off

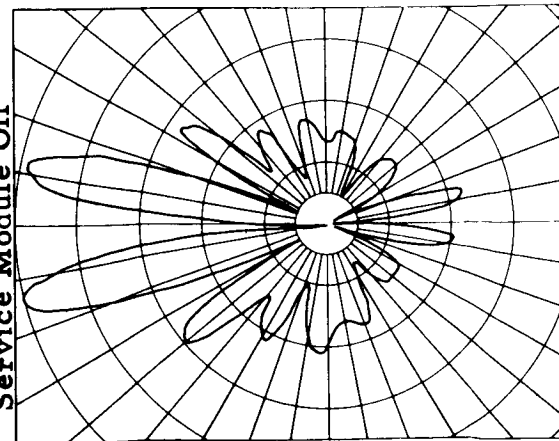
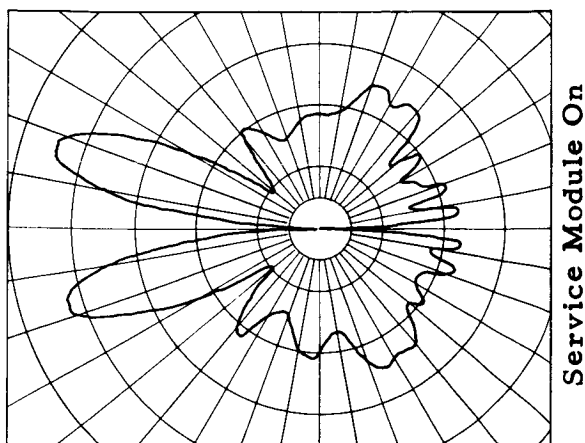
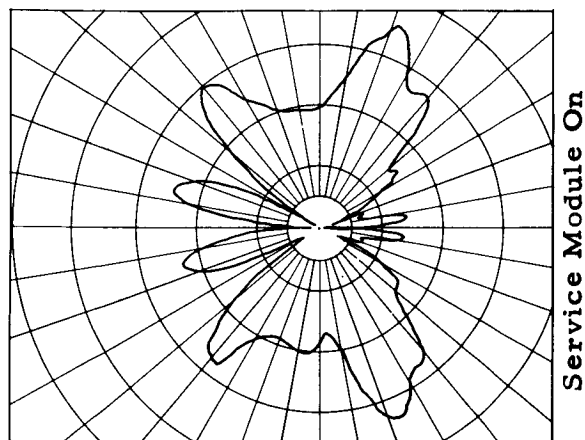
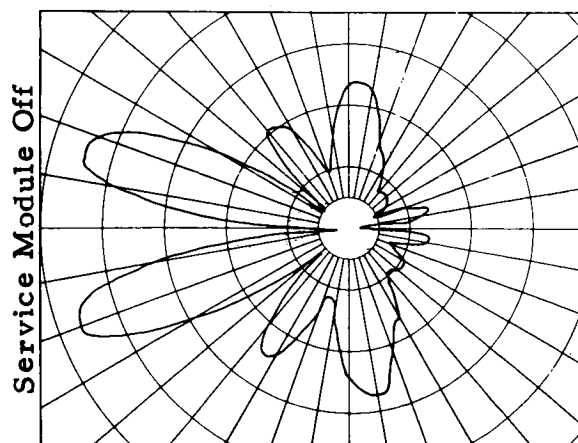


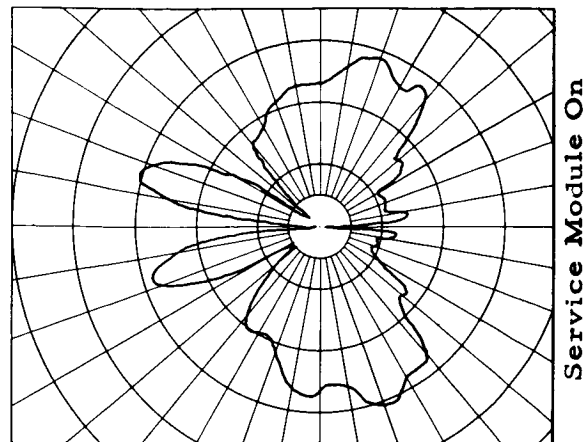
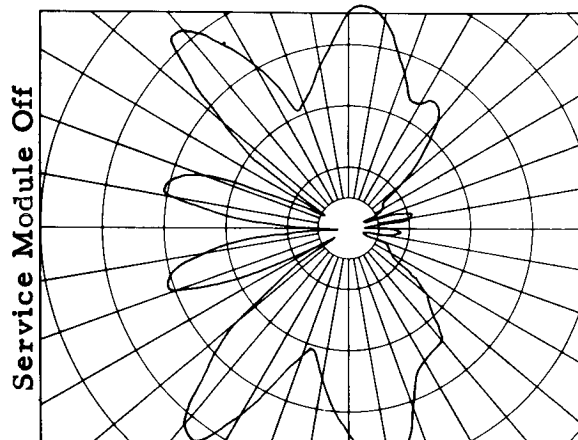
Figure 93 Relative Field Radiation Patterns In Pitch Plane Showing Effect Of Service Module
On 230 MC Antennas At Station 30



Eight Antennas, E_{θ} , $\phi = 0^{\circ}$



Four Antennas, E_{θ} , $\phi = 0^{\circ}$



Three Antennas, E_{θ} , $\phi = 0^{\circ}$

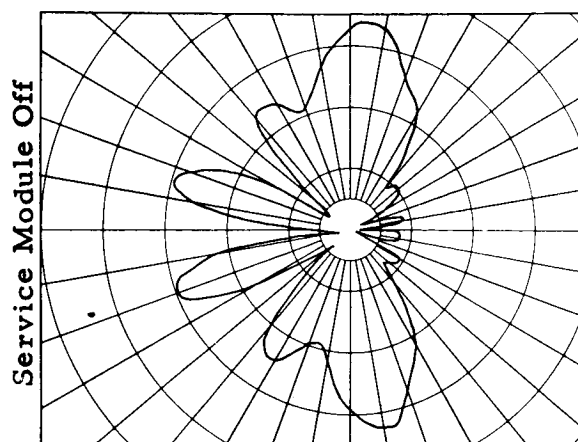


Figure 94 Relative Field Radiation Patterns In Pitch Plane Showing Effect Of Service Module On 230 MC Antennas At Station 68

with and without the service module for otherwise identical installations of eight, four and three antennas at Station 30. Figure 94 shows a corresponding set of patterns measured with the antenna located at Station 68. In both cases it will be noted that the average amount of radiation aft is somewhat greater when the service module is attached. Further, the radiation aft has sharper nulls with the service module off. Because the vehicle will be close to earth during the phase of its mission when the service module is off, the effect of this should not be harmful.

The next sets of patterns shown were also measured at 230 mc and are those of an array of only two elements, the minimum that can possibly be satisfactory. For this installation the antennas were installed with the plane of the loop canted at 45 degrees to the Y-Z plane in order to increase the E_{θ} component of radiation. The antennas were both tilted in the same direction (when viewed from a comparable point outboard of each antenna) and were fed out of phase. For these measurements balanced half loops were used as the radiating elements. Such an antenna is essentially identical in its radiation patterns to the prototypes. For illustrative purposes a single one of these half loops was mounted in the center of a 24 inch diameter round ground plane, thereby modelling at 1/4 scale the set-up used for testing the prototypes. The E plane pattern obtained at 920 mc is shown in Figure 95. Comparison with Figure 75 which showed the full scale patterns of

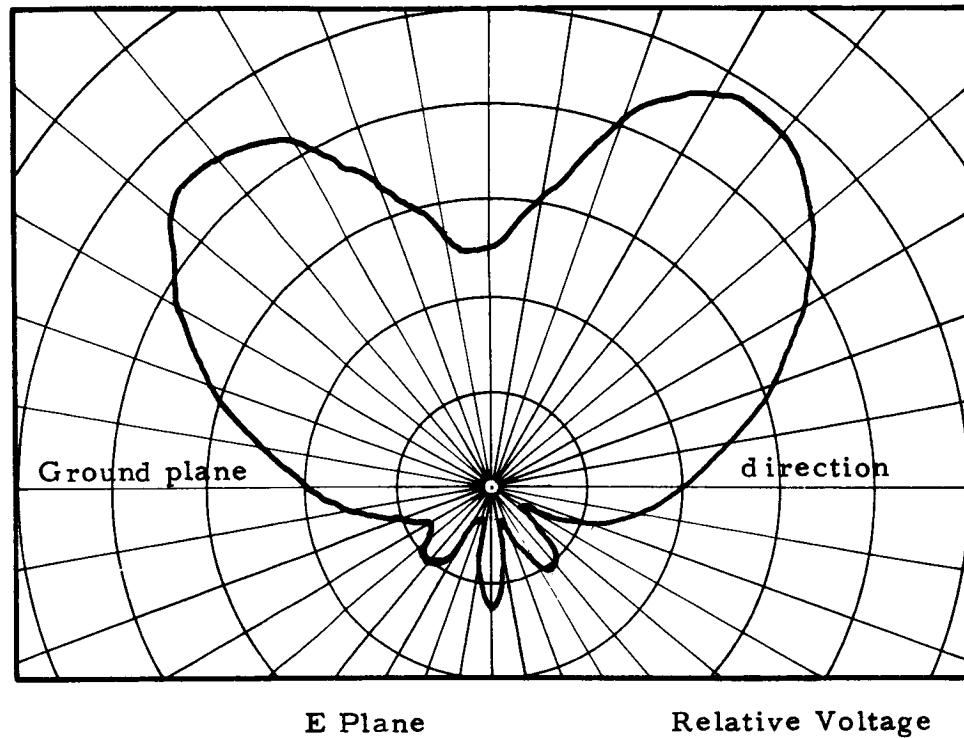
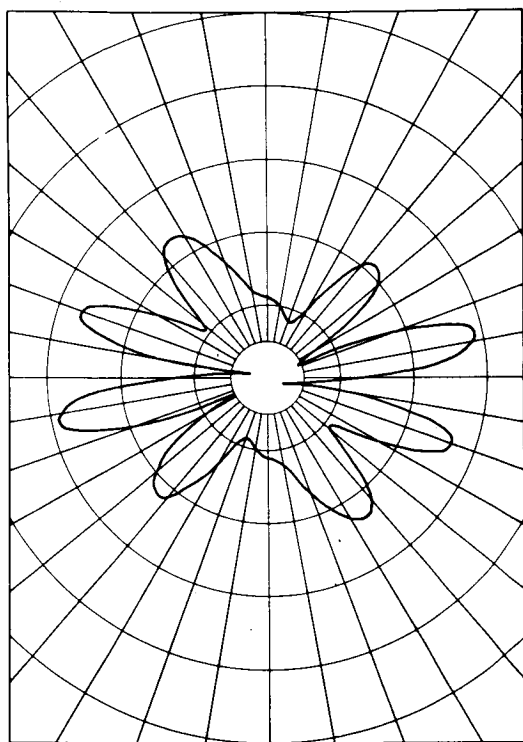


Figure 95 Measured Pattern Of Small Half-Loop Antenna On
Two Foot Diameter Ground Plane At 920 MC

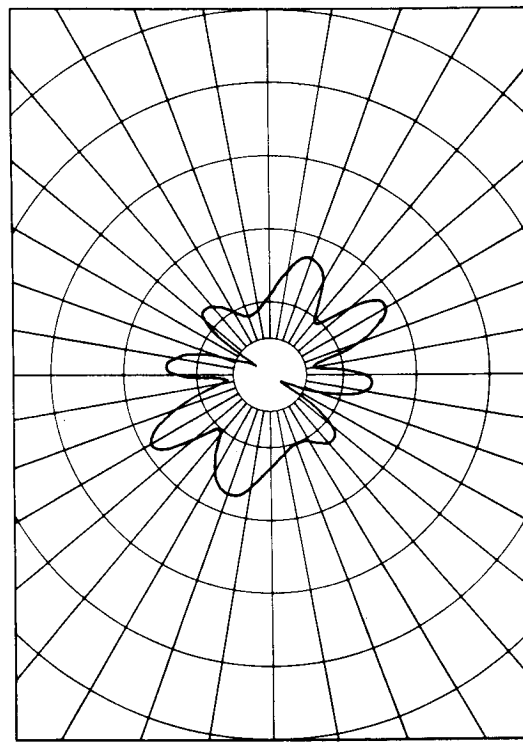
the 237.8 mc model and of the reference half loop used then shows that the inherent patterns are similar.

The roll plane patterns obtained with this installation are shown on Figure 96. Figures 97, 98 and 99 show representative pitch-yaw plane patterns. It will be noted that they possess the desired characteristic. The minima of the two components tend to fall in different directions.

The next sets of patterns shown were obtained at scale frequencies corresponding to 450 mc. The first of these were taken with a set of three antennas installed at Station 25. These were obtained with balanced loops equispaced around the capsule, running straight up and down, and excited with equal amplitude progressively phased excitation (i.e., the relative phases of the antennas were 0 , 120° and 240°). A set of patterns with the antennas excited in phase was also obtained. Except for the symmetry null that appears in both x directions they are not appreciably different from those shown. The next set shown was obtained with only two of these half loops installed diametrically opposite each other at Station 25 and excited out of phase. Following these patterns are a set that is similar, differing only in that the loops were canted 45 degrees with respect to the X-Y plane. Patterns obtained with these various installations are shown in Figures 100 through 108. It will be seen that although the straight two element array is substantially inferior to the three element one, that the canted two element one (again, assuming polarization diversity for the earth stations) is superior to either.



E_ϕ



E_θ

Figure 96 Relative Field Radiation Patterns In Roll Plane Of Two
Canted 230 MC Antennas At Station 68

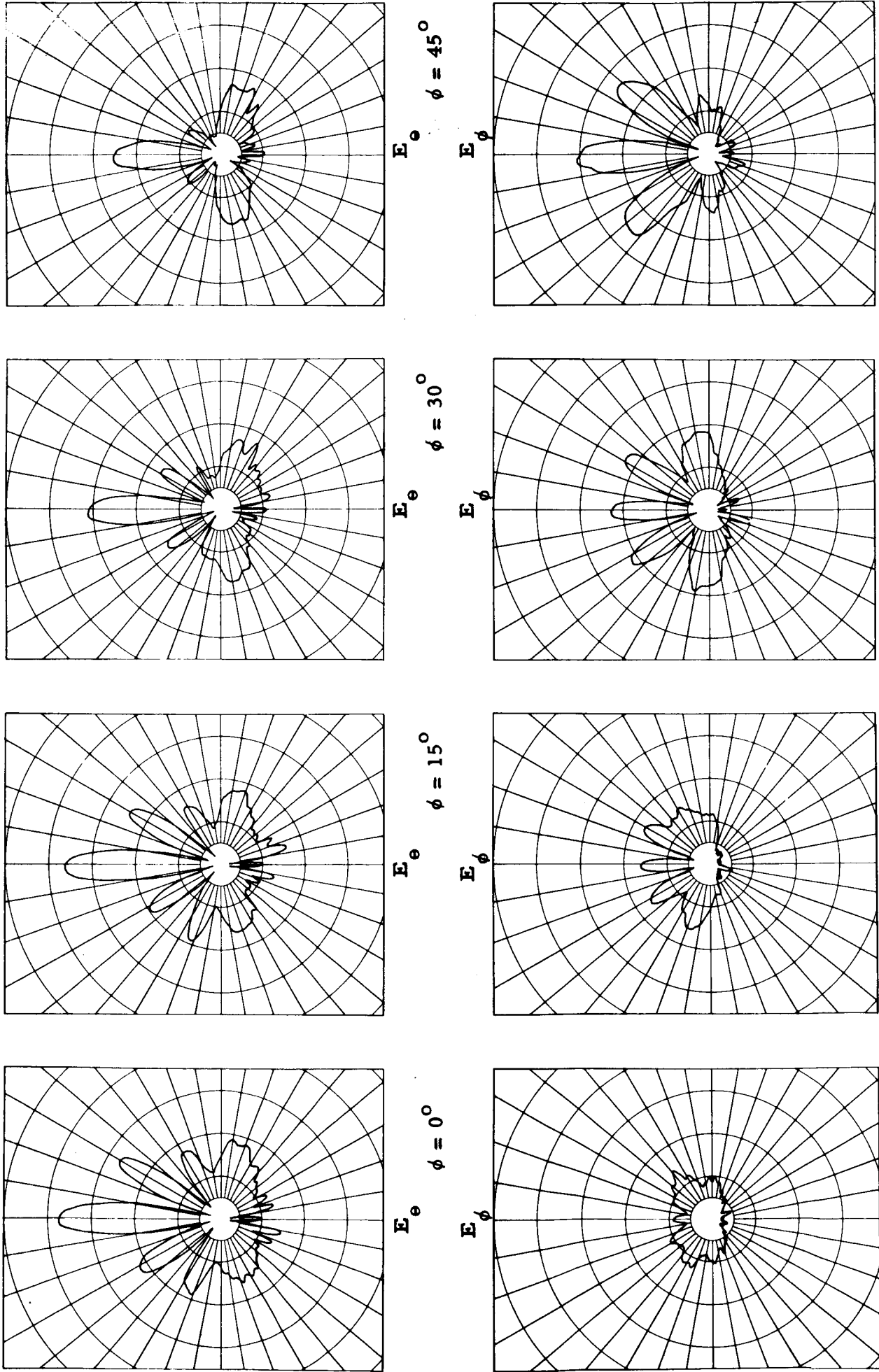


Figure 97 Relative Field Radiation Patterns In Pitch-Yaw Planes Of Two Canted 230 MC Antennas At Station 68

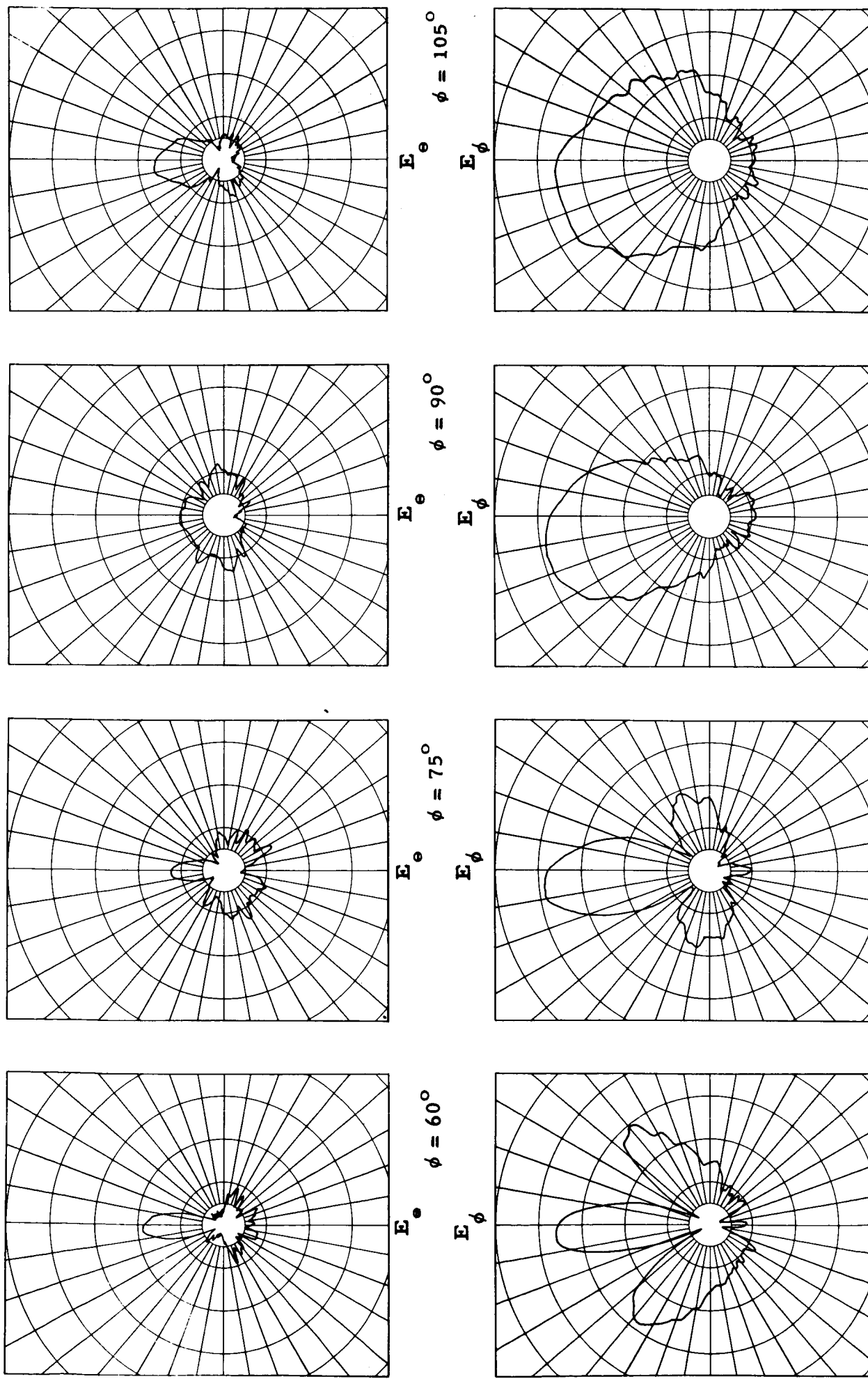


Figure 98 Relative Field Radiation Patterns In Pitch-Yaw Planes Of Two Canted 230 MC Antennas At Station 68 Continued

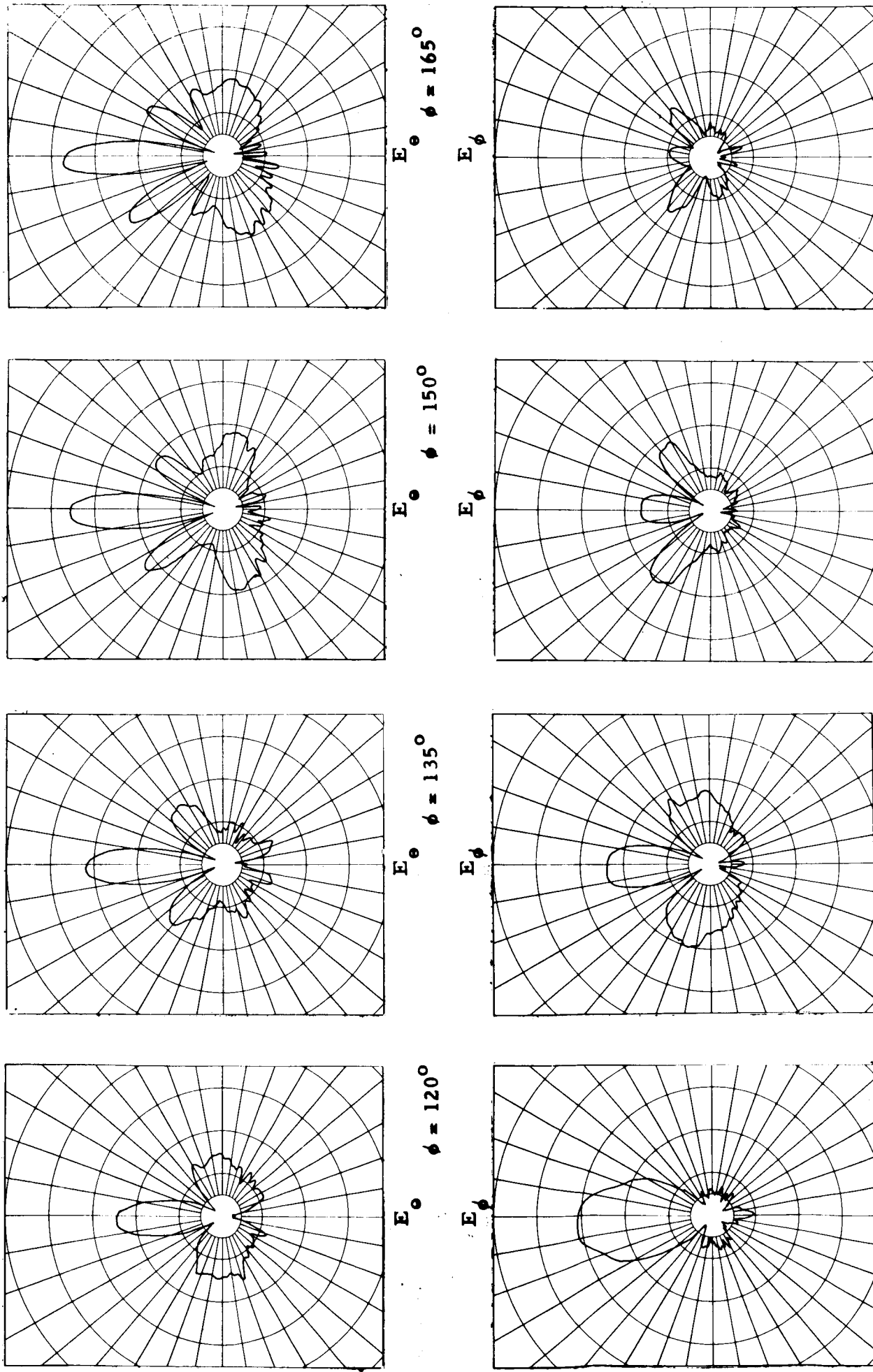


Figure 99 Relative Field Radiation Patterns In Pitch-Yaw Planes Of Two Canted 230 MC Antennas At Station 68 Continued

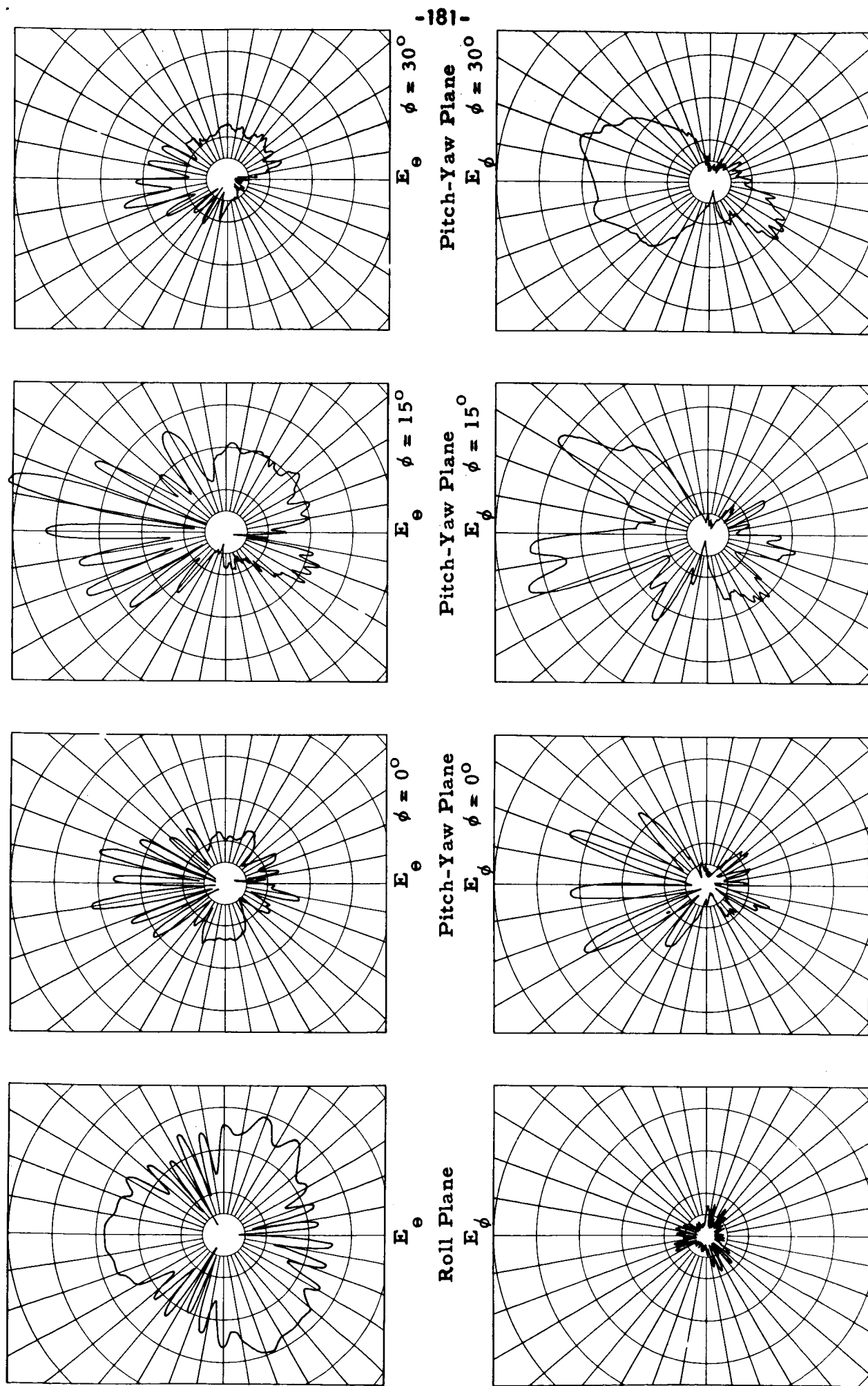


Figure 100

Relative Field Radiation Patterns Of Three Element Array Of 450 MC Antennas At Station 25

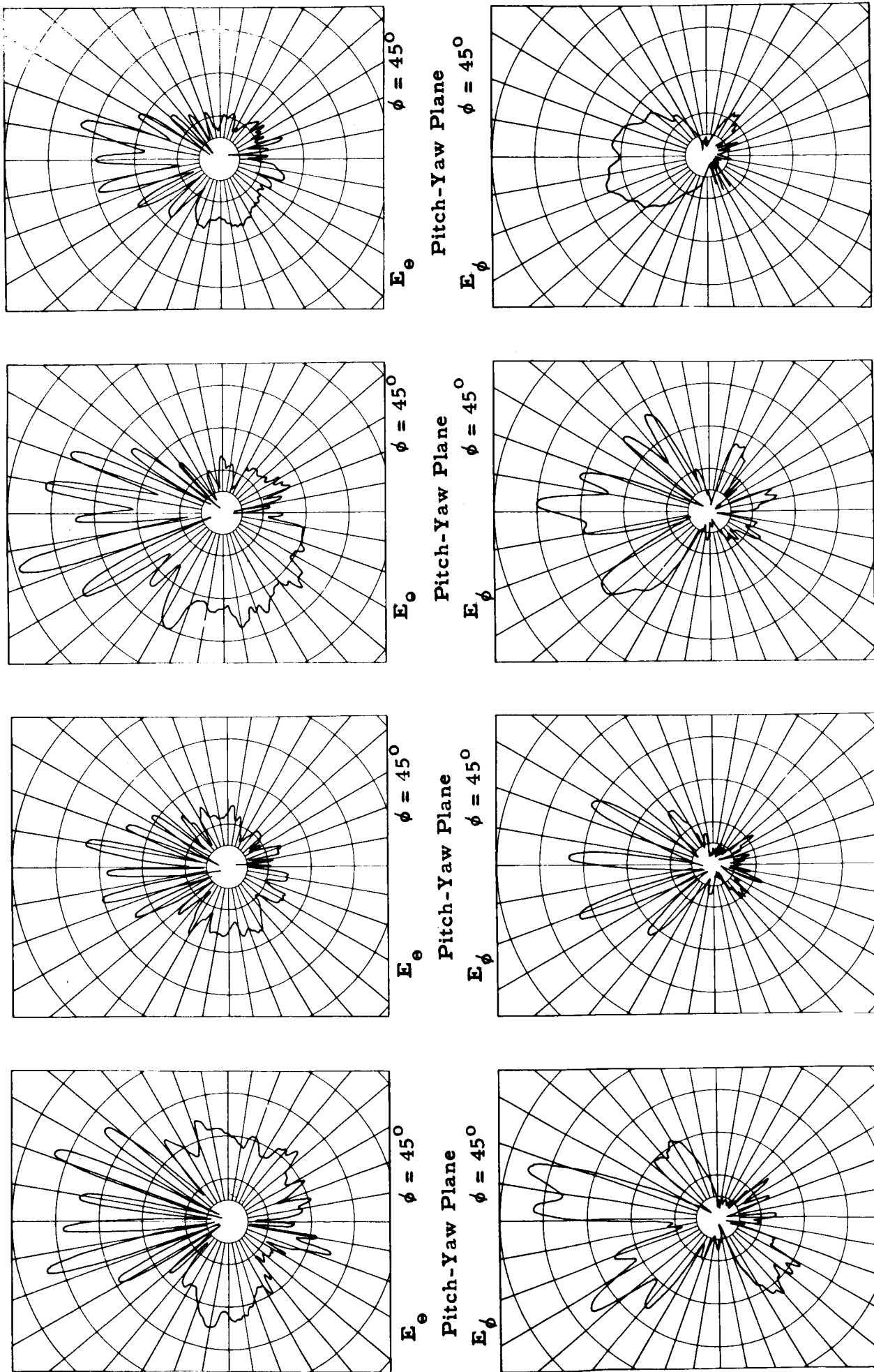
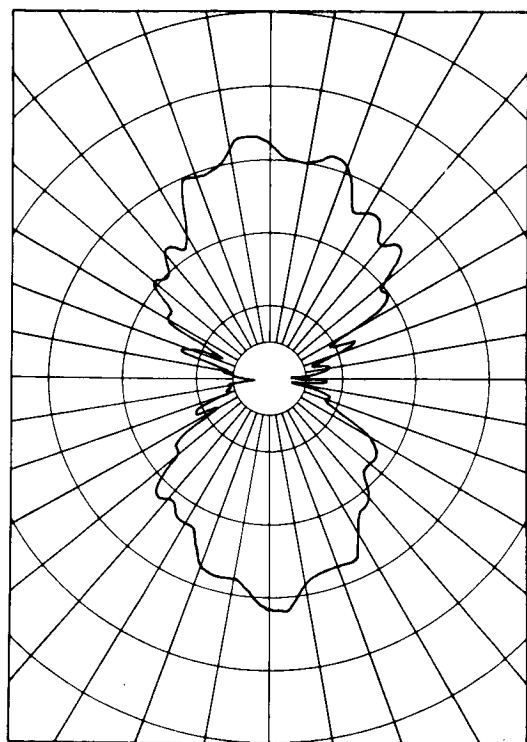
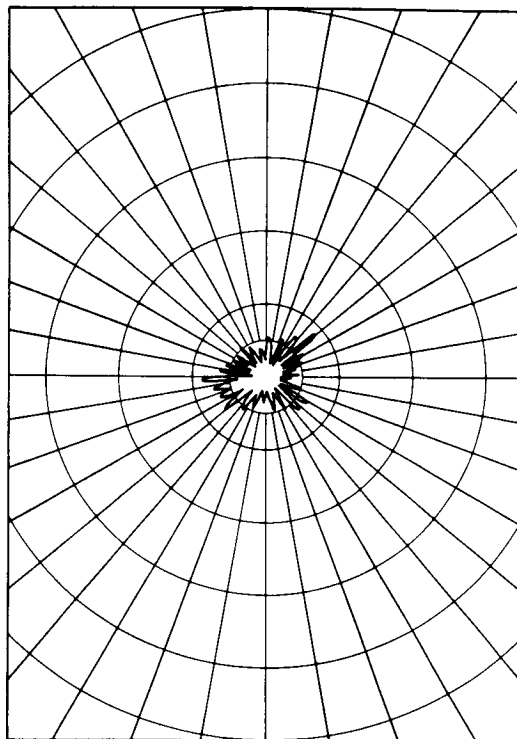


Figure 101 Relative Field Radiation Patterns Of Three Element Array Of 450 MC Antennas At Station 25 Continued

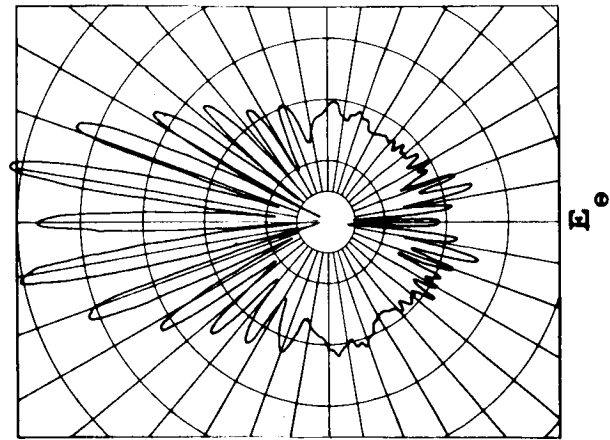


E_e

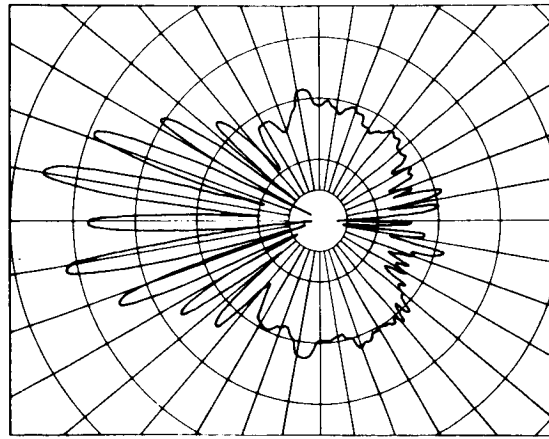


E_ϕ

Figure 102 Relative Field Radiation Patterns In Roll Plane Of Two Element Array Of 450 MC Antennas (Not Canted) At Station 25

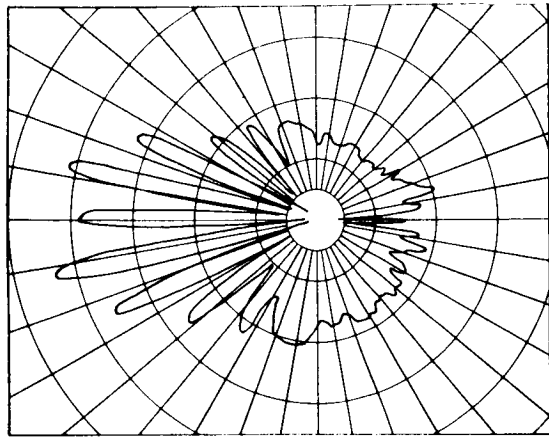


E_e



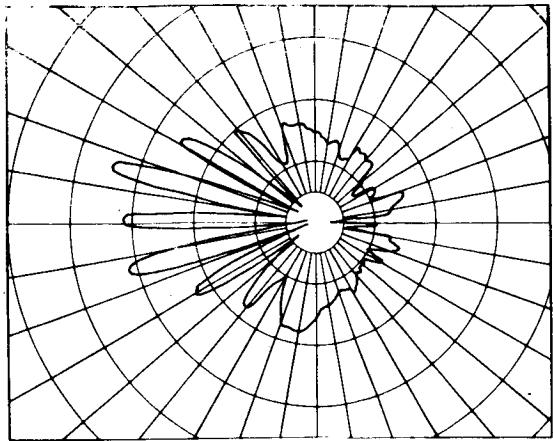
E_e

$\phi = 15^\circ$



E_e

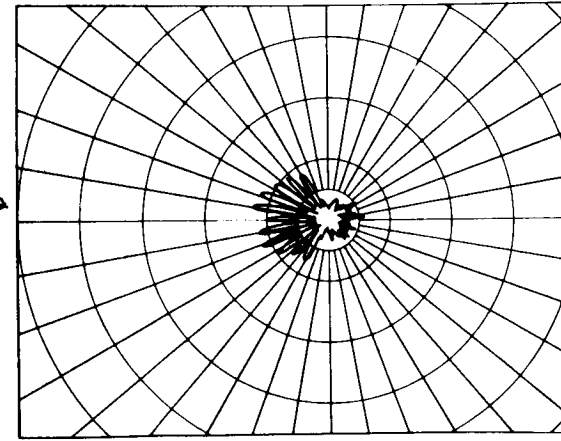
$\phi = 30^\circ$



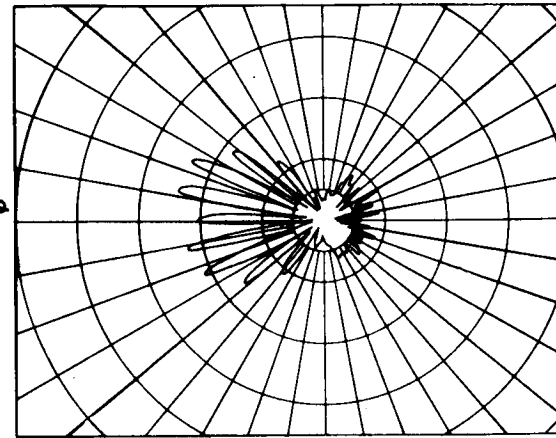
E_e

$\phi = 45^\circ$

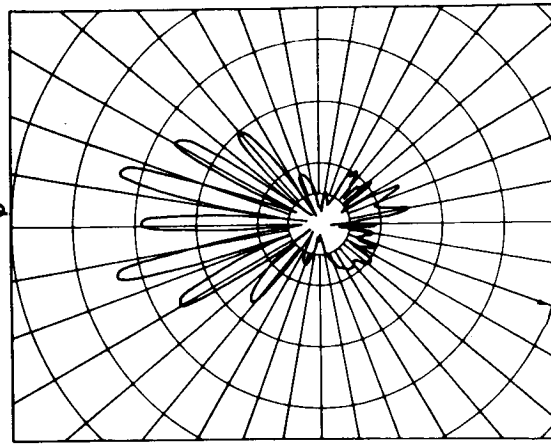
$\frac{1}{2} \lambda$



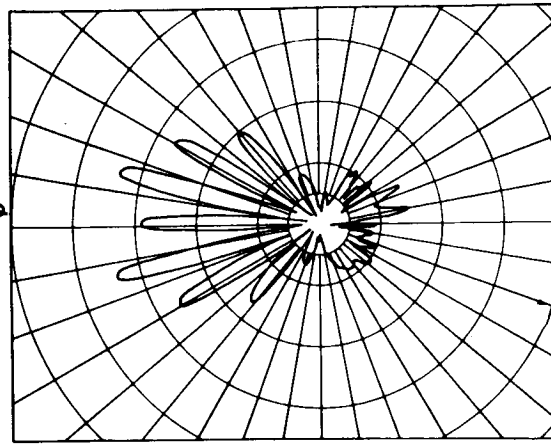
E_ϕ



E_ϕ



E_ϕ



E_ϕ

Radiation Below
Noise Level

Figure 103

Relative Field Radiation Patterns In Pitch-Yaw Planes Of Two Element Array Of 450 MC
Antennas (Not Canted) At Station 25

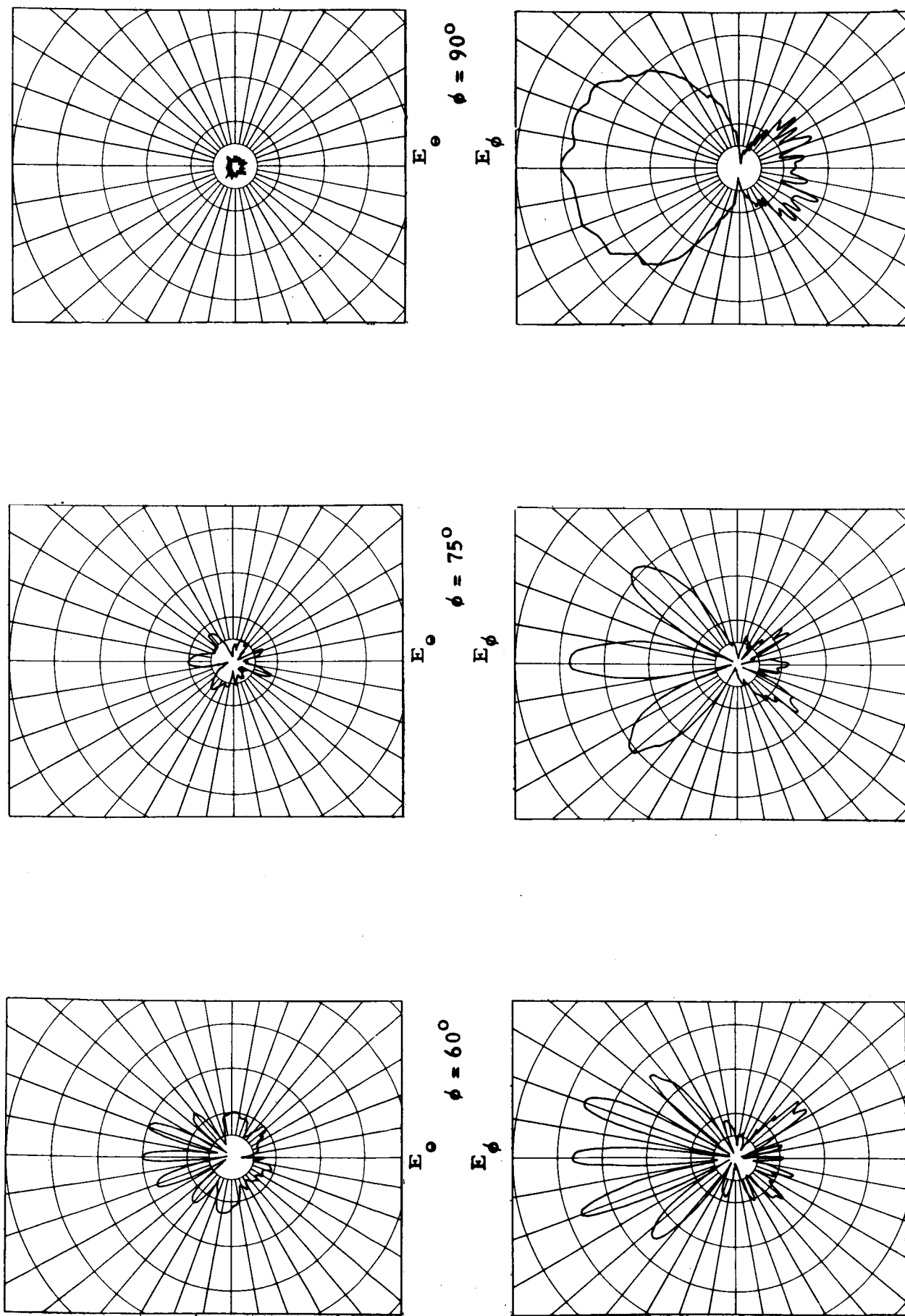
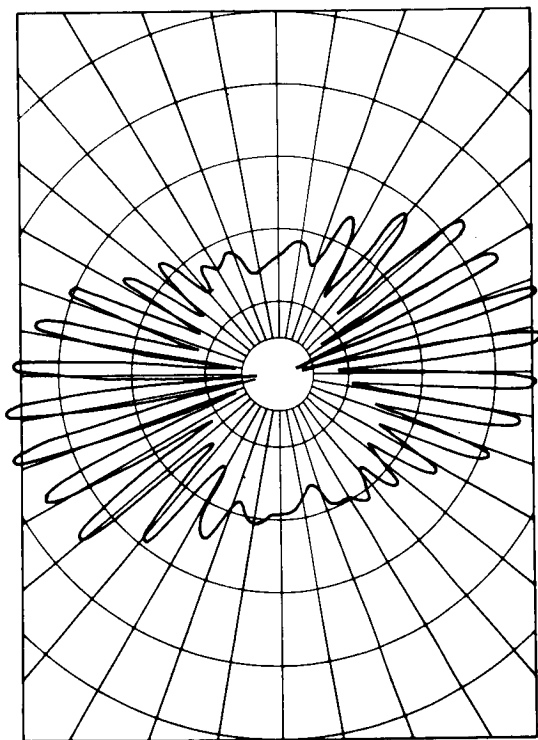
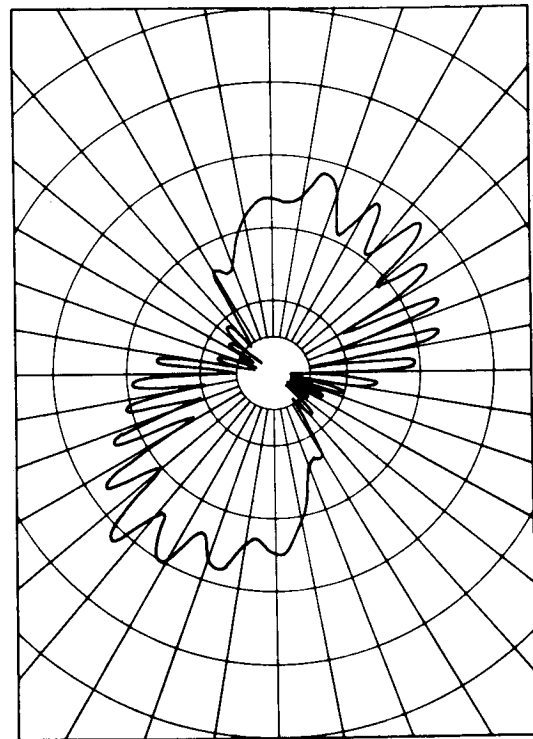


Figure 104 Relative Field Radiation Patterns In Pitch-Yaw Planes Of Two Element Array Of 450 MC Antennas (Not Canted) At Station 25 Continued



E_{θ}



E_{ϕ}

Figure 105 Relative Field Radiation Pattern In Roll Plane Of Two
Element Array Of Canted 450 MC Antennas At Station 25

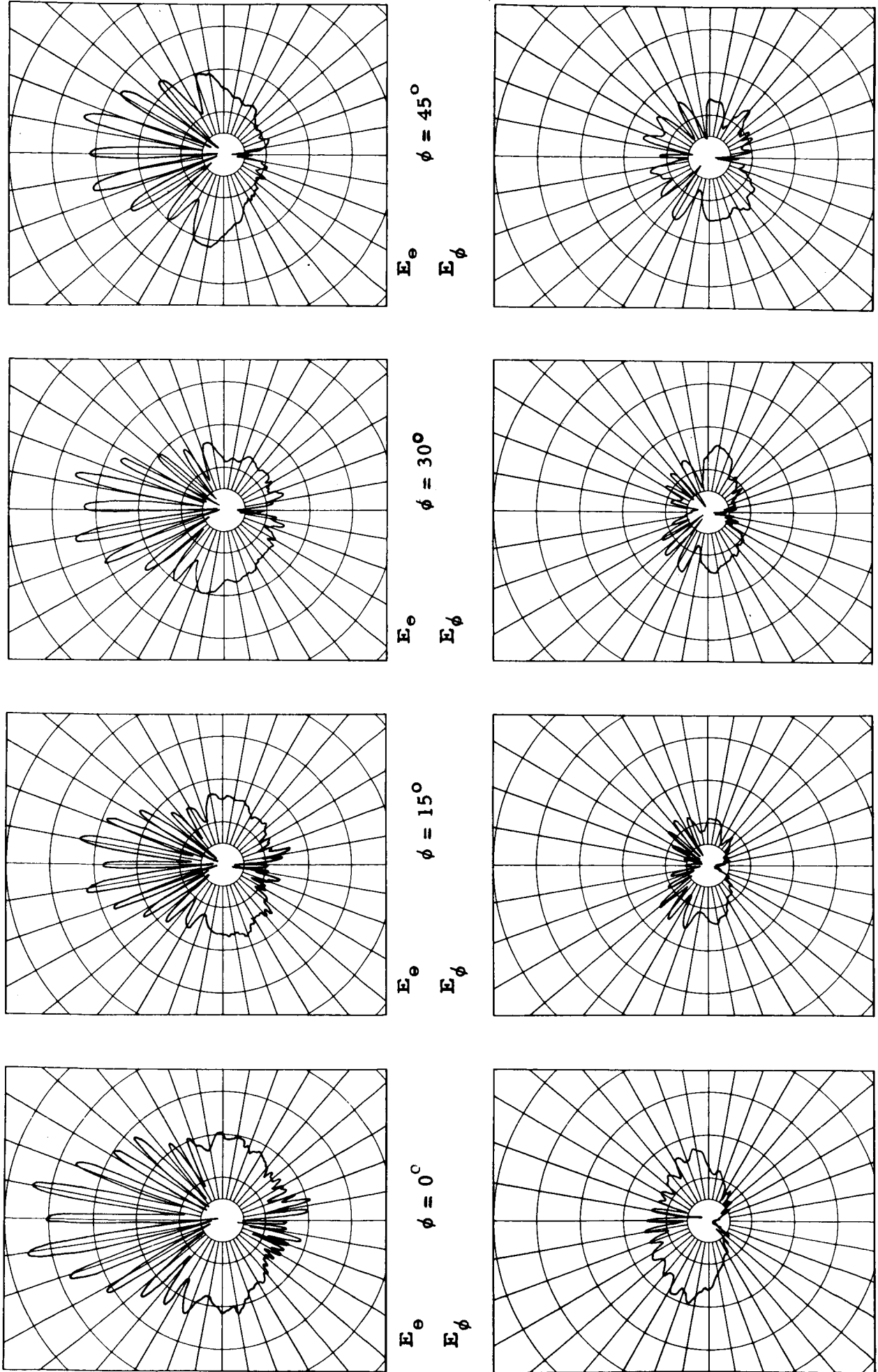


Figure 106 Relative Field Radiation Patterns In Pitch-Yaw Planes Of Two Element Array Of Canted 450 MC Antennas At Station 25

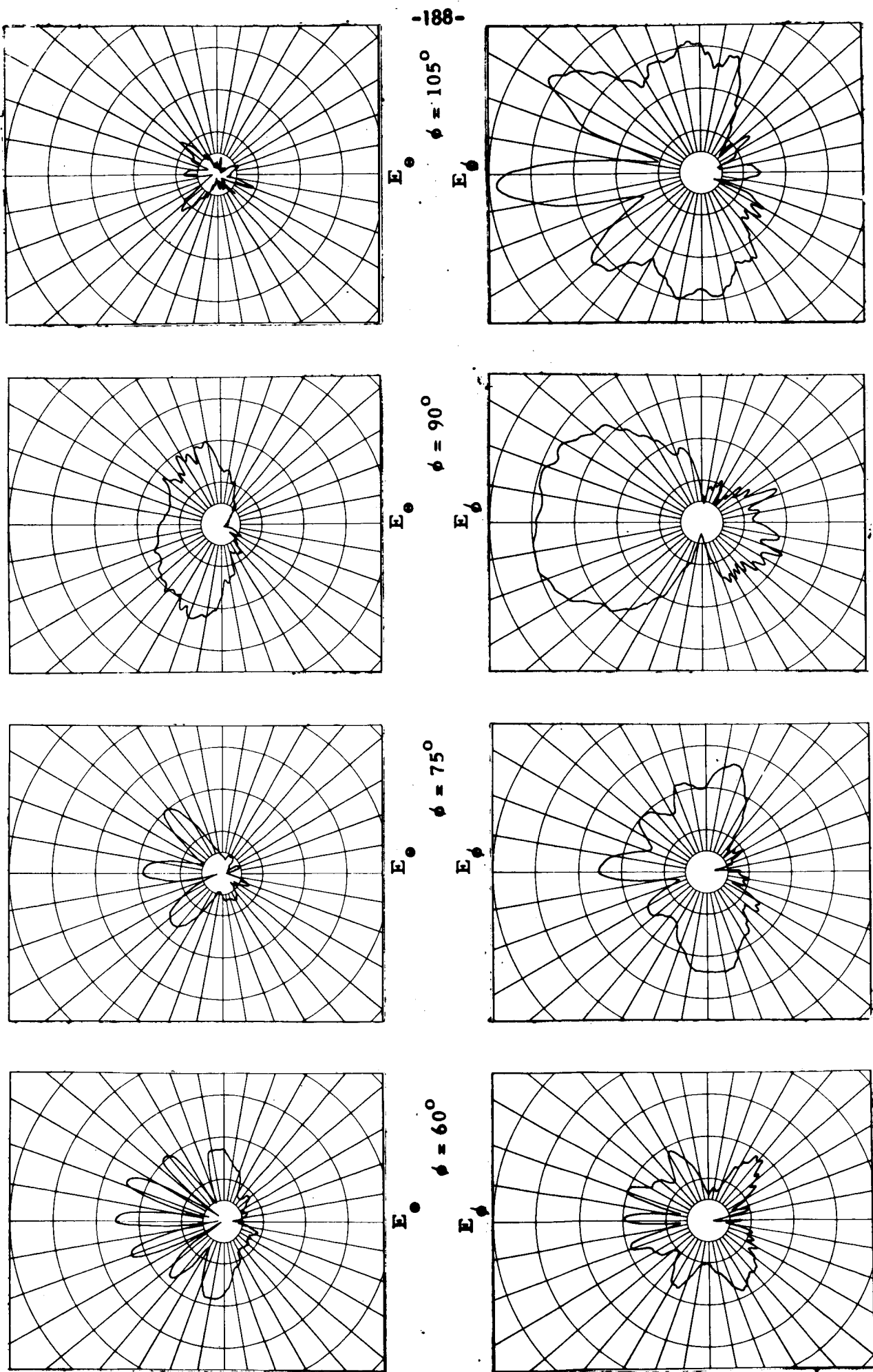
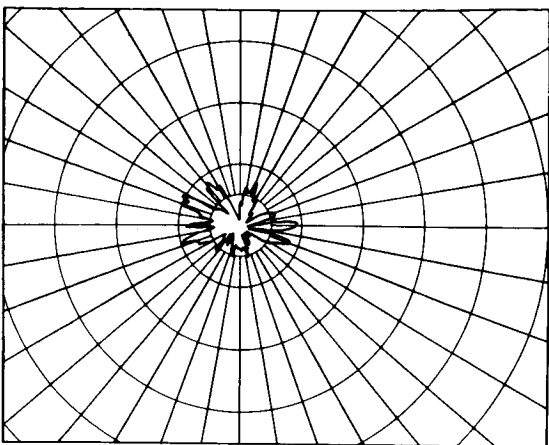
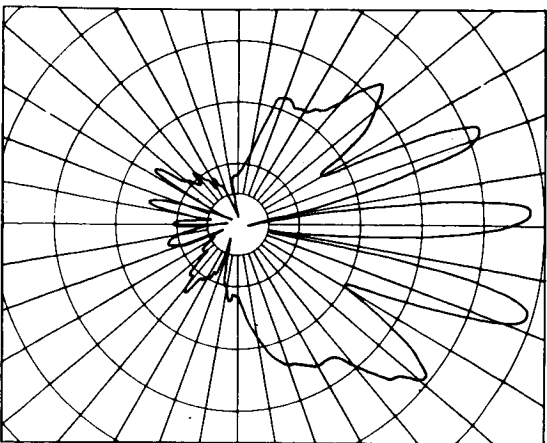


Figure 107 Relative Field Radiation Patterns in Pitch-Yaw Planes Of Two Element Array Of Canted 450 MC Antennas At Station 25 Continued



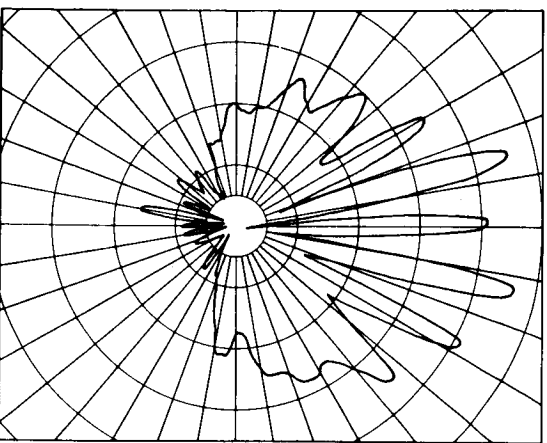
$\phi = 120^\circ$

E_ϕ



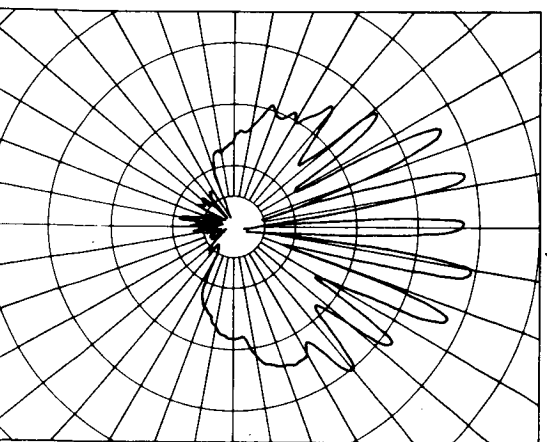
$\phi = 135^\circ$

E_ϕ



$\phi = 150^\circ$

E_ϕ



$\phi = 165^\circ$

E_ϕ

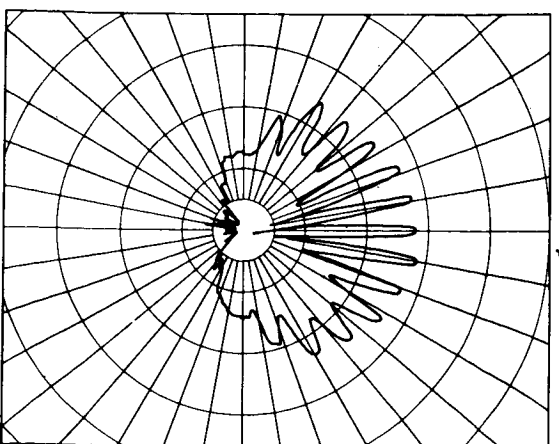
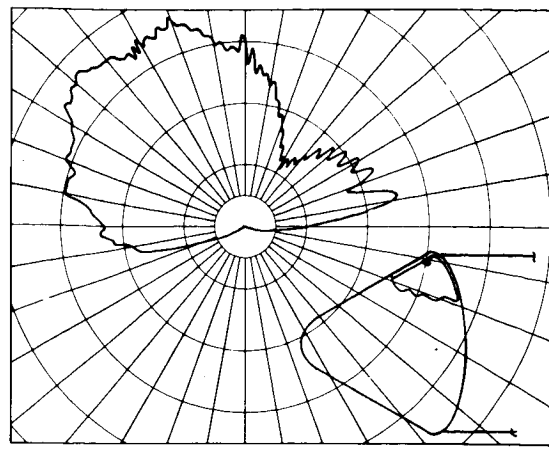


Figure 108 Relative Field Radiation Patterns In Pitch-Yaw Planes Of Two Element Array Of Canted 450 MC Antennas At Station 25 Continued

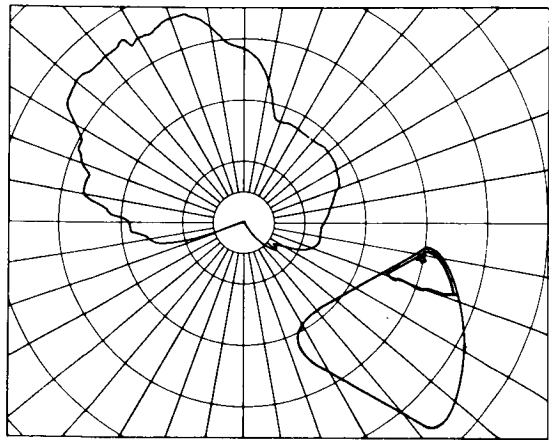
The S-band telemetry pattern problem was next approached. It was anticipated that the ablative material at S-band would prove to be the primary cause of pattern difficulty. No practical means of reducing the losses in the ablative remote from the antenna aperture seems possible. However, because of the shape of the capsule, if the antennas are located low upon it, in most directions the effects of this loss will be tolerable. On the other hand, both because of the vehicle shape and because of the configuration of the region between the command and service modules, it was judged that a serious problem with aft radiation was possible.

A sectional 1/4 scale mockup was constructed whose dimensions are shown in the sketch on Figure 109. A single circular aperture generating the pattern of a linear slot antenna was installed on the mockup. Radiation patterns were recorded under a variety of conditions in order to clarify the effects present. Figure 109 shows patterns measured with the following conditions:

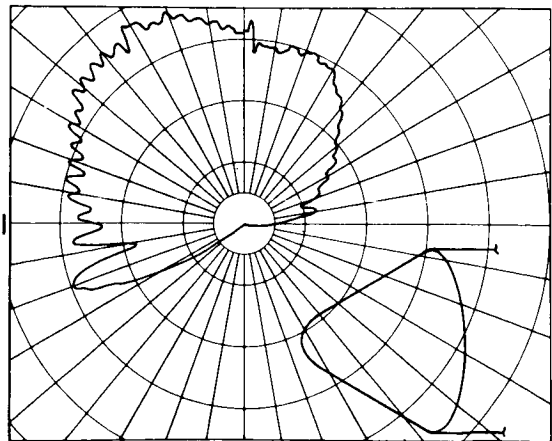
- a. Pattern of a single antenna, command module only, no ablative.
- b. Pattern of a single antenna, command and service module, no ablative.
- c. Pattern of a single antenna, command module only, ablative.
- d. Pattern of a single antenna, command and service module, having no physical contact between metallic structures, ablative.



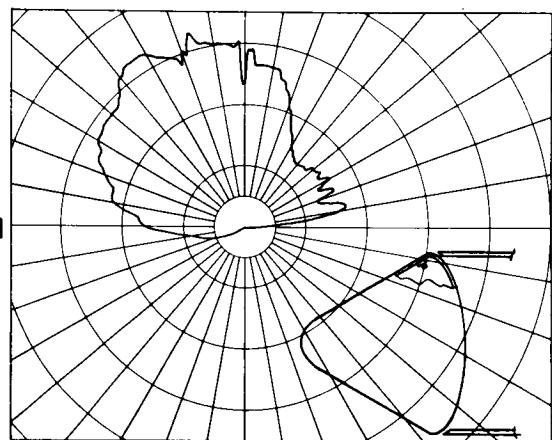
a



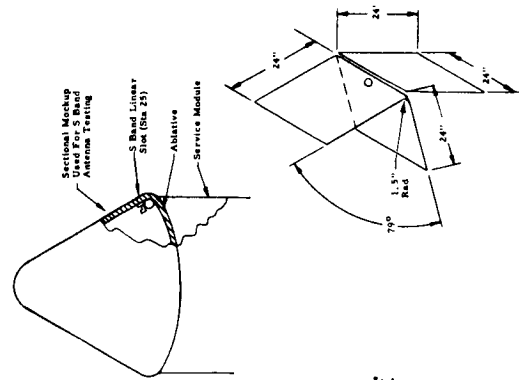
b



c



d



e

See text for explanation of conditions.

Figure 109 Relative Field Radiation Patterns Of Single, One-Quarter Scale S Band Antenna On Flat Sectional Mockup

- e. Command module and service module connected metal-to-metal physical contact, ablative.

Examination of these patterns shows the radiation aft to be significantly less with the ablative-filled gap than when this gap is bridged, and that at best the radiation in this sector is sufficiently low so that further reduction is undesirable. From these patterns taken on the flat mock up, it was judged important to investigate this effect further. Accordingly, the one-fourth scale model of the command module was covered with a layer of cork ablative and three S-band antennas were installed 120 degrees apart at Station 21. These antennas were scale models of the prototypes furnished and were installed with the planes of the radiating structures running straight up and down. First, a single antenna was fed. Its principal plane patterns are shown in Figures 110 through 112; Figures 110 and 111 showing the H plane patterns (which fall in the roll plane) and Figure 112 showing the E plane patterns (which fall in the pitch plane). Cross polarization is not shown in the E plane because it was negligibly small. From the roll plane patterns it appears that cross polarization is somewhat higher than it was when measured on the prototypes on the flat ground plane. Some of this may have been caused by differences between the full and scale model antennas. However, the curvature of the capsule

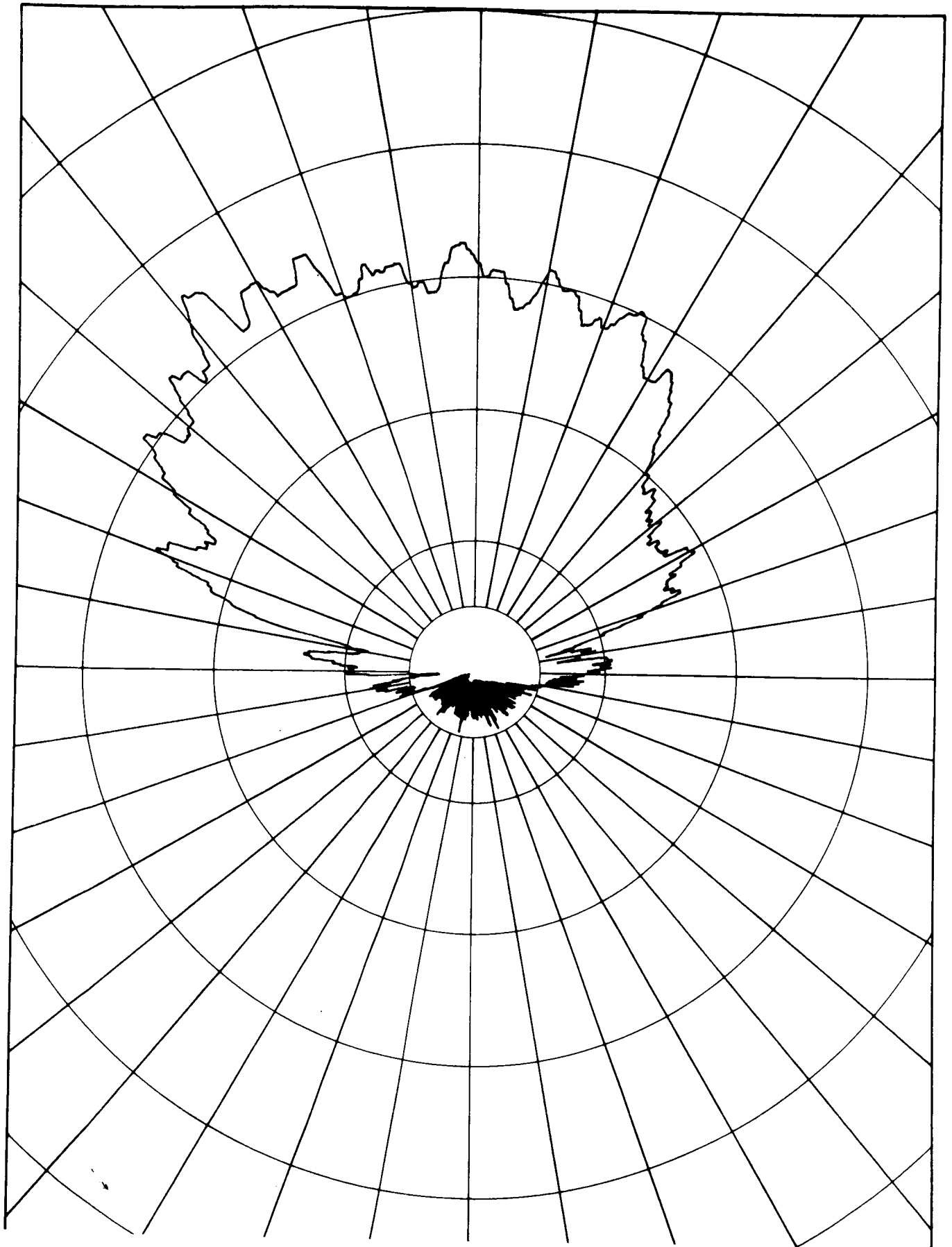


Figure 110

Relative Field Roll Plane Radiation Pattern Of Single
S Band Antenna At Station 21. Principal Polarization
Component; Gap Unbridged.

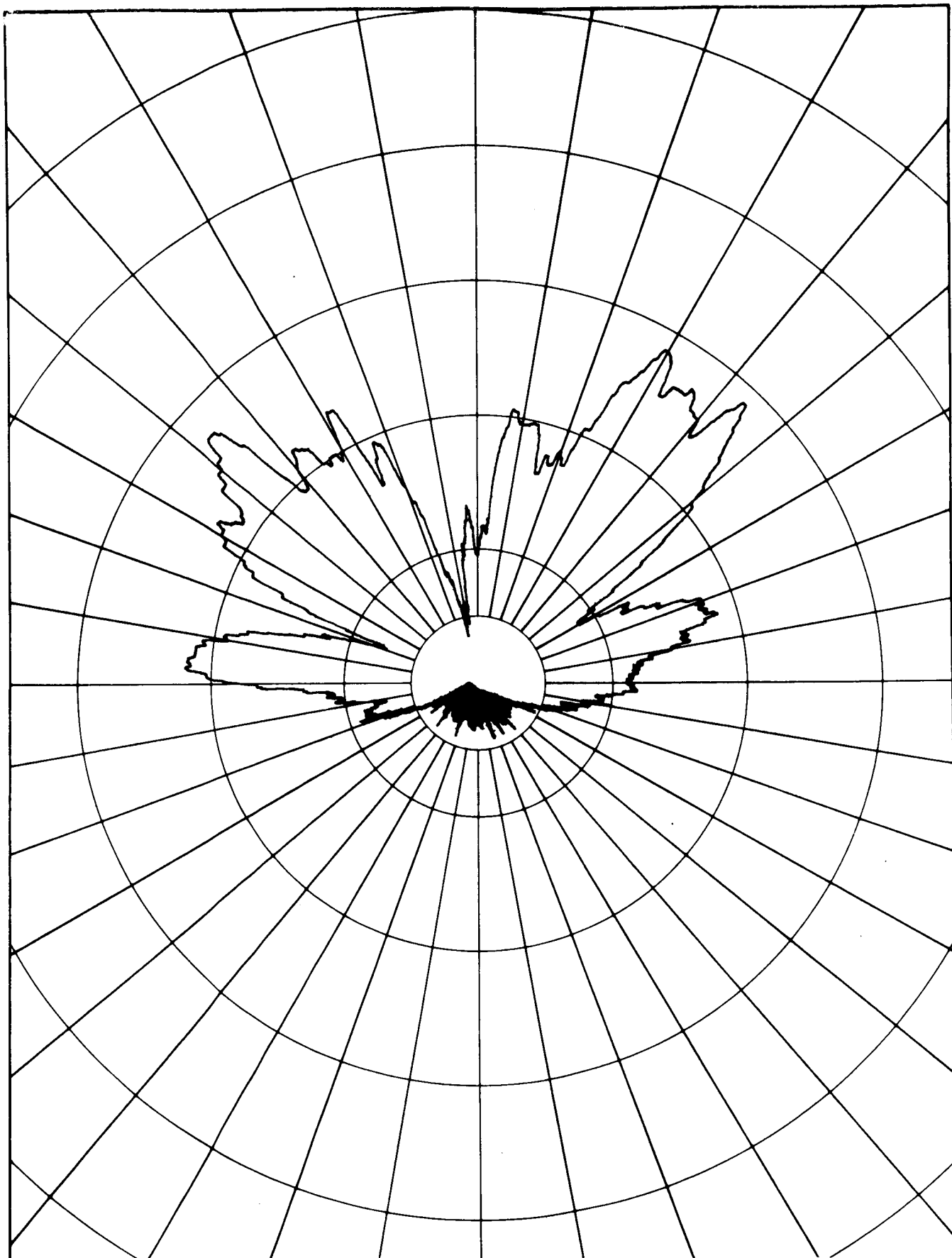


Figure 111

Relative Field Roll Plane Radiation Pattern Of Single
S Band Antenna At Station 21. Cross Polarization
Component; Gap Unbridged.

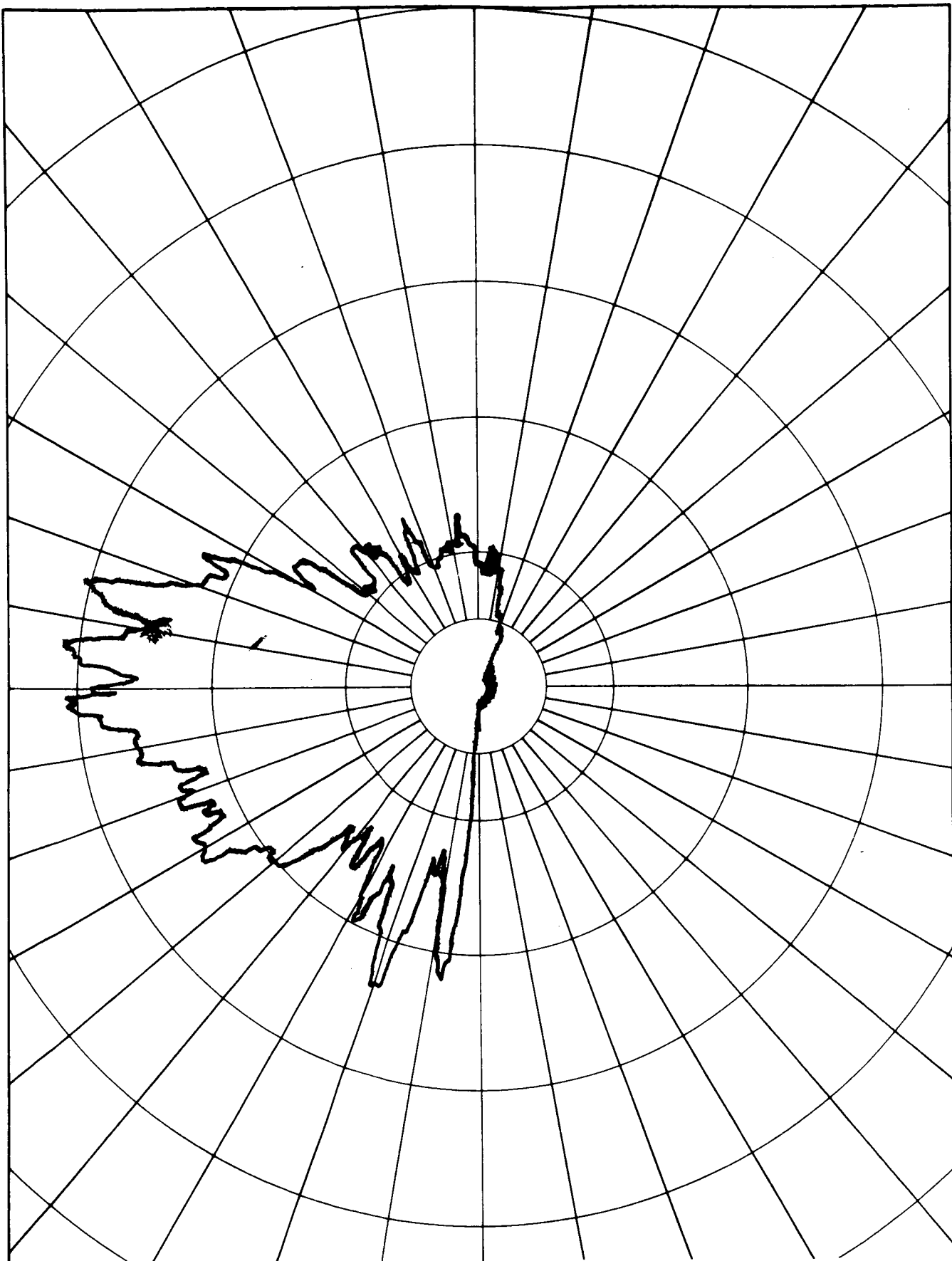


Figure 112

Relative Field Pitch Plane Radiation Pattern Of Single
S Band Antenna At Station 21. Principal Polarization
Component; Gap Unbridged.

is probably the principal cause. In the pitch plane it is seen that radiation in the aft sector is good because of the inherent antenna directivity of this design. However, it cuts off sharply within about 5 degrees of straight aft. This effect is similar to that which was found with the corresponding pattern on Figure 109. The gap between the two modules was then bridged with sheet metal and the patterns remeasured. The E components of radiation in the pitch plane is shown in Figure 113. A significant increase in aft radiation is evident. (Other patterns did not show significant change.)

All three antennas were then fed in phase and sets of roll and pitch-yaw plane patterns were measured, both with the gap unbridged and bridged. Representative patterns from the first set are shown in Figures 114 through 121, and those of the second set in Figures 122 through 127. Contrary to expectations, the two sets of patterns are only slightly different. Apparently, with three antennas the overall geometry is such that the effect is small. On larger models, where the modeling is more complete this effect would appear worth further investigation. The large number of sharp interference lobes is the dominating aspect of the patterns. The magnitude of this effect could be considerably reduced with operational units by sharpening the H plane patterns. This could readily be accomplished with an increase

of their width by about one inch.

Figure 128 shows the E plane pattern of a single antenna (bridge across the gap) moved up to Station 40. Comparison with Figures 110 and 114 shows that location of the antennas this high on the capsule reduces aft radiation so much that it should be avoided if at all possible.

As with the previous sets of patterns the desirability of polarization diversity in the earth-based antennas is indicated.

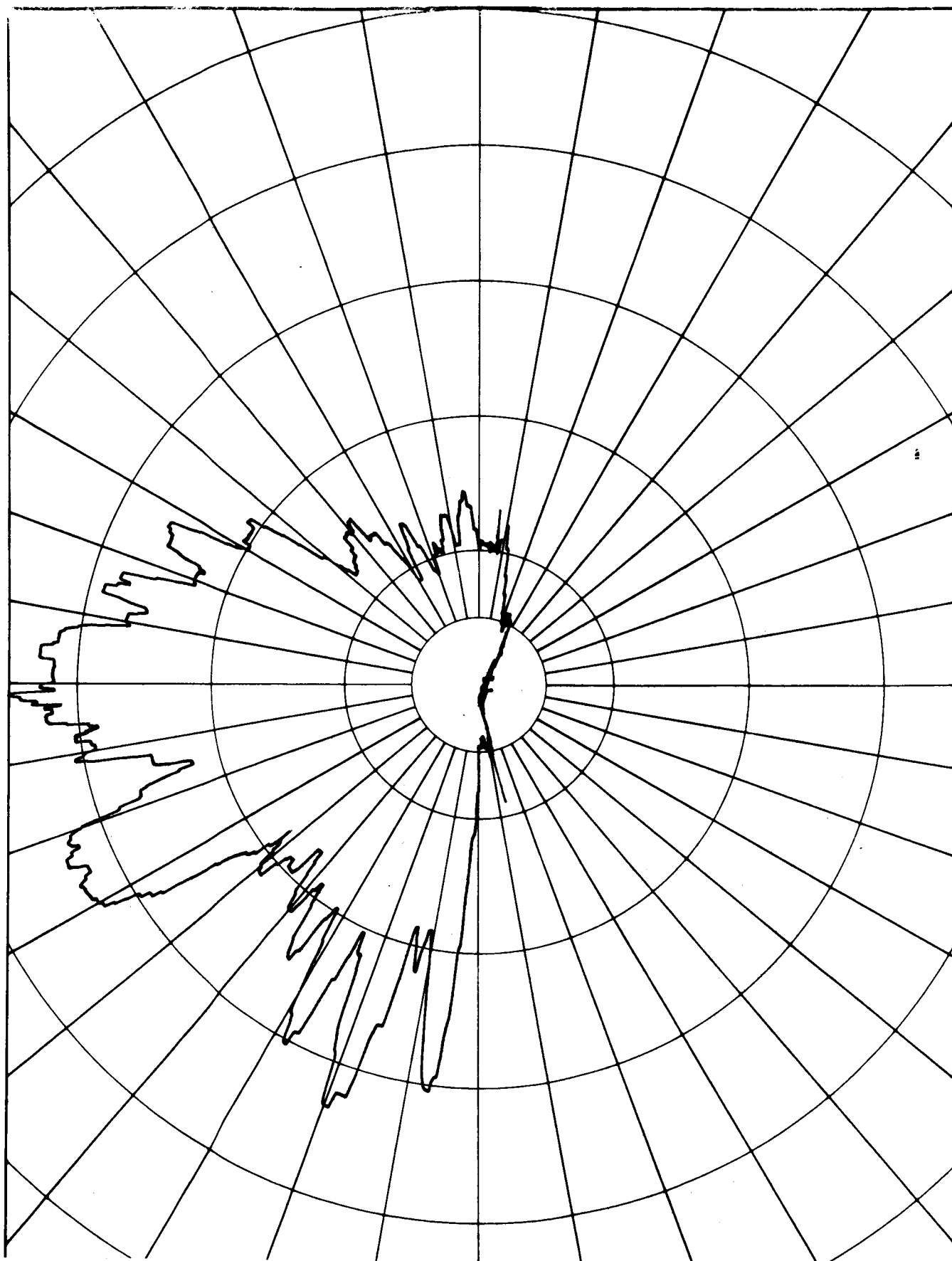


Figure 113

Relative Field Pitch Plane Radiation Pattern Of Single S Band Antenna At Station 21. Principal Polarization Component; Gap Unbridged.

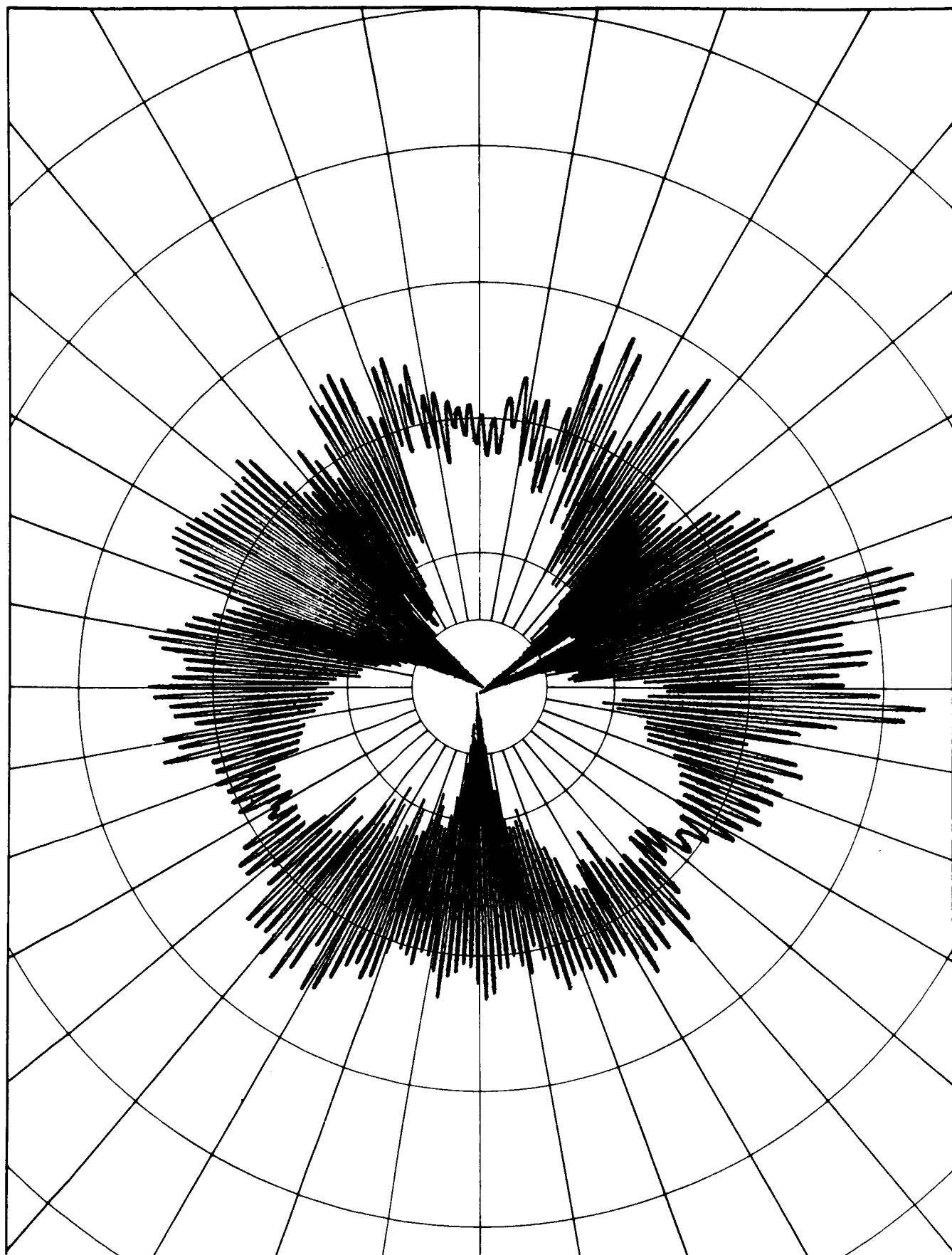


Figure 114

Relative Field Roll Plane Radiation Pattern Of Three S Band Antennas At Station 21. Principal Polarization Component; Gap Unbridged. Antennas At 0° , 120° , and 240° .

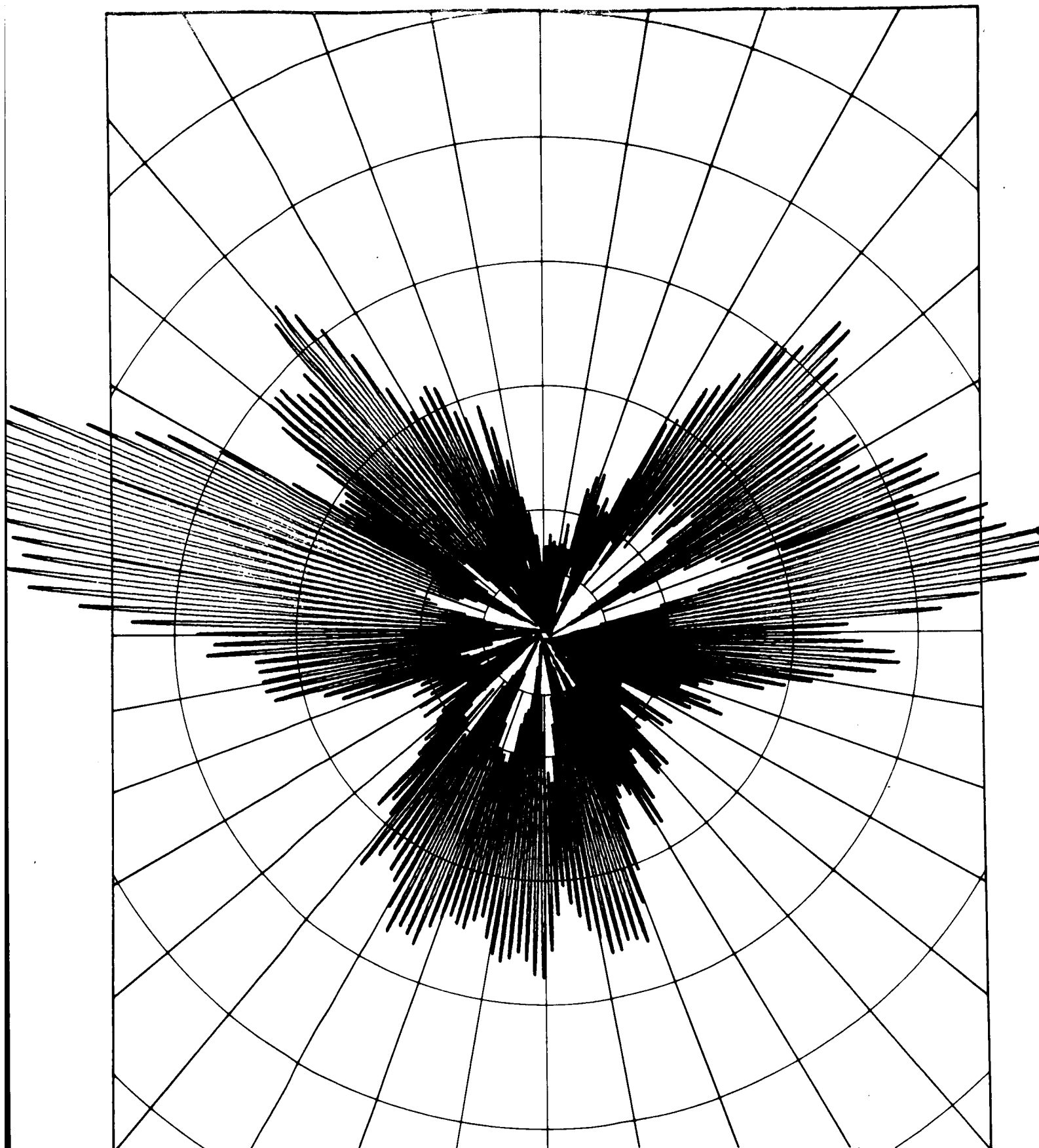


Figure 115

Relative Field Roll Plane Radiation Pattern Of Three S Band Antennas At Station 21. Cross Polarization Component; Gap Unbridged. Antennas At 0° , 120° , and 240° .

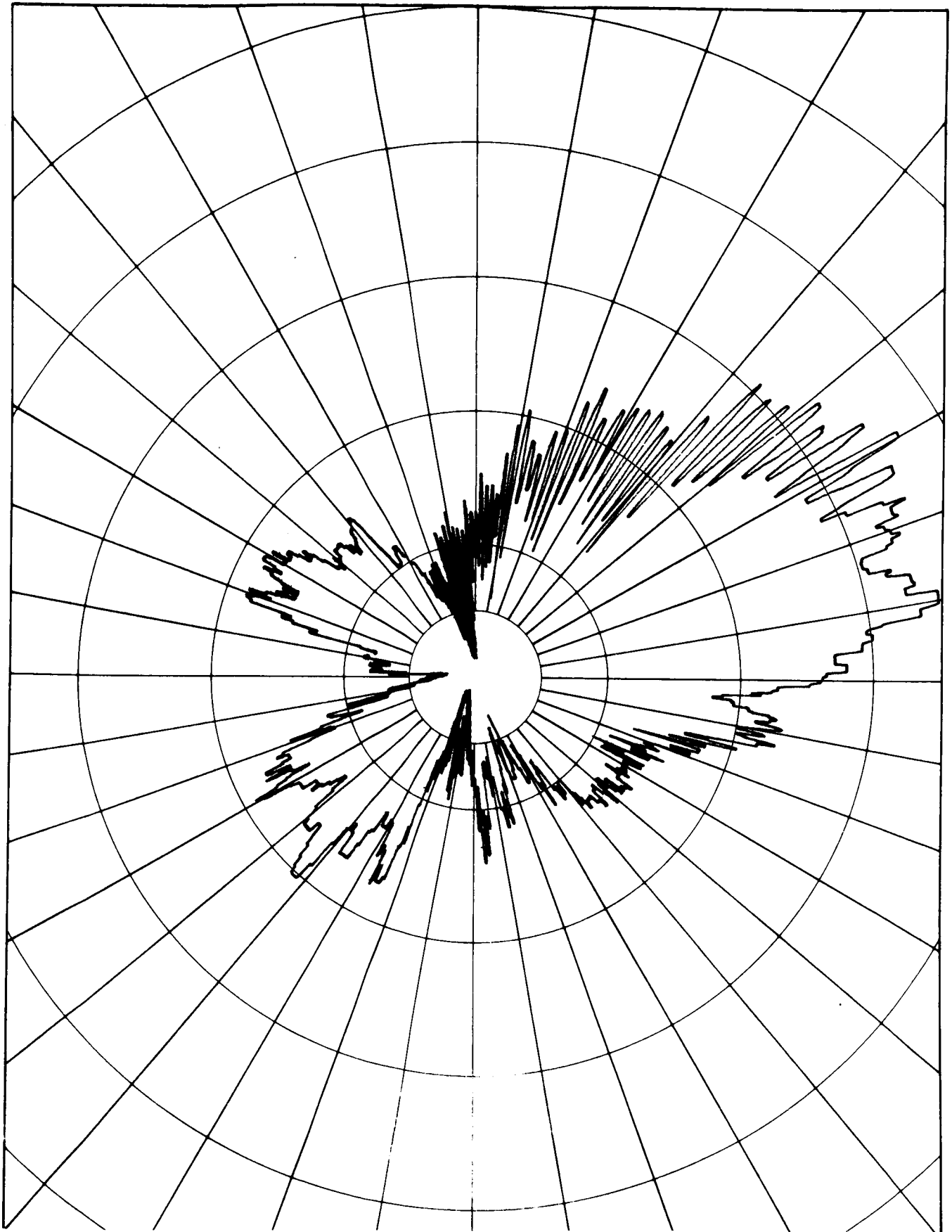


Figure 116

Relative Field Pitch-Yaw Plane Radiation Pattern Of
Three S Band Antennas At Station 21. Principal
Polarization Component; Gap Unbridged. One Antenna
In Plane Of Pattern.

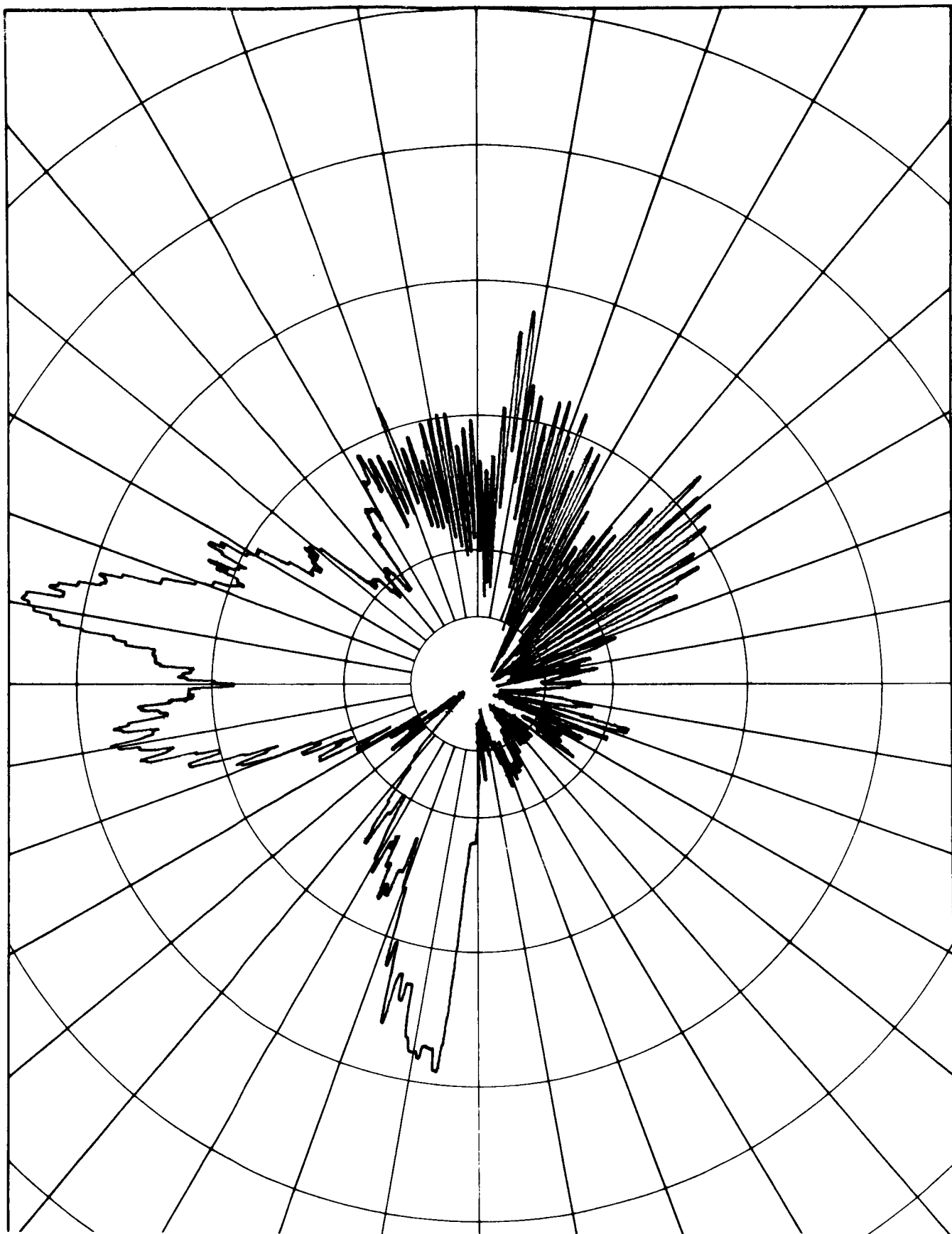


Figure 117

Relative Field Pitch-Yaw Plane Radiation Pattern Of
Three S Band Antennas At Station 21. Cross Polarization
Component; Gap Unbridged. One Antenna In Plane Of
Pattern.

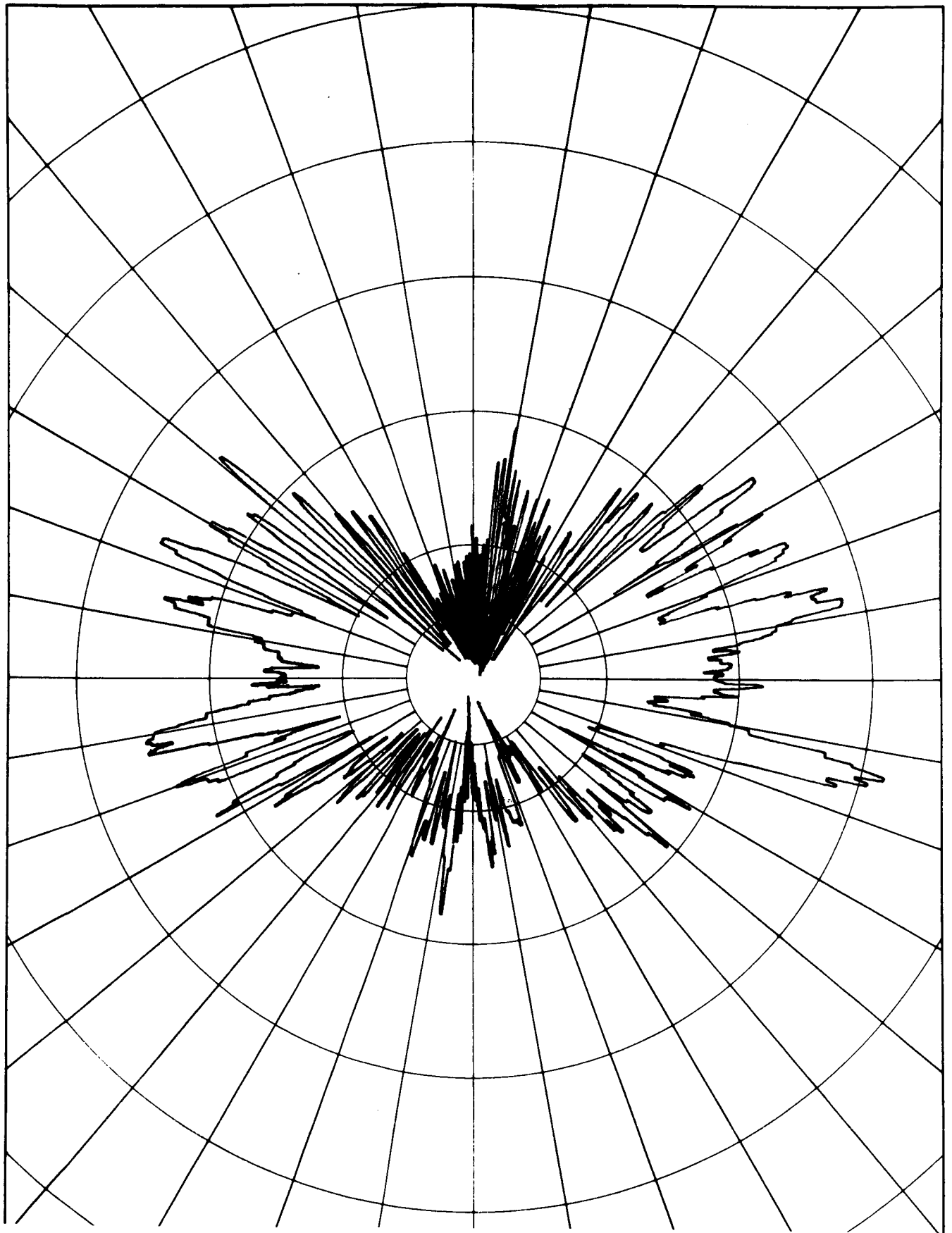


Figure 118

Relative Field Pitch-Yaw Plane Radiation Pattern Of
Three S Band Antennas At Station 21. Principal
Polarization Component; Gap Unbridged. Plane Of
Pattern 30° From Plane Containing Antenna.

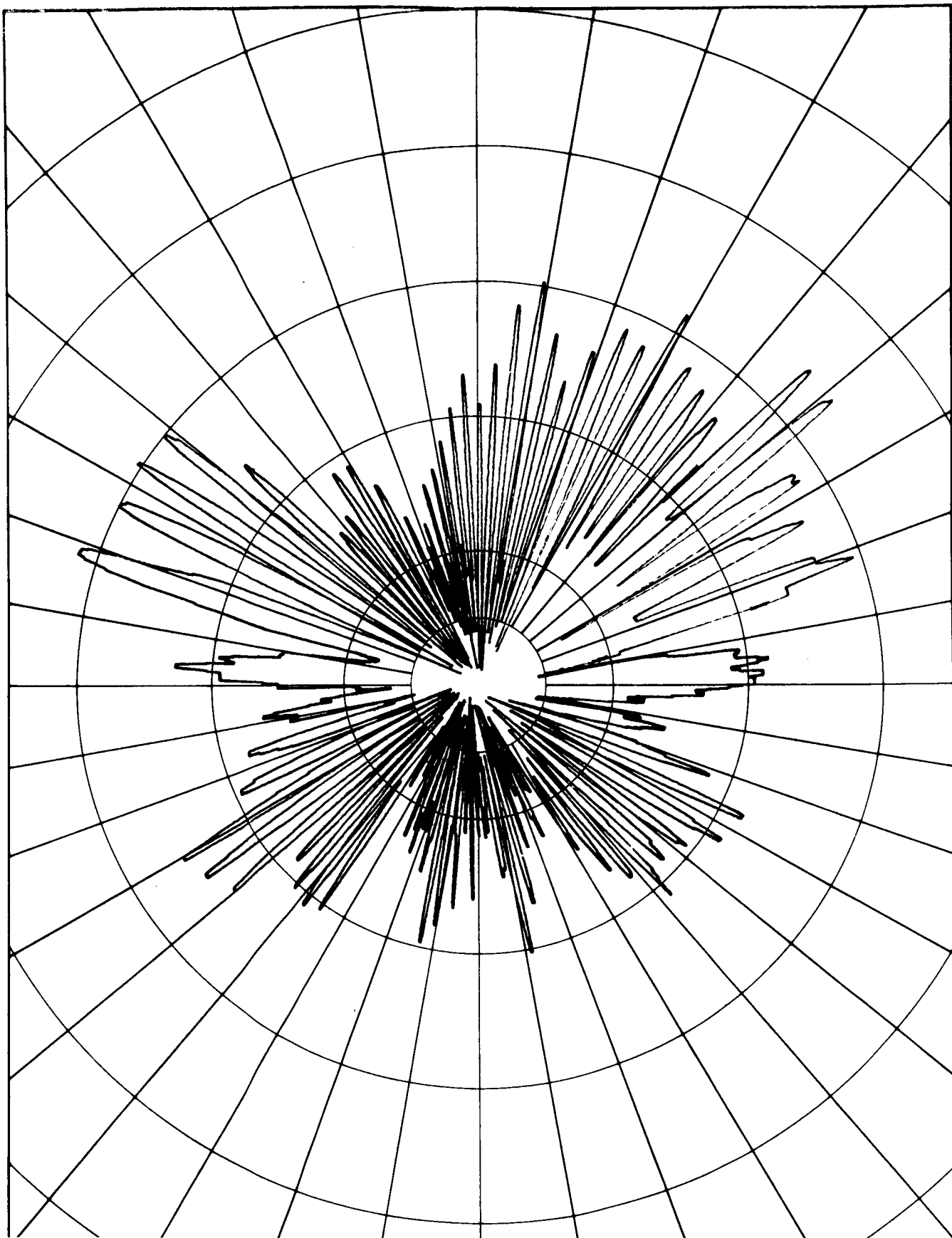


Figure 119

Relative Field Pitch-Yaw Plane Radiation Pattern Of
Three S Band Antennas At Station 21. Cross
Polarization Component Of Radiation; Gap Unbridged.
Plane Of Pattern 30° From Plane Containing Antenna.

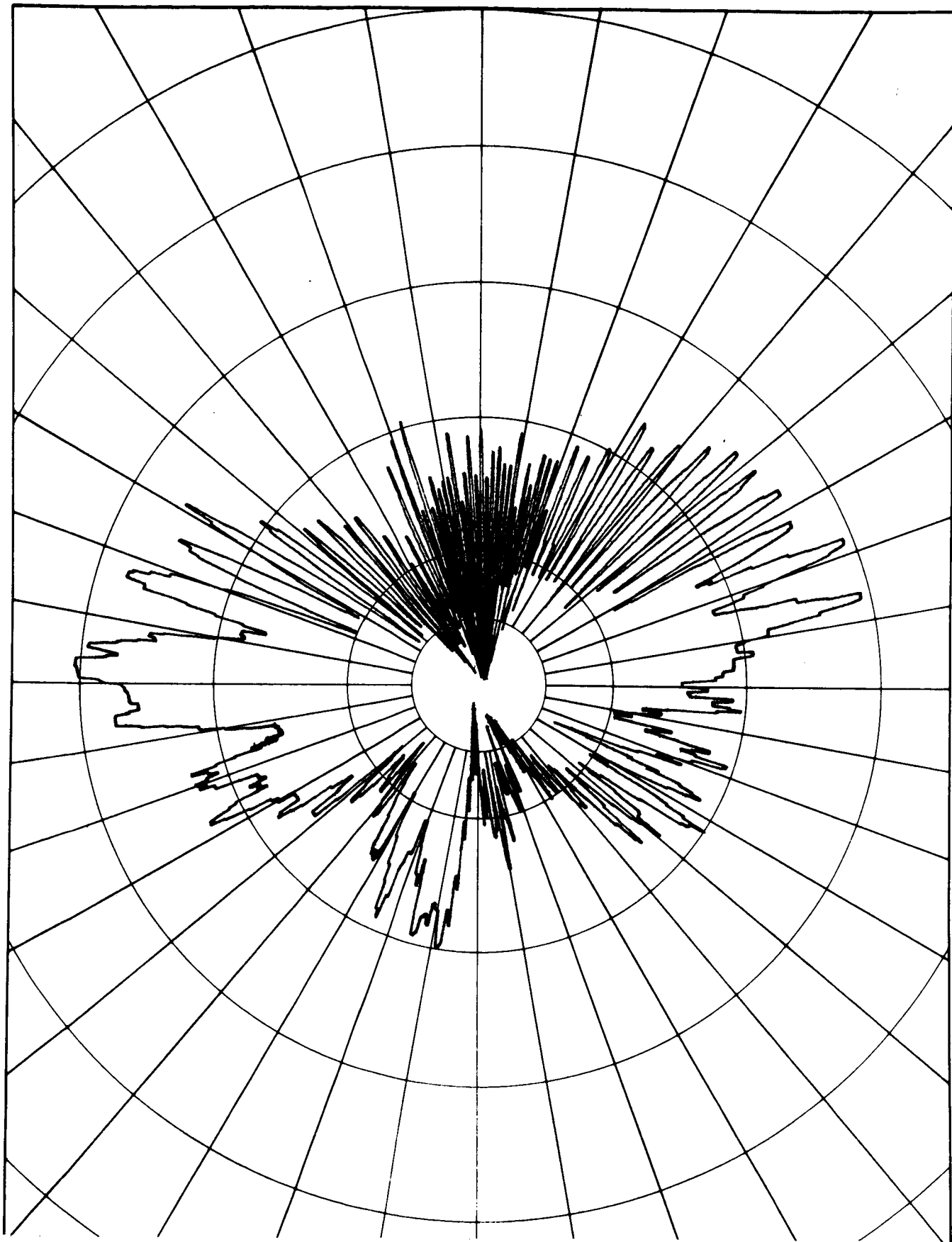


Figure 120

Relative Field Pitch-Yaw Plane Radiation Pattern Of
Three S Band Antennas At Station 21. Principal
Polarization Component; Gap Unbridged. Plane Of
Pattern 60° From Plane Containing Antenna.

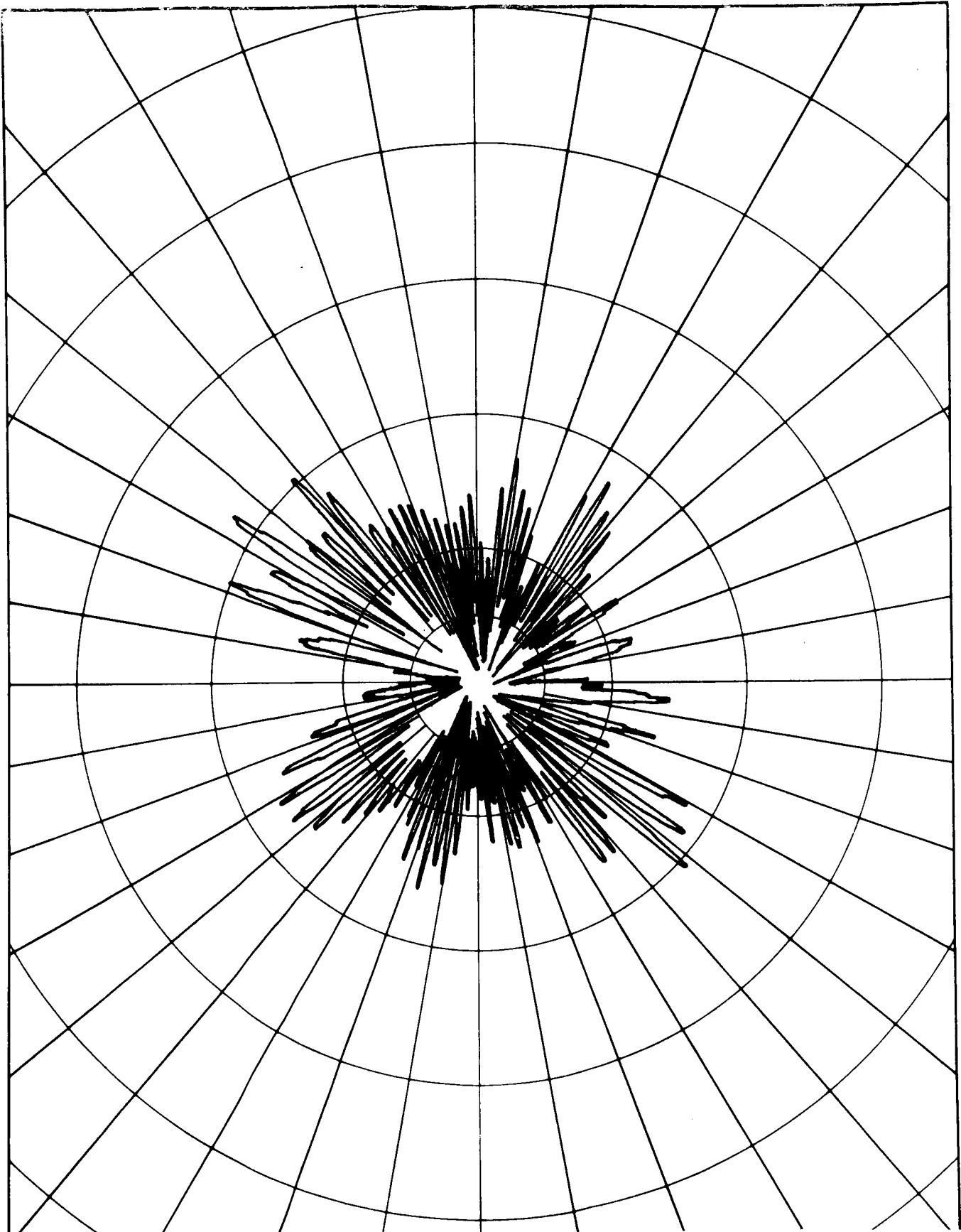


Figure 121

Relative Field Pitch-Yaw Plane Radiation Pattern Of
Three S Band Antennas At Station 21. Principal
Polarization Component; Gap Unbridged. Plane Of
Pattern 60° From Plane Containing Antenna.

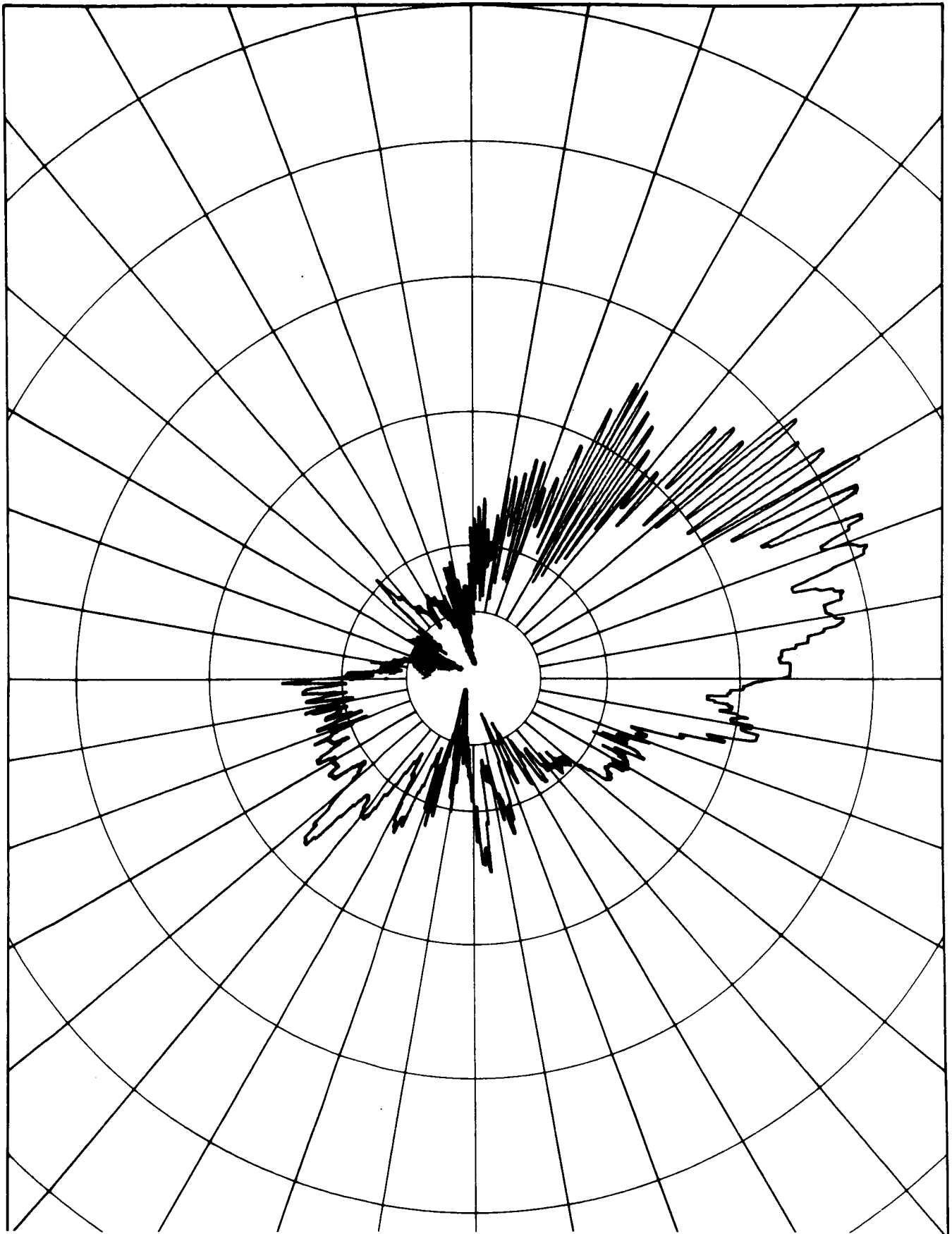


Figure 122

Relative Field Pitch-Yaw Plane Radiation Pattern Of
Three S Band Antennas At Station 21. Principal
Polarization Component; Gap Bridged. One Antenna
In Plane Of Pattern.

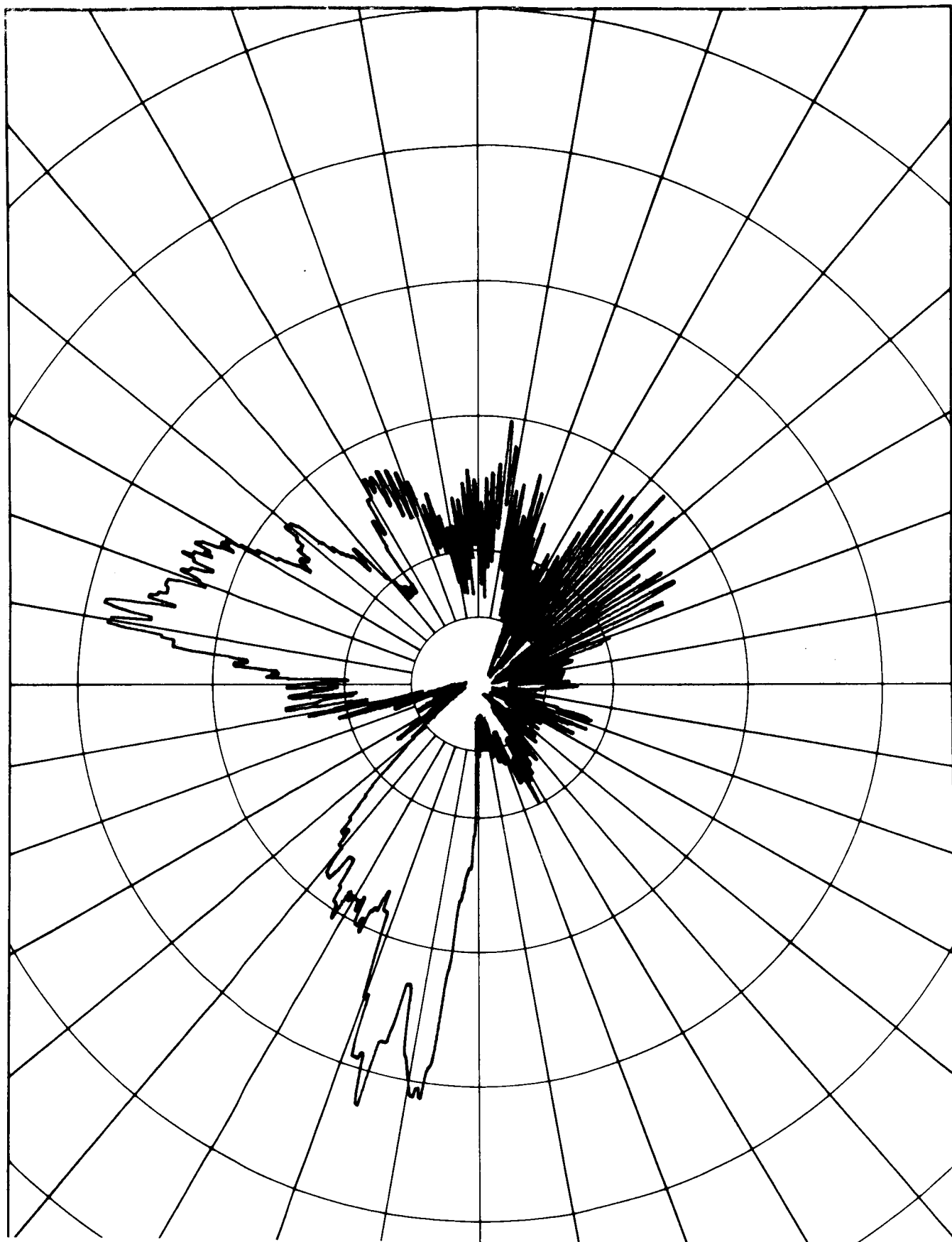


Figure 123

Relative Field Pitch-Yaw Plane Radiation Pattern Of
Three S Band Antennas At Station 21. Cross Polarization
Component; Gap Bridged. One Antenna In Plane Of
Pattern.

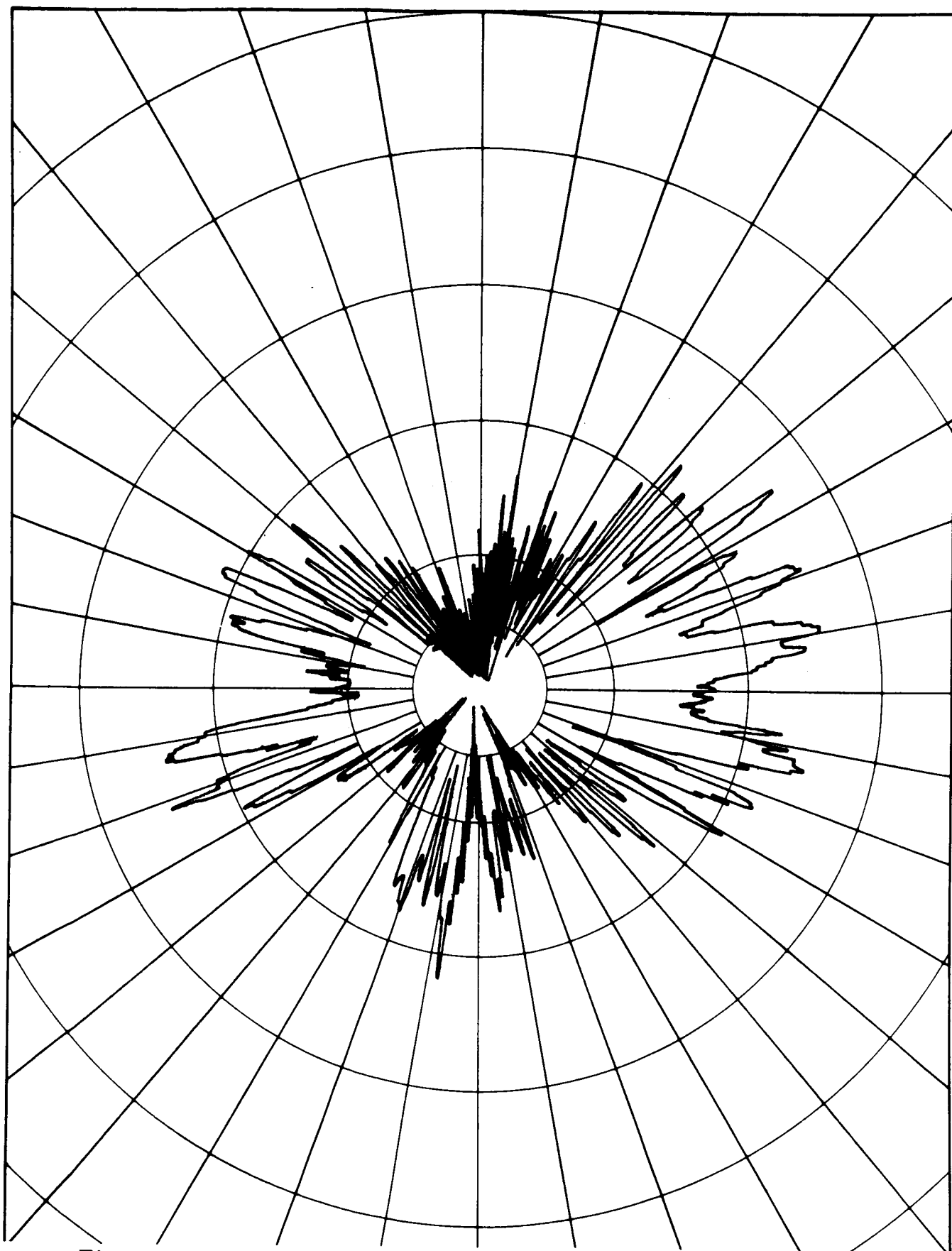


Figure 124

Relative Field Pitch-Yaw Plane Radiation Pattern Of
Three S Band Antennas At Station 21. Principal
Polarization Component; Gap Bridged. Plane Of
Pattern 30° From Plane Containing Antenna.

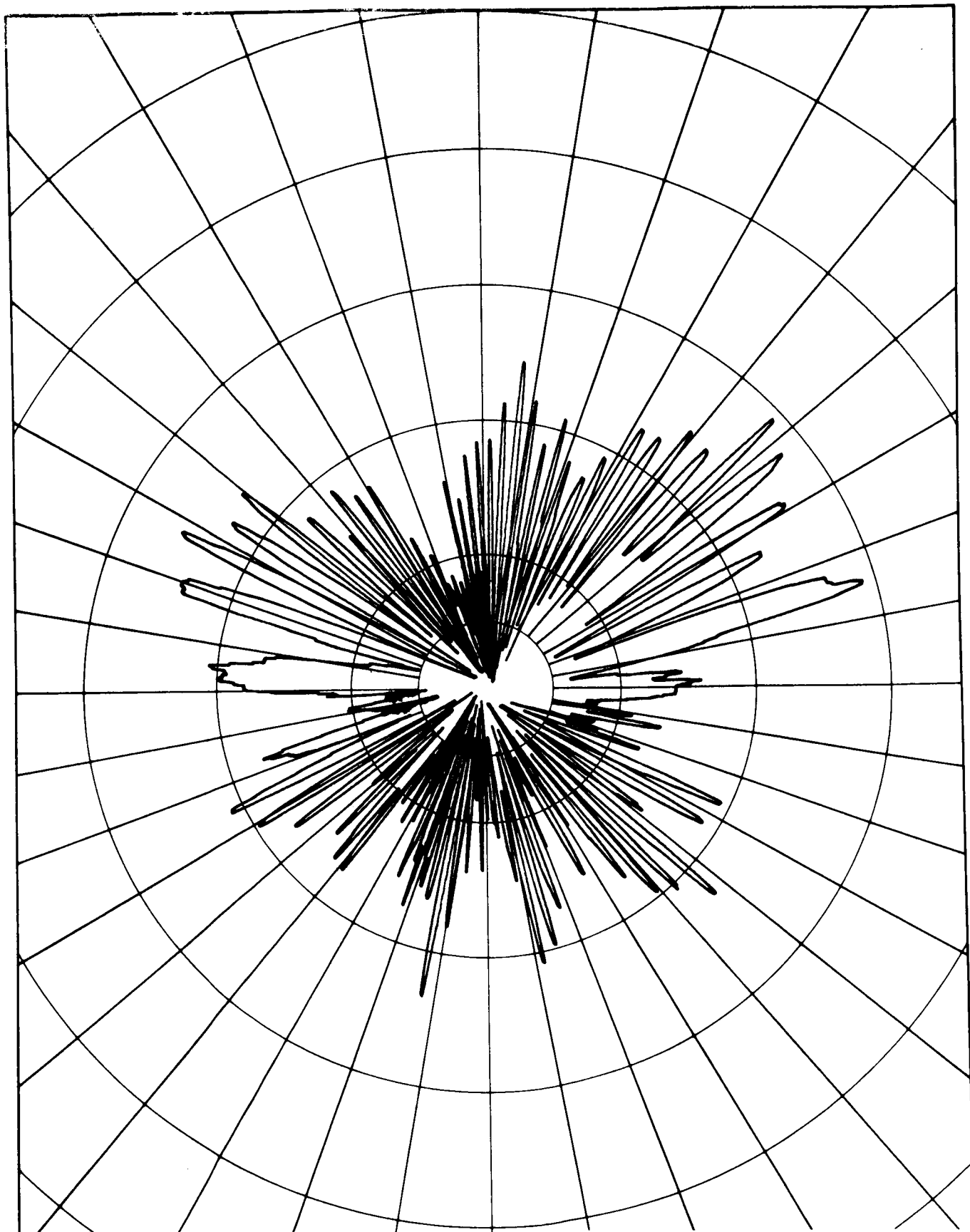


Figure 125

Relative Field Pitch-Yaw Plane Radiation Pattern Of
Three S Band Antennas At Station 21. Cross
Polarization Component Of Radiation; Gap Bridged
Plane Of Pattern 30° From Plane Containing Antenna.

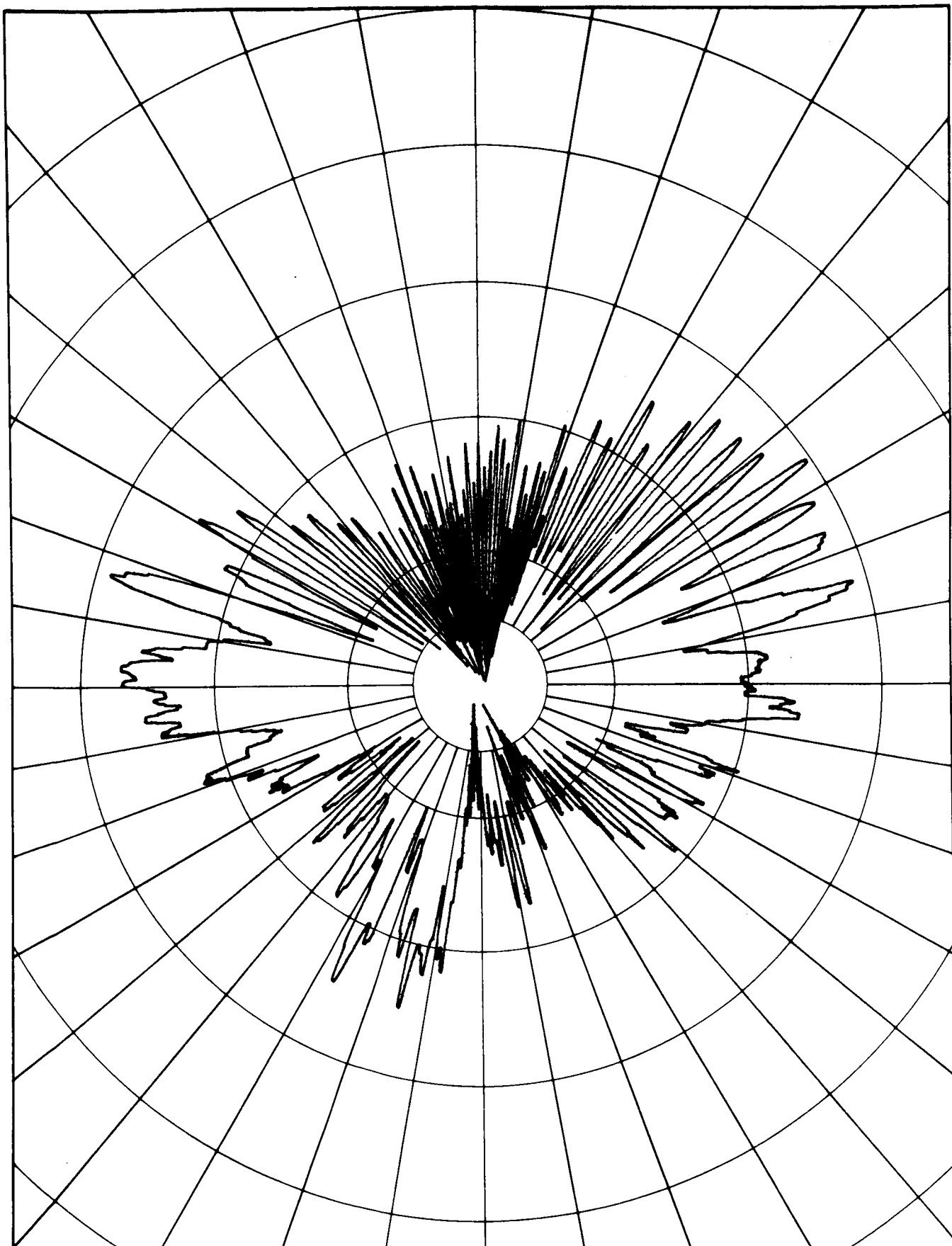


Figure 126

Relative Field Pitch-Yaw Plane Radiation Pattern Of Three S Band Antennas At Station 21. Principal Polarization Component; Gap Bridged. Plane Of Pattern 60° From Plane Containing Antenna.

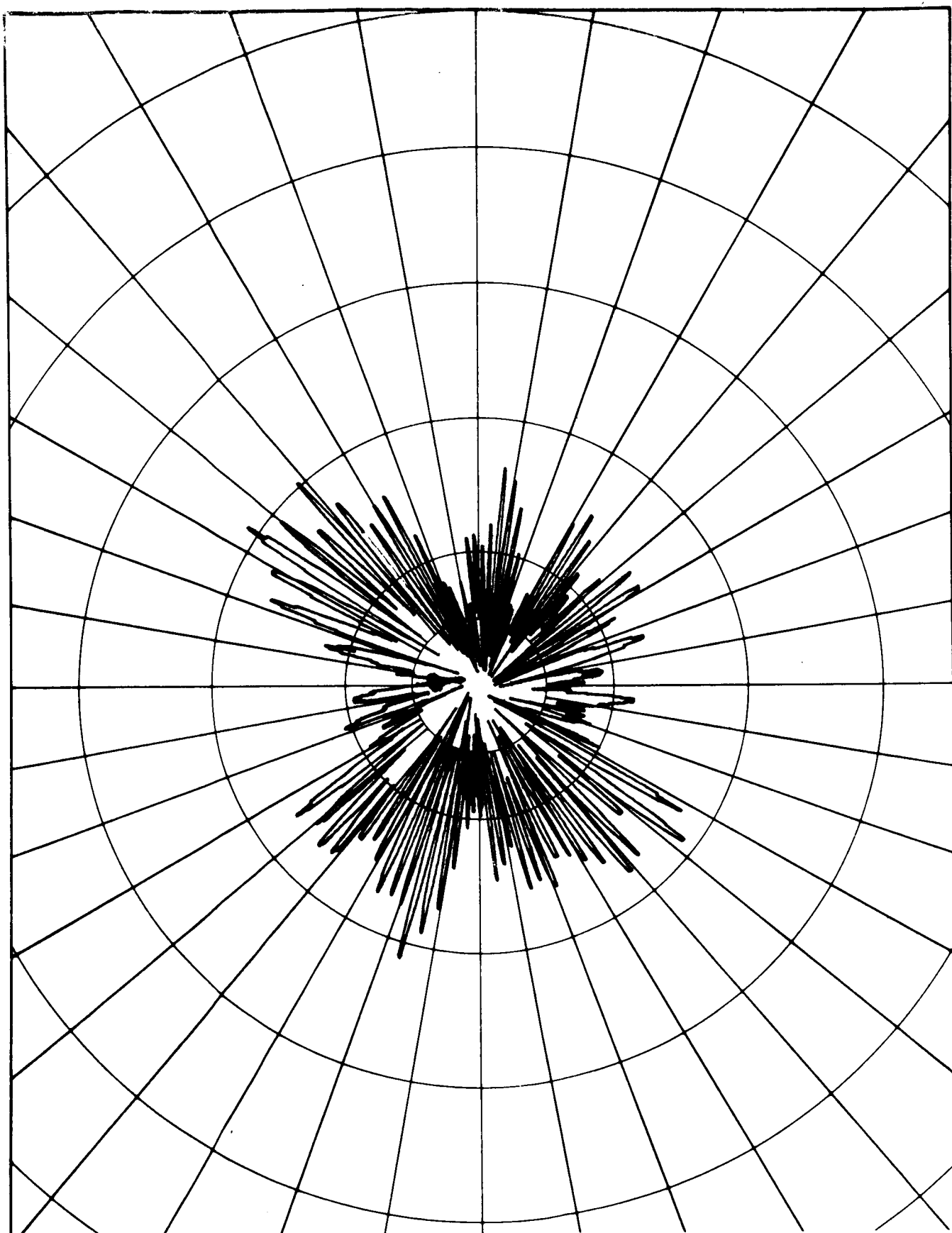


Figure 127

Relative Field Pitch-Yaw Plane Radiation Pattern Of
Three S Band Antennas At Station 21. Principal
Polarization Component; Gap Bridged. Plane Of
Pattern 60° From Plane Containing Antenna.

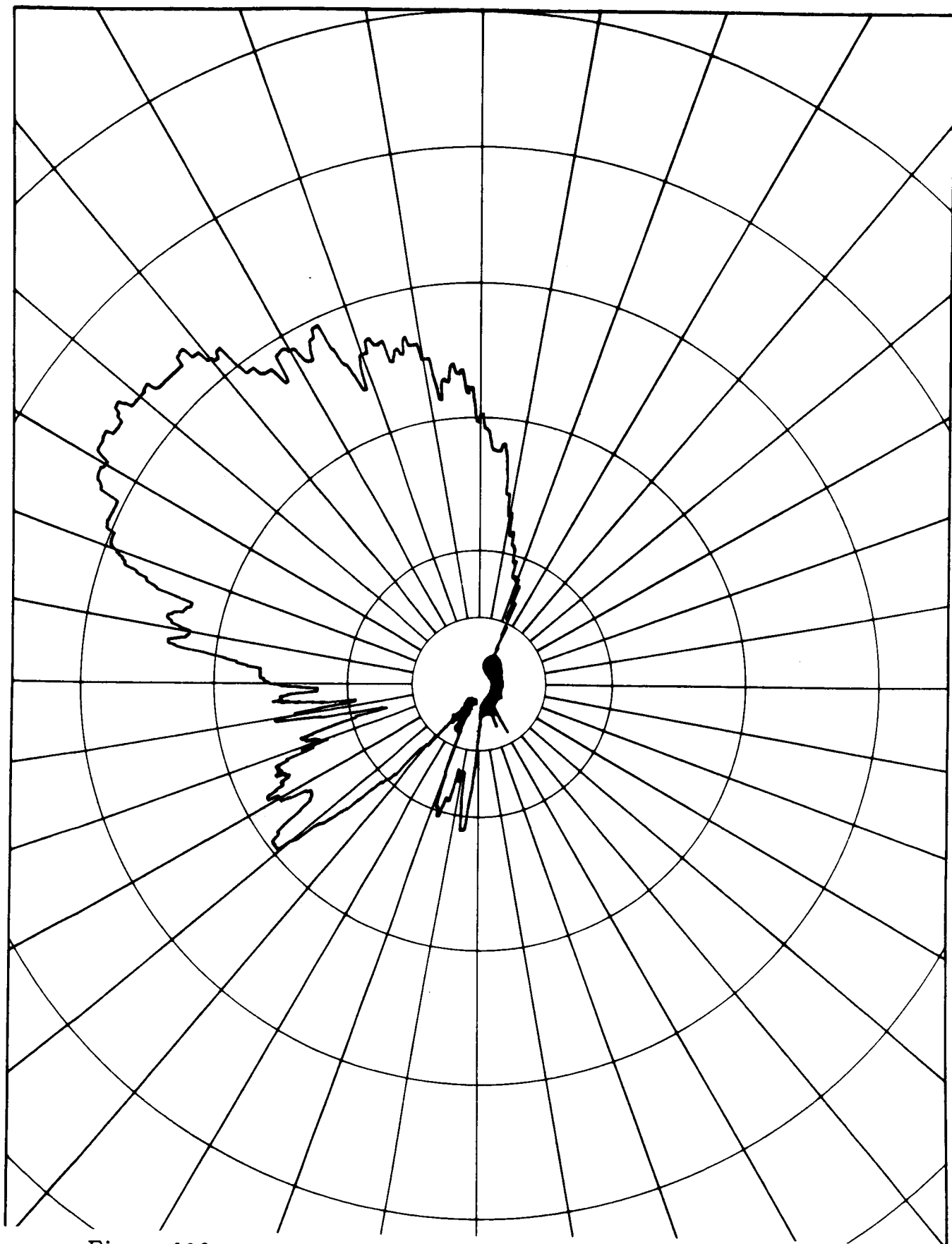


Figure 128

Relative Field Roll Plane Radiation Pattern Of Three S Band Antennas At Station 40. Principal Polarization Component; Gap Unbridged. Antennas At 0° , 120° , and 240° .

6.0 CONCLUSIONS

The antenna design study has indicated two approaches to the design of antennas for utilization as components of flush mounting nondirectional radiating systems on manned space flight vehicles. One of these, which utilized cavities as the antennas, was judged unsuitable for the Apollo Mission. A set comprising one each of the antennas which this approach would lead to if designed for the Apollo Command Module would weigh approximately 28 pounds. At least two, and preferably three, of these sets would be required to make up a full omnidirectional system. If such a system were used the installed weight would be substantially greater than the weight of the antennas alone because of the additional structure that would be required to carry the structural loads around the antenna mounting holes. This additional weight would preclude their use.

The other approach, which utilizes radiating structures embedded in the ablative shield itself, was judged suitable for Apollo use. Laboratory models were constructed, which confirmed this, indicating that it would be feasible to construct satisfactory operational units embodying this approach. If the operational units were of exactly the same size as the laboratory models the weight of a complete set of one each of these antennas would be about 14.5 pounds. As with the cavity antennas two, or preferably three sets, would be required for a complete nondirectional antenna system. But in the case of these ablative shield

antennas, unlike the cavity antennas, no significant additional weight would be required for structural changes in the course of their installation.

It was noted that final units might have to be increased in size in order to obtain acceptably small losses in the ablative material surrounding the antennas. If all of the antennas were increased in both length and width by one half inch (corresponding to the one quarter inch thick layer of teflon which was placed adjacent to the sides of the laboratory models) the weight of a complete single set would be increased by 4.2 pounds. How much, if any, weight increase of this kind would actually be necessary with operational units cannot be determined at this time. It would probably be less than the 4.2 pounds. It could possibly be slightly more. The actual final weight would depend upon many factors, including: the relative importances that were assigned to weight and radiation efficiency; the curvature of the capsule surface at the locations selected for the antennas; the exact final electrical properties of the ablative covering; and whether or not post-entry performance were required. In any case, it should be noted that because the antennas replace ablator having a density about one fourth that of the antennas themselves, that the weight increase is only about three quarters as large as the weights themselves.

The cavity antennas, although not recommended for Apollo, at least at present, may be useful in the future. If, at some time, thinner ablative coverings are used there will not be room for ablative shield antennas. At the same time the weight of cavity antennas for such vehicles would decrease almost in proportion to the decrease of ablative, because about 80% of the weight of these antennas was in the window covering them.

Additional work would be required to produce operational units of either type. In the case of the ablative shield antennas most of this would consist of the development of fabrication techniques for making the quartz-metal assemblies and of environmental testing. On the basis of the bandwidths obtained and the experiences thus far, relating to the response of the antennas to minute dimensional changes it is judged that it would not be difficult to achieve final designs having the stability demanded by the environmental requirements.

The pattern study indicated that as many of the antennas as possible should be located in the bilge area and that this is increasingly important as the operating frequency is increased. In the case of S and C-band antennas it is essential for aft radiation that the antennas be located at Station 21 or very close to it. It also indicated that as few as two antennas per frequency could be used at the lower frequencies, provided that they were canted to produce both E_0

and E_{θ} radiation. It was noted that utilization of this type of installation would require that earth-based antennas have polarization diversity. Better performance would be obtained with three canted antennas at each of the lower frequencies. If weight considerations permit, this is the type of installation that is judged the most appropriate for the application.